INTEGRATED GRASSLAND FIRE DANGER ASSESSMENT FOR GOLDEN GATE HIGHLANDS NATIONAL PARK USING GEOSPATIAL TECHNIQUES

Dipuo Olga Mofokeng

2004199796

A thesis submitted to the Department of Geography, Faculty of Natural and Agricultural Science, at the University of the Free State, in fulfilment of the academic requirements for the degree of Doctor of Philosophy in Environmental Geography

November 2023

Phuthaditjhaba; Free State Province; South Africa

Promoter: Prof Samuel Adelabu

ABSTRACT

Grasslands are key to the earth's system and provide crucial ecosystem services. However, the global degradation of grassland ecosystems is increasing at an alarming rate, and fire is regarded as one of the major drivers of degradation. Fire has been an integral evolution factor of grassland ecosystems, key in shaping and maintaining grassland's ecological functioning. With global changes such as anthropogenic climate changes that alter fire regimes, fire is perceived as a destructive factor associated with negative impacts on the environment, society and economy. Moreover, there is numerous evident showing that over the past several decades and predicted to continue, average temperature area rising, predicted to continue, rainfall patterns are changing, resulting in more frequent and longer lasting drought across all ecosystems; protected and grassland areas are becoming progressively more challenging with threat to biodiversity and tourism operations and activities due to bush-encroachment, fauna and flora and species losing their natural inhabitant and competition, destroy tourism infrastructure and alter the attractiveness of tourist destination and loss of revenue and landscape ecosystem services.

Integrated fire risk assessment systems provide an integral approach to fire prevention and control and mitigate the negative impacts of fire. Fire danger assessment, as one of the components of integrated fire risk assessment, is regarded as an extremely challenging endeavour owing to the confluence of factors that influence fire ignition and fire behaviour. Most global fire danger systems and indices are based on meteorological data, do not consider fire causes and have limited spatio-temporal dimensions of fire drivers or switches; therefore, they are deemed outdated and inadequate in accuracy and validating estimation of fire danger.

Numerous methods have been employed to quantify the complex interrelation between fire switches and fire occurrence to estimate fire danger or susceptibility with different precision outcomes, thence, the prediction accuracy is still debated. However, most of these studies focused on northern hemisphere forest fires; therefore, grassfire research is limited, particularly in the African and Latin American grassland ecosystem. This study, therefore, developed an integrated grassland fire danger assessment model in a protected Afromontane grassland ecosystem, the Golden Gate Highland National Park (GGHNP) as the study area, taking into account all four fire drivers adapting the fire danger assessment component of the framework for fire risk assessment. Geospatial technology such as remote sensing (RS), geographical information system (GIS), Google Earth Engine (GEE) and Climate Engine (CE) were used to evaluate the spatial and temporal variation of the fire drivers.

Lightning is a well-known natural fire ignition source and has been used as the proxy for such, and is inadequately represented in fire ignition models due to lack of quantitative spatial pattern on flash

density. The study developed the Lightning Hazard Map (LHM) from 11-year lightning strikes data (2007 – 2017) using GIS spatial analytic techniques (hotspot analysis, Global Moran I and spatial autocorrelation analysis). The results revealed December, 15:00 and 17:00 as the month and hours with the highest lightning activity, respectively. Clustering was observed throughout the year, except in July and the early to late morning hours at 06:00, 08:00 and 09:00 South African Standard Time (SAST). The clustering of lightning strikes at the park is at a distance of about 1.2 km. This connotes that strikes clustered with other strikes are not likely to strike an individual specific location from the centre of the cluster of strikes much beyond a circle with a radius of 1.2 km. While clusters starting at 2 km to 8 km. Forty-nine (49%) and 16% of the study area was found to be highly to extremely prone to lightning-caused fire.

Humans cause 90% of fires globally through land clearing and agricultural activities, however, most of the fire danger systems do not consider the temporal dimension of human-caused fire ignition. The study temporal modelled and evaluated the human behaviour as an agent of human-caused fires using distance from roads and tourist infrastructure (INFRA) as indicators using 11-year fire occurrence data. The results showed that INFRA and roads influenced all models at different times. The INFRA had influence during weekend days (Saturday and Friday) of both winter and spring seasons, while ROADS had influence during weekday (Monday to Friday) of both seasons.

The inaccuracy of most fire danger systems and indices often lies in the coarse spatial resolution data, particularly at the landscape scale. Using the GEE platform, this study developed a data fusion method termed "Blend-then-Index" (BI) by blending indices from Sentinel-2 and MODIS sensors to a 10 m spatial resolution to estimate the degree of grass curing (DoC). Grass curing is the transformation of live fuel to dead fuel component of the fuel bed and is one of the crucial input parameters for the grassland fire danger system or index, also inadequately represented in fire danger assessment systems due to sparse measurement systems which are too expensive and time-consuming, data scarcity and inaccessible. The results revealed September, February and May as the months with the highest, lowest and onset of degree of curing, respectively. Based on grass curing, over 80% of the study area was prone to fire danger. The results showed that over 90% of fire points fell under grass curing maps' (GCMs) high and extreme fire danger. Moreover, the study revealed an inverse correlation between grass curing indexes (GCIs) and precipitation and soil moisture. Owing to this precision, the "BI" data fusion method was used in the study to measure other fuel factors.

Finally, the study developed prediction fire danger map models taking into consideration the relationship between the confluence of fire drivers and fire danger and 20 variables were selected. Namely: LHM, proximity from road, infrastructure, rivers, GCI, global vegetation moisture index (GVMI), vegetation condition index (VCI), bare soil index (BSI), soil bulk density, coarse fragments, soil moisture content, total plant available water holding capacity (TAWCP) elevation, aspect, slope, topographic positioning index (TPI), topographic ruggedness index (TRI), topographic water index (TWI), land surface temperature (LST) and wind speed. All the models showed that almost 85% of the study area is prone to fire, ranging from low to extremely dangerous. In comparing the best-performing models in predicting fire danger, the results revealed trade-off between statistical and machine learning methods. Decision trees (DT) showed high precision on model fit and success rate (ROC/AUC value of 0.93, 0.96 and 0.50); however, it was outperformed by weight of evidence (WoE) (0.83, 0.82 and 0.7) in predictive rates. Other models, frequency ratio (FR) (0.92, 0.95 and 0.66) for model-fit, success rate and predict rate validation, logistic regression (LR) (0.63, 0.64 and 0.59), random forest (RF) (0.91, 0.94 and 0.53), support vector machine (SVM) (0.63, 0.64 and 0.59). The WoE method showed robust performance in all three accuracy assessments (model fit, success and prediction rates). and therefore, based on that, the study suggests a hybrid approach of statistical and machine learning methods for improving the accuracy of fire danger prediction. Furthermore, based on the WoE model, almost 53% of the park is highly prone to fire, observably concentrated in the southern, south-western and eastern parts.

The study revealed that the geospatial techniques used are effective and can effectively model fire danger. The results also revealed that the study area's fire regime was fuel-driven and caused by lightning and humans. This suggests that a fire management strategy should be based on a fuel management strategy that considers the local fuel conditions. Therefore, there is an urgent need to identify and determine the thresholds of fuel conditions (fuel load, fuel moisture content, and other fuel characteristics in relation to fire ignition and fire behaviour). This study assists in meeting sustainable development goal including SDG 15, i.e., life on land including protection of natural landscape and biodiversity, and conservation of mountainous ecosystems.

PREFACE

The research work described in this thesis was carried out in the Faculty of Natural and Agricultural Sciences, University of the Free State, Phuthaditjhaba from January 2018 to December 2023, with Prof. Samuel Adelabu as promoter (Department of Geography).

I declare that the study described in this research thesis has, at no time been submitted in any form at any form to any other university. It, therefore, represents my original work except where due acknowledgements are made.

Dipuo Olga Mofokeng: ____________________ Date: December 2023

As the candidate's promoter, I certify the above statement and approved this thesis for submission

Prof. Samuel Adelabu: ____________________ Date: December 2023

DECLARATION-1: PLAGIARISM

I, Dipuo Olga Mofokeng, declare that:

1. The research reported in this thesis, except where otherwise indicated, is my original research.
2. This thesis has not been submitted for any degree or examination at any other university.
3. This thesis does not contain other persons' data, pictures, graphs, or other information unless specifically acknowledged as being sourced from other persons.
4. This thesis does not contain other person's writing, especially acknowledged as being sourced from other researchers. Where other written sources have been quoted, then:
   (a) Their words have been re-written, but the general information attributed to them has been referenced.
   (b) Where their exact words have been used, then their writing has been placed in italics and inside quotation marks and referenced.
5. This thesis does not contain text, graphics, or tables copied and pasted from the internet unless specifically acknowledged and source being detailed in the thesis and the references section.

Signed: ________________________________

DECLARATION 2: PUBLICATIONS AND MANUSCRIPTS

1. Mofokeng, D.O., Adelabu, A.S., Adepoju, K. and Adam, E., 2019, July. *Spatio-temporal analysis of lightning distribution in Golden Gate Highlands National Park (GGHNP) using geospatial technology*. In IGARSS 2019-2019 IEEE International Geoscience and Remote Sensing Symposium (pp. 9898-9901). IEEE.
2. Mofokeng, DO., Olusola, A. & Adelabu, S. 2022. Development of Lightning Hazard Map for Fire Danger Assessment Over Mountainous Protected Area Using Geospatial Technology. Remote Sensing of African Mountains: Geospatial Tools Toward Sustainability. Springer
3. Mofokeng DO and Adelabu SA (2021). *Modelling and assessing distribution of anthropogenic factors in a protected area for fire danger assessment*. Journal of Geography & Natural Disaster .11: p358
4. Olga D. Mofokeng, Samuel A. Adelabu, Olufemi S. Duronoju and Efosa. A. Adagbasa. (under review), *Grass Curing- driven fire danger index in a protected mountainous grassland using fused MODIS and Sentinel-2 data*, (TRES-PAP-2023-1758) International Journal of Remote Sensing.
5. Olga D. Mofokeng, Samuel A. Adelabu and Colbert M. Jackson. (accepted). *Integrated grassland fire danger assessment of Golden Gate Highlands National Park using geospatial techniques* (Fire – 2824067). Fire (ISSN – 2571-6255)

ACKNOWLEDGEMENTS

I humbly present my gratitude to my family especially my grandmother Christinah Khakhu Molaudzi for unconditional love and valuable teachings of life including the value of education and almighty God, without whom my life would not have been successful.

I am extremely grateful to all those directly and indirectly assisted me to conduct this study and to bring out this thesis. Without whom this thesis would have never been realized. I am greatly indebted to my promoter supervisor Prof Samuel Adelabu whom made this thesis possible. I thank you for your attentively support and guidance from the initial to the final, which enabled me to complete this thesis. A special thank you to Dr Efosa Adagabasa for all your technical inputs and advice received from you facilitated the completion of this thesis. Dr Kayode Adepoju, I thank for advices and guidance.

I would like to thank different organizations in particular South African National Parks (SANParks) for granting permission to conduct this study on one of their protected areas (Golden Gate Highlands National Park). South African Weather Service (SAWS) for data provision. National Research Foundation (NRF-RISA) for financial support. The Rectorate Office for awarding me the top achiever bursary and the Centre for Graduate Support, without these financial supports this thesis would not be realized.

My deep thanks go to all staff members of GGHNP for providing valuable data, special thanks go in this regards to Dr. Ernest Daemane, Science Manager: Park Interface and Restoration Ecology.

Last but not least, warm thanks to all the personnel and postgraduate students of the Department of Geography, Qwaqwa Campus of the University of the Free State, no words may powerfully express the time we had together particularly during postgraduate seminars before the COVID pandemic.

DEDICATION

To my loving and caring family, my husband (Thatho Mofokeng), children (Langi, Oratile) grandchildren (Lesedi and Hloni) grandmother, late mother (Jeane Molaudzi), late daughter (Linde) and her daughters (Lerato)

TABLE OF CONTENTS

LIST OF TABLES

LIST OF FIGURES

CHAPTER 1
GENERAL INTRODUCTION

1.1 Grassland Ecosystem and Fire

Grasslands collectively constitute the largest ecosystem in the world, representing 40.5 (%) of the Earth's vegetation cover comprising of open grassland, grassy shrublands and savannah (Suttie *et al.*, 2005; Neary and Leonard, 2020). Grasslands are found mainly in tropical and subtropical Africa and Australia, and temperate and high mountain areas in China and Tibet and in the Middle East and North and South America. In contrast to forests, for which satellite-based products such as the Global Land Cover dataset clearly defines eight distinct types, there is a profusion of grassland definitions with no well-established categorization system (Leys *et al.*, 2018). Generally, grassland is defined as ground covered by vegetation dominated by grasses, with little or no tree cover. The United Nations Educational Scientific and Cultural Organization (UNESCO) defines grasslands as land covered with herbaceous plants with less than 10% tree and shrub cover, and wooded grasslands have 10 to 40% tree and shrub cover (Suttie *et al.*, 2005). In their effort of mapping global grassland, Dixon *et al.* (2014) proposed a systematic definition of grasslands as "a non-wetland type with at least 10% vegetation cover, dominated or co-dominated by graminids and forbs, and where the trees form a single-layer canopy with either less than 10% cover and 5 meter (m) height (temperate) or less than 40% cover and 8 m height (tropical)".

Grasslands are a key component of the Earth system, playing critical roles through the variety of ecosystem services they provide. These ecosystem services include livestock grazing areas, water supply and regulation, biodiversity reserves, tourism sites, recreation areas, religious sites, wild food sources, and natural medicine sources, carbon storage and climate mitigation, pollination and cultural services (O'Mara, 2012; Steiner *et al.*, 2020). Despite the importance of grasslands, their degradation is widespread and accelerating at a global rate of 49.25% (Gang *et al.*, 2014). Climate change and human activities are the underlying drivers of grassland degradation. Examples of such human activities are unsustainable agricultural practices and urban development, overgrazing, grassland reclamation, changes in land tenure and a lack of enforcement of land use rights (Bardgett *et al.*, 2021). Climate change has disturbed grassland ecosystems, especially through frequent, intense fires and droughts (Gang *et al.*, 2014).

Although the contribution of the factors of grassland degradation or change across the region and continent are varied and vigorously debated, fire stands out as one of the major factors that affect world grassy biomes (Jolly *et al.*, 2015). Fire is a widespread process in the earth system and is key in ecosystem composition and distribution (Bond and Keeley, 2005). Fire is an integral evolutional factor shaping and maintaining grassland ecological functioning and biodiversity in Afromontane grasslands (Everson and Everson, 2016). Roughly 80% of global fires occur in the grassland biome, mainly in Africa and Australia during dry winters but intensively in America, Asia, and Europe (Leys *et al.*, 2018). The significant role of fire in the continued existence of these grasslands is easily overlooked in light of the negative effect of fire in the context of global climate changes and concern for sustainable development. Negative impacts include loss on human lives and property, huge economic losses and marked increase of Greenhouse gases (GHG) emissions (Robinne *et al.*, 2018)**.** However, Keeley and Pausas (2019) postulated that fire *per se* is not an issue but rather perturbations in the fire regime due to anthropogenically driven global warming.

The extent of fire activity on the African continent has been well documented, with Africa dubbed the "fire continent" (Archibald *et al.*, 2009). In Southern Africa, the grassland biome covers an area of 360 589 km^2, one of the nine biomes accounting for roughly 28% of the terrestrial region (Carbutt *et al.*, 2011) and the most extensive grassland watershed (White *et al.*, 2000; Xiao *et al.*, 2002). However, grasslands are one of the most critically threatened southern African ecosystems (Rutherford and Westfall, 1994) and have relatively little international protection (Carbutt *et al.*, 2017)**.** In South Africa, the proportion of grassland increased from 3% at the end of 2000 to 4,6% at the end of 2020 (Statistics South Africa (StatisticsSA), 2021). Fires are part of the landscape of South Africa (Le Maitre *et al.*, 2014) and an intrusive disturbance in grasslands. Grasslands are fire-dependent and fire-prone, thus requiring burning at regular intervals to maintain the health of the ecosystems in such environments (van Wilgen *et al.*, 2012; Le Maitre *et al.*, 2014). Hence, the conservation of biodiversity and landscapes typically requires the judicious application of fire often by means of prescribe burning (van Wilgen *et al.*, 2012)

1.2 **Fire Danger Rating (FDR)**

In order to comprehend FDR, it is vital to make a distinction between these three concepts, namely: "Fire Risk", "Fire Danger" and "Fire Hazard". In its multidimensionality, fire risk has to be seen in accordance with different scientific concepts and disciplines. Nonetheless, following the fire science approach, the United States of America National Wildfire Coordinating Group (NWCG) refers 'fire hazard' as the potential fire behaviour associated with 'static' properties of fuel type, regardless of fuel moisture condition on a given day. 'Fire risk' is the chance of fire starting as determined by the presence of causative agents. The concept of fire danger is broader and describes the factors affecting the inception, spread and resistance to control, and subsequently fire damage (National Wildfire Coordinating Group (NWCG), 2006). In this line, Wang et al. (2013a) described fire danger rating as an assessment tool of both fixed and variable factors of the fire environment that determine the ease of ignition, rate of spread, difficulty to control and impact of wildland fires.

(Food and Agriculture Organization (FAO), 2005) defined fire danger rating as a component of fire management system that integrates the effects of selected fire danger factors into one or more qualitative or numerical indices. Taylor and Alexander (2006) referred fire danger rating as the process of systematically evaluating and integrating individual and combined effects of factors influencing fire potential. In disaster science, the concept ‘risk’ is commonly defined as the combination of the probability of an event and it has potential consequences (United Nations International Strategy for Disaster Risk Reduction (UNISDR), 2009). Based on this approach, Bachmann and Allgower (2001) defined fire risk as the probability of wildland fire occurring at a specified location and under specific circumstances together with its expected outcome as defined by its impacts on the objects it affects. Several researchers adopted this approach and defined fire risk as the combination of the physical probability that fire ignites and spreads and the expected damages caused by fire behaviour. They termed the former ‘fire danger’ and the latter ‘fire vulnerability’ (Chuvieco *et al.*, 2010; Thompson *et al.*, 2011; Chuvieco *et al.*, 2014; Eskandari and Chuvieco, 2015). Henceforth, this study also refers fire danger as the probability that a fire ignites and spreads.

Fire danger rating has its roots in Australia, Canada, the United States of America and Russia with research tracing back to the 1920s (de Groot *et al*., 2015). The primary role of FDRS is to enable fire managers to properly judge levels of preparedness needed and corresponding suppression resources required to keep wildfire losses or adverse impacts to a minimum (Taylor and Alexander, 2006). In a nutshell, the primary purpose of FDRS is preventing, controlling and mitigating wildfires. Willis *et al.* (2001) recommended that the system should consist of the following elements:

(a) The capacity to monitor, on a continuous basis, the conditions that would affect fire danger;

(b) The ability to delimit the regions that would be affected by high fire danger conditions;

(c) The ability to take relevant factors into account, using appropriate formulae and this will often require the use of the models which simulate the ease of ignition and potential fire behaviour;

(d) The ability to identify high fire danger, and listing of precautions that should be taken when the fire danger is predicted to be high; and

(e) The ability to communicate the fire danger ratings and necessary precautions effectively.

There are numerous national FDRSs currently in operational globally. Recently, Zacharakis and Tsihrintzis (2023a) reviewed 63 most used and well-performing fire danger rating systems from across the globe with the quest of creating an integrated forest fire danger system for Greece. The Russian Nesterov Flammability Index (NI), Keetch-Byram Drought Index (KBDI), Sharples’ Fuel

Moisture Index (SFMI), the Australian (McArthur) Forest Fire Danger Rating System (FFDI), Soil Dryness Index (SDI) were found to the top-performing indices for Greece. They concluded that the most complete systems, such as the Canadian Forest Fire Danger Rating System (CFFDRS) and the United States Fire Danger Ranger Rating System (NFRDRS) would improve their performance if the systems adapted better to local conditions.

1.3 Fire Behaviour in Grassland

According to Trollope *et al.* (2004), fire behaviour is the general term used to refer to the release of energy during combustion as described by the rate of spread of the fire front, fire intensity, flame characteristics and other related phenomena such as crowning, spotting, fire whirlwinds and fire storms. Food and Agricultural Organisation (FAO) (2007) refers to fire behaviour as how fuel ignites, flame develops, spreads, and exhibits other related phenomena as determined by the interaction of fuels, weather, and topography. Hence the analysis of fire behaviour requires the understanding of these factors that affect it. For any fire to start, three (3) conditions must be met, i.e., (a) sufficient flammable fuel in a continuous fuel bed to allow fires to spread; (b) warm, dry and windy weather conditions; and (c) a source of ignition (Stott, 2000; Archibald *et al.*, 2009; Kraaij and van Wilgen, 2014). However, Bradstock (2010) added a fourth element, i.e., dryness or drought, and called them "fire switches" (Clarke *et al.*, 2020). As explained by (Jin, 2010), at the local scale, fire occurrence needs three basic components, i.e., oxygen, fuel and heat, known as the fire triangle. At the landscape scale, fire behaviour is determined by three principle environmental factors, i.e., fuel, weather and topography. At the regional or global scale, fire is influenced by climate, vegetation and land use.

Fire behaviour reacts to a constantly changing confluence of these factors. However, this interaction complexity is further highlighted by the cause-effect of fire on the environment or two-way interaction termed "feedback" by Archibald *et al.* (2018). For instance, high temperature increases the probability of fire occurrence and intensity (Flannigan *et al.*, 2009). However, increased temperatures can negatively or positively affect vegetation productivity (Pausas and Ribeiro, 2013), resulting in shorter fire return periods, leading to less fuel and, thus, less intense fire (Archibald *et al.*, 2013). The following section describe the driving factors that influence the probability of fire danger and behaviour.

1.3.1 Grasses vegetation as a fuel

Fuel amount, type, continuity, structure, moisture and chemical composition are critical elements determining vegetation's susceptibility to fire. Unlike forest fires, grass fires have a high rate of spread and rapid combustion because of fine-sized fuel particles, well-aerated structure and high surface-to-volume ratio of grass leaf, its high thermal conductivity, and low density (Cheney *et al.*, 1998; Sullivan, 2010; Cruz *et al.*, 2022). Furthermore, grass is often fully exposed to sunlight, which speeds up drying (Sjöström and Granström, 2023). However, they can burn slowly when fuel is compacted. Fuel compaction refers to the placement of individual pieces of fuel in relation to one another (Trollope *et al.*, 2004).

Fuel load is regarded as one of the most important factors influencing fire behaviour because the total amount of heat energy available for release during fire is related to the quantity of fuel. Quantities of available fuel in grassland and shrublands range between 2-10 Mg ha^{-1} (Stavi, 2019), hence, grass fires have a relative lower intensity per unit area as compared to the forest fires (Trollope *et al.*, 2004). In contrast to (Cheney *et al.*, 1993; Cheney *et al.*, 1998), the study by (Cruz *et al.*, 2017) indicated that there is a statistically significant inverse relationship between grass fuel load and rate of fire spread. Nonetheless, both studies found that fuel load influences flame height and depth, fire intensity, and, thereby, the difficulty of suppression.

Fuel Moisture Content (FMC) is the mass of water contained within the vegetation (fuel) in relation to the dry mass; it is a critical factor in determining the fire behaviour as it affects ignition, combustion, the amount of available fuel, fire severity and spread as well as smoke generation and composition (Trollope *et al.*, 2004; Aguado *et al.*, 2007; Yebra *et al.*, 2013). Fuel Moisture Content (FMC) is distinguished into dead (DFMC) and live (LFMC). The LMFC is determined by the balance between water inputs through root system and the water outputs by plant evapotranspiration (Silva *et al.*, 2010). The DFMC is a function of fuel size, local atmospheric condition and precipitation (Nolan *et al.*, 2016).

Unlike the LFMC, which regulates water losses through stomatal closure and water uptake by roots, the DFMC is subject to sorption, precipitation and latent heat processes (Nieto *et al.*, 2010); thus it changes quickly. When dead fine fuel is introduced to an environment at constant temperature and relative humidity, the FMC either increases or decreases until it reaches a constant value called equilibrium moisture content (EMC) (Lopes *et al.*, 2014). The EMC fluctuates in response to changes in air temperature and relative humidity, and the lower the EMC value, the drier the fuel (Nolan *et al.*, 2016). Grasses experience substantial moisture changes in relatively short periods can reach their EMC within two (2) hour (Sullivan, 2010). Yebra *et al.* (2008) reported that FMC is the most critical factor affecting fire ignition. However, (McAllister and Weise, 2017) demonstrated that this alone cannot explain the ignition behaviour of the fuel.

Curing, the transition of fuel from live to dead, significantly influences the ability of fires to develop and spread in grasslands (Kidnie *et al.*, 2015). Sullivan (2010) defines grass curing as the process of dying and drying out that an annual grass plant undergoes during senescence following flowering and setting of seeds. The curing state of grassland is the percentage of dead material in the sward, a crucial factor of fire behaviour, largely determined by seasonality (Cheney and Sullivan, 2008; Anderson *et al.*, 2011; Cruz *et al.*, 2015). Kidnie *et al.* (2015) used NDVI-based FMC as a proxy for the estimation of grass curing, while (Martin *et al.*, 2015) compared various indices for grass curing estimation, and Global Vegetation Moisture Index (GVMI) based model outperformed the other indices.

1.3.2 Weather

The primary weather factors influencing fire behaviour are air temperature, relative humidity, wind speed and direction, precipitation and atmospheric stability. Air temperature and relative humidity strongly influence fuel moisture, thus determining how the fuel will burn (Kraaij and van Wilgen, 2014). Relative humidity is the ratio between the amount of water vapour in a parcel of air to the amount that would be present at saturation point, at the same temperature (Food and Agriculture Organization (FAO), 2005). A high relative humidity translates to a high percentage of moisture in the air (Trollope *et al.*, 2004). The highest relative humidity rate is in the morning and the lowest in the afternoon; hence fires are generally more difficult to control in afternoon, especially when relative humidity is below 30% (Trollope *et al.*, 2004).

Air temperature directly influences the fuel temperature and, consequently, the heat energy required to its ignition point. Moreover, its indirect impacts include relative humidity of the atmosphere and moisture losses by evaporation (Trollope *et al.*, 2002). Temperatures are cool at night and peak between 12:00 to 15:00. Simultaneously, fire intensity may rise, making it difficult to suppress (Trollope *et al.*, 2004). High temperatures increase plant evaporation, leading to decreased FMC and favouring the fire ignition (Chuvieco *et al.*, 2004b; Guo *et al.*, 2016a). The global studies by (Aldersley *et al.*, 2011; Forkel *et al.*, 2019) detected a substantial correlation between air temperature and fire behaviour. They showed that an increase in temperature would lead to an increase burnt area.

Wind significantly impacts fire behaviour due to the fanning effect (Ghodrat *et al.*, 2021). Hence, it is fundamentally involved in heat transfer between fuels, including pre-ignition heating and flame transfer (Nelson Jr and Adkins, 1988). Wind affects the convection column, which promotes preheating of unburnt fuels in front of the fire, carrying burning embers that have been lifted aloft by convection air and starting spot fires, moving moist air over fuels causing an increase in moisture content or moving moist away from fuels, causing them to dry out and providing continuous supply of oxygen to the fire (Trollope *et al.*, 2004; Moon *et al.*, 2013). Hence, wind is one of the main controlling factors that specifies fire direction, spread rate and configuration (Ghodrat *et al.*, 2021).

Fire burns in the direction of the prevailing wind, therefore, each side of the fire is described as “head”, “back or rear” and “flank”. The “head” is the most active downwind section of fire perimeter, characterized by high flames and intense fire behaviour. The “back or rear” is the section of fire burning into the wind with low flames and less intensity. The “flank” is the part of the fire spreading perpendicular to the wind, characterized by the alternating behaviour of the head and back of the fire (Sullivan, 2010). The effect of wind speed and slope on fire spread rate and flame length was examined by Weise and Biging (1994). The study concluded that the current formulation of an empirical wildland fire spread model was unfitting. As a result, Sharples *et al.* (2010) developed a range of techniques that predicted the rate of fire spread based on topographic slope and wind. The relationship between average open wind speed ($U_{10,}$ km^{h-1}) and average rate of fire spread (R, km^{h-1}) in conifer forests, eucalypt forests and shrubland fuel types was investigated by (Cruz and Alexander, 2019). The resulting rule of thumb revealed that the forward rate of spread of wildfire burning in forests and shrublands in relatively dry conditions is approximately 10% of the average 10-m open wind, where both values are expressed in the same units. However, the 10% rule of thumb was deemed not applicable to grasslands.

Precipitation in the form of rainfall, dew, fog or snow influences fuel moisture and quantity. Chen *et al.* (2017) show that the variability in precipitation associated with El Niño/ Southern Oscillation (El-ENSO) influences fuel availability in northern Australia and Africa. In grasslands, the knowledge of grass life cycle and the effects of drought on them is paramount for fire behaviour (Cheney and Sullivan, 2008). A wet spring and rain in early summer will produce abundant growth, while early summer with little or no rain will fast-track the senescence and drying of grasses.

African natural grasslands are dynamic, i.e., summer rainfall can be followed by long, dry winter periods; therefore, curing will produce above-average fuel, leading to grassfires (Trollope *et al.*, 2004). A strong relationship between rates of precipitation and fire activity was observed by (Van Wilgen *et al.*, 2000) in Kruger National Park, South Africa. Similarly, Archibald *et al.* (2009) presented that, in Africa, a high wet season followed by a long dry season supports high fire frequencies. Archibald *et al.* (2010) also ascertain the significant correlation between rainfall and fire activity over six (6) southern African protected areas.

1.3.3 Topographic features

The behaviour of fire becomes unpredictable in a rugged terrain. Particularly when and where topography interacts with local wind direction and microclimates, thereby affecting fuel type, loads and moisture content (Moreira *et al.*, 2011). The main topographic factors important to fire behaviour are slope, aspect, shape of the terrain (landform) and elevation. Slope, defined as the degree of inclination or steepness of an area, significantly influences the forward rate of spread of surface fire, by modifying the degree of preheating of the unburnt fuel immediately in front of the flames (Trollope *et al.*, 2004). Moreover, the process of heat convection can be enhanced by wind effects due to fire behaviour. Debano et al.1998 cited in (Bian *et al.*, 2013) as stronger fire induced winds behind the fire and other complex interactions between wind and terrain (Sharples, 2009). Argañaraz *et al.* (2015) found a significant correlation between increased fire frequency with steeper slopes.

Aspect, defined as the compass direction that slopes face, substantially impacts fuel drying rates and, subsequently, fire behaviour (Trollope *et al.*, 2004). Thus, it is proportional to the amount of solar radiation an area receives. In the Southern Hemisphere, northern aspects have more direct sunlight exposure, higher temperatures, receive less rain, and low humidity. In contrast, south-facing slopes have less direct sunlight exposure, and rainfall is significantly higher; thus, there is higher vegetation moisture content, and consequently, vegetation growth is more significant than in the north facing slopes (Trollope *et al.*, 2004). Additionally, eastern aspects tend to receive more direct solar radiation during the morning hours and less during the late afternoon as compared to western aspects (Adab *et al.*, 2013).

Elevation plays a crucial role in fire behaviour by influencing the amount and timing of precipitation. Elevation is also associated with temperature, moisture, air humidity and wind (Adab *et al.*, 2013). Therefore, it influences vegetation structure and fuel. Hernandez-Leal *et al.* (2006) revealed that humidity and temperature significantly influence fire at higher elevations. The opposite is true for fire at lower altitudes. Regarding the influence of elevation on fire ignitions, (Catry *et al.*, 2009) estimated higher probabilities of fire ignition at high altitudes because of a higher likelihood of lightning, whereas De Vasconcelos *et al.* (2001) found high fire ignition is associated with flat and lower elevated areas due high population density, proximity to road or urban interfaces.

1.3.4 Soil properties

Soil is vital in supporting a healthy and functioning ecosystem by providing a medium for vegetation growth, cycling nutrients, and filtering water through systems (Erickson and White, 2008; Strydom *et al.*, 2019). Although the significance of soil properties such as soil moisture conditions for fire behaviour is not a novel discovery, recent research advanced the understanding of how soil influences fire occurrence. Prominent fire danger rating systems in Australia, Canada and the United States of America have been using moisture indices (moisture codes: Fine Fuel Moisture Code (FFMC), Duff Moisture Code (DMC), Drought Code (DC)) to represent the moisture of surface organic layers (Wotton, 2009). The well-known Keetch-Byram Drought Index (KBDI) was designed to indicate the moisture deficit in the top 760 - 890 mm for soils with fine textures and at greater depth for coarse-textured soils (Keetch and Byram, 1968).

In contrast with the effect of fire on soil, the soil influence on fire is gaining traction in fire science. The influence of soil on fire ignition and spread is based on the soil-vegetation-atmosphere relation, Zhao *et al.* (2022) demonstrated two processes whereby soil moisture influences fuel moisture content for fire danger, namely (i) vapour flux from the soil, through the influence on local air humidity and

(ii) capillary flow from the soil. Recently, Krueger *et al.* (2022) reviewed how researchers revealed the influence of soil moisture on fire occurrence and behaviour. In addition, the influence of soil hydraulic properties such as infiltration, saturated hydraulic conductivity, soil water retention and available water capacity on fire occurrence and behaviour has been studied. Krueger *et al.* (2015) demonstrated that large fires in Oklahoma, USA, occurred exclusively when Fraction of Available Water Capacity (FAW) was extremely low. (Sharma *et al.*, 2020) have shown the relationship between FAW and the herbaceous vegetation moisture content and curing rate in grassland. Archibald *et al.* (2009) used the percentage of sand in the soil as the indicator of soil fertility in determining the fuel load for fire danger in southern Africa. Mathu (2020) examined how soil texture affects wildfire occurrence and behaviour in the Netherlands. The study revealed that more than 80% of fires occurred on sandy soils.

1.3.5 Sources of ignition

No matter how dry the weather conditions and the vegetation flammability, an agent or heat source to provoke or spark fire is essential. Spatial and temporal variation in ignition probability have been established, with varying patterns observed based on the type of ignition sources being examined (De Vasconcelos *et al.*, 2001; Genton *et al.*, 2006; Archibald *et al.*, 2009; Massada *et al.*, 2012; Vacchiano *et al.*, 2018; Clarke *et al.*, 2019; Martín *et al.*, 2019). Camia *et al.* (2013) reviewed all fire causes across European Union (EU) countries and established a harmonized classification scheme. Ganteaume and Syphard (2018) comprehensively explained wildfire sources of ignition. Typically, to understand fire's origins better, known ignition sources are categorized into two groups, i.e., natural or anthropogenic/human–induced ignitions.

Ignitions caused by humans may be either indirect or unintentional (accidental), direct and unintentional (negligence), direct and intentional (voluntary). Human-induced ignitions are associated with human presence and activities such as proximity to roads, railway lines or housing density, land use and land cover (LULC) change (Martínez *et al.*, 2009; Clarke *et al.*, 2019; Martín *et al.*, 2019). Researchers have also revealed the most important characterization of human ignitions in that the number of ignition sources can increase without a concomitant increase in the area burnt (Archibald *et al.*, 2009; Syphard and Keeley, 2016) in particular population/human density (Archibald *et al.*, 2012). Guyette *et al.* (2002) demonstrated the positive non-linear relationship between the percentage of area burnt and human density. In theory, low population densities should be associated with fewer ignitions. However, Archibald *et al.* (2009) found that lower population densities did not reduce burnt area.

Natural Ignitions, described as any fire caused by natural origin without human involvement, include lightning, volcanism, gas emission and meteorite strikes (Ganteaume and Syphard, 2018).

Lightning strikes are the primary source of natural ignition. Most natural-induced fires are started by dry lightning, where little or no rain accompanies a stormy weather disturbance (Ganteaume and Syphard, 2018). For instance, the Elandskraal fire in Western Cape, South Africa, was caused by the positive lightning observed on 22 March 2017 (Frost *et al.*, 2018).

Despite being less frequent than human-caused fires, lightning-caused fires may result in extensively large areas burnt in some parts of the globe. (Stocks *et al.*, 2002; Cha *et al.*, 2017) showed that 72% of Canadian fires were lightning-induced, accounting for 85% of the total area burnt. Lightning has been parameterized as a driving factor of fire behaviour or danger globally (Archibald *et al.*, 2009; Chuvieco *et al.*, 2010; Chuvieco *et al.*, 2014; Eskandari and Chuvieco, 2015; Huang *et al.*, 2015). Lightning was found to be the least important predictor by (Archibald *et al.*, 2009). Therefore, human and natural ignitions have distinctive spatial and temporal patterns worldwide, which can be readily quantified using human and biophysical explanatory variables (Massada *et al.*, 2012; Martín *et al.*, 2019). However, Massada *et al.* (2012) distinguished two goals of ignition modelling: (a) explanatory modelling to test hypotheses about the role that different factors play in causing ignitions, and (b) predictive modelling to identify those areas that are most prone to ignitions and where fire prevention or fuel reduction can be targeted.

1.4 Remote Sensing and Geographic Information System (GIS) techniques for Fire Danger Assessment

The role of RS in fire danger assessment is mainly focused on generating the required input variables (Chuvieco, 2005). For instance, indicators of weather conditions, such as land surface temperature, can be generated from the thermal bands of satellite imagery (Li *et al.*, 2013). Notably, numerous studies, if not all have based their fire danger assessment on fire environmental factors (Chuvieco and Congalton, 1989; Adab *et al.*, 2013; Bian *et al.*, 2013; Wang *et al.*, 2013; Banu *et al.*, 2014; Chuvieco *et al.*, 2014; Chowdhury and Hassan, 2015; Eskandari and Chuvieco, 2015; Yu *et al.*, 2017; Van Dijk *et al.*, 2019). Wang *et al.* (2013) assessed fire danger in Northern China using an analytical hierarchy process based on five environmental factors, including land surface temperature, vegetation curing, equivalent water thickness, vegetation continuity degree and fuel weight derived from MODIS satellite. (Bian *et al.*, 2013) developed a grassland fire danger index for Mongolia grasslands. They integrated fuel, fire climate, accessibility, human social factors, and topography data into the MLR model in which NDVI was used as an indicator for fuel continuity.

Remote Sensing offers a method for assessing vegetation or fuel conditions and monitoring changes across vast geographic extent, thus a helpful tool for supporting the development of fire danger indices. Some researchers, e.g., (Jurdao *et al.*, 2012; Arganaraz *et al.*, 2016; Luo *et al.*, 2019) have used RS techniques to measure the spatio-temporal variation of FMC for fire danger assessment. Jurdao *et al.* (2012) developed Ignition Probability (IP) index converted from LFMC measurement using NOAA-AVHRR imagery and fire occurrences from MOD14. They have compared several multivariate linear regression techniques. Logistic Regression (LR) was found to be the most advantageous. The researchers concluded that the LFMC from one week before the fire detection was the most influential variable in the statistical analysis.

Arganaraz *et al.* (2016) constructed a linear model between LFMC and spectral indices derived from MODIS imagery. The study linked LFMC to the fire risk and generated a fire danger map in the Chaco Serrano Sub-region of Argentina. (Yebra *et al.*, 2018; Luo *et al.*, 2019) applied a PROSAIL model for LFMC inversion from MODIS imagery. Yebra *et al.* (2018) constructed a physical-based retrieval model to estimate FMC from MODIS data using radiative transfer mode (RTM) inversion. Logistic regression models were developed to generate a flammability index for Australia. Similarly, Luo *et al.* (2019) demonstrated the relationship between the pre-fire RTM- based LFMC and fire events in China. Recently, an extensive global database of LFMC measurement has been developed by Yebra *et al.* (2019) and can be useful for fire danger assessment.

Apart from LFMC, researchers utilized RS and GIS techniques to estimate the degree of curing (DOC) for fire danger assessment (Newnham *et al.*, 2010; Newnham *et al.*, 2011; Turner *et al.*, 2011; Martin *et al.*, 2015; Chaivaranont *et al.*, 2018; Li, 2020). Newnham *et al.* (2011) assessed Relative Greenness (RG) for predicting DOC in grasslands in Australia from MODIS data. The results revealed that RG explained a greater proportion of the variance and provided a more accurate estimate of DOC than linear regression against NDVI. Martin *et al.* (2015) compared the performance of NDVI, EVI, SAVI, GVMI, and $NDWI_6$ from MODIS imagery on the MLR model for estimating DOC. The combination of the NDVI and GVMI performed best. Using similar methods, Chaivaranont *et al.* (2018) also utilized MODIS data; however, they replaced GVMI with vegetation optical depth (VOD). Results suggested that VOD-based DOC estimation can reasonably reproduce ground-based observation. (Li, 2020) combined NDVI and GVMI extracted from Landsat 8 data due to its high spatial resolution, to calculate DOC; the study reported precisions comparable to ground measurements.

Several studies have provided evidence of the potential benefits of moisture in fire danger assessment. Pellizzaro *et al.* (2007) reported that soil moisture was more highly correlated with Live FMC than weather variables or drought indices in shallow-rooted perennial shrubs. Levi and Bestelmeyer (2016) demonstrated that soil-landscape properties have significantly influenced the spatial distribution of fire in desert grassland region of the south-western USA, with soil available water holding capacity (AWHC) explain more variability of fire ignition in the Madrean Archipelago regions as compared to Chihuanhuan desert. Similarly, Krueger *et al.* (2016) found that soil moisture is significantly related to wildfire probability during growing and dormant seasons. Qi *et al.* (2012) found that in situ soil moisture measurements were strongly correlated with LFMC in shrubs than several remote sensing proxies.

Although in situ measurement methods yield a high level of accuracy, they are time-consuming, costly, often require destructive sampling and are labour intensive. These traditional methods are usually point-based measurements that suffer estimation errors from data interpolation techniques and do not have uniform and extensive spatial coverage of study areas (Leblon et al., 2012; Wang et al., 2013). Alternatively, remote sensing methods have been employed to address the spatial interpolation limitation associated with conventional methods with the obvious advantage of spatial and regular temporal coverages and non-destructive way for vegetation studies at remote, inaccessible mountainous areas (Arganaraz *et al.*, 2016).

Optical, thermal infrared, and microwave remote sensing techniques can generally measure near-surface soil moisture content (Walker, 1999). The remotely sensed soil moisture of both optical and thermal techniques is considered vulnerable to contamination by weather conditions and many other noise sources, and their precision can hardly satisfy the needs of operational or practical applications. However, aerosol data can be used for atmospheric correction (Chaivaranont *et al.*, 2018). In contrast, numerous studies have shown that microwave passive and active remotely sensed soil moisture has good potential for operational applications in different fields. Microwave satellites, including Advanced Scatterometer (ASCAT) on the Meteorological Operational Satellite (METOP), Advanced Microwave Scanning Radiometer for Earth Observing System (AMSR-E), National Aeronautics and Space Administration (NASA) Soil Moisture Active Passive (SMAP) and Microwave Imaging Radiometer with Aperture Synthesis (MIRAS) on the Soil Moisture and Ocean Salinity (SMOS) and are used to acquire near-surface soil moisture data. Several studies, e.g., Bartsch *et al.* (2009); (Chaparro *et al.*, 2016; Holgate *et al.*, 2016; Holgate *et al.*, 2017) have opened a path forward in applying microwave-derived soil moisture products in fire studies. Therefore, these studies verify that fire danger assessment informed by remotely sensed soil moisture may improve existing techniques because soil moisture directly influences the amount and the rate of water that can be supplied to growing vegetation. The increasing availability of soil moisture data presents an opportunity for its use in fire danger assessment but research regarding the influence of soil moisture on fire danger is scarce or limited, especially in grassland mountainous ecosystems.

1.5 Integrated Grassland fire danger assessment modelling

With the advance of geospatial technology, many previous researchers have used multi-criteria decision techniques or knowledge-based methods like analytic hierarchy process (AHP) to explore the correlations between fire drivers and fire occurrence and fire danger modelling in a protected area (Kumari and Pandey, 2020; Zhao *et al.*, 2021b; Maniatis *et al.*, 2022). Though these studies accurately delineated the fire danger area, these methods are subjective and lack uncertainty (Xie *et al.*, 2022). Building a physical model is mostly dependant on fire ignition, intensity and propagation mechanisms, which are more expensive and have a specific application scenario (Peng *et al.*, 2023). Therefore, statistical and machine learning are two dominant modelling techniques used for fire danger modelling. Statistical modelling assume the response data are generated by a specific stochastic model that involves other predictors (Phelps and Woolford, 2021). Most applied statistical approach include regression-type models. Si *et al.* (2022) and Zapata-Ríos *et al.* (2021) used logistic regression and to predict fire danger in plateau mountainous Lijiang area, northwest of Yunnan province in China and mountainous area of the Andes in Ecuador respectively. They prediction power of the LR model was 86,9% and 84% respectively. To capture the non-stationary pattern of grassfire drivers, geographical weighted logistic regression model has been tested (Chuvieco *et al.*, 2012; Rodrigues *et al.*, 2018; Cao *et al.*, 2020; Chang *et al.*, 2023). Weight of Evidence (WoE) (Hong *et al.*, 2017; Jaafari *et al.*, 2017; Ye *et al.*, 2017; de Santana *et al.*, 2021; Pradeep *et al.*, 2022) modelling techniques have been applied for fire danger prediction as they adept in explaining the statistical relationship between drivers and fire danger and predictive fire danger likelihood in the form of probability. Frequency ratio (FR) have been tested (Romero-Calcerrada *et al.*, 2008)

The application of machine learning (MP) algorithms to construct the fire danger models mostly focusing on comparative evaluation of different ML methods has drawn increasing attention from the fire science community (Jain *et al.*, 2020; Bot and Borges, 2022; Chicas and Østergaard Nielsen, 2022; Alkhatib *et al.*, 2023). A scoping review by Jain *et al.* (2020) covering 300 publications revealed random forest (RF), artificial neural networks (ANN), decision tree (DT), support vector machines (SVM), maximum entropy (MaxEnt) and genetic algorithms (GA) as the most common used ML techniques in fire management. Chicas and Østergaard Nielsen (2022) conducted a literature review covering fire susceptibility or danger modelling for the period of 2001-2021. The study identified RF, LR and AHP as the models implemented most and out of these three, RF had the highest reported average accuracy, however, bayesian belief network (BBN) and multiple linear regression as the highest and lowest accuracy rate respectively. Slope, elevation and distance from road were reported as the most used factors and soil moisture, shrub and livestock density as the least used driving factors for building fire danger models. Iran, India and Vietnam were revealed as the countries where most researches were conducted. Most researchers compared different methods in quest for the best-fitted fire danger modelling particularly in protected areas (Tien Bui *et al.*, 2016; Pham *et al.*, 2020; Chicas *et al.*, 2022). Appendix 1 show some exemplary studies that have compared statistical and ML methods in fire danger or susceptibility modelling. It is evident that models vary in their capacity to predict the fire occurrence probability and fire danger mapping. Furthermore, no study has proven that a particular method is applicable to all areas in different environment (Pham *et al.*, 2020). Most of the studies are based on lowland forest environment and can be misrepresentative when applied in rugged terrain grassland.

1.6 Problem Statement

Natural disturbances such as fire are principal management tool in Afromontane grassland ecosystem in achieving its conservation and societal goals (Everson and Everson, 2016). However, fire gradually negatively impact the resources for human well-being and functions of the ecosystem. Fire "per se" is not an enemy but the perturbations in fire regimes (Keeley and Pausas, 2019). Global climate change, land use changes, population growth and introduction of species are reshaping the fire regimes, climate change as the primary driver of fire regime changes as it changes fire activity by increasing drought frequency, lengthening fire season and frequency of fire season in different regions of the world (Jolly *et al.*, 2015; Bowman *et al.*, 2017; Ruffault *et al.*, 2018). The resulting fire from fire regime can have a large range of destructive ecological and social impact that may reverse or delay progress towards United Nation Sustainable Development Goals (SDG) (Martin, 2019). For instance, fire burning release particulates and volatile gases and this emission of carbon dioxide, methane, nitrous oxide and aerosols have short and long-term effects on global warming, i.e. linked to SDG 13 (climate change); on air quality and affect human health (SDG 3: good health and well-being). Global warming affect precipitation patterns and thence affect food production (SDG 2) and exacerbate poverty (SDG1). Fire promotes desertification and land degradation by reducing soil fertility and exacerbate soil erosion by wind and water which is also linked to SDG 15 (life on land). Fire can directly destroy human lives, livestock, property, and infrastructure and can alter hydrology and reduce water quality(Food and Agricultural Organisation (FAO), 2007).

For protected areas (PAs), Pereira *et al.* (2012) dubbed the application of fire in PAs as "paradoxical or conundrum" Likewise, South African National Parks (SANParks) have applied a range of interventions to achieve its mandatory goals, including the use of fire as a management tool (Van Wilgen *et al.*, 2011). Steered by its ecological goals (conservation of biodiversity and landscapes), fires in PAs, including the GGHNP are not regarded as a "foe "as in non-PAs but a crucial ecological process that can be manipulated to achieve a particular goal. In this stance, firstly, fire is applied at a particular frequency, season or intensity, or fire is intentionally avoided or supposed to influence identified aspects of vegetation structure and composition directly. Secondly, fire is applied to promote a diversity of fire patterns across the landscape (mosaic of fire return periods, seasons, intensities and sizes) (Nieman *et al.*, 2021). Guided by societal goals, the use of fire in PAs has to contend with its effects within the landscape. For instance, unplanned or natural fires that would otherwise be beneficial or even necessary for maintain healthy ecosystems may pose serious threats and have to be suppressed of contained for safety reasons (Van Wilgen *et al.*, 2011).

Considering the causes-effects of fire on climate change, the degradation of grassland and along with the projections that future climate conditions will lead to extreme fire event, it is, therefore, imperative to develop an integrated fire management strategy to prevent and mitigate the negative impacts of fire. However, implementation of integrated fire management system is complex and remain incomplete due to the limited knowledge on the spatial and temporal dimension of fire (Chuvieco *et al.*, 2010; van Wilgen *et al.*, 2012; Müller *et al.*, 2020). Most applied fire danger rating systems worldwide are based on meteorological data measured from sparsely distributed weather stations and often do not consider natural or anthropogenic activities that potential triggers the fire (Müller *et al.*, 2020). When human activities are incorporated in fire danger model , the temporal dimensions of fire-triggers factors are frequently overlooked implying that no temporal variation in its influence as fire triggers (Martín *et al.*, 2019). Lightning strikes activities lack quantitative spatial patterns of flash density (Amrhein, 2017).

Zacharakis and Tsihrintzis (2023a) proved that environment-based fire danger rating systems and indices are inadequate and outdated in terms of accuracy and validating fire danger estimation. The inaccuracy of most of fire danger systems and models is attributed to the fact that most of countries including South Africa, the fire danger is at national level at the spatial resolution not less than 1km^2. The spatial resolution might be insufficient for mountainous landscape owing to topographic effects on temperature, precipitation, wind and other meteorology variables (Sharples, 2009) and thence inaccurate approximation of fuel conditions (Müller *et al.*, 2020). Fire danger assessment process takes into consideration multitude factors. In that these factors act in concert to produce fire. However, understanding all these interrelationship complexities is not always apparent, yet is the fundamental for sustainable management of grassland ecosystem in changing world. The influence of fire drivers varies in time and space (Archibald *et al.*, 2013; Pausas and Ribeiro, 2013; Pausas and Keeley, 2021). However, the degree of influence of the complex suite of biophysical and human drivers of fire remains controversial and incompletely understood (Bowman *et al.*, 2011b; Clarke *et al.*, 2020).

With the advent of geospatial technology, RS and GIS based methods and techniques have been developed to assess the influence of fire drivers to aid fire danger modelling and mapping (knowledge–based, statistical, machine learning and simulation models) globally. No single best model can be effectively applied in all fire-prone landscape (Jaafari *et al.*, 2019), hence the accuracy of prediction and the competency of models are still debated (Pourtaghi *et al.*, 2016; Zhang *et al.*, 2019; Achu *et al.*, 2021). Chicas and Østergaard Nielsen (2022) observed fire-prone areas where this type of research is not being implemented, especially in Africa and Latin America. Furthermore, previous studies focused more on forest fires—grassland fires have been relatively overlooked. Montane grasslands have long been known to be highly sensitive to the direct impact of climatic warming and drying, so fires in these ecosystems are expected to increase globally (Abatzoglou *et al.*, 2019). The South African montane grasslands are no exception. Fire regimes in Afromontane grassland ecosystems are not well studied, and the conditions under which fires occur in these landscapes still need to be fully understood.

1.7 Aim of the study

The aim of the study was to develop an integrated grassland fire assessment model utilizing geospatial techniques to serve as a fire management tool in the protected mountainous Golden Gate Highlands National Park (GGHNP).

1.8 Objectives of the study

The objectives of the study were to:

1. develop Lightning Hazard Map (LHM) of GGHNP from lightning strike activities using statistical spatial techniques;
2. use machine learning technique to assess and model the temporal dimension of anthropogenic activities that trigger fire danger for GGHNP;
3. estimate and asses the spatial and temporal patterns of degree of curing (DoC) for fire danger assessment in GGHNP using data fusion techniques; and
4. explore statistical and machine learning fire danger modelling techniques and develop an integrated grassland fire danger model for GGHNP.

1.9 Thesis Outline

In order to achieve the objectives of this study, the thesis is organized as a compilation of four (4) research articles that have been submitted to peer reviewed conferences, book chapter and journals. Out of these, two have been published, and other two accepted and under review respectively. Each chapter has been written as a stand-alone article that can simply be read independently from the rest of the thesis. However, reference to other chapters are made. Although the background literature review of the thesis presented chapter 1, there are still minimum repetitions and similarities in the introduction and methods sections of different chapters. The thesis comprises of six chapters as follows:

Chapter 1 serves as the introduction to study, provides a general background literature about the driving factors of fire occurrence and behaviour, role of the geospatial technology in data acquisition for fire danger assessment and fire danger rating systems as well as the fire danger modelling techniques. The study arguments and objectives are also presented in this chapter. Following on from this introductory chapter 1, the description of the study area is detailed in chapter 2, describing the physical and climatic characteristics, general vegetation and soils, the socio-economic and cultural features, and finally, significance of protected areas on achieving sustainable development goals (SDGs) in the context of GGHNP and a brief history of the GGHNP fire management plan.

Chapter 3 provides for the natural-induced fire ignitions part of fire danger by examined the use of statistical spatial analytic techniques such as Global Moran I, Spatial Autocorrelation and Hotspot analysis to assess the spatio-temporal patterns of the lightning strikes activity of the GGHNP. The methods and tools used (i.e. inverse diverse weighted (IDW) interpolation and Zonal statistics) to develop Lightning Hazard Map of the GGHNP were also described in this chapter.

Chapter 4 presents the human-induced source of fire ignition, describing the two mostly used anthropogenic factors (Roads and tourist infrastructures) and modelling approach used (MaxEnt modelling) to determine the temporal variation and influence of each factor on fire occurrence. This includes explanation of the of the data, methods and tools used to create temporal scenarios of the model (dependant variables) and preparations of the independent variables of the model (multi-ring buffer zone method).

Chapter 5 provides information on the data fusion method (Index-then-Blend, (IB) method) applied to improve the spatial resolution data (MODIS and Sentinel-2) used to estimate grass curing indices (GCIs). The spatio temporal patterns of degree of curing (DOC), and methods to develop GCI based fire danger map of the study area were presented in this chapter.

Chapter 6 uses the lightning hazard map (LHM) from chapter 3, anthropogenic factors (roads and tourist's infrastructure) from chapter 4, and downscaling method from chapter 5 to measure fuel conditions (GCI, global vegetation moisture index (GVMI), vegetation condition index (VCI), and bare soil index (BSI)). And other driving factors of fire danger (weather, topographic, proximity to river and soil properties as the driving factors (fire switches) of the study area. Three statistical (weight of evidence (WoE), logistic regression (LR) and frequency ratio (FR) and three conventional machine learning (random forest (RF), decision tree (DT) and support vector machine (SVM) were explored to evaluate the degree of relationship between these driving factors and fire occurrence as well as to the predict the probability of fire occurrence and fire danger modelling and fire danger mapping of the study area.

Finally, chapter 7 summarises the findings from chapter 3 to 6 in the context of global climate change. Limitations of the study and future research recommendations on the fire danger modelling and mapping are emphasized. The reference list, the GEE/computer codes developed and some of the results are provided at the end of the thesis as appendices.

CHAPTER 2
DESCRIPTION OF THE STUDY AREA

2.1 Introduction

Protected Area (PA) defines geographical space recognized, dedicated and managed through legal or other effective means to achieve the long-term conservation of nature with associated services and cultural values. Due to its topography (1892–2829 m above sea level), the Golden Gate Highlands National Park (GGHNP) was proclaimed as a national park in 1963. The GGHNP covers 32 690 ha. and is situated in the foothills of the Drakensberg (Maloti) Mountains, (28°27'S – 28°37'S and 28°33' E - 28°42'E) in the eastern Free State Province of South Africa between the town of Clarens and Phuthaditjhaba on the provincial road that meanders through the middle of the park as shown in Figure 2.1. However, the road increases the probability of anthropogenic - induced fire ignition with the park ((Martín *et al.*, 2019). The Caledon River delineates the southern boundary of the park and the border between Free State and Lesotho (South African National Parks (SANParks), 2020). The GGHNP is the tourism hub of the province owing to its great scenery. Figure 2.2 depicts the tourist's infrastructure available within the park. The presence of humans may increase the probability of of human-caused fire ignitions, however, they may decrease the spreading of fire (Archibald *et al.*, 2009).

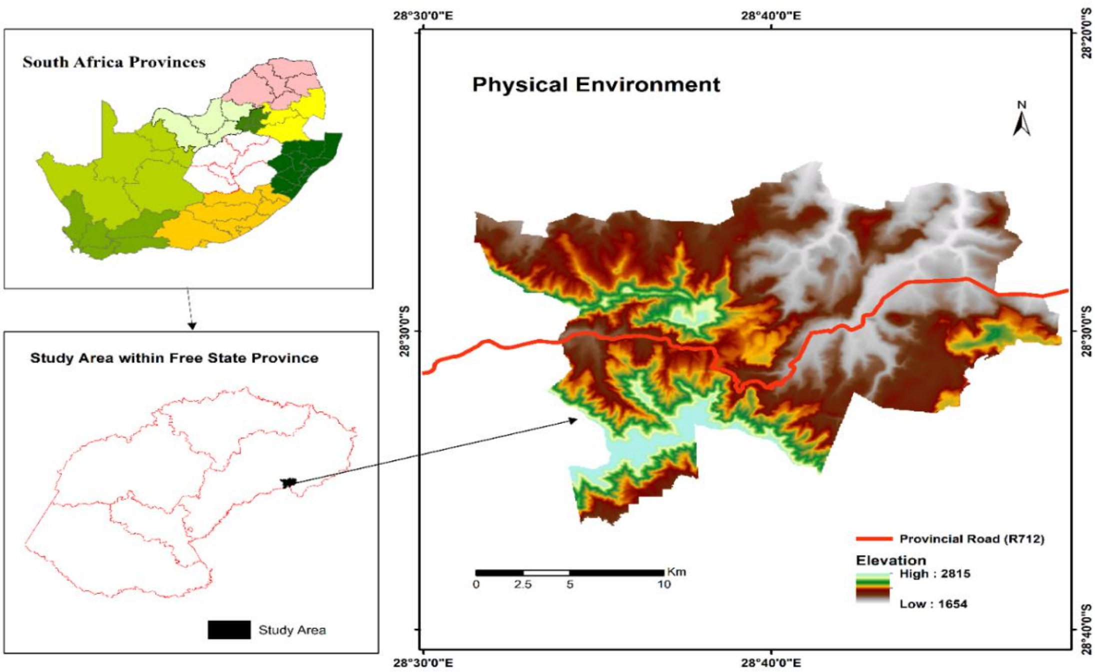

Figure 2.1: Spatial location of GGHNP in the Free State Province of South Africa

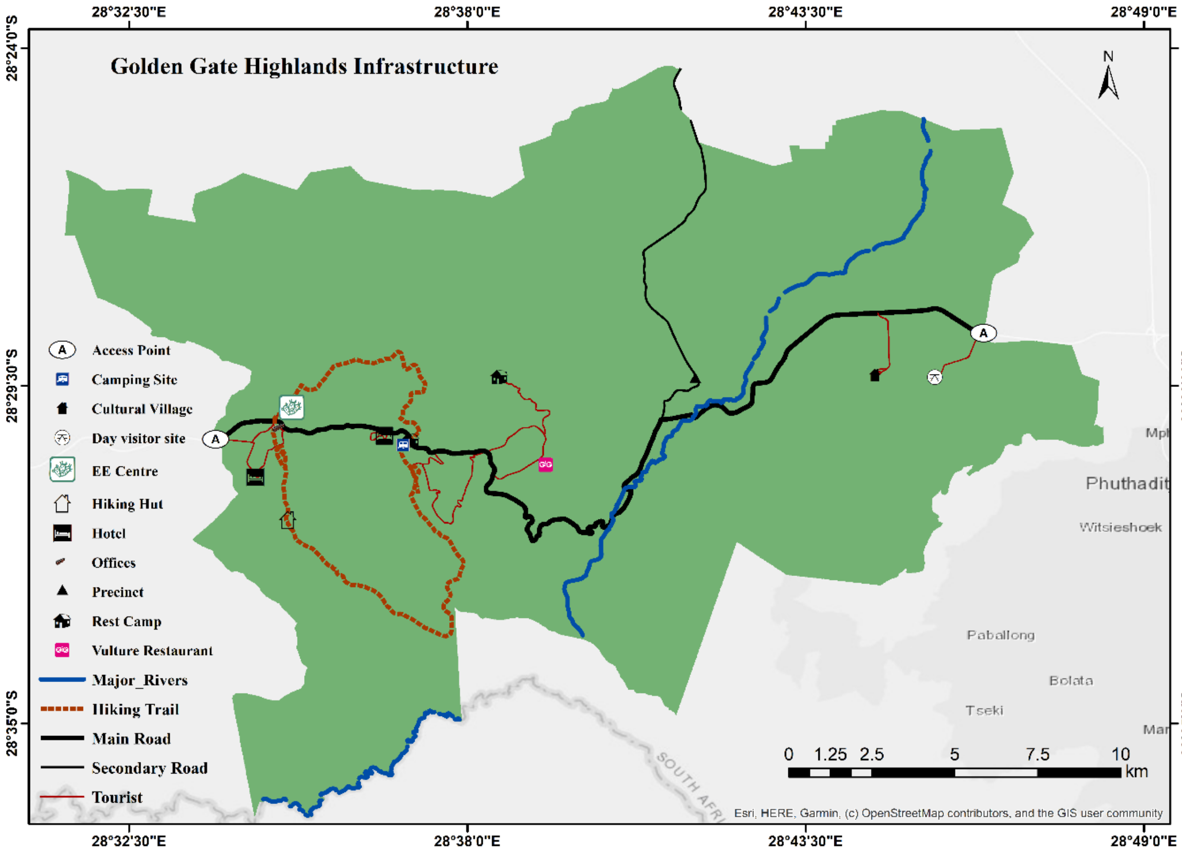

Figure 2.2: Road networks, facilities and other infrastructure within the GGHNP

Currently, in SA, 13.2% of the terrestrial area, including land (9.2%) and freshwater (4%) is protected (United Nations Enviroment Program - World Conservation Monitoring Centre (UNEP-WCMC), 2021). Grassland biome, on which the study area is categorized is the second lowest proportion biome protected within the country (Statistics South Africa (StatisticsSA), 2021). The primary purpose of PAs is to conserve biodiversity, i.e., protecting ecosystem types, species and genetic diversity. The GGHNP was established to protect the pristine sandstone formation, and the montane and Afro-Alpine grassland biome (South African National Parks (SANParks), 2020). Protected areas (PAs) are not only essential for the conservation of biodiversity but also regarded as natural solutions to global challenges such as climate change, land degradation , food and water security, health and well-being (International Union for Conservation of Nature (IUCN), 2020). The contribution of PAs in achieving Sustainable Development Goals (SDG(s)) is well documented (Dudley *et al.*, 2017; International Union for Conservation of Nature (IUCN), 2020; MacKinnon *et al.*, 2020). The most prominent links are SDG 14 and SDG 15, life below water and life on land, respectively. Well-managed PAs may help people to cope with climate change (Dudley *et al.*, 2009).

Other SDGs provide opportunities to underscore the importance of PAs to human welfare and well-being. For instance, SDG 1: The PAs generate monies to help support livelihoods and address poverty reduction via job creation. More than 20 000 jobs have been created in the wildlife economy and conservation-related industries (Driver *et al.*, 2019). The GGHNP has 203 permanent employees and has created over 1400 temporary jobs through its Extended Public Works Programme (EPWP). On SDG 3, PAs provide a variety of health benefits, by maintaining vital supplies of both local and national medicine. Moreover, Stolton and Dudley (2010) regarded PAs as “green gyms” and places for the treatment of people with mental health and addiction issues. Pertaining to SDG 16, PAs may contribute to maintaining peaceful societies and mitigating conflict risk (Dudley *et al.*, 2017). The utilisation of “Park for Peace” Initiatives, the Cordillera del Cóndor Transboundary PA was declared as a part of the resolution of a boundary dispute between Peru and Ecuador. It showed how communities can come together and build understanding and cooperation after the cessation of conflicts (Sandwith and Besançon, 2010).

In addition to “Park for Peace”, initiatives like “Transboundary Conservation were introduced, for example the Maloti Drakensberg Transfontier Conservation and Development Area was declared with the aim of addressing conservation and community development issue in the Maloti-Drakensberg Mountain; a 300 km long alpine and montane zone along the southern, eastern and northern of the landlocked mountain Kingdom of Lesotho and the Republic of South (Sandwith and Besançon, 2010). Thus, GGHNP form the part of this Transboundary conservation and development area.

2.2 **The brief history of fire management in GGHNP**

In contrast with Kruger National Park (KNP), which has a long and well-documented history of fire management, the first prescribed burning in GGHNP was introduced in 1978 with regular burning in September (just after the good summer rainfall) aiming to rotate the wildlife and to prevent homogenous use of the veld as well as to control game movement with the park (South African National Parks, 2013; Daemane *et al.*, 2018.). In the 1980s, the fire policy was adjusted based on agricultural practices and fire was used to address issues related to overgrazing and accumulation of moribund material. Burning was applied on a rotational basis, and the timing of fire burning was also adjusted to include burning before the first rainfall. Fire breaks, as required by the South African Fire legislation (Forest Act,1984 (Act No. 122 of 1984), were also introduced between May to July at 07 - 50m wide (Daemane *et al.*, 2018.).

Subsequently, the abandonment of the fire programme was based on the study of van der Walt and van Zyl, (Kay *et al.*, 1993), which recommended that the park (GGHNP) be divided in 16 burning compartments. They recommended that the fire regime should be triennial burns in the *Festuca caprina* and Alpine Grass veld, biennial early spring burn in areas which are higher than 1861 m in elevation, biennial early burn in areas lower than 1861 m (i.e. valleys) and annual early spring burn in areas called the Old lands. Guided by her study on the geomorphological effects of veld burning in the park (Bird, 1996) recommended that instead of formulating a rigid prescriptive fire policy, the burning should be guided by the fuel load. Thus, her recommendations included:

(a) Burning should apply to the areas where the build-up of fuel is such that it poses an unacceptable fire hazards,
(b) Blocks should be assessed at the beginning of the burn season to determine both the fuel load and erosion risk that the area poses;
(c) Prescribe or Controlled burns should be applied in the spring from late August to the beginning of October; and
(d) Rotation of fire-breaks burnt and burning should not be in spring.

The park fire policy has since been significantly evaluated, reviewed, and updated in 2006, 2011, and 2018. Fires in GGHNP like all SANParks are managed based on patch mosaic fire philosophy whereby fires are ignited at the selected localities and left to burn creating patch mosaic of burnt and unburnt patches. At this point, the study area is divided into five burning partitions based on the plant communities found within the park. Each burning partition has a certain fire regime to achieve ecological and/or management objectives (Daemane *et al.*, 2018).

The park has experienced burnt areas in the past. A fire severity assessment of the park was conducted by (Adagbasa *et al.*, 2018). The results revealed that in the year 2000, 30 704 ha burnt with low to high severity, 31 352.13 ha in 2005, 20 198 ha in 2013, and 30 009.33 in 2017. Only 1120.14 ha of the park was unburnt. This implies that the study area is very prone to fire, mainly occurring between May and November which coincides with the onset of dry season, and ends at the beginning of the rainy season (Adelabu *et al.*, 2020).

2.3 Ecological Description

Rutherford *et al.* (2006) classified the study area as a grassland biome, representing the Drakensberg Grassland Bioregion (Gd) and the Mesic Highland Grassland Bioregion (gd). According to Mucina and Rutherford (2006), the vegetation of the study area has been classified into five (5) types. The Mesic Highveld which includes (a) Eastern Free State Sandy Grassland (Gm4) and (b) Basotho Montane Shrubland (Gm5); The Drakensberg (c) Northern Drakensberg Highlands Grassland (Gd5), (d)Drankensberg-Amathole Afromontane Fynbos (Gd6), and (e) Lesotho Highlands Basalt Grassland (Gd8). The Gm4, Gm5, and Gd8 have a high conservation importance (Skowno *et al.*, 2019).

Figure 2.3. (a) shows the distribution of fire ecology types in the park based on the key plant communities of the GGHNP. *Protea* woodlands found in the park are *Protea caffra, P. subvestion and P. roupellia.* This *Protea* woodlands are characterized by a grass-dominated herbaceous understory such as *Pteridium aquilinum* (Daemane *et al.*, 2018). *Leucosidea* open woodland community is dominated by scrubland species such as *Leucosidea sericea, Buddleja salviifolia, Rhus pyroides, Clutia Pulchella and Rhamnus prinoides.* Grass species found in rocky highland grassland include *Festuca caprine, Themedea Triandra, Merxmuellera disticha and Xerophyta viscosa.* While lower lying mid-slope grassland consist of *Microchloa caffra, Eragrotis lehmanii, Rhus discolour and Monocymbium ceresiiforme.* Grass species such as *Aristida junciformis, Digitaria monodactyla, Heteropogon contortus, Melwilla natalensis, Adiatum capillus-veneris* are found at outcrop/middle plateau grassland. *E. curva, Helichrysum capense and Felicia filifolia* are grass species in old cultivated land. Plateau grassland communities include grass species such as *Cynodon dactylon, Hyparrhenia Hirta, E.capensis, E.racemos* and *Sporobolus africana*. Forest patches classified as Olinia Podocarpus Forest community include *Olinia emarginata, Podocarpus latisfolius, Kiggelaria africana, Halleria lucida, Cussonia paniculat,* and *Pittosporum viridiflorum.* Wetland /drainage vegetation found in the park are primary represented by *Phragmites communis, Cyperus marginata, Fuirena pubescens* and *Paspalum dilatatum* species (Kay *et al.*, 1993; Daemane *et al.*, 2018; South African National Parks (SANParks), 2020).

The park is home to a wide spectrum of faunal diversity, including 58 large and 52 small mammal species, 22 amphibians, 257 birds, roughly three (3) fish, 117 invertebrates and 20 reptile species (SANParks), 2020). According to SANParks (2020), the soil types of the park include shallow rocky soil (Glenrosa and Mispah), deep soil along lines (Oakleaf), well-developed sand soils (Hutton and Clovelly) and Clayey structure soil (Milkwood and Tambakulu).

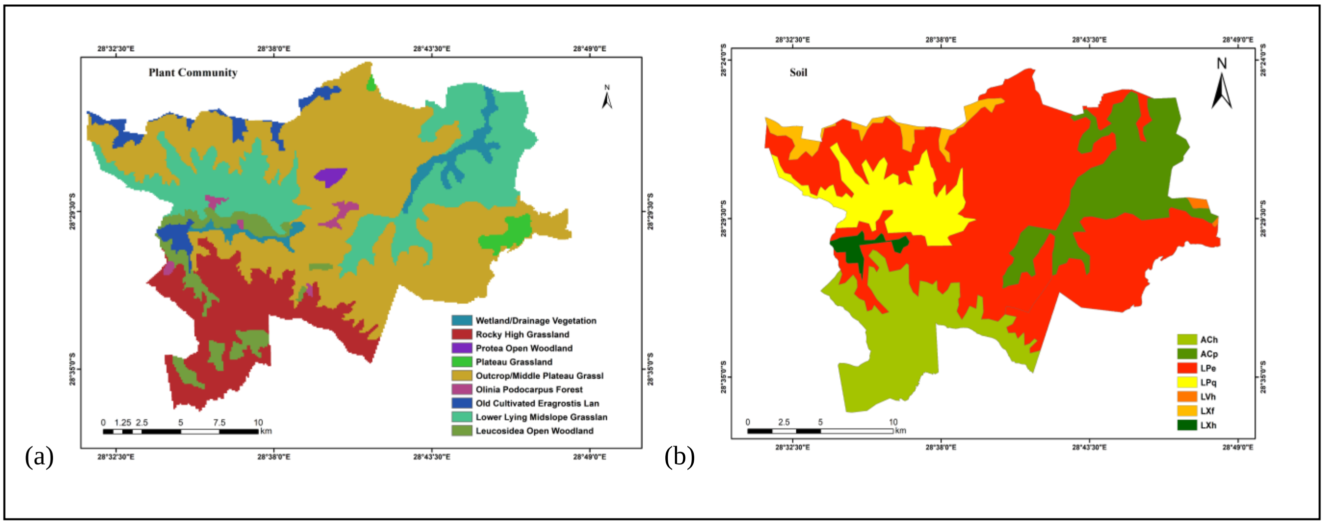

Figure 2.3: (a) Plant Community (b) Dominant Soils of the Golden Gate Highlands National Park

Figure 2.3.(b). show the soil map of the GGHNP as classified by ISRIC-World Soil Information and FAO, where ACh = Haplic ACISOLS; ACp = Plinthic ACISOLS; LPe = Eutric LEPTOSOLS; LPq = Lithic LEPSOLS; LVh = Haplic LUVISOLS; LXf = Ferric LIXISOLS; LXh = Haplic LIXISOLS (Dijkshoorn *et al.*, 2008).

The park is part of the most important water catchment in Southern Africa, called Maloti Drakensberg catchment complex (South African National Parks (SANParks), 2020). The southern parts of GGHNP drain into the Caledon River. In the northern section of the park, the Perskeboom and Klerspruit are tributaries which drain towards Wilge River; this river network forms part of the Vaal River basin, where water is used for the domestic, agricultural and industrial needs part of Gauteng, Mpumalanga, and North-West of the country (Russell and Skelton, 2005; Moloi *et al.*, 2020). The Little Caledon is the largest river that flows about eight (8) km through the park (Russell and Skelton, 2005). The Little Caledon river drains towards the Gariep Dam and Orange River (South African National Parks (SANParks), 2020).

2.4 Climatic elements of the study area

According to the Köppen-Geiger climate classification, the GGHNP falls under the sub-tropical highland climate, also known as the *Cwb* climate subgroup (Spatial Temporal Evidence for Planning South Africa (stepSA), 2015). The *Cwb* climate subgroup is temperate, with dry

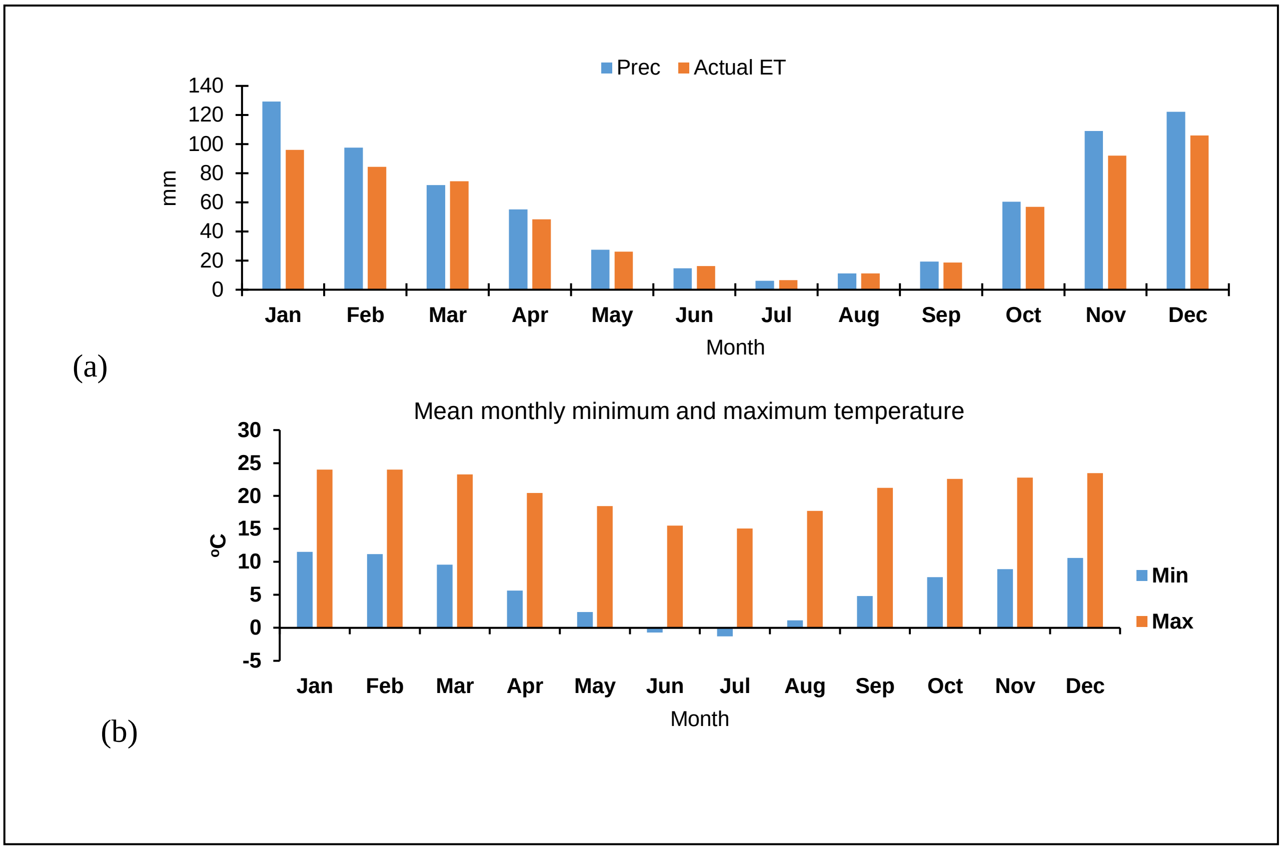

Figure 2.4. Climate Summary of the study area for the period from 2007- 2021 showing (a) Mean Monthly Precipitation (mm), and (b) Mean Minimum and Maximum Monthly Temperatures (^{o}C)

winters and warm summers. More than 80% of the precipitation occurs during the austral summer month from October until March, peaking in January with an average 129 m and is typically scare in the month of July in the middle of winter, with an average of 9mm (Fig. 2.4(a)). Evapotranspiration rates are also high during this period (October –March) (Fig.2.4(a). due to the higher temperature (Fig 2.4(b)). Mean monthly temperatures range from -1.3 ^{o}C (July) to 24 ^{o}C (Jan & Feb) Fig 2.4(b).

2.5 Political, socio-economic and land tenure

Conflict over the land access have long history as human settlement itself in Southern Africa. The amalgamation of former Qwaqwa national park to GGHNP in November 2008 was the emergence of conflict in the park as the consequences of the inhabitants who rented the land on Qwaqwa national park to graze their livestock showing displeasure on the lack of consultation on the incorporation process (Slater, 2002). Conflict persisted after the amalgamation of two parks with farmers still allowing domestic livestock to graze in the protected (Rademeyer and van Zyl, 2014). Today domestic livestock are seen grazing throughout the park. Conflict is regarded as the as a hidden drivers of changes in fire regime (Kelly *et al.*, 2023).

Land use and ownership around the park is diverse and complex to apprehend as it includes private landowners, land claimant (about 1800 ha of the park is under claim for restitution of land rights), private tourism operations, agriculture and traditional communities ((South African National Parks (SANParks), 2020). The park is situated in one of the poorest parts of South, the Eastern Free State one of the presidential nodal point due to the prevailing high levels of poverty and employment(South African National Parks (SANParks), 2020). The nearest towns are Clarens and Phuthadjhaba under Maluti-a-Phofung and Dihlabeng Municipality respectively. Dihlabeng Local Municipality comprises of 140 044 people and 4687 households with agricultural sector as the major contributor of the economy. While Maluti-a-Phofung over double the population of Dihlabeng with 355 784 people and 100 228 households with the government sector contributing more on economy(South African National Parks (SANParks), 2020). All these dynamic factors, land tenure, economic, poverty level and human population have influence on changes of fire regimes. For instance, (Aldersley *et al.*, 2011) found that economy (Gross Domestic Product, GDP) having a strong link to habitant fragmentation and there effect of the region fire regime.

CHAPTER 3

DEVELOPMENT OF LIGHTNING HAZARD MAP FOR FIRE DANGER ASSESSMENT OVER MOUNTAINOUS PROTECTED AREA USING GEOSPATIAL TECHNOLOGY

This chapter is based on:

Mofokeng, D.O., Adelabu, A.S., Adepoju, K. and Adam, E., 2019, July. Spatio-temporal analysis of lightning distribution in Golden Gate Highlands National Park (GGHNP) using geospatial technology. In IGARSS 2019-2019 IEEE International Geoscience and Remote Sensing Symposium (pp. 9898-9901). IEEE.

Mofokeng, DO., Olusola, A. & Adelabu, S. 2022. Development of Lightning Hazard Map for Fire Danger Assessment Over Mountainous Protected Area Using Geospatial Technology. Remote Sensing of African Mountains: Geospatial Tools Toward Sustainability. Springer

Abstract

Lightning is regarded as a leading cause of fatalities, injuries, property damages, and interruptions to businesses. As against some other tropical countries, especially around the equator in Africa and South America, South Africa does not experience as much lightning activity; however, it is still considered a lightning-prone country. With the advent of remote-sensing technology and its capabilities, the world can detect nearly all lightning strikes in real-time with the ability to also geolocate the strike with high temporal and spatial accuracy. This study aims to advance the understanding of the geography of CG lightning activity in South Africa through the application of geospatial technology. Using spatial analysis techniques, this research evaluated 11-year lightning data (2007–2017) to develop a lightning hazard map for Golden Gate Highlands National Park. The monthly strike count of lightning increases from the minimum value in July (0.08%) and displays a peak in December (23.80%). The average diurnal variation (2007–2017) suggests that lightning is more prevalent in terms of occurrence from 14:00 to 18:00 South African Standard Time (SAST) with two clear maxima at 15:00 SAST and 17:00 SAST. The lowest lightning activity is during the morning hours at 05:00 and 06:00 SAST, and yet again at hour 08:00 SAST. The average diurnal variation (2007–2017) suggests that lightning is more prevalent in terms of occurrence from 14:00 to 18:00 SAST with two clear maxima at 15:00 SAST and 17:00 SAST. The lowest lightning activity is during the morning hours at 05:00 and 06:00 SAST, and yet again at hour 08:00 SAST. Spatial autocorrelation analysis revealed that the clustering of lightning strikes at the park is at the distance of about 1.2 km. This connotes that strikes clustered with other strikes are not likely to strike an individual specific location from centre of cluster of strikes much beyond a circle with a radius of 1.2 km. Furthermore, Global Moran I revealed clusters starting at 2km to 8km.

Keywords: *Lightning · Spatial Statistics techniques · Remote Sensing · Fire Danger Assessment*

3.1 Introduction

Lightning as an activity most likely predates human existence (Rakov and Uman, 2003; Gijben *et al.*, 2017) and even a critical meteorological phenomenon. Lightning is regarded as a leading cause of fatalities, injuries, property damages, and interruptions to businesses (Cha *et al.*, 2017; Gijben *et al.*, 2017). By definition, lightning can be described as the release of static electricity in the sky or between the clouds and the ground (Rakov and Uman, 2003; Gijben *et al.*, 2017). On a global scale, lightning is responsible for not more than 24,000 deaths and 240,000 injuries on an annual basis (Blumenthal *et al.*, 2012). From Earth Observation Satellites (EOS), about 39-49 lightning flashes are captured around the globe per second. This is translated to about 1.4billion flashes per day on a Cloud-to-Ground (CG) scenario (Christian *et al.*, 2003; Gijben *et al.*, 2017).

As against some other tropical countries, especially around the equator in Africa and South America, South Africa does not experience as much lightning activity; however, it is still considered a lightning-prone country (Bhavika, 2010; Gijben, 2012). Yearly death rates from lightning in South Africa is 6.3 per million of the population, which is 15 times more than the global average (Gill, 2009). This figure is presumed to be underestimated per actual mortality rate. This underestimation is likely to be because lightning deaths are not rigidly reported in rural areas (Gijben *et al.*, 2017). As a natural ignition source for global fire, lightning activities were recently operationalized as one of the driving factors in fire danger or risk modelling (Chuvieco *et al.*, 2014; Eskandari and Chuvieco, 2015; Huang *et al.*, 2015). According to Cha *et al.* (2017), an average of 816 fires were ignited by lightning each year globally.

During 2005, lightning fire burnt a large area of fynbos and commercial timber plantation in Tsitsikamma, Western Cape Province of South Africa (Durrheim, 2010). According to the Council for Scientific and Industrial Research (CSIR) report on the Elandskraal fire that ravaged approximately 9440 hectares, it was revealed that the positive lightning strike observed on the 22 March 2017 was responsible for the fire which started on the 07 June 2017 (Frost *et al.*, 2018). With the advent of remote-sensing technology and its capabilities, the world can detect nearly all lightning strikes in real-time with the ability to also geolocate the strike with high temporal and spatial accuracy. Numerous studies have focused on understanding lightning activities in many countries using different lightning location systems (Christian *et al.*, 2003; Rakov and Uman, 2003; Kigotsi *et al.*, 2018). Most of the lightning systems detect electromagnetic reading using Time of Arrival (ToA) and Magnetic Direction Findings (MDF) methods or a combination of ToA and MDF. A summary of literature relating to the methods can be found in (Gill, 2009). These systems are either ground-based or satellite lightning sensors. The latter detects lightning from space through the earth-orbiting satellite which either detects light or electromagnetic waves from lightning discharge (Rakov and

Uman, 2003). The well-known satellite-lightning sensors include National Aeronautical & Space Administration (NASA) Optical Transient Detector (OTD) and Lightning Imaging Sensors (LIS) on-board the Tropical Rainfall Measuring Mission (TRMM) (1997–2014) (Christian *et al.*, 2003; Kigotsi *et al.*, 2018). Formerly, sensors which detect electromagnetic pulse in very low frequency (VLF) or low frequency (LF) include regional Lightning Detection Network (LDN) such as United States of America National Lightning Detection Network (USA NLDN) and Southern African Lightning Detection Network (SALDN) in South Africa. Global LDN includes World Wide Lightning Location Network (WWLLN) and the Global Lightning datasets (Kigotsi *et al.*, 2018).

The spatio-temporal lightning flash density and occurrence have been investigated in the United States (Bentley and Stallins, 2005), Canada (Cha *et al.*, 2017), Europe (Anderson and Klugmann, 2014), Mediterranean (Price and Federmesser, 2006), India (Dewan *et al.*, 2018) Africa (Mayet, 2016; Kigotsi *et al.*, 2018) at the global scale (Christian *et al.*, 2003; Cecil *et al.*, 2014). According to Evert and Schulze (2005)), studies on lightning have been in existence for about eight decades. However, in the past couple of years, there has been tremendous growth in South Africa as a result of the introduction of the National System (see Gill (2009)). Gill (2009) was the first to utilize the 2006 SALDN data in the development of the climatology of South Africa. This was later updated by Gijben (2012) using the 2006–2010 dataset. Recently, Evert and Gijben (2017) utilized the 2006–2017 SALDN data to update the national lightning flash density map over South Africa. In their study, (Evert and Gijben, 2017)observed that the highest flash density occurs along the eastern escarpment of the country with values exceeding 15 flashes km^{-2} yr^{-1}.

Despite the availability of geo-coordinated lightning data, most CG lightning studies found within the country (South Africa) typically only focus on visualizing the distribution of CG lightning activity as a flash density for the simple purpose of identifying areas of high flash density rate. These forms of studies often do little in explaining the observed spatial patterns of flash density. Furthermore, based on the uniqueness of the country's physiography, there are landscapes across the country that are unique to lightning activities, such as montane environments. Montane environments within South Africa are unique, in that they serve as places of water towers for South Africa and some neighbouring countries, also these areas preserve very unique grasslands that are endemic to South Africa and of global interest. Also, montane environments in South Africa are witnessing the impact of the changing climate through the emergence of invasive species and incessant lightning strikes. Therefore, this study aims to advance the understanding of the geography of CG lightning activity in South Africa through the application of geospatial technology. Using spatial analysis techniques, this research evaluated 11-year lightning data (2007–2017) to develop a lightning hazard map for Golden Gate Highlands National Park by examining the statistical spatial and temporal patterns of lightning activity of Golden Gate Highlands National Park and their relationship with environmental characteristics, namely, elevation, slope, aspect, fire scars, and the vegetation type.

3.2 Methodology

3.2.1 Materials

3.2.1.1 CG Lightning Data

CG lightning data was acquired from the Southern African Lightning Detection Network (SALDN) of the South African Weather Services (SAWS). The SALDN became operational in 2005 and underwent a series of upgrades. From 2015, the network consisted of 25 Vaisala CG lightning sensors that can detect all cloud-to-ground lightning discharges with a 90% efficiency measure (Evert and Gijben, 2017). The SALDN is capable of detecting lightning with a location accuracy of ~0.5 degree (500 m) covering all of South Africa, Lesotho, and Swaziland (Bhavika, 2010; Evert and Gijben, 2017; Gijben *et al.*, 2017). The network records lightning events chronologically. The attribute information of each lightning strike is recorded including date and time, latitude, longitude, peak current with negative (-) or positive (+) polarity, major and minor ellipsoid angle, and the number of direction finders that sensed the event (Bhavika, 2010). As recommended by International Electrotechnical Commission Standards (IEC 62858), lightning data for at least 10 years is required to ensure that short-term scale variation in lightning parameters due to a variety of meteorological oscillations are accounted for (Javor *et al.*, 2018). Therefore, in this study, lightning strike data for 11 years from January 2007 to December 2017 was utilized.

3.2.1.2 Terrain Elevation, Slope, and Aspect

Advanced Spaceborne Thermal Emission and Reflection Radiometer-Digital Elevation Model (ASTER-DEM) data at 30 meters (m) freely obtained from USGS EarthExplorer (http://earthexplorer.usg.gov) was used for retrieval of elevation, aspect, and slope values. These values were selected due to its known role of orographic lifting to the enhancement of convection and consequently to lightning (Kotroni and Lagouvardos, 2008).

3.2.1.3 Vegetation Type

Vegetation plays a pivot role in the universal climatic variation together with the convective growth and lightning activity (Dissing and Verbyla, 2003; Mushtaq *et al.*, 2018). Vegetation type of GGHNP was attained from Fire Ecology Department, South Africa National Park (SANParks), in the polygon shapefile providing GIS coverage that shows vegetation types in community and habitat.

3.2.1.4 Historical Fire

Historical fire scar/spot data was received from the Fire Ecology and Biogeochemistry Department, SANParks, with their geographical coordinates in polygon shapefile format. The significance of these data in lightning activity is that a possible-induced thunderstorm can be conceived from all sides of fire scars (Kilinc and Beringer, 2007).

3.2.2 Methods

Lightning data was provided in a formatted text (.cvs) that was first parsed and saved in a spreadsheet and then converted into a point vector layer in a GIS environment using Microsoft Excel and ArcMap 10.2. software, respectively. The geo-reference UTM Zone 35S was used as the projection. A Clip Tool was employed to extract the study area. Databases of lightning activity by year, monthly, and hourly were then created by using the Select by Attributes tool.

3.2.2.1 Temporal Distribution of Lightning Strikes Activity

Lightning strikes counts were analysed to explore temporal patterns of lightning activities over GGHNP. Annually, monthly, seasonal, and diurnal distributions were calculated with the summation of counts for respective periods. To evaluate the influence of season on lightning activity, monthly data was summarized according to four seasons: summer (Dec, Jan, Feb), autumn (March, April, May), winter (June, July & August), and spring (Sept, Oct, Nov). For diurnal, a series of graphs and tables were created using Excel to visualize the temporal distribution of lightning activity of the park.

3.2.2.2 Spatial Distribution of Lightning Strikes Activity

To capture the spatio-temporal distribution of lightning activity, maps for visualization showing the individual CG lightning strikes as points and density were created. In this study, the Hex binning analysis was employed. This analysis helps in aggregating spatially lightning strike data. The reason here is that the Hex binning as used in this study will help to spatially aggregate the dataset (lightning strike) in a hexagonal manner. The assumption stems from studies (Carr *et al.*, 1992; Genton *et al.*, 2006) that have posited that hexagons are visually appealing and have better symmetry of nearest neighbour than square or rectangular bins. The hex grid (100 m) for each of the dataset (lightning) were created using MMQGIS plugin version 2018.1.2 and the lightning data was spatially joined to the hex grid using the join by location attribute in QGIS 2.18.5. The lightning flash density attribute was added to the new feature table and calculated using the Field Calculator tool by dividing the 'count' by cell area and then by the number of years spanning the dataset resulting in a count per km^2 per year (Ng).

Hot Spot Analysis was employed to determine whether or not there is clustering and also to measure the degree of spatial autocorrelation of CG lightning in the study area. Hot Spot Analysis was performed using lightning strikes density data as an input. Several analyses or processes precede hotspot analysis. First, we determined the specific threshold distance or distance band for neighbouring feature, which is called neighbourhood. The neighbourhood consists of features that are analysed together to assess local clustering and this is made possible through the use of a threshold distant band (TDB). To determine the TDB, the Incremental Spatial Autocorrelation (ISA) tool in ArcGIS was conducted.

ISA is a measure of spatial autocorrelation. The Z-score here depicts the spatial clustering intensity and statistically significant peak z-score indicates where spatial processes promoting clustering are most pronounced. These peak distances were used to determine a distance band or threshold distance band for hot spot analysis using Getis–Ord G_i* (Environmental Systems Research Institute (ESRI), 2013; Cha *et al.*, 2017).

Furthermore, ISA calculates Global Moran I. Moran's I is a measure of the correlation where negative correlation indicates the dispersion of similar values, positive correlation indicates clustering of similar values (either high or low), and zero correlation indicates complete spatial randomness. It informs us whether a set of features is clustered, dispersed, or random. It is based on spatial covariation divided by total variation as shown in Equation 3.1 (Moran, 1950; Amrhein, 2017).

$$I = \frac{n\sum_{j=1}^{n}\sum_{j=1}^{n} W_{ij}(y_i - y)(y_j - y)}{\left(\sum_{i=1} n(y_i - y)^2 \left(\sum_{i=1} n \sum_{j=1}^{n} w_{ij}\right)\right)} \qquad \text{Equation 3.1}$$

Where, n is the total number of features, w_{ij} is the spatial weight matrix between feature *i* and *j*, the variable *y* is the features attribute value.

Values for Moran's I range from -1 (dispersion) to +1 (clustered). A Z-score and p-value are also calculated for Moran's I statistic. For statistically significant positive Z-scores, the null hypothesis of spatial randomness is rejected, and the high and low values in the dataset are considered to be more clustered than expected. For statistically significant negative Z-score, the spatial distribution of high and low values is considered dispersed and the null hypothesis is rejected (Moran, 1950; Amrhein, 2017). Results were represented in the form of line graphs of Moran I and Z-score vs distance.

To explain a spatial pattern of the CG lightning strike density, hotspot analysis was eventually performed using Hot Spot Analysis Getis–Ord G_i* Tool of ArcMap. Getis–Ord G_i* evaluates the spatial correlation from a local scale perspective. The G_i* as a statistic helps in determining areas of high and low clusters by looking at local averages to global averages. The G_i*statistic ranges in values from -3 to -3 and is calculated for each feature and produces a Z-score indicating the intensity of the high or low clustering with respect to its neighbourhood depending on the sign of Z-score. A statistically significant 'hot spot' is one where a feature with high value is surrounded by other features with high values (positive Z-score). Likewise, a 'cold spot' is one where a feature with low value is surrounded by other features with low values (Getis and Ord, 1992; Environmental Systems Research Institute (ESRI), 2013; Cha *et al.*, 2017). The G_i* is calculated using Equation 3.2.

$$\mathrm{Gi}* = \frac{\sum_{j=1}^{n} w_{i,j},, x_j - X\sum_{j=1}^{n} w_{i,j}}{S\sqrt{\sum_{j=i}^{n} xj^2 - (X)^2}} \qquad \text{Equation 3.2}$$

where x_j is the attribute value for feature j, w_{ij}, is the spatial weight between i and j, and n is equal to the total number of features. Also, X and S are shown in Eqs. 3.3 and 3.4, respectively.

$$X = \sum_{j=1}^{n} x_j \qquad \text{Equation 3.3}$$

$$S = \sum_{j=1}^{n} x^2 j - (X)^2 \qquad \text{Equation 3.4}$$

3.2.2.3 Development of Lightning Hazard Map

For the spatial distribution of Lightning Hazard Map (LHM), the Inverse Distance Weighted (IDW) technique of ArcMap 10.2 was employed. LHM was developed from the Z-score of the Hot Spot Analysis. The output of the IDW was normalized to range between 0 and 1 using the Raster normalization tool (ArcGIS), while the Reclass tool was used to stratify the entire data layer into five classes based on lightning potential risk of lightning activities guided by previous researches. These classes are categorized as follows: almost danger-free (0-0.2), minimal danger (0.2-0.35); moderate danger (0.35-0.50); severe danger (0.50-0.75); and extreme danger (0.75-1).

3.2.2.4 Relationship of Lightning Hazard Map with Topography (Elevation, Slope, Aspects, Vegetation Types, and Fire Scar)

Regression analysis was undertaken to explore the relationship of LHM with terrain parameters, (elevation, slope, and aspect), vegetation types, and fire scars. Statistical analysis of the data, namely, Coefficient, Probability or Robust Probability, and Variance Inflation Factor (VIF), as well as t-test were used to assess each variable. In preparing the data for statistical analysis, the study area elevation data was prepared using methods by (Adelabu *et al.*, 2020). Slope and aspect were calculated using the Surface Tool. All raster layers were converted into vector layers (polygons) to align with vegetation types and fire scar layers and resampled to 1000 m. All six (6) layers were overlaid using the Spatial Join Tool of ArcMap. Regression analysis was performed using Ordinary Least Squares (OLS) Modelling spatial relationship Tool of ArcMap 10.2 software. The diagnostic results were displayed in the form of a table.

3.3 Results

3.3.1 CG Lightning Strike Events and Density Maps

Within the GGHNP, a total of 114,720 lightning strikes were recorded between January 2007 and December 2017. About 94.86% were of negative polarity and 5.14% of positive polarity. In general, most of the previous studies showed a similar pattern of positive polarity accounting for less than 10% of total CG activities (Dewan *et al.*, 2018). Since the CG lightning point event map is difficult to visually interpret, a lightning flash density map on the hexagon polygon grid for the entire 11-year period is displayed in Fig. 3.1. The map showed that the density of lightning strikes is not uniform throughout the park. Areas of high density (in red) can be seen throughout the park. These observed variations in the CG lightning pattern follow the topography of GGHNP. The highest density was prominent at a highly elevated area within the park.

3.3.2 Temporal Analysis

From Fig. 3.2. it can be observed that the GGHNP experienced the highest number of lightning events during 2016 (16,365). The distribution shows that the years 2015 (7071 events) and 2017 (7067 events) witnessed the lowest number of individual lightning strikes in the park. Based on the inter-annual variability (Fig. 3.2 and Table 3.1), there is a possibility that the occurrence of these strikes is related to a large-scale climate phenomenon, such as the ElNino Southern Oscillation (ENSO) and the Southern Annular Mode (SAM) (Dowdy, 2016, Guha et al., 2017, Mariani et al., 2016). However, there is still the need to carefully unravel this relationship using standard climatic procedures.

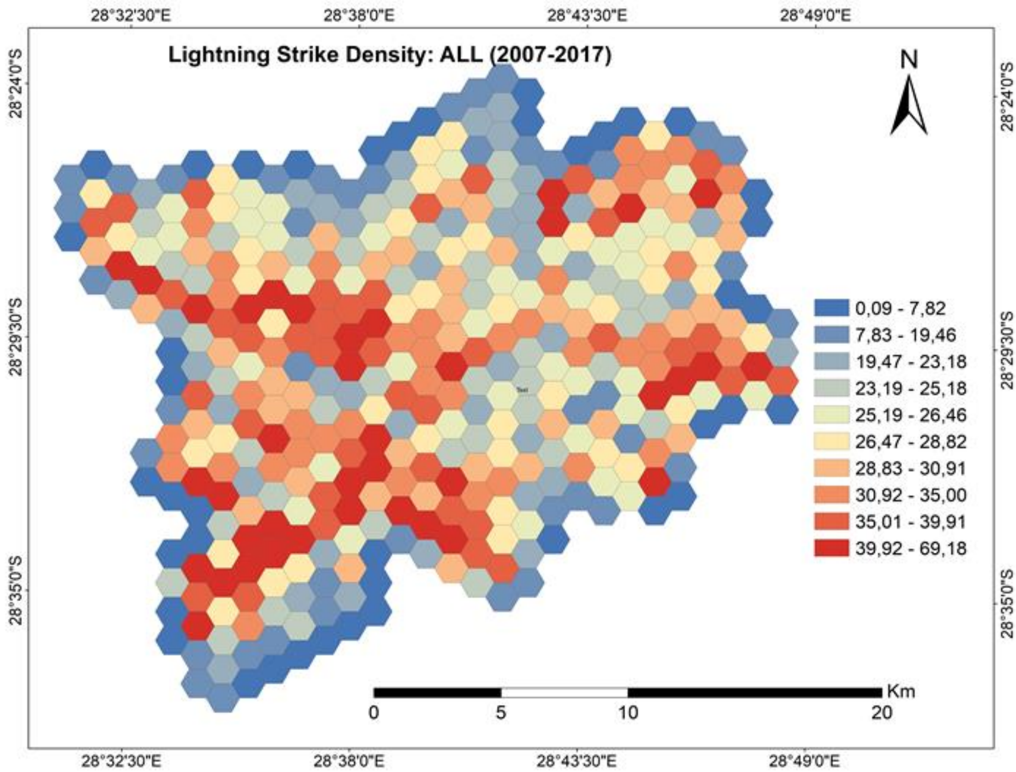

Figure 3.1: Map depicting the spatial density of CG lightning flashes within GGHNP between 2007 and 2018. Lightning density (Ng) displayed the number of CG lightning events per km^2 per year

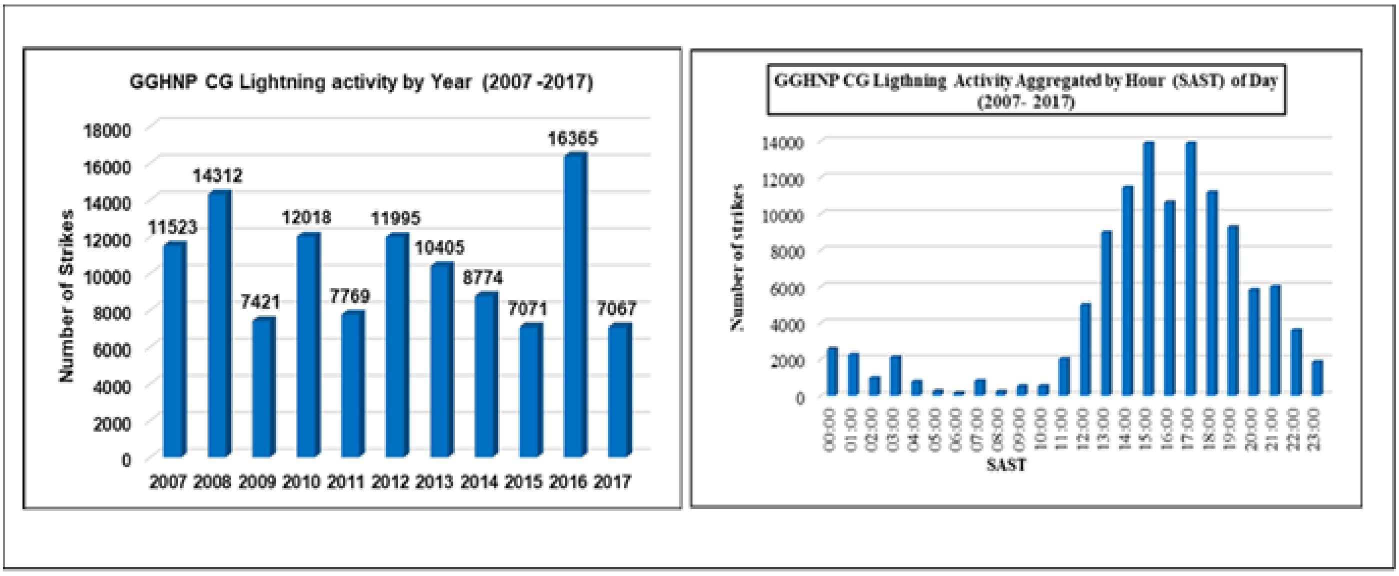

Figure 3.2: Graph of lightning events by year and hour

Table 3.1: Percentage of lightning strikes count by month and season from 2007 to 2017

Month	Percentage	Season	Percentage
Dec	23,80%	Summer	56,26%
Jan	17,57%		
Feb	14,89%		
Mar	10,71%	Autumn	14,22%
Apr	2,82%		
May	0,69%		
Jun	0,47%	Winter	0,68%
Jul	0,08%		
Aug	0,13%		
Sep	1,90%	Spring	28,84%
Oct	13,38%		
Nov	13,56%		

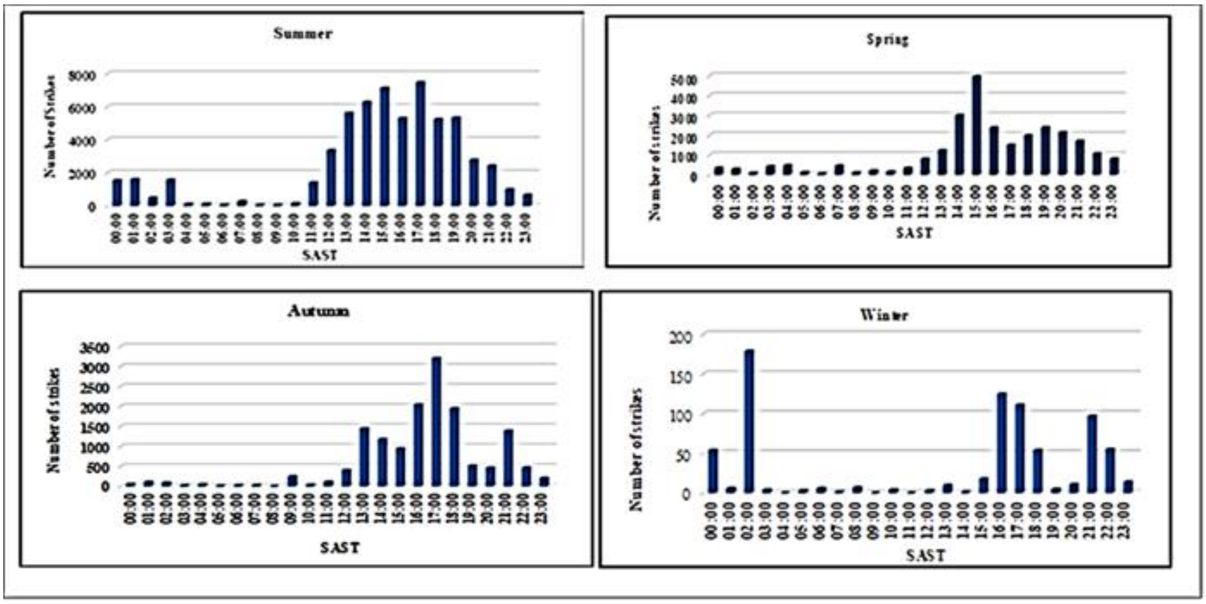

Figure 3.3: Seasonal variation lightning strikes over GGHNP

3.3.3 Spatial Pattern Analysis

3.3.3.1 Global Moran 1

Output from Moran I analysis on the monthly scale, as depicted in Fig. 3.4(a), revealed that the Moran I values are greater than 0 ranging from 0.01 to 0.49 throughout the year, with the exception of July. This indicates positive spatial autocorrelation of clustering of either high or low values of CG lightning density. However, the Moran I value of July is smaller than 1 indicating that the spatial pattern is randomly distributed. In winter months (June, August, and September), Moran I values range from 0.01 to 0.07, which reveals that spatial pattern is close to the random distribution pattern of CG lightning density. The z-score values are above zero (see Fig. 3.4(b)) and observed p-values are low, therefore, the spatial pattern is statistically significant and rejected the null hypothesis that lightning density is randomly distributed except in the month of July. The CG lightning density and the Moran I curves show the bias of lightning density with distance. From Fig. 3.4, it can be posited that the spatial distribution of lightning density within the protected area is clustered at a distance of about 1.2 km which becomes closer to random as the neighbourhood distance increases.

From Fig. 3.5(a), (b), the CG lightning density shows a persistent decrease with distance for afternoon and evening hours ranging from 0.00 to 0.48 at 1.2 km to values less than 0.0 at 8.3 km. On the other hand, the Moran I curve for late morning hours suggests a random pattern since the morning hours is less than zero and negative for 06:00 SAST and 09:00 SAST (Fig. 3.5). From Fig. 3.5b, the observed Z-score (Z > 0 and positive) curves for early morning, afternoon, and evening hours are above zero and are positive signalling a positive spatial auto-correlation and an indication of a significant clustered pattern (p < 0.5). Based on Fig. 3.5b, the Z-score (Z < 0 and negative) for late morning hours 06:00 and 08:00 SAST suggests a negative non-significant spatial correlation, hence, lightning activities within GGHNP during 06:00 and 08:00 are likely to be random. Furthermore, Figs.3.4 and 3.5 revealed that clusters starting at 2km to 8km.

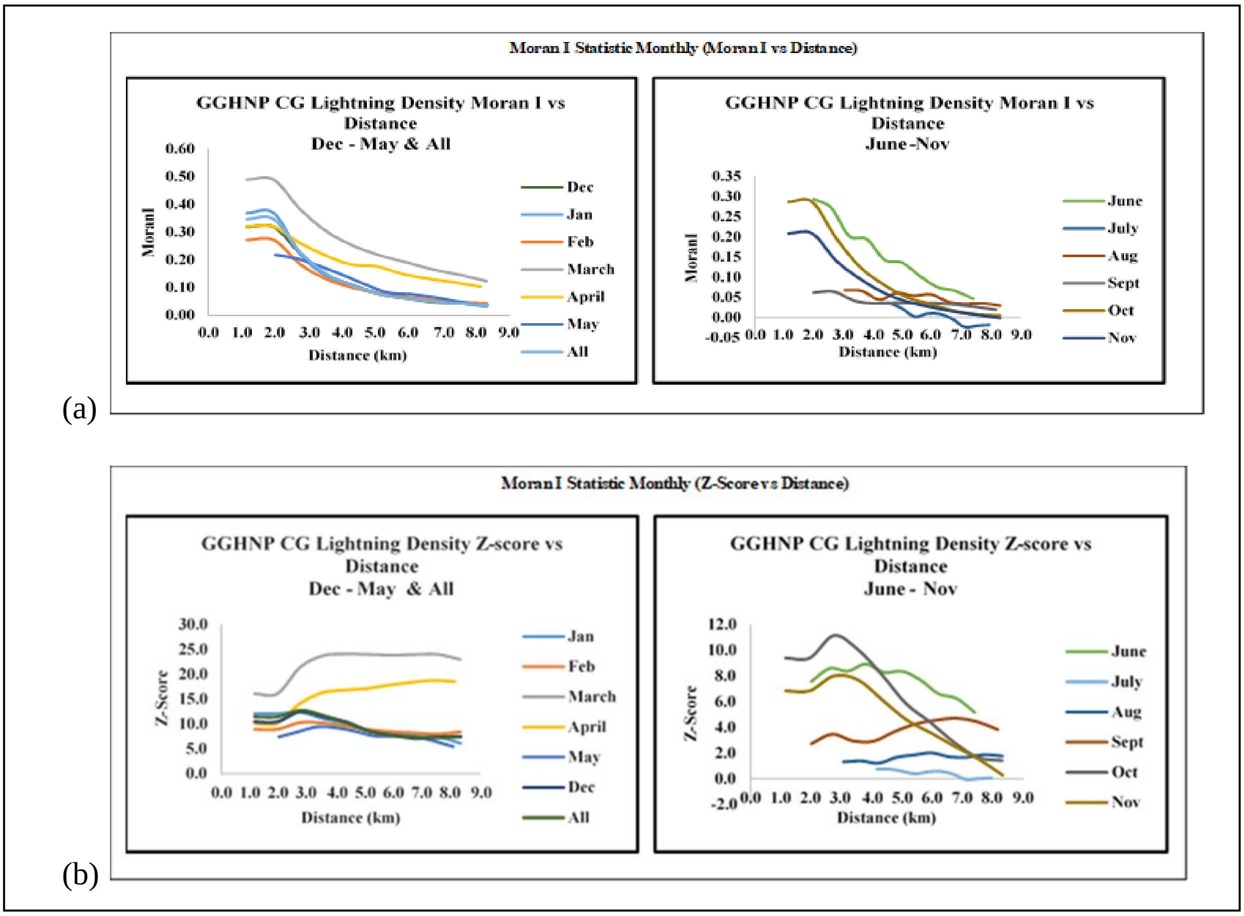

Figure 3.4: Global Moran I statistic results for monthly data (a) Moran I vs Distance, (b) Z-score vs Distance

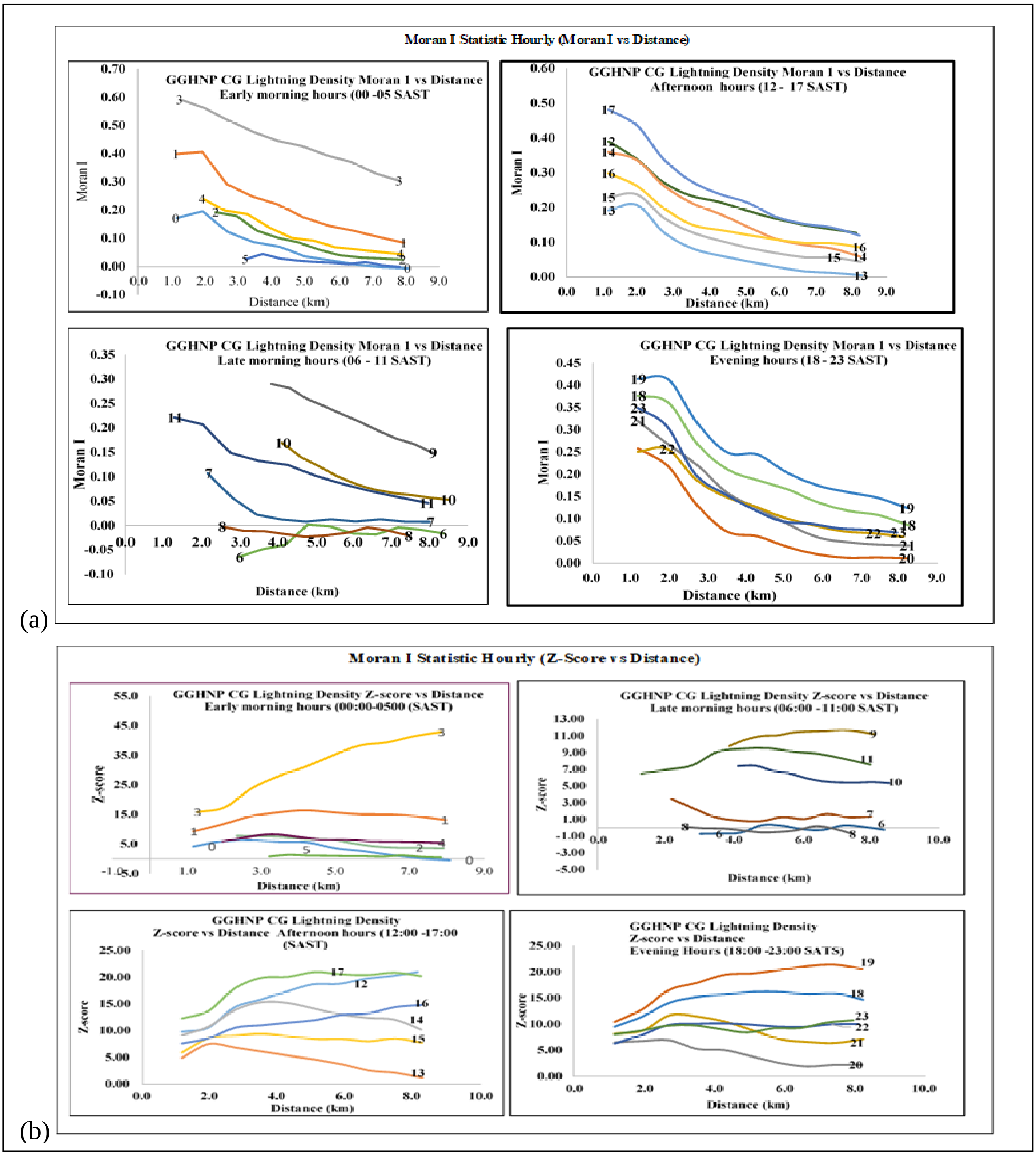

Figure 3.5: Global Moran I statistic diurnal data (a) Moran I vs Distance, (b) Z-score vs Distance

3.3.4 Hotspot Analysis Getis-Ord G_i*

The map of Hotspot Analysis Getis–Ord G_i*statistic using the 11-year lightning activity is presented in Fig. 3.6. It illustrates the regions of a statistically significant cluster of high and low values (hot and cold spots) presented in shades of red and blue based on the calculated Z-score and p-values. From Fig. 3.6, the main clusters are large and are identified as hot spots. These are at a higher elevation within the park such as in the south-western through the north-western and eastern part of the park. These hotspot areas cover 23.76% of the study area. Clusters of statistically significant low values or cold spots are mainly located in the northern part of the park. While 13.43% was found as statistically significant and identified as a cluster of low values (cold spot).

The results of the Getis–Ord G_i^*statistic for aggregated monthly data are revealed in Fig. 3.7. It showed that July and August (winter months) have a smaller area of coverage of high values of clustering and non-existing low values of clustering. Large coverage is identified as clusters of high values for all months between September and June. Table 3.2 showed the percentage of the area identified as clusters of high values (hotspot) and low values (cold spot), as well as non-significant for the monthly dataset. February and March have the largest coverage identified as clusters of high values (hotspot). During winter months when the lightning activity is at least, the largest area of coverage of hotspot is located in June (18.27%) followed by August (12.38%) and July (10.36%) and located in the south-western part of the park and a small portion at the centre of the park.

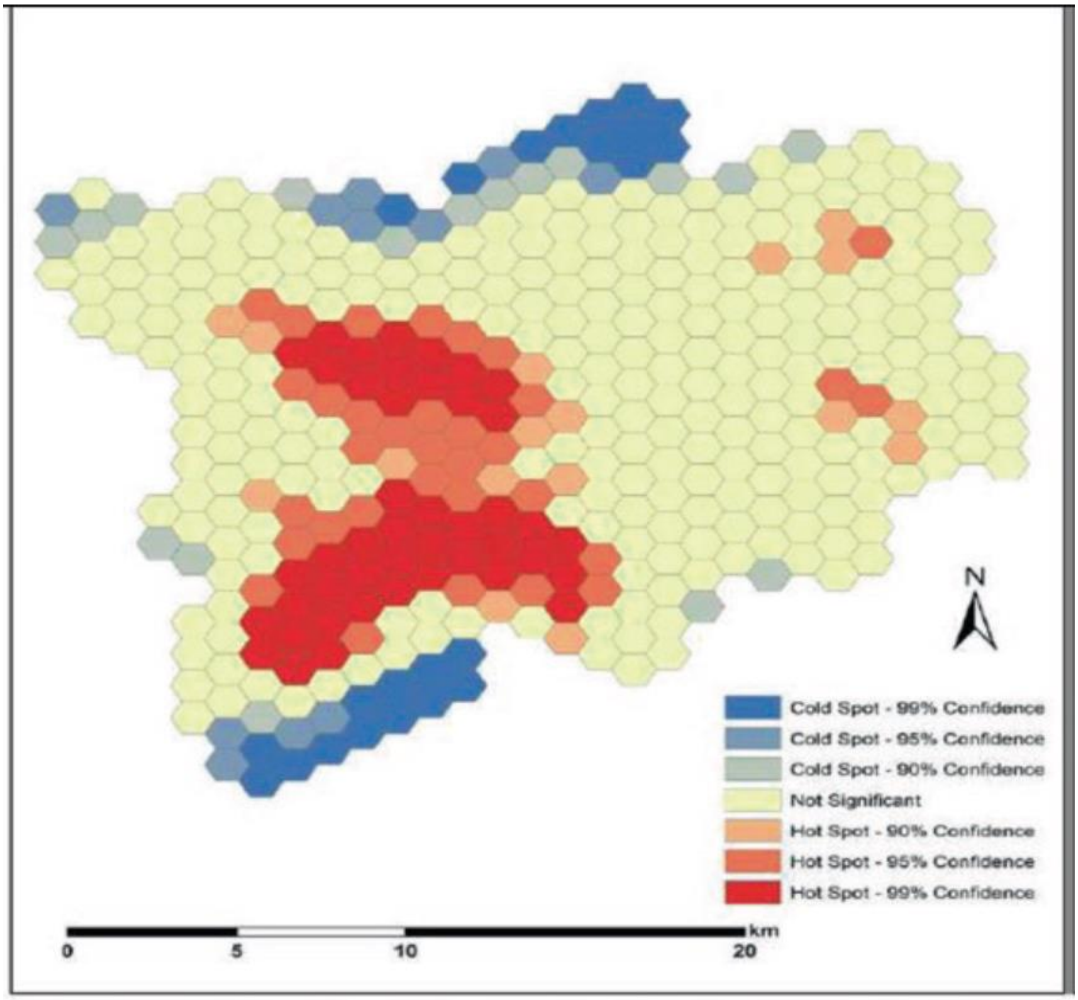

Figure 3.6: GGHNP lightning strike density showing hot and cold spots

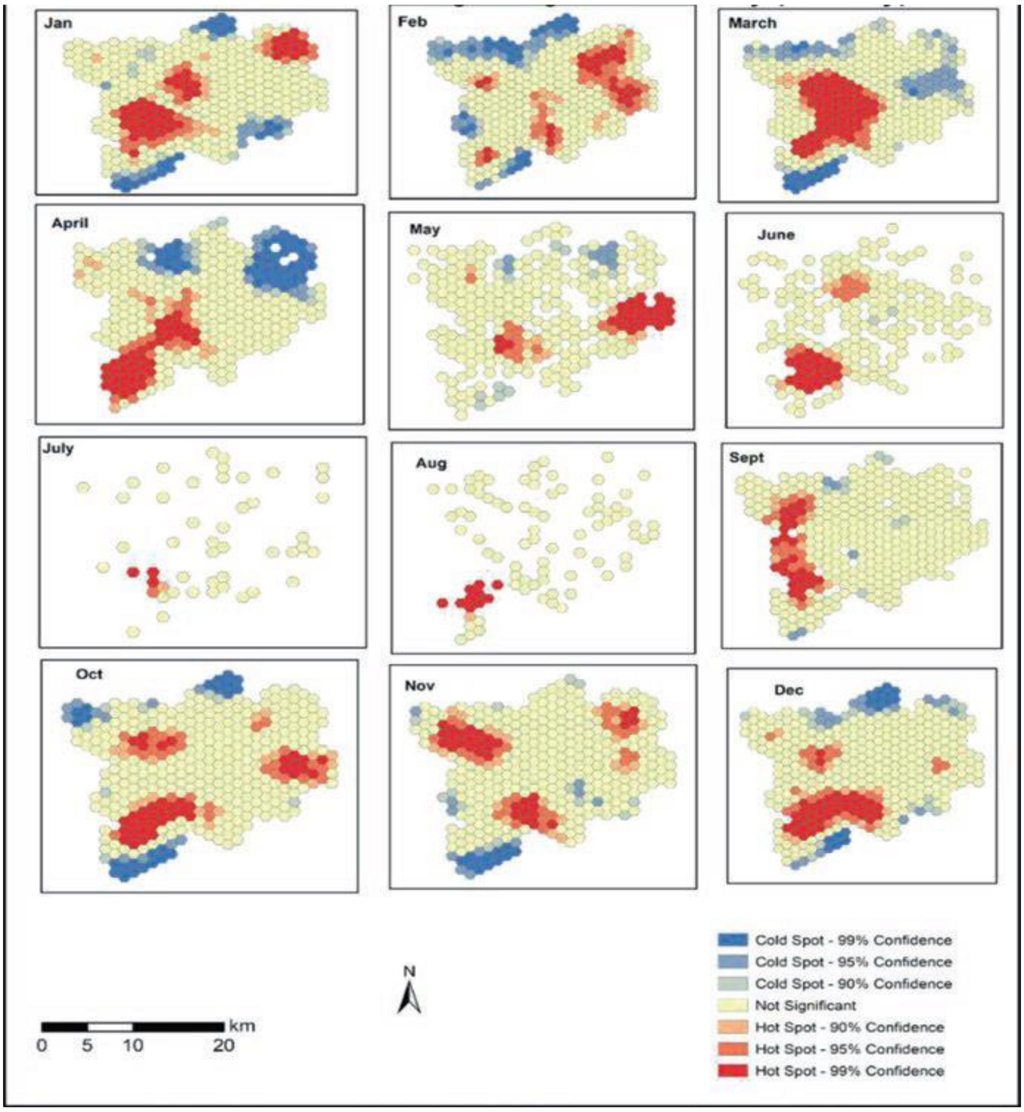

Figure 3.7: GGHNP monthly lightning strike density showing hot and cold spots

Table 3.2: Summary of monthly Getis–Ord G_i*result showing the percentage of area identified as clusters of high values (hotspot), low values (cold spot), and non-significant

Month	High	Low	Non-significant
Jan	23,21	13,03	63,76
Feb	23,7	18,86	57,44
Mar	23,7	23,25	53,05
Apr	19,32	19,91	60,77
May	15,43	7,12	77,44
Jun	18,27	0,96	80,77
Jul	10,36	0	89,64
Aug	12,38	0	87,62
Sep	14,75	3,64	81,62
Oct	21,6	10,99	67,41
Nov	21,4	9,24	69,62
Dec	19,36	13,43	67,21
All	23,76	12,85	63,4

During summer months when lightning activity is at its peak, the largest areas of coverage of hotspots are observed in February (23.70%) located in north-east and eastern parts of the park, followed by January (23.21%) and December showing the least (19.36%) and concentrated more in the south-west part of the park. During the autumn season, March (23.70%) contributed the highest area of coverage of hotspot located extremely at the central part followed by April (19.32%) located in south-western and May (15.43%) located in the eastern part of the park. The high values of the cluster during the spring season are high in October (21.60%) concentrated mostly in the south-western region and less in the eastern part of the park and followed by November (21.14%) located in the north-west portion, September with the least (14.75%) in north and south-western part of the park. The cold spots of lightning strike density are large in coverage during April and non-exist in July and August.

The hotspot coverage appears to be at its greatest during 22:00 SAST (30.08%), 03:00 SAST (26.19%) and 17:00 SAST (25.75%) as shown in Fig. 3.8 and Table 3.3. The north-western, south-western, and central mountains have a consistently high level of hotspot during these time periods and through 06:00 SAST (3.33%) where it is almost non-existence. In the mountains of north-eastern and eastern GGHNP, the hotspot coverage in this region of the park is consistent but relatively smaller in coverage expect during 01:00, 04:00, 12:00, 16:00, and 19:00 SAST. Cold spot coverage appears to be at its greatest during 03:00 SAST (38.11%) and occurs mostly over the north-eastern flat terrain region of GGHNP. Therefore, the results of the Getis–Ord G_i* test reveal localized hot and cold spots of CG lightning activity within GGHNP and vary with the seasons on the monthly time scale as well as diurnally hour of the day. The hot spots are generally located in or near the mountains while most of the cold spots are located in the flat terrain of GGHNP.

Table 3.3: Summary of hourly Getis–Ord Gi*result showing the percentage of area identified as clusters of high values (hotspot), low values (cold spot), and non-significant

Hour	**High**	**Low**	**Non-significant**	**Hour**	**High**	**Low**	**Non-significant**
00	18	10,25	71,75	**12**	22,14	22,43	55,47
01	18,14	15,61	66,25	**13**	12,51	9,26	78,22
02	16,03	7,77	76,2	**14**	24,46	20	55,54
03	26,19	38,11	35,69	**15**	22,25	8,33	69,4
04	21,32	5,98	72,7	**16**	23,03	18,9	58,06
05	16,39	0	83,61	**17**	25,75	21,24	53,75
06	3,33	0	96,6	**18**	20,86	14,98	64,16
07	13,56	3,71	82,73	**19**	18	15,99	66,01
08	7,8	0	92,2	**20**	16,17	8,55	75,28
09	17,61	0	82,39	**21**	22,25	14,09	63,77
10	12,6	6	81,4	**22**	30,08	13,29	56,63
11	23,4	17,08	59,52	**23**	19,1	12,62	68,28

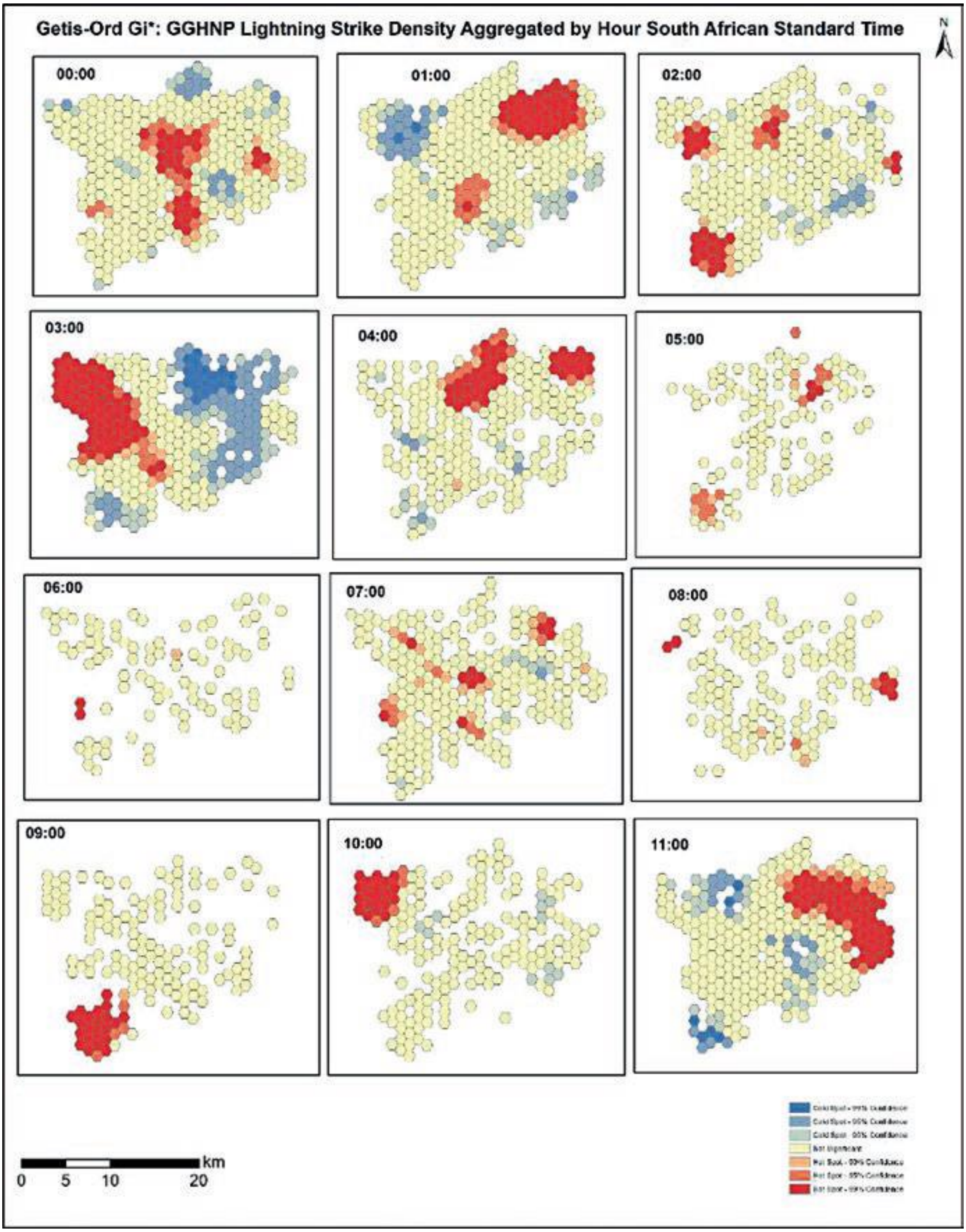

Figure 3.8: GGHNP average hourly lightning strike density showing hot and cold spots

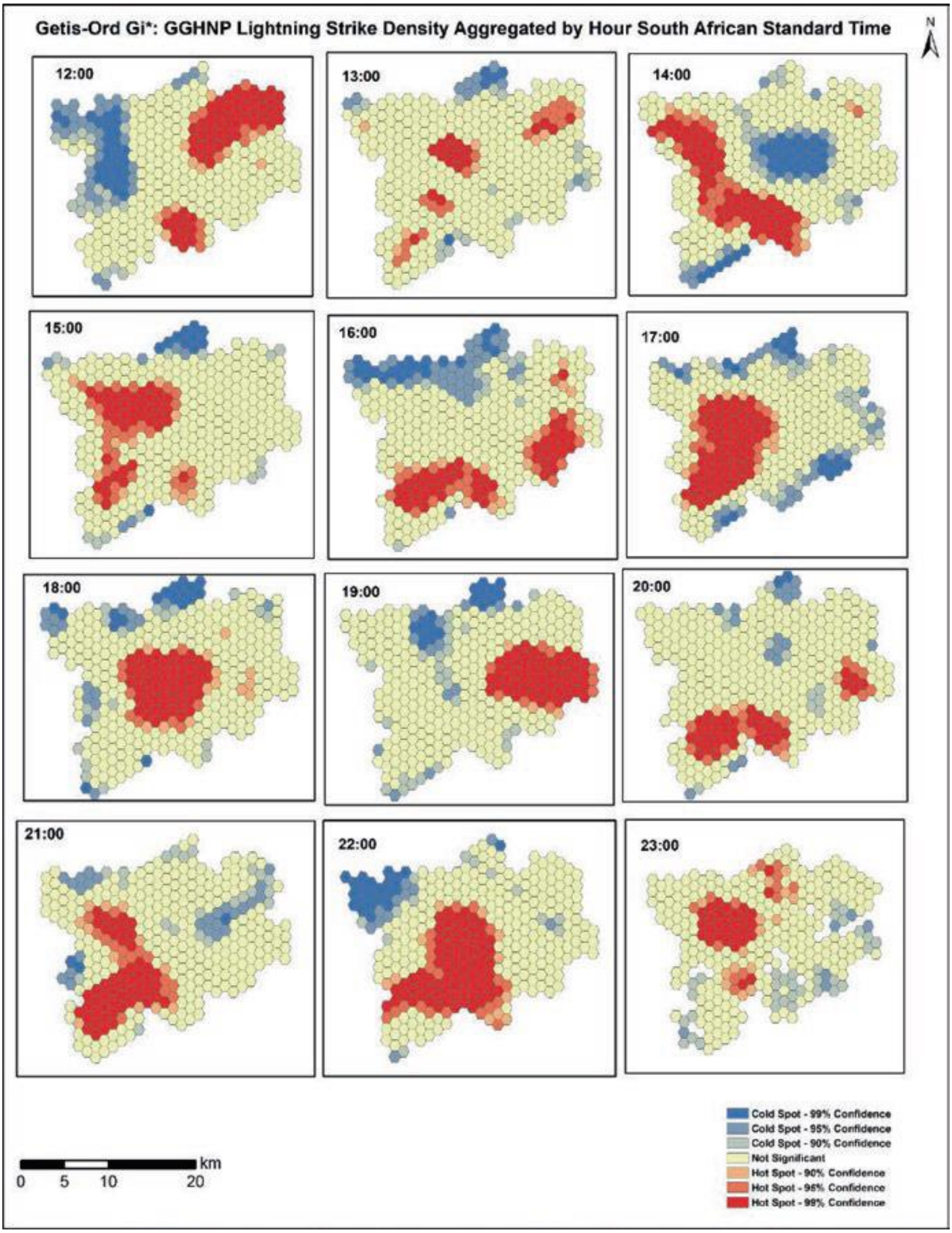

Figure 3.8:.(cont..) GGHNP average hourly lightning strike density showing hot and cold spots

3.3.5 Development of Lightning Hazard Map

The development of LHM was drawn from the Z-score of Hotspot analysis, interpolated, normalized, and classified according to the potential of lightning hazard. The map showing coverage extent of hazard severity is illustrated in Fig. 3.9. It revealed that 48.76% of the entire landmass of the GGHNP falls under the severe danger zone. Two patches of the extreme danger zone are seen on the map towards the south-western part and north-central portion of the map. Only very few portions of the entire landmass fall under almost danger-free zone, suggesting that the entire landmass of the GGHNP is largely prone to lightning hazard (Fig. 3.9).

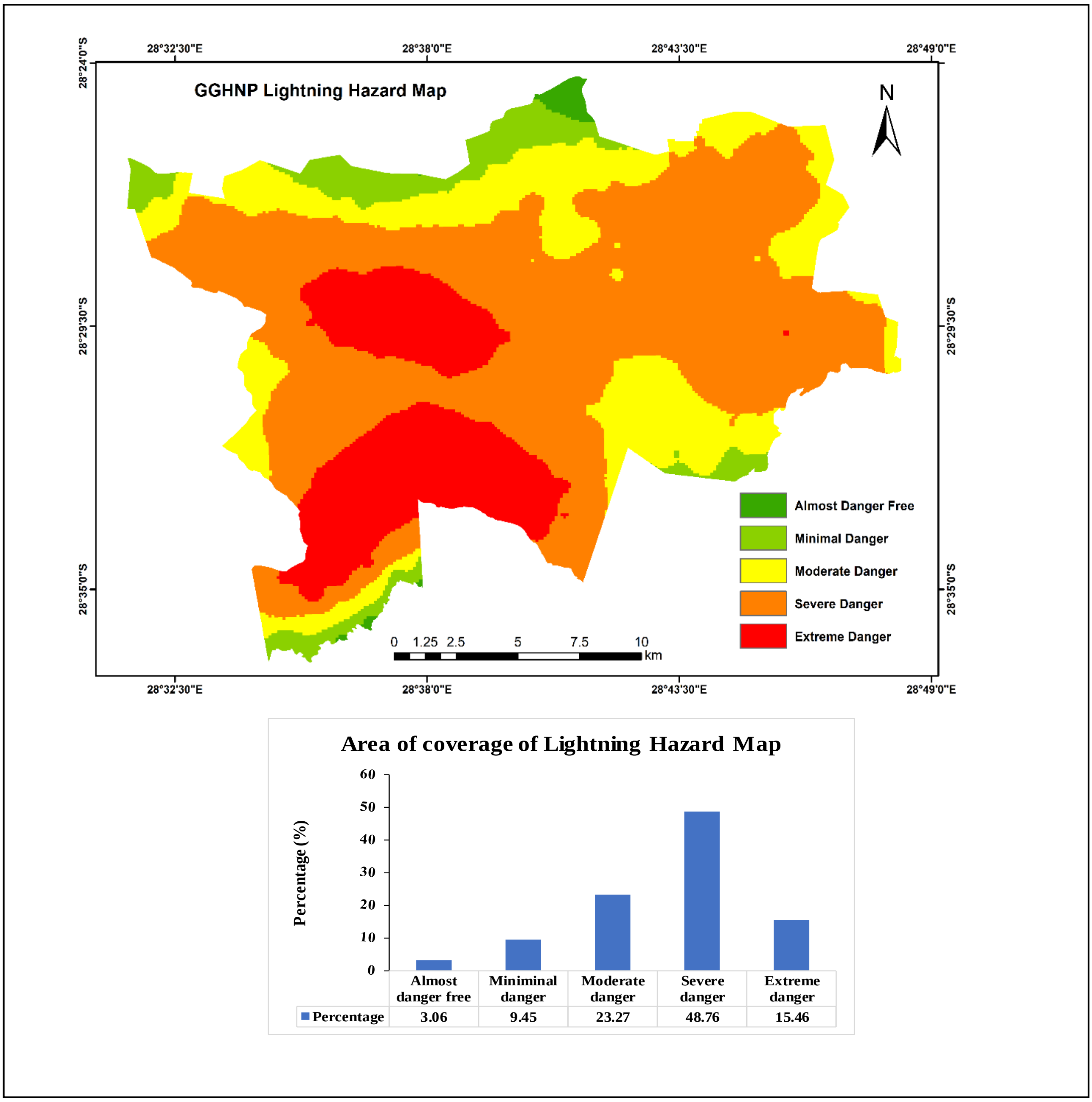

Figure 3.9: Lightning hazard map for GGHNP (2007–2017) showing coverage extent of hazard severity

3.3.6 Regression Analysis

In order to explore the relationship between the developed LHM and the terrain parameters (aspect, slope, and elevation), vegetation type, and fire scars, the regression analysis was executed. OLS regression (Table 3.4) yielded a model that explained 77% of the variation in lightning hazard map as explained by R2 value of 0.77. The coefficient statistic which explains the type and strength of co-relation showed negative relationship between LHM and aspect (-0.0424). However, positive and statistically significant relationship was found on fire scars (4.5668), slope (0.683), vegetation (0.021), and elevation (0.0029). These results are in agreement with the study conducted in Yellowstone National Park (Amrhein, 2017), whereby there was no relation of any aspect with lightning activity. The predictor variables used to predict spatial clustering all have variable inflation factor (VIF) less than 7.5 (Table 3.4) indicating little redundancy amongst variables except fire scars. However, fire scars have a robust relation with LHM.

The model was identified as statistically significant owing to the very low value of Joint F- and Wald-Statistic that is smaller than 0.05. With the Koenker (BP) statistics showing no statistical significance indicate that the model is consistent in data space, the variation in the relationship between predicted lightning strike density and explanatory variables does not change within explanatory variable magnitude. Therefore, there is no heteroscedasticity (non-constant variable or non-stationary) in the model. The Jarque–Bera Statistic test was also not statistically significant indicating that the regression residuals are normally distributed with a p-value higher than 0.05, therefore the model is unbiased. The adjusted R2 and AICs values of the model are 0.63 and 73.66, respectively, validating the sound performance of the predicted model.

Table 3.4: OLS regression diagnostic for the entire dataset

Dependent variable	Lightning					
Variables	Coefficient	StdError	t-Statistic	Probability	Robust_Pr	VIF
Aspect	-0.0424	0.0606	-0.6949	0.4970	0.4884	1.41
Elevation	0.0029	0.0008	3.5989	0.0024*	0.0003*	2.14
Slope	0.0683	0.0699	0.9773	0.3429	0.2706	1.72
Vegetation	0.0211	0.0676	0.3125	0.7586	0.6393	1.35
Fire	4.5668	6.1007	0.74857	0.4649	0.008631*	37.164
R-Squared	0.770884	**Wald-Statistic**	0.000000*			
Adjusted R-Squared	0.670646	**Koenker (BP)**	0.415350			
(AICc)	73.663751	**Jarque-Bera**	0.789538			
F-Statistic	0.000382*					

3.4 Discussion

The study revealed the outcomes in assessing the spatio-temporal patterns of CG lightning activity over the GGHNP. The application of statistical spatial autocorrelation and clustering techniques such as Global Moran I and Getis–Ord Gi* was effective in delineating the LHM, identifying what areas of the park experience clusters of lightning activity. The regression analysis was performed testing the relationship between the developed LHM and physical properties of GGHNP terrain.

The monthly strike count increases from the minimum value in July (0.08%) and displays a peak in December (23.80%) as shown in Table 3.1. It was observed that the maximum lightning strikes count occurred in the summer months (DJF), accounting for 56.26% of the total lightning strikes. This is followed at a distance by the spring (SON) and autumn (MAM) months. SON and MAN accounted for 28.84% and (14.22%), respectively, with the lowest count in the winter (JJF) months (0.68%). Also, it was observed that as the winter season progresses, that is April upwards, lightning strikes count showed a decreasing trend. This decreasing trend during the autumn season moving into the winter season is constituent with (Dewan *et al.*, 2018) who reported a shift in lightning strikes count with the change in season in Bangladesh. The summer peaks and the consistent monthly variability are consistent with (Bhavika, 2010) and (Mayet, 2016). The lightning strikes observed during summer months are associated with the nature of the terrain leading to orographic forcing; the increase in the total precipitable water column as a result of abundant moisture in the atmosphere; an increased surface temperature due to intense solar heating leading. The persistent heating of the land atmosphere creates instability in the atmosphere, by enhancing convection activities leading to severe storms heralded by lightning.

The average diurnal variation (2007–2017) as depicted in Fig. 3.2 suggests that lightning is more prevalent in terms of occurrence from 14:00 to 18:00 SAST with two clear maxima at 15:00 SAST and 17:00 SAST. The lowest lightning activity is during the morning hours at 05:00 and 06:00 SAST, and yet again at hour 08:00 SAST. A 24-h distribution of lightning activity was divided by 6-h periods revealed the following pattern: early mornings (00–05:59) 7.82%, late morning (06:00–11:59) 3.72%, afternoon (12:00–17:59) 55.60%, and evening (18:00–23:59) 32%. From the foregoing, within the GGHNP, the lightning activity follows an afternoon–evening maxima. A comparison of diurnal variation across the seasons reveals that lightning activity is predominantly late afternoon-type, although it is not evident in the winter season. Both summer and autumn have prominent peak at 17:00 SAST and spring at 15:00 SAST. During winter, lightning activity is greatly diminished, however, there is a prominent peak at 02:00 SAST. The diurnal variability and inter-seasonal diurnal variability observed in Figs. 3.2 and 3.3 are in agreement with the study by (Dewan *et al.*, 2018), which found that peak lightning activity usually occurs during the afternoon-evening hour.

Number of factors may be related to this type of diurnal variation; these include diurnal solar cycle leading to destabilisation of the atmosphere and development of convective particular in springs and summer seasons (Williams, 1994). In south-western and north-central part of GGHNP, topography forcing the Thaba Bosiu Plateau and the foothills of Maloti Mountains allow convection and associate lightning to develop. Thus, topography in conjunction with synoptic system may lead to convective development (Qie *et al.*, 2003) subsequently to the development of thunderstorm and lightning. Early morning peaks observed in winter season might be attributed to land and sea breezes circulation, nocturnal valley wind which promotes convection to early mornings and vertical wind shear for local convection (Dewan *et al.*, 2018).

Regional road that passes through the GGHNP may enhance aerosol in atmosphere caused by increased anthropogenic activities within and adjacent to the park. The study by Mushtaq *et al.* (2018) showed that presence of aerosol in the atmosphere may affect the lightning activity. South-western and northern central part of GGHNP support the notion that mesoscale convective is higher in the mountainous area. Qie *et al.* (2003) articulated three trigger mechanisms of such concept as (a) orographic and terrain effects, (b) presence of wind discontinuity line or dry line, and (c) availability of vegetation moisture. Since these areas of the park are dominated by moderate height terrain, orographic lifting with respect to complex terrain could initiate conditional instability of atmosphere which favours the development of thunderstorm-facilitated lightning. Therefore, these mechanisms influence the spatial clustering of lightning activity over the study area.

Spatial autocorrelation analysis revealed that the clustering of lightning strikes at the park is at a distance of about 1.2 km. This connotes that strikes clustered with other strikes are not likely to strike an individual specific location from centre of cluster of strikes much beyond a circle with radius of 1.2 km. While Global Moran *I* revealed that clusters are between 2km to 8km Spatial regression analysis (OLS) identified that elevation, slope, vegetation type, and fire scars are as statistically significant and positive in predicting the development of LHR. The vegetation-type variable was statistically significant showing a positive relation with LHM. This relation of vegetation type with LHM could be viewed in light of the vegetation of the study area. GGHNP is predominantly an Afromontane grassland park. There is a conjecture that grassland has much higher sensible heat flux because they have senesced during dry season, and an increased sensible heat flux may drive thermal convection and increase lightning activity. Although fire scars were found to be the only variable with the highest IVF values, which is responsible for multicollinearity and the most variables with the robust correlation with the LHM. This multicollinearity is due to the fact that the short-period dataset (I year dataset) was used for this variable; therefore, increasing the sample size or long-period dataset could be a solution (Environmental Systems Research Institute (ESRI), 2013). A small fire scar will show an increase in heating, but its impact on the heating of the boundary layer will be minimal (Kilinc and Beringer, 2007).

3.5 Conclusion

To the best of our knowledge, this is the first study of its kind to make use of SALDN data over the mountainous protected area to explore the statistical spatial and temporal patterns of lightning activity: the first to employ spatial analysis techniques to determine the clustering of CG lightning within the GGHNP. Global clustering spatial pattern was calculated using Global Moran *I* employed on lightning-strike for the entire dataset (2007–2017), and monthly and hourly data revealed that there is strong evidence of global clustering and spatial patterns are statistical spatially significant and appear to be clustered except in July, late morning hour of 06:00, 08:00, and 09:00 SAST. The study demonstrated that the overall spatial pattern of CG lightning activity varies with time due to regional and local weather patterns as influenced by a large scale of climatic nodes (ENSO and SAM). This relationship still needs to be explored. Monthly variation revealed that lightning activities are at peak during summer, in December, while diurnal variation revealed afternoon-evening maxima attributed to orographic effect, availability of abundant moisture, and diurnal solar heating cycle. The developed LHM revealed that almost 16% of the study area is at extreme risk of lightning. OLS helped to identify the key factors contributing to the lightning threat being elevation. The study is a step towards new information regarding the spatio-temporal distribution of CG lightning. The data derived from this study would be of significance for wildfire models used to predict, monitor, and assess the lightning-induced wildfire. Knowing where and when lightning is mostly to cluster will allow managers to preposition suppression, plan for fuel treatment, and prepare fire prevention and public safety(Van Wagtendonk and Cayan, 2008). Although this study furnished some initial results, incorporating strikes characteristics (polarity, multiplicity, and strength), regional climate conditions and local weather patterns that result from physical geography of GGHNP would advance the understanding of spatio-temporal distribution of CG lightning activity. Knowledge of why positive or negative clusters occur in the study area can be used to improve lightning-induced wildfire models.

CHAPTER 4

MODELLING AND ASSESSING TEMPORAL DISTRIBUTION OF ANTHROPOGENIC FACTORS IN A PROTECTED AREA FOR FIRE DANGER ASSESSMENT


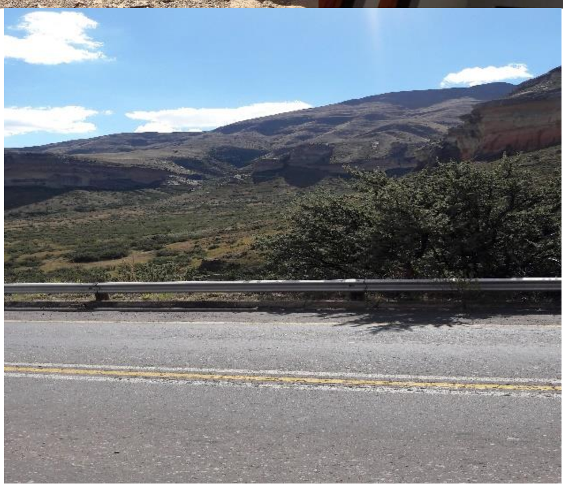

This chapter is based on:

Mofokeng DO and Adelabu SA (2021). Modelling and assessing distribution of anthropogenic factors in a protected area for fire danger assessment. Journal of Geography & Natural Disaster .11: p358

Abstract

Human activities threaten the effectiveness of Protected Areas in preserving key natural resources. Ignoring the temporal dimension of human on fire occurrence can lead to ineffectiveness fire management and preserved outcomes. This study explored the intra-annual dimensions of fire occurrence and two (2) mostly used anthropogenic fire triggers, i.e. distance from the roads (ROADS) and tourist infrastructures (INFRA) for the Golden Gate Highlands National Park of South Africa. MODIS Terra Collection 6.1 fire hotspot data for the period of 11-years (2007 -2017) was used to construct four (4) occurrence data scenarios (models) by splitting occurrence data into two seasons (Spring and Winter) and further into weekdays and weekends. MaxEnt method was used to assess the performance of the models and to explain the importance of each explanatory variable. Results revealed INFRA as the most important factor across all the models and had the highest contribution to the Winter_W_End and Spring_W_End models. ROADS as the most contribution to the Winter-W-Days and Spring-W-Days models. In addition, we observed strong temporal variation with ROADS strongly influencing weekdays of both seasonal scenarios while INFRA shows strong influence in the weekends. Model overall performance is satisfactory, above 0.8 AUC values for all the models (Winter Weekend = 0.977; Winter Weekday = 0.929; Spring Weekend = 0.896) except Spring Weekday (0.641). In addition, Winter models are more robust in explaining the temporal distribution of human-caused fire ignition factors of the study. The results are reliable and significant for advising practical wildfire management and resource allocation as well as to predict the human-caused fire ignition.

Keywords: *Wildfires; human/anthropogenic factors; MaxEnt; temporal dimension. Protected area*

4.1 **Introduction**

Fire is a natural disturbance in many ecosystems and is applied as one of the management tools for maintaining a healthy ecosystem particularly in Protected Areas (PAs). International Union for Conservation of Nature (IUCN) defined PA as a clearly defined geographical space, recognized, dedicated and managed through legal or other effective means to achieve the long-term conservation of nature with associated services and cultural values (Molaudzi and Adelabu, 2018). Africa has a long history of fire longer than any other continent but current fire management issues on the continent are complicated. For instance, the global pressure to initiate climate mitigation programme in Africa often involve changes in how fire is applied (Archibald, 2016). Application of fire in the PAs is conundrum driven by the safety policies and regulations that have led to the reduction of fire ecological benefits (Pereira *et al.*, 2012; Mansuy *et al.*, 2019).

Fire management strategy which includes fire prevention may be the most cost-effective and effective mitigation programme (Food and Agricultural Organisation (FAO), 2007). The strategy includes but not limited to awareness campaigns and or risk mitigation. In wildfire, risk is a chance of fire starting and spreading (danger) as well as its potential damage over environmental and human resources (vulnerability)(Chuvieco *et al.*, 2010; Eskandari and Chuvieco, 2015). Therefore, wildfire risk is a combination of wildfire “danger” and vulnerability. The concept of wildfire danger describes the factors affecting the inception, spread and resistance to control (Martín *et al.*, 2019). Wildfire danger is related to both fire ignition and propagation. The former depends on the fuel amount and moisture and the presence of external cause (anthropogenic or natural) leading to fire start (Eskandari and Chuvieco, 2015).

While fire ignition is an integral component of wildfire factors, it is critical in wildfire danger because the chances of wildfire to start is minimal no matter how dry weather conditions and how the vegetation flammability is (Ye *et al.*, 2017). As confirmed by data all over the world, human presence in landscape increases the number of ignitions even above the background from lightning. Human affects fire regime directly by altering the number and timing of ignition of fire and indirectly by altering fuel (Archibald, 2016). Henceforth, an improved understanding of wildfire risk should address the patterns of human activity and its relation to fire ignition. A key resource for wildfire risk is risk zoning and mapping, a subject on which Geospatial technology (Geographic Information Systems and Remote Sensing) and spatial statistic have been traditional applied (Martín *et al.*, 2019).

Noteworthy, studies have been undertaken to explore the relationship between wildfire and its causative factors with the main aim of building predictive and explanatory models. A review study on human cause fire occurrence modelling by Costafreda-Aumedes *et al.* (2018) revealed that on annual average 14 papers were published between 2012 and 2016. Most of these researchers construct these models with the different motivations ranging from fire prevention, fire suppression, for supporting fire management strategies and to develop early warning system as well as for conservation goal. However, Ye *et al.* (2017) suggested that modeling on human activity and its pattern is more appropriate for supporting decision making in wildfire preventions rather than firefighting and management after ignition. Although modeling and evaluating of human activity as an agent of ignition is a complex task since it requires the identification and quantification of human behaviour, a number of authors have showed that fire ignitions exhibit strong preference for distance to roads, settlement and infrastructure (Genton *et al.*, 2006; Martínez *et al.*, 2009; Arndt *et al.*, 2013; Martínez-Fernández *et al.*, 2013; Vilar *et al.*, 2016; Zhang *et al.*, 2016; Ye *et al.*, 2017; Mancini *et al.*, 2018; Vacchiano *et al.*, 2018; Martín *et al.*, 2019). However the effects of different human-related drivers on fire ignition change over time and space, and among ecosystems (Vilar *et al.*, 2016).

Several methods have been employed to model and evaluate the human-related drivers to fire ignition. Logistic regression has been intensively applied as they can handle unbalanced sample for rare wildfire presence versus common wildfire occurrence (Martínez *et al.*, 2009; Arndt *et al.*, 2013; Zhang *et al.*, 2016; Mancini *et al.*, 2018) and Geographically Weighted Regression (GWR) (Martínez-Fernández *et al.*, 2013). However, most of the used techniques suffer from multicollinearity problems (Costafreda-Aumedes *et al.*, 2018). Machine learning algorithms such as Random Forest (RF) (Archibald *et al.*, 2009), Classification And Regression Trees (CART) (Sturtevant and Cleland, 2007) and Weight of Evidence (WoE) (Ye *et al.*, 2017) properly predict and explain fire occurrence. One of the advantages of these algorithms is that they are non-parametric models and their input explanatory variables interrelationship are not defined a prior but rather derived from iterative training and testing using random data subset (Vilar *et al.*, 2016). Recently, one of the existing machine learning tools, presence only Maximum Entropy (MaxEnt) saturated the wildfire literature since it demonstrated high prediction and explanation accuracy than other plant and animal species distribution methods. As fire ignition distribution may be compared to species distribution, some researchers applied MaxEnt to model human-related drivers to wildfire occurrence (Massada *et al.*, 2013; Vilar *et al.*, 2016; Mansuy *et al.*, 2019; Martín *et al.*, 2019).

Wildfire occurrence contain a temporal dimension which often requires temporal perspective (Carmona *et al.*, 2012). However, these temporal perspectives of anthropogenic drivers are frequently overlooked and these drivers enter the modelling as structural “static”. For instance the models developed by (Chuvieco *et al.*, 2010; Del Hoyo *et al.*, 2011; Eskandari and Chuvieco, 2015). This implies that they have no temporal variation in its influence as fire-trigger factors as explained by (Martín *et al.*, 2019). By considering the temporal dimension of fire occurrence and fire-trigger factors in their study, they found out that modelling utilizing temporal scenarios enhances understanding of anthropogenic drivers. Although previous studies have created the models for predicting and explaining the human-related drivers in wildfire occurrence, fewer studies have focused on Afromontane grassland protected landscape or taking into account the temporal dimension of these drivers. This study using fire occurrence data spanning for 11-year period (2007 to 2017) aim to create seasonal and day-type models that consider temporal behaviour of anthropogenic drivers over wildfire occurrence applying MaxEnt method to explore the influence of anthropogenic drivers as a causal agent of the fire ignition either by accident or negligence to each model and how sensitive are these models are to the anthropogenic drivers. Finally, determine the best temporal model that can be used to facilitate the decision making on the preparation of the fire prevention plan.

4.2 **Methodology**

4.2.1 Datasets and source

4.2.1.1 Fire occurrence data

The dependent variable – Wildfire occurrence was obtained from Moderate Resolution Imaging Spectroradiometer (MODIS) Collection 61 of NASA Fire Information for Resource Management (FIRM). The dataset has limitations as it does not distinguish between fire causes (either natural or human) and as a result makes it difficult to analyze each explanatory variable in its causality context (Zhang *et al.*, 2016). However, the MODIS active fire points represent fire activities being recorded at given times and locations that implies they contain information on both ignition and spread. The provisions of how the dataset is acquired and algorithms used are available on Davies *et al.* (2008) . The fire events of the 11 years spanning from 2007-2017 was selected for this study.

4.2.1.2 Independent variables

According to the basis of variable performances and their relationship with wildfire ignitions, the distances to roads and railways, and tourist sites are mostly considered as anthropogenic drivers that possible cause of wildfire ignition by accident or negligence (Archibald *et al.*, 2009; Martínez *et al.*, 2009; Arndt *et al.*, 2013; Ye *et al.*, 2017; Costafreda-Aumedes *et al.*, 2018; Mancini *et al.*, 2018; Ricotta *et al.*, 2018; Vacchiano *et al.*, 2018; Mansuy *et al.*, 2019; Martín *et al.*, 2019). Hence, this study used roads and tourist site as the variable to evaluate the influence of human activities on fire occurrence. Several anthropogenic factors that can be used are discussed (Section 1.3.5). A polyline vector of road map and a point vector of tourist sites map were obtained from South African National Parks (SANParks), Scientific Service Department. Furthermore, global position coordinates of tourist sites as shown in Figure 2.2. were obtained for verification.

4.2.2 Methods

4.2.2.1 Fire occurrence data

The fire hotspot data was downloaded in a point vector layer, and projected to UTM Zone 35S. The attribute information contains acquisition date of the fire point. Select by attribute table tool of ArcMap software was used to select the months according to the seasons and days of the week. Figure 4.1. illustrates the uneven temporal distribution of wildfire at both monthly and daily scale for the period of 11-year (2007 -2017). The monthly distribution shows bimodal pattern with peaks in August and September, which is conditioned by tourism seasonality of human beaviour and weather conditions as described by Martín *et al.* (2019). Similarly, the daily distribution is biased towards weekends showing a variation in the temporal pattern of wildfire activity.

Fire points by season was created resulting into two (2) seasons, i.e. Winter (June, July, August) and Spring (September, October, and November). The calendar of specific year was used to determine the days of week on which the fire occurrence to further split season's layers into days of the weeks. Monday to Friday was categorized as weekdays while Saturday and Sunday was categorized as weekend. Database of fire occurrence by days of the week of the seasons were created. This led to creation of four (4) intra-annual scenarios and serve as dependent variable of each model (Table 4.1). To meet the requirement of MaxEnt model, the dependent variables were converted into comma delimited (.csv) format.

4.2.1.2 Independent variables

Multi-ring buffer zone method was employed to create multiple buffer zone at the distance of 100m, 200m, 300m, 400m, 500m respectively for these two layers (ROAD and INFRA) in order to determine how many fire points intercept each buffer zone. Since the output of multi-ring buffer analysis is polygon, polygon to raster conversion tool was used to convert the layers into a raster format at cell size of 30 meter. As the MaxEnt model dictate for input variables should be in ASCII raster format, raster to ASCII conversion tool was used to convert independent variables into spatialized in ASCII raster format. ArcMap Software was used as

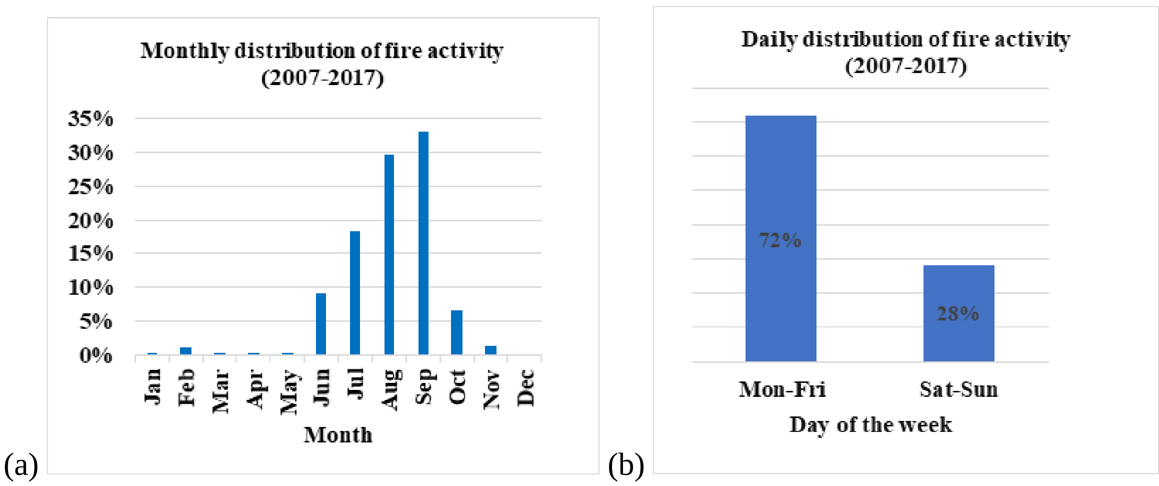

Figure 4.1: Distribution of fire activity for the period from 2007 -2017 (a) Monthly; (b) Daily

Table 4.1: Temporal Scenario

Model	Name	Description
1	Winter_W_Day	Weekdays of Winter
2	Winter_W_End	Weekend of Winter
3	Spring_W_Day	Weekdays of Spring
4	Spring_W_End	Weekend of Spring

4.3 Modelling approach

Maximum Entropy (MaxEnt), a machine learning method was applied for modeling the anthropogenic factors for fire ignition in this study. MaxEnt is described as estimating a distribution across geographic space and was originally developed to be used for species distribution and environmental niche (Phillips *et al.*, 2006). The method has been extensively used for fire modeling studies (Parisien *et al.*, 2016; Vilar *et al.*, 2016; Mansuy *et al.*, 2019; Martín *et al.*, 2019). MaxEnt iteratively contrasts environmental layers (anthropogenic predictor values) at occurrence location (fire ignition points) with those large backgrounds sample of random locations taken across the study area (Elith *et al.*, 2011). Data for running MaxEnt software, sample data (fire occurrence data) and environmental predictors (roads and tourist's facilities _ infra) were prepared guided by the approach applied by Brown (2014) using ArcMap. A standalone MaxEnt Species Distribution Modeling Version 3.4.1. software version was chosen and the following were checked before the model runs: create a responsive curve, make pictures of predictions and do jackknife to measure variables importance.

A jackknife test was used to investigate the importance of an individual anthropogenic variable for MaxEnt predictions. The blue bars depict the accuracy and performance of the variable when used in isolation. While the turquoise bars represent the model's overall accuracy when each variable ix excluded from the model. The area under the curve (AUC) of the receiver operating characteristics (ROC) was used to measure each model 's performance and validation (Clarke *et al.*, 2019). The ROC curve is a graphical representation of the false-positive error (1-specificity, where specificity is the proportion of incorrect prediction) versus the true positive rate (also known as sensitivity or proportion of correct prediction) for binary classifier system and different values of the discrimination threshold (Zhou *et al.*, 2009). AUC is a threshold-independent metric because it evaluates the performance of a model at all possible threshold values by adding up the area between the ROC and random performance line (Martín *et al.*, 2019). AUC is valid to estimate AUC values range from 0.5 to 1. Excellent model performance is suggested by AUC values higher than 0.9, a moderate good performance by values between 0.7 and 0.9, and poor model performance by values from 0.5 to 0.7 (Fawcett, 2006).

4.4 Results

4.4.1 Variable contributions to the models

The analysis of variable contributions as depicted in Fig.4.2 revealed that INFRA as the highest variable contributing to Spring_W_End model accounting for 97.9% (Fig 4.2(d). However, INFRA was the lowest variable contributing to Winter_W_Day model accounting for 16.6%. ROADS as the highest variable contributing to the Winter_W_Day model accounting for 83.4%. However, ROADS was lowest contributor in favour of INFRA with 2.1% and 97.9% in the Spring-W-End model respectively. INFRA was revealed as the most important variable in all the models, the top most observed during Winter_W_End (79.3%), followed by Spring_W_End (71.3 %), Winter_W_Day (54.9%) Spring_W_Day (52.9%).

Figure 4.3 represents the jackknife test results of the models indicating the most significant variables influencing the fire occurrence. According to the jackknife test of variable importance, the anthropogenic variable that gains most was ROADS during weekdays when it was omitted, which therefore appeared to have more information that was not present in INFRA (Fig 4.3.). In contrast, INFRA performance a key role during weekends in both Summer and Winter seasons.

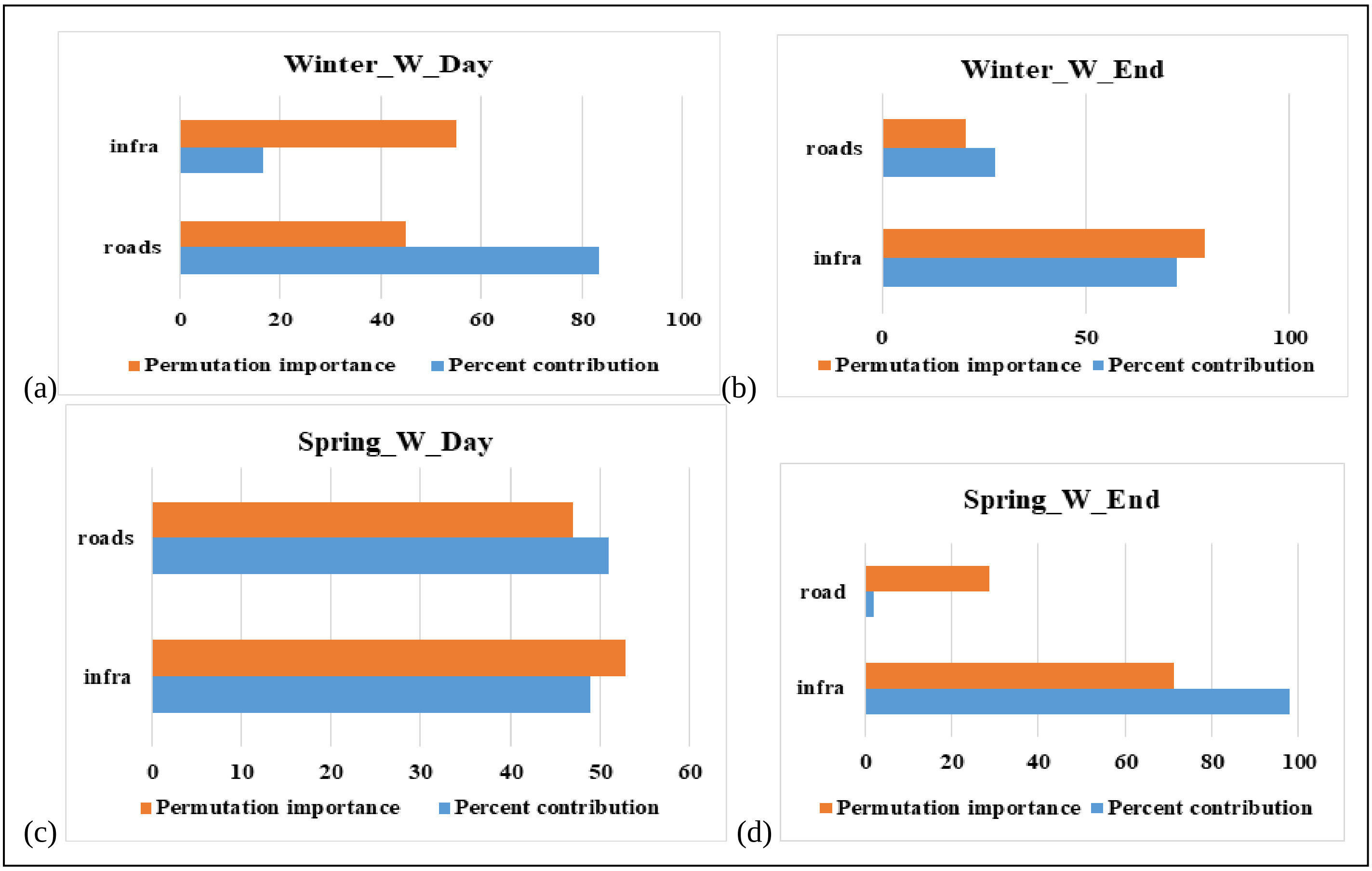

Figure 4.2: Contribution of the anthropogenic variables to the models (a) Winter_W_Day; (b) Winter_Wend; (c) Spring_W_Day; and (d) Spring_W_End

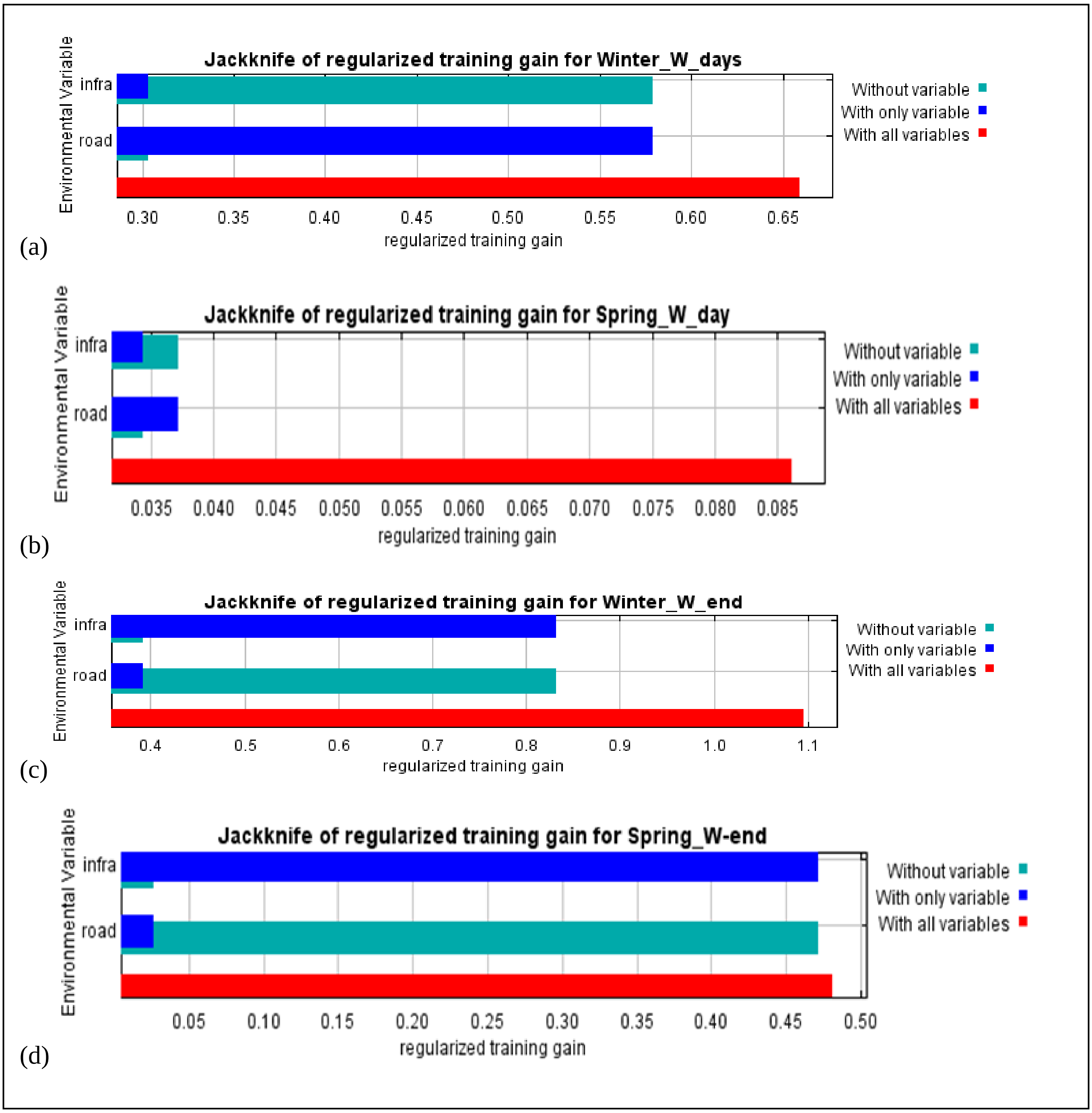

Figure 4.3: Jackknife estimation of variables importance to the models: (a) Winter_W_Day; (b) Winter_W_End; (c) Spring_W_Day; and (d) Spring_W_End

The response curve of fire occurrence to the anthropogenic variables classifies the quantitative relationship between logistic probability and anthropogenic variables. Moreover, we can deepen the niche of fire ignition by explaining the response of each model to the distance of these variables. According to the response curve as shown in Fig 4.4., which reveals that the likelihood of fire ignition is higher at 100m from the distance to the infrastructure during weekdays, 200m during weekends in Winter. While in Spring models are at 200m and 400m during weekdays and weekends respectively.

Looking at the response curve of winter models to ROAD, a higher likelihood of fire ignition in relation to distance to the road is observed at 500m and 200m during weekdays and weekends respectively. Both Spring weekday and weekend models show the maximum probability of likelihood of fire ignition is 300m from the distance to the road

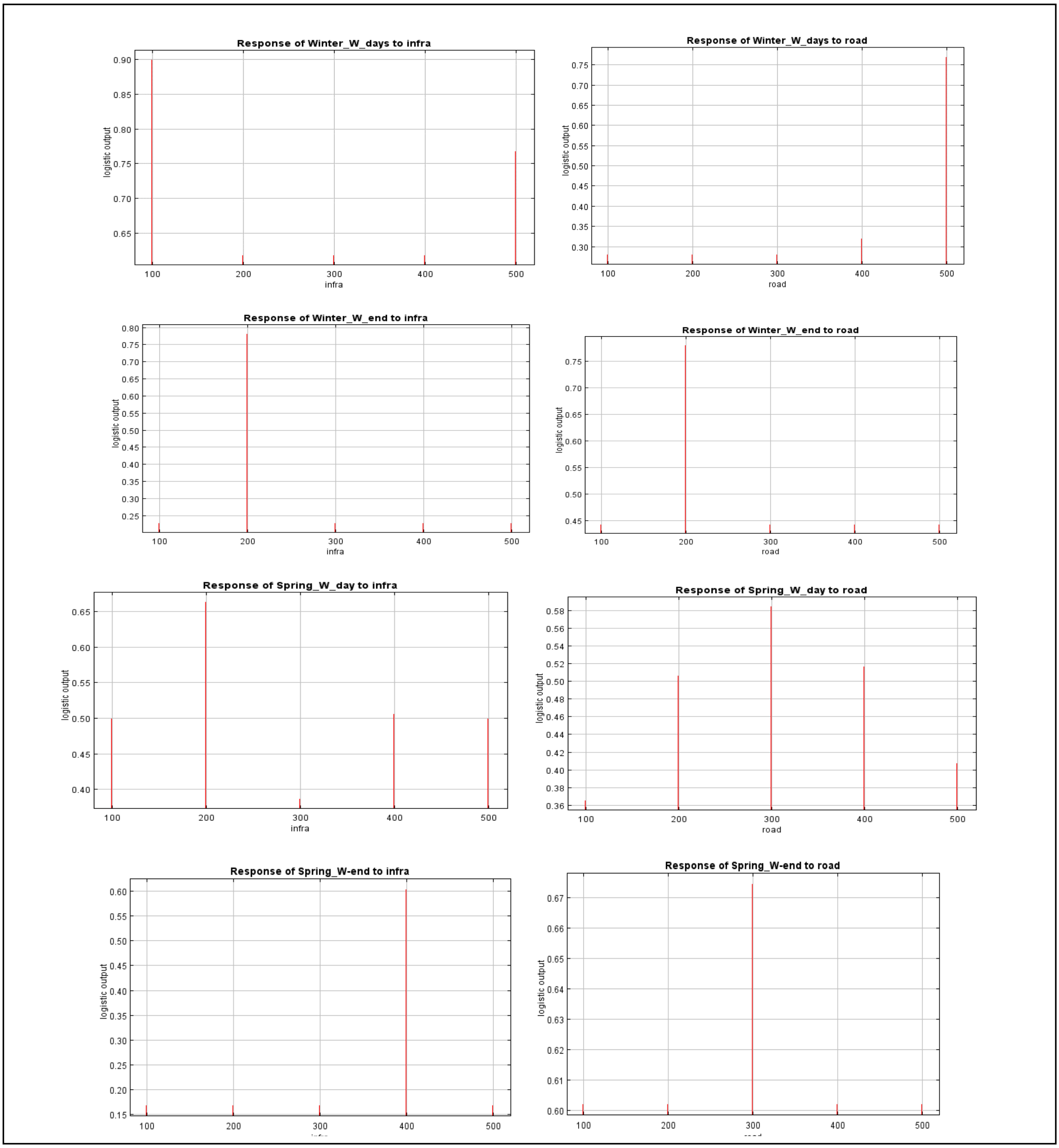

Figure 4.4: Response curves showing the relationship between anthropogenic drivers and fire occurrences of all models

.

4.5 Model Performance

Figure 4.5. represents the ROC results with AUC values of the models. According to AUC values, the highest prediction capacity is reached in winter especially during the weekend (0.977), followed by weekdays (0.929) and spring weekend with 0.896. While the lowest is found during spring weekday (0.641). However, the overall performance of the models based on the average performance is moderate good performance (0,861) as the prescribe accuracy threshold proposed by Fawcett (2006).

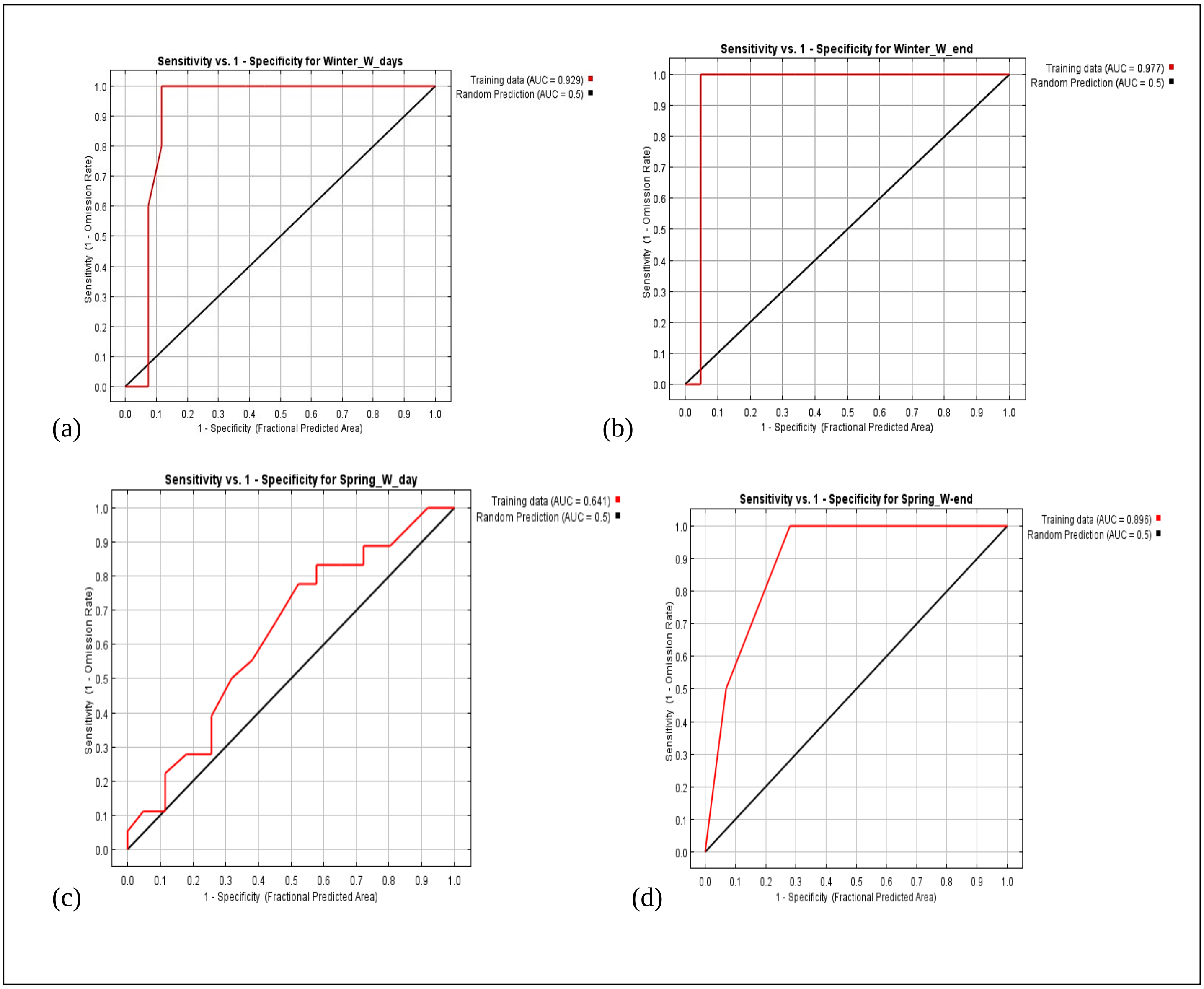

Figure 4.5: The ROC/ AUC curve of all the models; (a) Winter_W_Day; (b) Winter_W_End; (c) Spring_W_Day; and (d) Spring_W_End

4.6 Discussion

Our models can explore the influence of anthropogenic drivers as the causal agent of wildfire ignition. The results of this study confirm the dominance of infrastructure as the key contributor to wildfire ignition, which is in consistent with the findings of earlier studies (Arndt *et al.*, 2013; Massada *et al.*, 2013; Parisien *et al.*, 2016; Vacchiano *et al.*, 2018). Fire ignitions are more likely to occur close to roads due to accident, negligence or arson since roads act as conveyors for arsonists, careless drivers, and campers). INFRA is consistently the most important variable in all the models. However, the contribution to temporal distribution is not similar in all models, it was dominant in both Spring and Winter week end days. Similarly, as observed in Fig. 4.5 the influence of ROADS is highest during weekdays of both seasonal scenarios. This finding disagrees with the common conclusion that ROADS contribute more during weekends which can be attributed to the traffic increase experience during weekends and holidays as people tend to travel more frequently during these days especially in natural or forest environment (Martín *et al.*, 2019). The maximum importance of ROADS during weekdays in the study area may be attributed to the regional or public road (R712) passing through the park that connects major towns within the district (Fig 2.1). Activities by passers-by in such a road increase the probability of ignition. INFRA (tourist's facilities) finds its maximum contribution to the models during Spring Weekends the most important anthropogenic factor to models. Moreover, the influence of INFRA was found to be strong in weekends day-type of both seasonal scenarios. This coincides with the recreational activities in the park and tourism hub of the province (South African National Parks (SANParks), 2020). Furthermore, may be related to the favorable weather conditions of Spring warming, conditions that promote fuel dryness which leads to higher ignition probability.

Considering the sensitivity of models to the ROADS and INFRA, as we observe in Fig 5 wildfire ignition patterns vary with time and distance (space). This finding confirms the novelty of the relationship between human activity and wildfire occurrence is not linear (Bowman *et al.*, 2011a; Archibald, 2016). In Winter Weekend response to both ROAD and INFRA, area between 100m and 200m have high influence to fire ignition and likelihood decreases as the distance increase. This might be explained by the reality that most distant areas are highly rugged topography and not accessible to humans (Ye *et al.*, 2017). Similarly, in Spring Weekend higher ignition probability is observed in distance to INFRA of 100m to 200m. In Spring Weekday and Weekend wildfire is easily ignited by the human in a medium distance from the ROAD of 300m and Spring Weekend to INFRA (400m). The explanation might be illegal livestock shepherds' and arsonists seek remote areas to avoid capture. This finding shows how wildfire prevention or mitigation measures should proceed. Attention should be paid to areas directly adjacent to ROADS and INFRA during weekends in Winter and Spring Weekdays to INFRA. Distant zones should receive more attention during Spring Weekend to INFRA. Overall during weekends INFRA is the most influential anthropogenic factor while weekdays fire ignition probability is influenced by ROADS.

Nonetheless the drawbacks of MODIS active fire product including indistinguishable of its ignition sources, we use the MODIS data rather than the historical fire records in this study. Because of its accessibility, ability to assess the suitability of model and explore the variation of spatio-temporal pattern in the study area. Modelling human-caused ignitions probability by means of temporal dimension enhance our understanding of human activity to wildfire prevention. On average, the overall performance of our models is satisfactory (0.861). Our model outperform those other models based on intra-annual models. For example,Arndt *et al.* (2013) study in modelling human-caused fire ignition for assessing fire danger in Austria the models created using logistic regression method reported 60.5% of model performance. Furthermore, the reported performance of dynamic model proposed (Martín *et al.*, 2019), the highest prediction model process was 0.860 observed during summer months. It should be noted that their research considered the temporal dimension of human factors. The research was conducted in NE Spain using MaxEnt and wildfire data (2008-2012), they constructed eight fire occurrence data scenarios and assess their model accuracy using a cross-validation k-fold procedure. The reported performance of our models is clear low in Spring season particularly during weekdays, this might the explained by fewer fire occurrence experienced during this period. Our results have demonstrated that Winter fire occurrence data is more suitable for modelling and assessing the human-caused fire ignitions of the study area.

4.7 Conclusion

In this study, we used fire ignition data from MODIS spanning from 2007 to 2017 to construct four occurrence data scenarios. Considering the temporal dimension in modelling human-caused fire ignition is a foundation for efforts towards creation reliable and accurate predictions and explanation models. Application of MaxEnt method provided us with the mechanism for evaluating the performance of different temporal scenarios and the importance of the explanatory variables to the models. MaxEnt provided optimal opportunity to reflect distinct temporal distribution in different explanatory variables. Categorical MaxEnt proved to be a useful approach as it avoids problems of dealing with false, unreliable and pseudo-absences (Vacchiano *et al.*, 2018; Martín *et al.*, 2019) and it is relatively straightforward to implement and interpret. The study revealed that tourist's infrastructure (INFRA) as the most anthropogenic factor influencing fire ignition during week-end days (Saturday and Sunday) and roads influence fire ignition during weekdays (Monday to Friday). From this temporal perspective, the fire prevention or management plan of the GGHNP during the period in Spring and Winter should be adjusted according to the days of the week on which each human caused factor shows the influence on fire occurrence. Regardless of the overall performance of the model is satisfactory, improvement of the models would be achieved by introduction precise fire ignition or occurrence data that can identify source of ignition type, with lower omission error. Furthermore, the improvement of the model might be achieved by parsing the explanatory variables, for instance, distance to main road, secondary road, hiking trails, distance to hotels, campsite

CHAPTER 5

MODELLING AND ESTIMATION OF GRASS CURING FOR FIRE DANGER ASSESSMENT

This chapter is based on

Olga D. Mofokeng, Samuel A. Adelabu, Olufemi S. Duronoju and Efosa. A. Adagbasa. (under review), *Grass Curing- driven fire danger index in a protected mountainous grassland using fused MODIS and Sentinel-2 data*, (TRES-PAP-2023-1758) International Journal of Remote Sensing.

Abstract

Curing refers to the evolution of live fuel into dead fuel component of fuel is a critical factor in fire danger assessment however rarely incorporated because direct measurements are scare, expensive and time consuming. Furthermore, curing from sparse measurement systems are unsuitable for landscape scale. This study assessed the spatio-temporal variation of degree of curing (DOC) for the Golden Gate Highlands National Park (GGHNP) for the period from 2016 to 2020. To estimate GCI, Index-then-Blend fusion method was applied to downscale MODIS indices to spatial resolution of Sentinel-2 data. The approach assumption is that linear mixture model is applicable to indices. Four commonly used soil and vegetation moisture content indices (GCI_Global Vegetation Moisture Index, NDVI & GVMI; GCI_Normalized Difference Moisture Index, NDVI & NDMI; GCI_Shortwave Infrared Water Stress Index, NDVI & SIWSI; GCI_Surface Water Capacity Index, NDVI & SWCI) were computed using Google Earth Engine (GEE) applying MapVictoria Algorithm. GCIs were converted into Grassland Curing Maps (GCMs) which were then synthesized into fire danger maps. The GCMs were used for correlation analysis with precipitation and soil moisture. For accuracy assessment, derived fire danger maps were overlaid with active fire points from VIIRS (FIRM). The results showed September and February as the month of highest and lowest DOC respectively, May as an onset month of increase of DOC. The GCMs revealed that almost 90% of the park vegetation is susceptible to fire. Accuracy assessment showed that all candidate GCIs exhibited the capability to estimate of DOC as maximum number of active fire points fell under high to extreme fire danger zone with GCI_NDMI (99%) outperforming other indices. The study contributes a valuable insight towards enhancing spatial resolution of fuel conditions for fire danger assessment and paved a way for the remotely sensed estimation of DOC for fire and fuel management of park and other fire agencies within mountainous grassland environment. The study can also be useful for the livestock agricultural practitioners and the games for pasture management.

Keywords: *Remote sensing, GIS, Grassland Curing Index, grass fire danger, Data-fusion*

5.1 Introduction

Grasses undergo large phenological transformation over the season, with dramatic changes in moisture content as the shoots emerged, mature and finally senesce and this transformation is commonly referred as “Curing”(Sjöström and Granström, 2023). Therefore, grass curing is refers to the process of grass senescence, or die-off and the transition of live fuels into the dead fuel component of fuel bed (Duff *et al.*, 2020). As a quantitative measure, (Kidnie *et al.*, 2015) describe curing as the proportion of dead material in grassland, as percentage , with significant effect on both the probability the fire to ignition and propagation (Anderson *et al.*, 2011). Curing influences how vegetation acts as fuel and is triggered by environmental factors such as photoperiod, water availability, competition and temperatures (McGranahan *et al.*, 2016). The timing of curing is strongly defined by productivity cycle, species adaptations and climatic conditions. For instance, in South Africa grasses will have their most significant die-off in Autumn (Everson *et al.*, 1988). Similarly, to tall grasses prairie grasses in southern Ontario, Canada which die-off in Autumn before snowfall (Kidnie and Wotton, 2015). On the contrary, in southern Australia, significant changes in grassland curing occurs in late spring (Martin *et al.*, 2015). In general, annual grasses grow in one season and die in the next season, a typical life cycle of annual grass species last to three to six months. Whereas perennial grasses may grow and live for several years. However, natural grassland may have an assortment plants with various life cycles resultant to patchy, heterogeneous curing patterns. Hence is it imperative to timely and accurately assess the degree of curing for fire management particularly where fire is used as the management tool.

Before the advent of remote sensing techniques, two direct field methods, namely, destructive sampling and visual observation were solutions to measure the degree of curing (DOC). Visual assessments depend on the field observers to estimate the general curing percentage over the landscape supported by photographic field guide (Anderson *et al.*, 2011). Hosking (1990) used visual assessment and developed an empirical grassland curing index (GCI) scaled 1 to 100 (percentage) that reveals the seasonal physiological development of grassland for Braidwood, New South Wales in Australia. Destructive sampling which entails collecting all fuel from a small area and sorting it into live and dead, and oven-drying (Everson *et al.*, 1988). These ground measurements were perceived as subjective, labour-intensity, cost-ineffective, time-consuming, vary significantly in their accuracy and are generally spatio-temporal sparse (Anderson *et al.*, 2011; Sharma *et al.*, 2020). Furthermore, non-destructive point intercept method of counting live and dead fuel touches a vertical pole, well-known as Levy Rod method was used by (Anderson *et al.*, 2011) and they found that this method provided an accurate estimate of DOC, however it was also time-consuming, tedious and expensive.

With the assumption that moisture content is proportional to the DOC, several studies used fuel moisture content for DOC estimation by solely using ground measurement or RS data or joint-use of RS data and ground measurement. For instance, Everson *et al.* (1988)in their study they developed a mathematical model which predicted the fuel moisture in Highland Sourveld at the Cathedral Peak' using field methods. Using fuel moisture their study found that curing is initiated at the end of April and progress rapidly up to middle of May. By June the grasses are 95% cured, increasing the fire danger in winter. Wittich (2011) observed an exponential relationship between decreasing grass-moisture content and increasing curing or yellowing level estimated from destructive sampling and gravimetrically. McGranahan *et al.* (2016) used fuel moisture from several species in two grassland locations in KwaZulu-Natal, South Africa to determine the variability of grassland fuel curing among species or across locations. The findings revealed that the magnitudes of variation do not suggest radical alteration of fire practice and planning.

Grassland Curing assessment that integrate satellite remotely sense and ground measurement data has been the subject of the earlier studies worldwide predominantly in Australia, where grasslands are the most widespread fuel type (Cheney and Sullivan, 2008). AVHRR and MODIS were most frequently adopted sensors in most studies but their poor spatial resolution of 1000 meter (m)and 500m limits the accurateness of the results as they failed to separate grassland from other land cover types (Li, 2020). Most recent study has estimated the inter-satellite variable (ISV) of three satellite sensors (Landsat, MODIS and Sentinel 3) to established on where and when to use which satellite for grassland observation (Li, 2021). Different spectral indices including NDVI, global vegetation monitoring index (GVMI), normalized difference water index (NDWI) have been adopted in most DOC estimation either as single variable or multiple variables through FMC and chlorophyll content monitoring (Kumar *et al.*, 2020). (Dilley *et al.*, 2004) used NDVI as a proxy of FMC from NDVI and relate to curing from ground measurement, and concluded that there was a strong negative linear relationship between curing and FMC, however with the different coefficient at different site. Similar exponential relationship between visual-curing and NDVI was observed by Allan *et al.* (2003) over red soils of the Victoria River District and Sturt Plateau region of the Northern Territory, Australia but with soil type variation. As they observed a linear relationship over black soils and year to year variations.

Chladil and Nunez (1995) established strong correlation between NDVI and GCI derived from time series of Soil Dryness Index (SDI). Newnham *et al.* (2010) used MODIS MOD0901 dataset over Australia and New Zealand to estimate curing from four models, namely, Map A: Linear Regression (NDVI), Map B: Multiple Linear Regression against NDVI, and Ratio of Band 7 and R6, Map C: Normalized Regression of NDVI (nNDVI), and Map D: Normalised Regression of Soil Adjusted

Vegetation Index (nSAVI). The results showed that Map B performed best in estimating curing in Australia. Furthermore, the study found that these satellite curing models tend to overestimate curing in the present of water pixel (Newnham *et al.*, 2010; Newnham *et al.*, 2011; Martin *et al.*, 2015). To eliminate the errors caused by bare soils and vegetation greenness , Newnham *et al.* (2011) placed NDVI collected from MODIS data in time series introduced relative greenness (RG) approach in the estimation of curing and provided more accurate estimation of curing than a direct linear regression between curing and NDVI. In attempt to resolve the NDVI limitation, researchers developed several methods for masking water using MODIS data such as global vegetation monitoring index (GVMI) (Ceccato *et al.*, 2002b), enhanced vegetation index (EVI) (Huete, 2012) normalized different water index (Xiao *et al.*, 2002).

With the commencement of questioning the robustness of spectral indices that focused on the Red and Near Infrared (NIR) reflectance for estimation grassland curing with conflicting results, (Martin *et al.*, 2015) tested a series of vegetation indices (NDVI, SAVI, GVMI, NDWI(6), EVI & DVI) using multiple linear regression method for curing assessment in Victoria , southern-eastern Australia and developed an integrated satellite model named "the Victorian Improved Satellite Curing Algorithm" well-known as MapVictoria model. The combination of the NDVI and GVMI performed best than other candidate indices. MapVictoria algorithm was also used by Li (2020) and validated the use of Landsat 8 data as an effective and accurate way for grassland curing monitoring in Greater Melbourne, Australia. Similarly, Chaivaranont *et al.* (2018) used MapVictoria method, however, instead of using optical satellite data, a passive microwave-based RS vegetation product vegetation optical depth (VOD) was used. The results suggested that VOD-based curing estimation can reasonably reproduce ground-based observation in space and time.

Potential application of soil moisture data as proxy for grassland fuel moisture and curing has recently gained traction in fire research. From literature, few researchers have demonstrated the relationship between soil moisture and the degree of grassland curing. In USA, Jolly *et al.* (2005); (Jolly 2018) constructed an integrated growing season index (GSI) plant phenology model. In this study the dead herbaceous fuel load was assessed as a function of degree of curing. The results revealed a negative relationship between GSI and grass curing in North Dakota. (Krueger *et al.*, 2015) provided evidence that soil moisture as Fraction of Available Water Capacity (FAW) impacted grass curing in Oklahoma, USA. Likewise, Sharma *et al.* (2020) used FAW to determine the relationship between rate and degree of curing and FAW. The study confirmed that the grass curing rate increases linear as FAW drops below 0.30. In South Africa, McGranahan *et al.* (2016) observed positive correlation between soil moisture and fuel moisture content during the curing period from the end of growing season into mid-winter. While in Germany, Wittich (2011) considering that soil moisture deficits promote curing, estimated the percentage of yellowed dead grass per unit grassland area termed it yellowing level to determine the relationship between grass moisture and curing to use as input into danger rating models of Deutscher Wetterdienst. For Australia, (Kidnie *et al.*, 2015), developed models to estimate curing level from fuel moisture content and soil dryness level from Keetch-Byram Drought Index (KBDI) and Soil Dryness Index (SDI). Overall results revealed that FMC was found to have a strong relationship with degree of curing when combined with SDI. However, the study found that due to misclassification of fuel components, visual curing assessment resulted in over-prediction bias of curing level and failed to capture the effect of the senescing process on fuel availability to burn.

The afore-mentioned studies used in-situ or modelled soil moisture data, however *in-situ* soil moisture measurements are sparse in most countries (Myeni *et al.*, 2021). For instance, the International Soil Moisture Network (ISMN) contains data from only 71 soil moisture monitoring networks and 2842 stations located all over the globe (Dorigo *et al.*, 2021) Although physical-modelled soil moisture datasets have been successfully to its spatio-temporal flexibility and capability to represent root-zone layer, its large computation requirements (Krueger *et al.*, 2022) hinder its application in curing estimation. With the advent of refined satellite based microwave sensors such but not limited to advanced scattermeter (ASCAT) on the meteorological operational satellite (METOP), Advanced Microwave Scanning Radiometer for Earth Observing System (AMSR-E), National Aeronautics and Space Administration (NASA) soil moisture active passive (SMAP),and microwave imaging radiometer with aperture synthesis (MIRAS) on the soil moisture and ocean salinity (SMOS) have proven the usefulness of assessing fuel properties such as fuel load, dead and live fuel moisture (Fan *et al.*, 2018; Jia *et al.*, 2019; Lu and Wei, 2021)**.** These microwave remote sense data products have a coarse spatial resolution and unsuitable for small scale application and high spatial resolution are inaccessible due to its cost (i.e. Vander sat Soil Moisture Product). Downscaling techniques has been used to obtain high resolution soil moisture data (Merlin *et al.*, 2015; Peng *et al.*, 2017; Sabaghy *et al.*, 2020). Estimation of degree of grassland curing from in-situ observation, physical-modelled and remotely sensed soil moisture data is basically limited.

Spatial and temporal data fusion techniques have been developed to obtain both fine spatial resolution and high temporal resolution data. Numerous studies have applied spatio-temporal data fusion such as spatial and temporal data fusion approach (STDFA) (Wu *et al.*, 2012), spatial and temporal adaptive reflectance fusion model (STARFM) (Zhu *et al.*, 2010), enhanced spatial and temporal adaptive reflectance fusion model (ESTARFM), flexible Spatio-temporal Data Fusion (FSDAF) (Meng *et al.*, 2019) and improved spatial and temporal data fusion approach (ISTDFA) (Wu *et al.*, 2015; Wu *et al.*, 2018). However, Jarihani *et al.* (2014); (Wu *et al.*, 2015) had demonstrated that index fusion strategy is more suitable than the reflectance fusion strategy when comparing these methods to NDVI data.

Although grass curing is regarded as a critical factor in fire danger assessment, however, curing is inadequately represented in fire danger models (Sharma *et al.*, 2020). Because direct curing measurements are rarely available, time consuming and expensive, and available on sparse measurement system which are unsuitable for landscape scale due to coarse spatial resolution. Therefore, the present study had employed Index-then Blend (IB) fusion technique, with the overall aim of assessing the spatio-temporal patterns of grassland curing for fire danger assessment using MODIS and Sentinel 2 data. Firstly, degree of grassland curing Index (GCI) was calculated from four candidates' vegetation and soil moisture indices and then converted into Grassland Curing Maps(GCMs). Secondly, the GCMs are synthesized to Fire Danger GCMs to investigate its effectiveness in assessing fire danger in grassland environment.

5.2 **Methodology**

5.2.1 Materials

This study utilized MODIS Terra MOD09A1 Version 6 product and Sentinel -2 satellite data spanning from 2016 to 2020 to calculate grassland curing indexes (GCIs) which were further converted into grassland curing maps (GCMs). MODIS Terra instrument was launched on December 18, 1999. MOD09A1 provides surface spectra reflectance of Terra MODIS Bands 1 through 7 and it has been corrected for atmospheric conditions such gasses, aerosols and Rayleigh scattering (Vermote, 2019). It consists of seven reflectance bands and two quality layers and four observation bands with temporal resolution of a day and spatial resolution of 500m (Vermote, 2019). MODIS data has the advantages of higher spectral and temporal resolutions.

Sentinel 2 was developed by the European Space Agency (ESA) with constellation of identical twin satellites, Sentinel -2A and Sentinel- 2B launched on the 23rd of June 2015 and 07th of March 2017 respectively. Sentinel-2 carries an optical instrument payload that samples 13 spectral bands, four bands at 10m, six bands at 20m and three bands at 60m spatial resolution and a revisit frequency of 5 days at the Equator. Each satellite individually in the Sentinel-2 mission have a single payload called Multi-Spectral Instrument (MSI). Further information on specifications of Sentinel-2 sensors are available on Sentinel-2 mission website (ESA). In comparison with MODIS data with a solid historical database, Sentinel-2 lacks that qualities. Nevertheless, is more advantageous in spatial resolution and has the ability to integrate imagery with compatible sensors (Misra *et al.*, 2020). All MODIS and Sentinel-2 satellite imageries were downloaded from Google Earth Engine (GEE) platform. GEE is a cloud-based computing platform that gives convenient web-based access to a numerous catalogue of satellite imagery and other geospatial data in a format that is analysis –ready (Gorelick *et al.*, 2017).

Visible infrared imaging radiometer suite (VIIRS) thermal anomalies/active fire 375m product data was utilized to validate GCMs. VIIR provide data from the VIIRS sensor aboard the joint NASA/NOAA Suomi National Polar-orbiting Partnership (Suomi NPP) and NOAA-20 satellites. The 375m data complements MODIS fire detection. They both show good agreement in hotspot detection however the improved spatial resolution of 375 m data provides a greater response over fires of relatively small areas, improved mapping of large fire parameters (Schroeder and Giglio, 2017). Furthermore the 370m data improve night-time performance and these data is well suited for use support of fire management (Schroeder and Giglio, 2017). Active fire points for 5-year fire period from 2016 to 2020 (May to November) were downloaded from FIRM NASA website (https://firms.modaps.eosdis.nasa.gov/download/).

Precipitation and soil moisture are the most significant meteorological factors impacting grass curing. Precipitation and soil moisture data was obtained from TerraClimate dataset. The dataset forms on integrated processes that interpolate and combine high spatial resolution climatological normal from the Worldclim dataset and produce a monthly dataset of climatic and surface water balance of spatial resolution of 4km from 1958 to present (Abatzoglou *et al.*, 2018). The data was downloaded from Climate Engine App (https://app.climateengine.org/climateEngine). This tool use GEE for processing, visualize and download satellite and climate dataset with a simple web browser (Huntington *et al.*, 2017). It enables the users to create maps and time series summaries without having to know how to code, therefore the tool overcome common big data barriers. The data was used for correlation analysis between estimated GCIs generated from different soil and vegetation moisture indices.

5.2.2 Methods

Index-then-Blend (IB) method of data fusion technique was employed to obtain a fine spatial resolution data. The IB approach was chosen because it is (a) less computationally expensive due to blending single index rather than multiple bands, (b) more accurate due to less error propagation, and (c) less sensitive to choice of blending algorithm (Jarihani *et al.*, 2014). In the IB approach, the assumption is that a linear mixture model is applicable to indices (i.e. the mixed index for each MODIS is the sum of the index weighted by the class area proportions. This assumption introduced a very small error when using indices directly into linear mixture model (i.e. IB) instead of using individual band reflectance data in the model (i.e. BI) (Kerdiles and Grondona, 1995; Jarihani *et al.*, 2014)

Four RS indices were selected as candidates indices for GCI estimation including the normalized difference vegetation index (NDVI), global vegetation monitoring index (GVMI) (Ceccato *et al.*, 2002b), the normalized difference moisture index (NDMI) (Gao, 1996; Wilson and Sader, 2002) , shortwave infrared water stress index (SIWSI) (Fensholt and Sandholt, 2003), and surface water capacity index (SWCI) (Du *et al.*, 2007; Chen *et al.*, 2009). The GEE Code Editor, a web-based integrated development environment (IDE) for writing and running scripts was used for calculations. Equations were coded into the scripts (Appendix 2). These indices are commonly used for the estimation of vegetation and surface (soil) dryness's and require optical spectral bands for calculations. Four Bands were utilized Red, NIR and SWIR and SWIR 1. Bands 4, 8, 11 and 12 of Sentinel 2 and Bands 1, 2, 5.6 and 7 of MODIS respectively.

5.2.2.1 Estimation of Degree of Grassland Curing Index (GCI)

Martin *et al.* (2015) developed an integrated satellite model for estimating the degree of curing based on historical satellite and ground-based observations named "the Victorian Improved Satellite Curing Algorithm" well-known as MapVictoria's algorithm. Curing degree was computed following these algorithms as shown in Equation5.1.

$$Curing = (NDVI * -88.41) + (GVMI * -67.71) + 113.80 \qquad \text{Equation 5.1}$$

where

$$NDVI = \frac{NIR-Red}{NIR+Red} \qquad \text{Equation 5.2}$$

and

$$GVMI = \frac{(NIR+0.1)-(SWIR+0.02)}{(NIR+0.1)+(SWIR+0.02)} \qquad \text{Equation 5.3}$$

i) GCI estimation using GVMI (GCI_GVMI)

The GCI_GVMI was calculated using Equation5.1. GVMI is a moisture index built on combination of near-infrared and shortwave infrared regions of electromagnetic. Instead of using Band 6 and Band 11 of MODIS and Sentinel-2 respectively, this study used Band 7 and Band 12 reflectance, because longer wavelength in SWIR has higher absorption co-efficient (Chen *et al.*, 2009) . Martin *et al.* (2015) demonstrated the efficacy of the indices for grass curing estimation.

ii) GCI estimation using NDMI (GCI_NDMI)

The GCI_NDMI was estimated by replacing the original MapVictoria algorithm GVMI with NDMI and is calculated using Equation 5.4.

$$Curing = (NDVI * -88.41) + (NDMI * -67.71) + 113.80 \qquad \text{Equation 5.4}$$

where

$$NDMI = \frac{NIR-SWIR}{NIR+SWIR} \qquad \text{Equation 5.5}$$

The NDMI is a normalized difference moisture index that utilizes NIR and SWIR to display moisture. An index that has been referenced with different nomenclatures with different authors such land surface water index (LSWI) (Xiao *et al.*, 2002; Chandrasekar *et al.*, 2022), normalized difference infrared index (NDII) (Hardisky and Smart, 1983; Hunt and Rock, 1989; Hunt *et al.*, 2012) and Normalized Different Water Index (Gao, 1996). The index has proven to be suitable indicator for root zone moisture storage in the Upper Ping Basin in northern Thailand (Sriwongsitanon *et al.*, 2015). Malakhov and Tsychuyeva (2020) established that NDMI performed well to be a promising approach for assessing vegetation biophysical parameters in semi-arid heterogeneous vegetation cover.

iii) GCI estimation using SIWSI (GCI_SIWSI)

The GCI_SIWSI was computed following Equation 5.6.

$$Curing = (NDVI * -88.41) + (SIWSI * -67.71) + 113.80 \qquad \text{Equation 5.6}$$

where

$$SIWSI = \frac{SWIR-NIR}{SWIR+NIR} \qquad \text{Equation 5.7}$$

The SIWSI is shortwave infrared water stress, a transpose of NDMI, constructed by Fensholt and Sandholt (2003). The index has the ability of reflecting the trend of soil moisture and monitor soil moisture without passing through the vegetation (Wang *et al.*, 2022). The efficacy in monitoring soil moisture has been positively proven in variety of studies (Fensholt and Sandholt, 2003; Yunhao *et al.*, 2007; Olsen *et al.*, 2013; Zhao *et al.*, 2013).

iv)* GCI estimation using SWCI (*GCI_SWCI)

The surface water capacity index (SWCI) is a soil moisture index constructed by utilizing the normalized differences between two SWIR bands and was developed by (Du *et al.*, 2007) based on the water absorptivity curve and soil reflective curve**.** Similarly, to NDMI, SWCI is referenced to different names by different authors**.** (Haubrock *et al.*, 2008); Alonso *et al.* (2019) referred to this index as Normalized Soil Moisture Index (NSMI). A non-dimensional measure that can be used to quantify gravimetric soil moisture (Haubrock *et al.*, 2008). The index has proved to be highly correlated with soil moisture at the 0 -50 cm layer (Hong-wei *et al.*, 2011). The GCI_SWCI is calculated following Equation5.8.

$$Curing = (NDVI * -88.41) + (SWCI * -67.71) + 113.80 \qquad \text{Equation 5.8}$$

where

$$SWCI = \frac{SWIR-SWIR1}{SWIR+SWIR1}$$ Equation 5.9

5.2.3 Generation of fire danger maps

After the calculation of grass curing indices (GCIs), it was discovered that some of GCIs have values beyond 100%, for instance GCI_NDMI of October 2010 has maximum curing of 114%. To accommodate the differences, all results were scaled to the range of 0 -100% (Li, 2020). QGIS 3.28.6 Raster Rescale tool was used for scaling. Finally, the rescaled maps were classified according to grass curing influence on fire danger and fire behavior as guided by Victoria County Fire Authoring (CFA) Grassland curing Guide (Victoria County Fire Authority (CFA), 2020) using Reclassify by Table Tool (Table 5.1) to generate fire danger CGMs**.**

Table 5.1: Classification of GCMs and Fire Danger Class

Curing Range (%)	**Will Fire ignite?**	**Fire Spread**	**Suppression difficulty**	**Grass Curing Fire Danger**	
				Reclassified Value	**Danger Level**
0-30	No	Fire fail to spread	N/A	1	Insignificant
30-50	Maybe	Fire front will be fragmented. Fire will be carried by thatch underneath current season growth. Fuel consumption will be patchy.	Low	2	Low
50 -60	Yes	Fragmented fire front with faster spread rates in areas of dry fuels. Patch fuel consumption.	Moderate	3	Moderate
60-80	Yes	Fire spread will be moderate to high. Patchy areas of green will slow spread, however fire spread will be fast under strong winds and will be difficult to suppress.	High	4	High
80 -100	Yes	Fire spread will be very fast under strong winds.	Very High	5	Extreme High

5.3 Results

5.3.1 Distribution of fire activity

Based on the cumulative number of fires occurred during the fire season of the study period, September was revealed as the month with the highest number of fire occurrences, with the year 2017, 2019 and 2020 revealing the similar results (56%, 55% and 58% respectively) as depicted in Figure.5.1. More than 60% of fire occurred was observed in the month of July for the year 2018. For the year 2016, the highest number of the fire was observed in the month of August (49%).

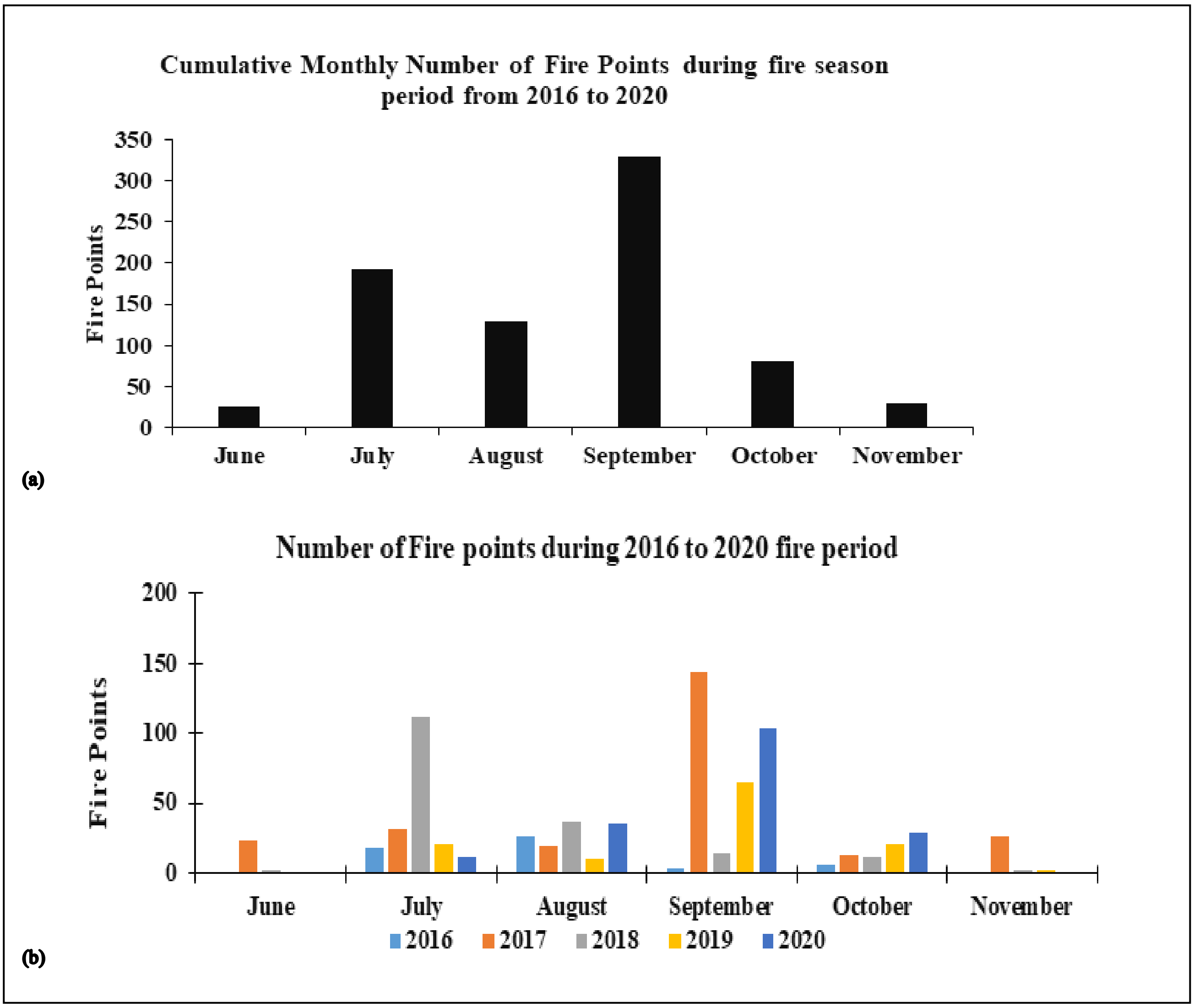

Figure 5.1: Number of fire points for the period from 2016 to 2020(a) Cumulative Monthly, (b) Monthly Fire points

5.3.2 Spatio-temporal distribution of grass curing

Examining monthly grass curing averages from 2016 to 2020 provided insight into the overall temporal pattern of grassland degree of curing over the period of five (5) years. All candidate indices have the highest degree of curing observed in the month of September with the minor time variation as shown in Fig.5.2. The lowest curing was observed in the month of February for all candidate indices except GCI_SWCI where the lowest curing was in March. The month of May was observed as the increase starting point of degree of curing for all candidate indices. Similar pattern of the lowest degree of curing was observed between GCI_GVMI and GCI_NDMI. Although the lowest degree of curing for GCI_SWCI was observed in the month of March, its pattern of highest degree of curing was similar with GCI_GVMI.

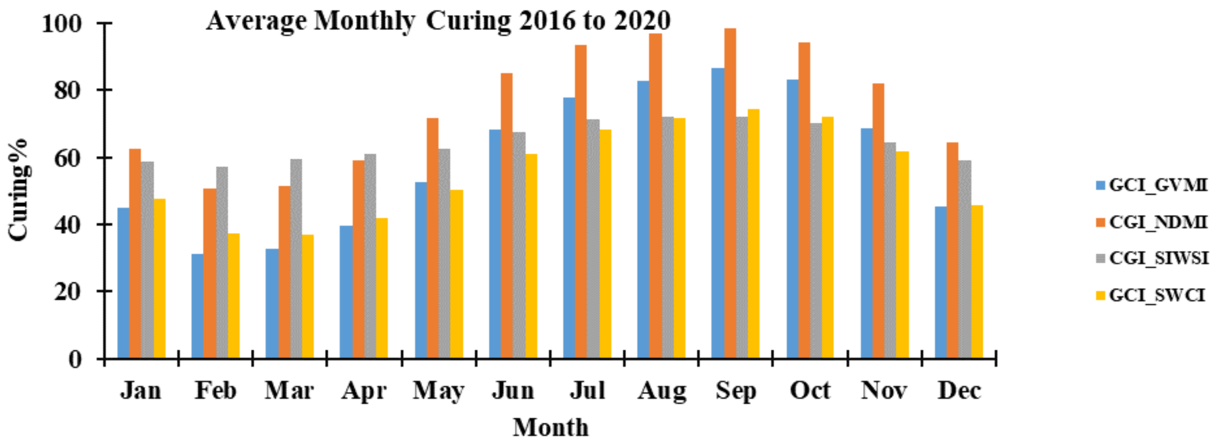

Figure 5.2: Monthly average curing for the period from 2016 to 2020 across all candidate indices

Figure 5.3 represents all candidate indices degree of curing estimation per year to assess annual similarity and variation amongst the candidate indices. For the year 2016, all candidate indices revealed uniformity of increasing curing with starting time of June until August. All candidate indices generally have similar high degree of curing in the month of August and lowest curing in the month of February, except GCI_SIWSI that the lowest curing was observed in the month of March. In the year 2017, the increase of degree of curing started in the month of May until September. Like in 2016 all candidate indices have lowest degree of curing in the month of February except GCI_SIWSI observed in January. All candidate indices have the similar peak time in the month of September. Similarly, the peak degree of curing was observed in the month of September for the year 2018 and all candidate indices showing the lowest curing in the month of February and uniformity of increasing degree of curing starting from June to September. For the 2019, all candidate indices revealed a starting point of increase of curing in June with the highest curing observed in the month of October and the lowest in the month of April. However, GCI_SIWCI have its peak curing in the month of September and lowest in the month of December. For the year 2020, though the peak and lowest degree of curing varied among the candidate indices, the starting point of increase of degree of curing was observed in the month of May to October. GCI_GVMI and GCI_SWCI depicted the similar pattern of the degree of curing.

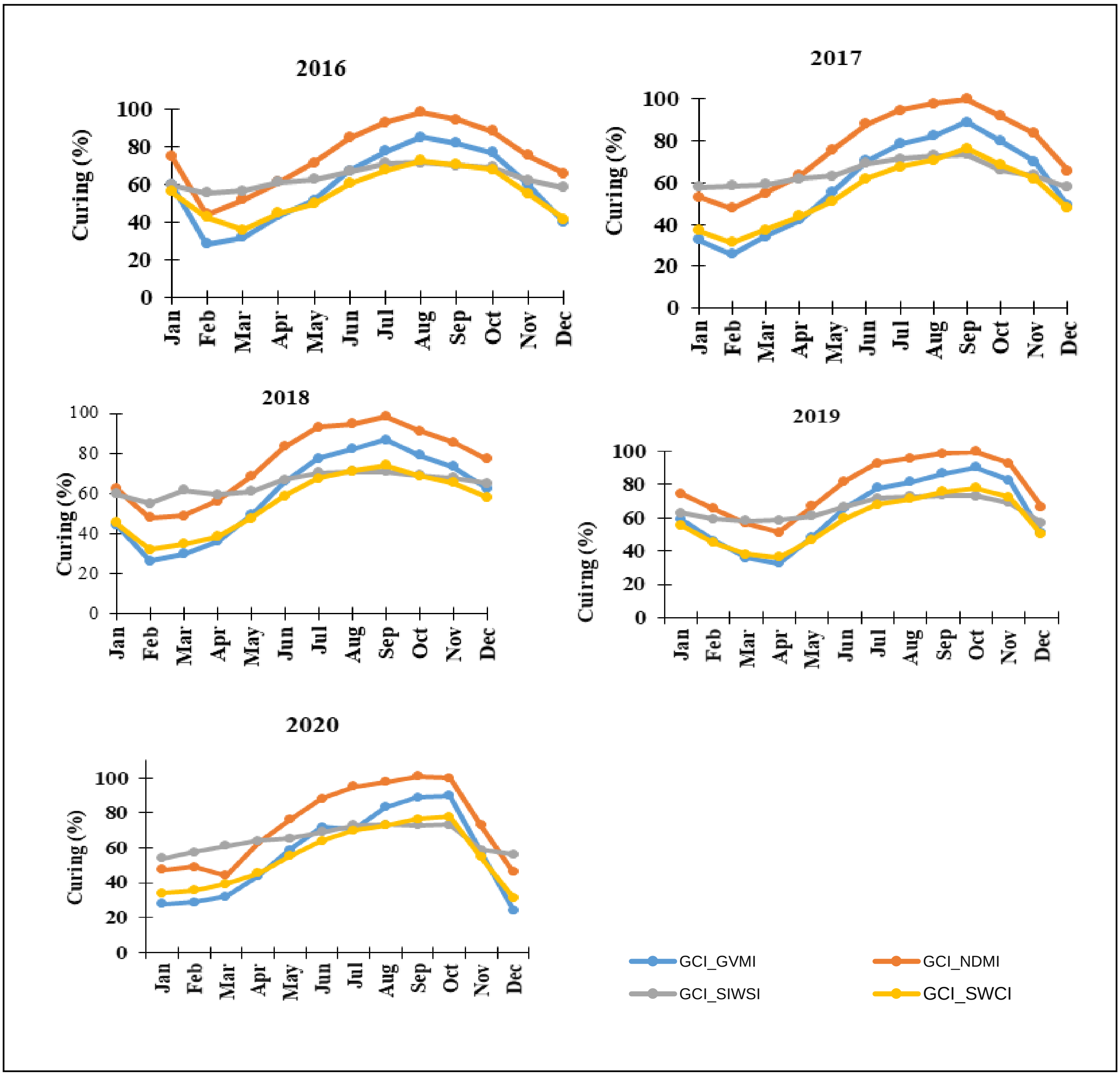

Figure 5.3: Annual average degree of curing for the period from 2016 to 2020 across all candidate indices

Figure 5.4. show the example of Grassland Curing Maps (GCMs). The spatial distribution of curing is not uniform throughout the park. Areas with fully cured fuel can be seen throughout the study area and varies monthly. The development of fire danger GCMs were drawn from GCMs classified according to the degree of curing prone to the spread of fire. Figure 5.5. represent fire danger GCMs of all candidate indices for the cumulative month of September for the period of 2016 to 2020. More than 85% of the entire landmass of the study area fell under high to extreme high fire danger zone as illustrated in Table 5.2. Less than 2% of the study area fell under danger-free danger zone and noticeable distributed around the rivers, fallows and south facing mountain ridges. These suggest that

the entire landmass of the study area is highly susceptible to fire. This is further confirmed by largest area of coverage of high to extremely high degree of curing as depicted in Figure 5.4.

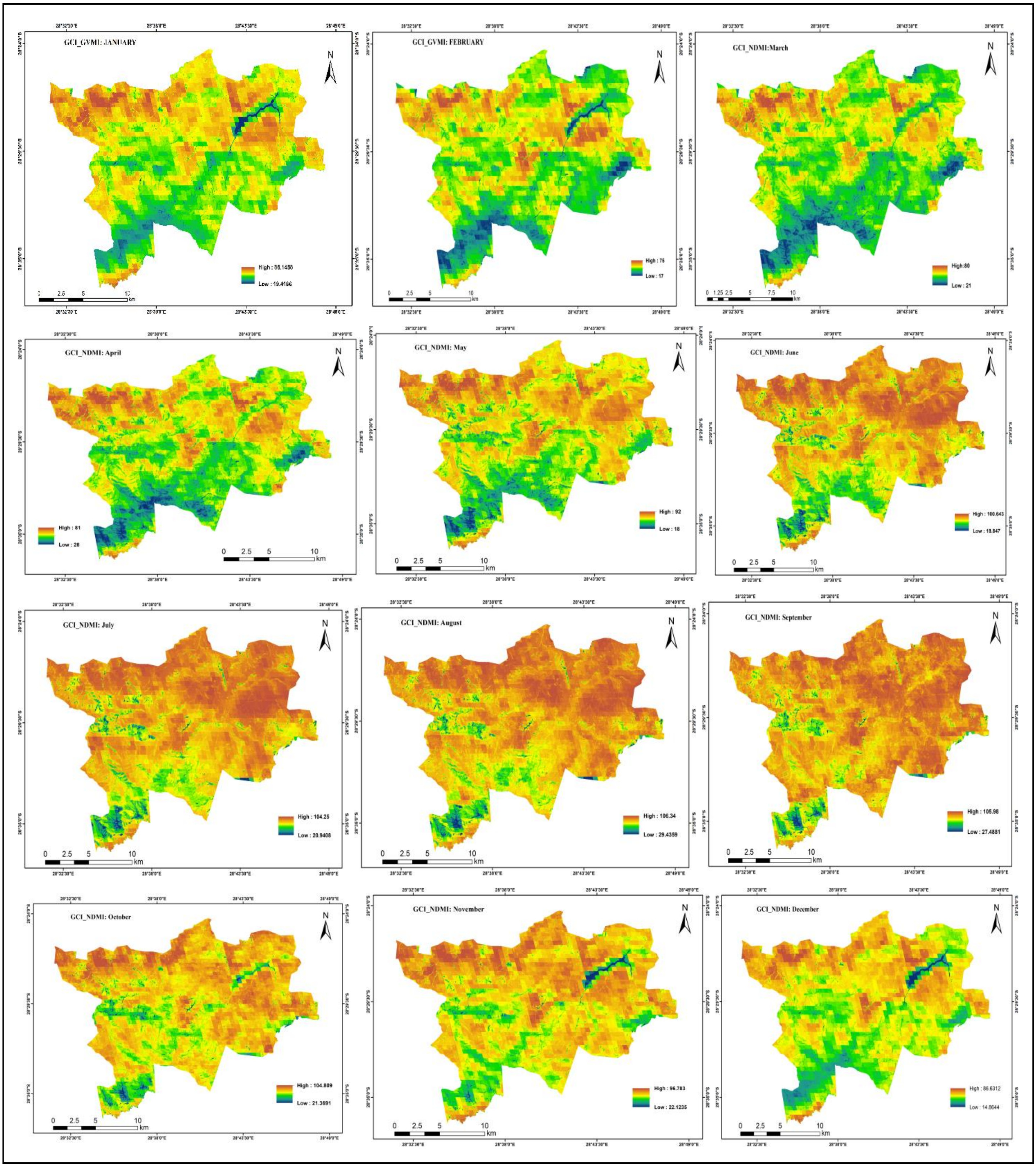

Figure 5.4: Monthly Grass Curing Maps for GCI_NDMI for the period of 2016 to 2020

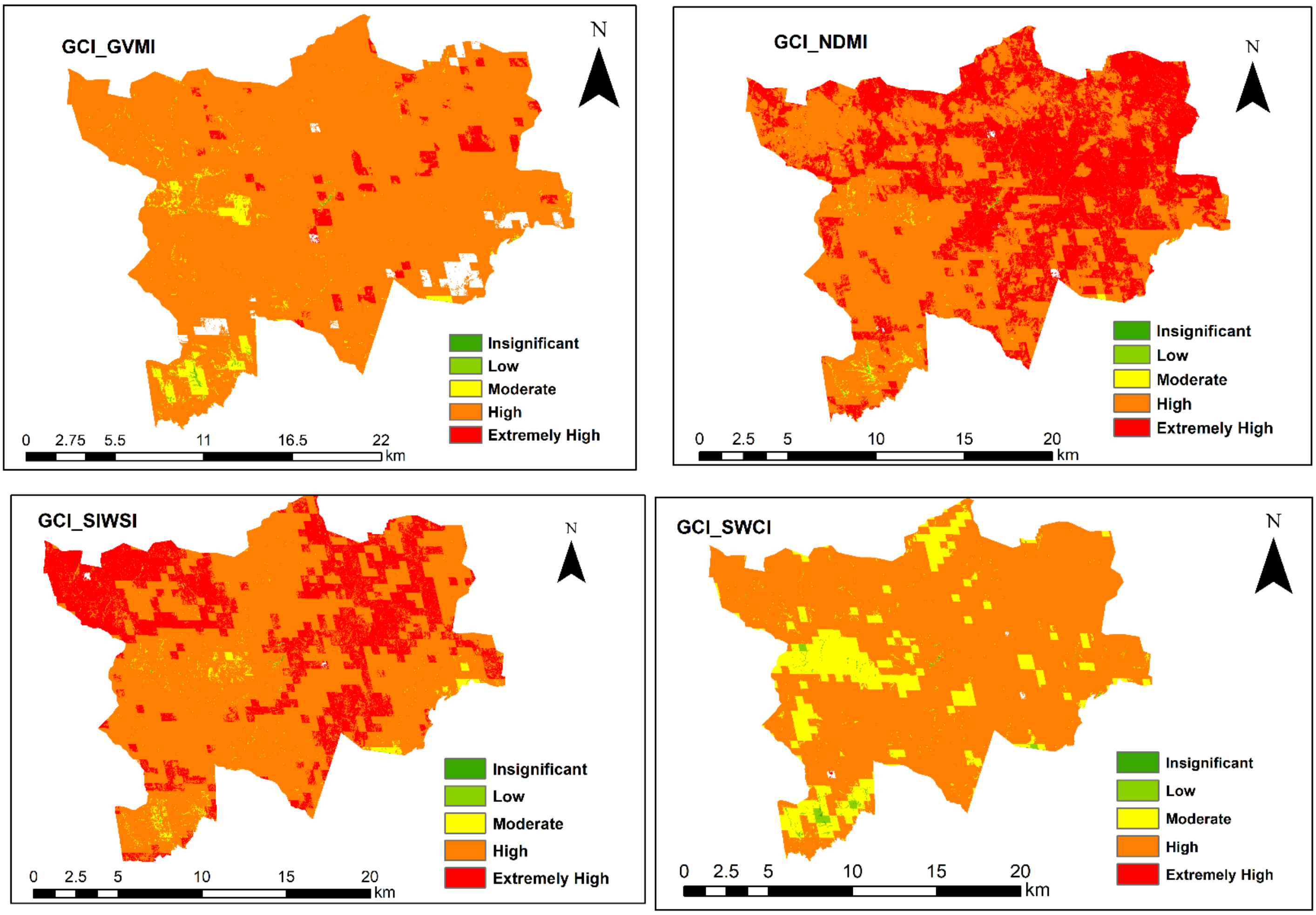

Figure 5.5: Fire Danger Grassland Curing Maps for the cumulative month of September for all indices for the study period from 2016 to 2020

Table 5.2: Percentage Area coverage of Fire Danger GCMs for the cumulative month of September for all indices for the study period from 2016 to 2020

FDI	GCI_GVMI	GCI_NDMI	GCI_SIWSI	GCI_SWCI
Insignificant	0.04	0.02	0.02	0.06
Low	0.28	0.16	0.14	0.70
Moderate	2.74	0.63	1.52	14.07
High	93.80	55.76	68.76	85.16
Extreme High	3.13	43.43	29.56	0.01

5.3.3 Accuracy Assessment

The accuracy of these Fire Danger GCMs was validated using active fire points from the VIIRS of FIRMS NASA website that offers hotspot location of the fire events after the satellite's overpass. The active fire points were overlaid to Fire Danger GCMs to calculate the accuracy of danger maps. The percentage of active fire points within fire danger GCMs for all candidate indices are shown in Figure 5.6. None of the fire points fell under an insignificant fire danger zone. Over 90% of the fire points fell under high to extremely high fire danger zone with the highest percentage observed in GCI_NDMI, followed by GCI_SIWSI, GCI_GVMI and GCI_SWCI (99%, 97%, 94 % and 92% respectively). Furthermore, the results showed that the highest percentage of fire points that fell under extremely fire danger zone was observed in GCI_NMDI (65%), whereas in case of GCI_GVMI was 42%, GCI_SIWSI was 35% and 31% for GCI_SWCI.

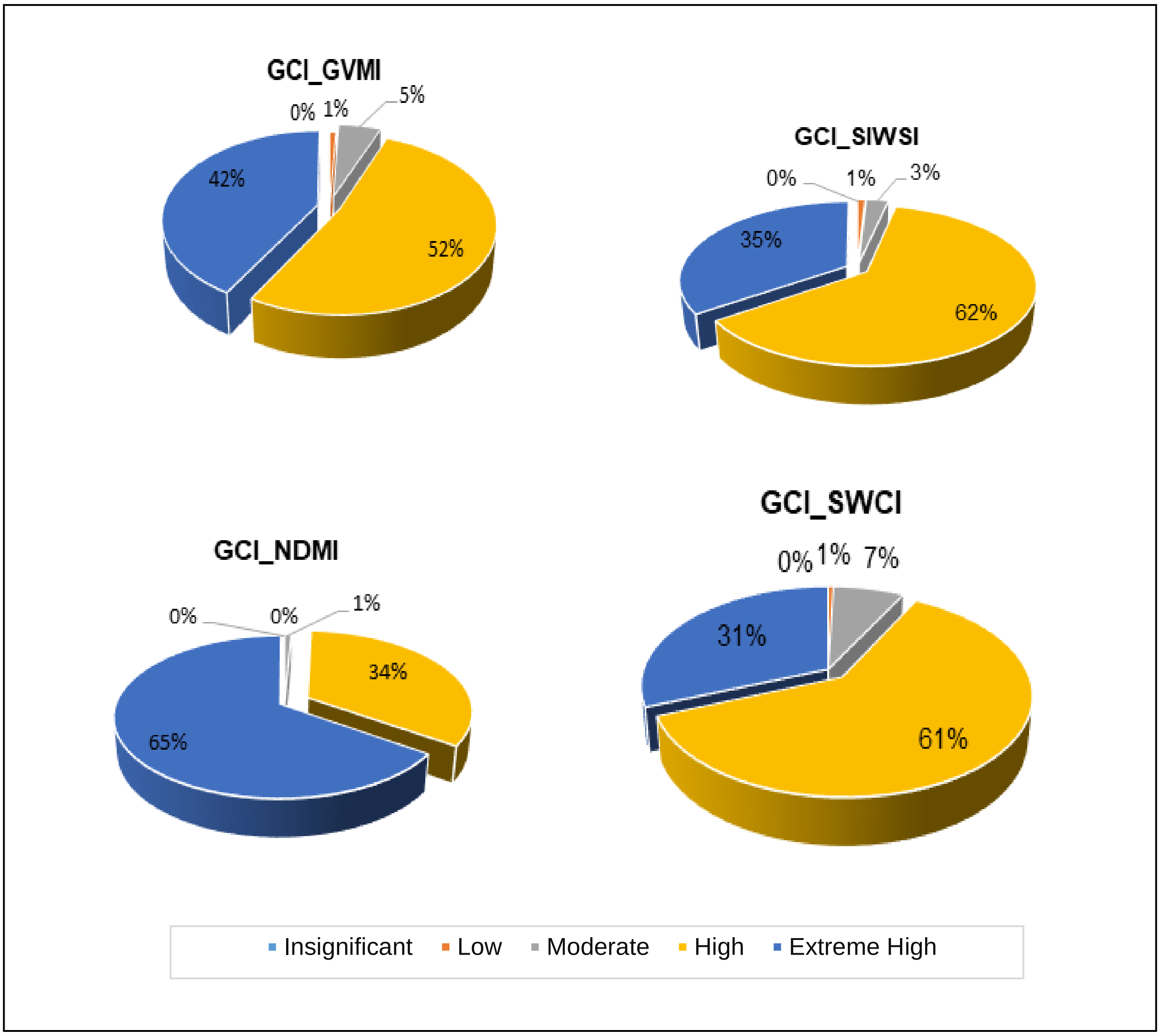

Figure 5.6: Percentage of area in each fire danger zone of estimated GCMs

5.3.4 Pearson correlation analysis

Pearson correlation analysis was used to determine the relationship between CGMs of all candidate indices and weather conditions i.e. precipitation and soil moisture content. The correlation results are presented in Fig.5.6 and Table.5.2. A significant negative correlation was observed between Precipitation and all candidate indices ($p<0.001$; GCI_GVMI (-0.54); GCI_NMDI (-0.57);

GCI_SIWSI and GCI_SWCI (-0.54)), indicating an inverse relation whereby for example higher precipitation is associated with lower degree of curing indices. A moderate inverse correlation was also observed between soil moisture and all candidate indices (p<0.01; GCI_GVMI (-0.39); GCI_NMDI (-0.38); GCI_SIWSI (-0.34); GCI_SWCI (-0.40)). A significant positive correlation was observed between soil moisture and precipitation (p<0.001; 0.57) indicating that the increase the precipitation the increase the soil moisture. Similarly, a perfect positive correlation among all candidates was also observed.

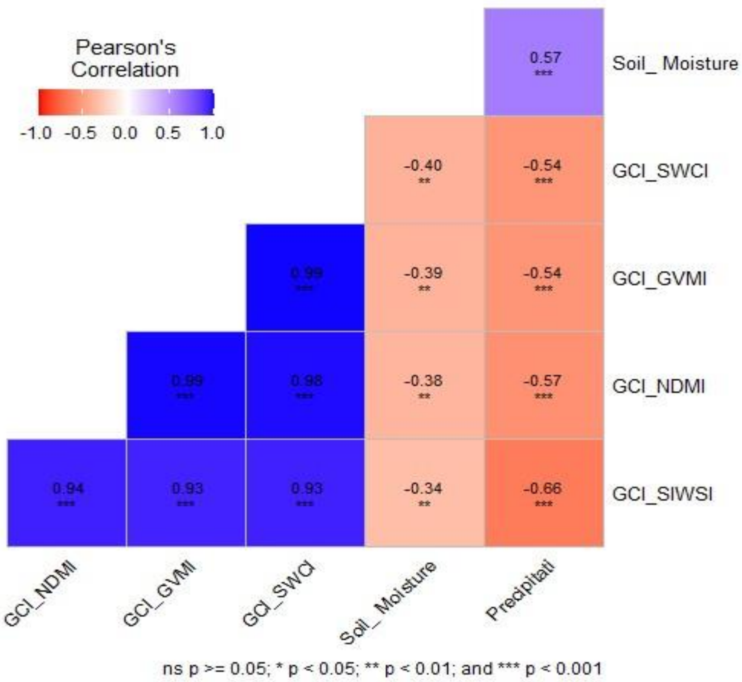

Figure.5.7: Pearson correlation analysis among precipitation, soil moisture and all candidates' indices

Table 5.3: Correlation matrix among precipitation , soil moisture and all candidates indices

	Precipitation	Soil Moisture	GCI_GVMI	GCI_NDMI	GCI_SIWSI	GCI_SWCI
Precipitation	1	0.57	-0.54	-0.57	-0.66	-0.54
Soil Moisture	0.57	1	-0.39	-0.38	-0.34	-0.4
GCI_GVMI	-0.54	-0.39	1	0.99	0.93	0.99
GCI_NDMI	-0.57	-0.38	0.99	1	0.94	0.98
GCI_SIWSI	-0.66	-0.34	0.93	0.93	1	0.93
GCI_SWCI	-0.54	-0.4	0.99	0.98	0.93	1

5.4 Discussion

Analysis of degree of grass curing is critical for determining grassland fire danger. In this study, using soil and vegetation moisture indices derived from fused remotely sensed data (i.e. MODIS and Sentinel 2), we examined the monthly and inter-annual spatio-temporal variability on degree of curing for the GGHNP. In general, the month of September experienced the highest degree of curing with the month of February experienced the lowest degree of curing. The month of May was observed as the starting point of rapid increase of degree of curing, steadily increasing from May to October and then start to slowly decrease from November to April. The observed trend is expected following the South African summer rainfall as one can assume that GGHNP rainfall would be the same. GGHNP as summer rainfall receiver, highest rainfall occurs in November to March coupled with extremely low precipitation occurring from June to August**.** Therefore, it is apparent that degree of curing will increase during low rainfall and increase during high rainfall rate. Hence the effect of rainfall or precipitation is important in degree of curing estimation. Moreover, the FIRM fire occurrence data showed that the fire occurrence in GGHNP during fire season for 2016 to 2020 were predominately during the month the September.

Everson *et al.* (1988) found a similar pattern of degree of curing. In their study on the curing rates in the grass sward of the Highland Sourveld in the KwaZulu-Natal Drakensberg in South Africa they found that curing is initiated at the end of April and progresses rapidly up to middle of May. After winter dryness, plant growth, photosynthesis and stomatal aperture may be limited under water deficient. Then as re-watering in the form of frost or fog and declines in temperature in winter, recoveries of the plant growth and photosynthesis would appear immediately throughout the growing new plant parts, reopening the stomata and decreasing peroxidation could explain the decrease onset of grass curing (Xu *et al.*, 2010; Li, 2020) Therefore, precipitation in the form of frost and dew have significant contribution to the grass curing during early winter.

Inter-annual degree of curing variability among the candidate indices was observed for the study period. The variability was observed in terms of the monthly highest degree of curing for candidate indices August (2016); September (2017); Sept (GCI_GVMI; GCI_NMDI) & Oct (GCI_SIWSI, GCI_SWCI) (2018; October (All candidate indices except GCI_SIWSI) (2019); August (GCI_SIWSI), September (GCI_NDMI) & October (GCI_GVMI &GCI_SWCI) (2020). These highest curing for these months (August, September and October) is expected due to windy, dry, hot weather conditions. In August, September and October vegetation is dormant and dry (Strydom and Savage, 2016) and the onset of summer rains when lightning prevails (Mofokeng *et al.*, 2022). August is known as dry and windy and the highest degree of curing might be attributed to the effect of Berg winds described as the hot dry winds characterized by very low humidity (Everson *et al.*, 1988). The inter-annual variation on the monthly highest degree of curing might be attributed to the timing of starting, end and length of growing season as determined by the topographical effects on climatic factors that influence plant phenology (Hua *et al.*, 2022)**.** Furthermore, the curing estimations are relatively in line with the VIIRS fire occurrence data. As shown in Figure 5.1 the highest number of fire occurrence was experienced in August for the year 2016 & 2020, for the year 2017 & 2019 in September and for the year 2018 in July.

The results of spatial distribution of degree of curing for the GGHNP was observed using the developed GCMs of the month of September for all the candidate indices since September was the month with the highest fire activities, and showed the heterogonous degree of curing pattern within the park. Almost the entire landmass is covered with higher degree of curing with small patches of low degree of curing observed within the park. Number of factors may be related to this type of spatial variation. The vegetation in the park is predominantly natural grassland with a very small percentage of shrubs forest and Afromontane along the rivers (Daemane *et al.*, 2021). According to the South African National Land Cover (SANLC) dataset more than 80% of the park is covered with natural grassland (Republic of South Africa, 2020). In general, natural grassland consists of high species diversity with different life cycles resultant to patches hence heterogeneous curing pattern (Duff *et al.*, 2020). The lowest degree of curing is prominent at fallow land dominated by perennial grasses, as they stay green longer and are more tolerant to stress and do not show immediately signs of drying due to its deeper roots (Wittich, 2011). Land cover types of the study can explain its spatial heterogeneity of degree of grass curing as (Yang *et al.*, 2022) land cover was found to be one of the main reason for spatial heterogeneity on vegetation phenology in the Yangtze River Delta however quantitative evaluation still requires further analysis.

In additional, spatial heterogonous pattern can be attributed to the topographical and environmental heterogeneity of the study area. The elevation of GGHNP ranges from 1654m to 2829m hence an Afromontane grassland ecosystem. A general tendency on the delayed start and decrease length of the growth period of vegetation with increasing in elevation has been globally observed however the rate of these variation is influenced by aspects or the slope (Hua *et al.*, 2022). Findings by Yang *et al.* (2022) showed that a longer growing season was observed at lower elevation and north-facing sunny slope. An *et al.* (2018) showed that the green-up onset did not find any significantly on aspect in steppe area however dormancy onset was earlier on shaded slopes than the sunlit slope.

The generated fire danger maps showed over 90% of the entire park is prone to fire danger based on the degree of curing. However, Chaivaranont *et al.* (2018) cautioned that the high curing values do not guarantee a fire as there is no accounting for ignition sources , rather higher curing value indicates that if a grassland fire were to start it would spread faster compared to low curing values given no fire suppression activity. Generally, fires in the grasslands will fail to sustain itself when the curing level is less than 20%, and above this level the rate of fire spread increases with curing level (Cruz *et al.*, 2015; Duff *et al.*, 2019). As tested by Cheney *et al.* (1998) the small fires occur on the grassland which are 60 -70% cured while large fires are possible at on grassland that are 80% cured. This implies that in the presence of ignition source and favourable weather conditions, the park is susceptible to large fires.

From the results of accuracy assessment of estimated degree of curing it can be identified that GCI_NDMI (NDVI and NDMI) has proven its accuracy in estimation of degree of curing in the rugged and heterogeneous grassland environment in comparison with other three (3) candidate indices, though in a small margin. NDMI can be effectively used to detect plant water stress according to the property of shortwave infrared (SWIR) reflectance which is negatively related to leaf water content and linear relationship between NIR/SWIR and leaf water content was discovered by (Hunt and Rock, 1989). Previous studies have proven the effectiveness of NDMI in phenological estimation and monitoring the changes of soil moisture. (Sriwongsitanon *et al.*, 2015) have proven that NDMI or NDII is an effective index for moisture storage in the rootzone during the time of moisture deficit and powerful indicator to assess drought with a correlation of R^2 value of 0.87. In the study of Martin *et al.* (2015), owing to the similarities of NDWI/NDMI and GVMI, they accuracy assessment analysis show a little variation between NDVI & NDWI and NDVI & GVMI model. Recent study by Gaznayee *et al.* (2023) revealed a notable correlation between soil moisture based on the NDMI and vegetation cover based on NDVI. Consequently, NDMI can be regarded as both soil and vegetation water content estimator. Likewise, SIWSI as the transpose of NDMI can be estimator of both soil and vegetation water estimator. SWCI as be estimator of soil moisture content (Alonso *et al.*, 2019). Whereas GVMI has been categorized as vegetation water estimator (Ceccato *et al.*, 2003; Qi *et al.*, 2012) and NDVI as chlorophyll content of vegetation (vegetation greenness) (Chuvieco *et al.*, 2002).

Correlation analysis showed a strong significant negative correlation between precipitation and all candidate indices. Similar correlation was observed by (Li, 2020), when the precipitation decrease, curing increases, and when the precipitation increases, curing decreases. Likewise, the correlation was negative between soil moisture and the indices. As expected the relationship between soil moisture and precipitation was significantly positive. A notable positive correlation among all the candidate indices was revealed. The significant positive relationship among all indices symbolize that all candidates has the capability of estimating degree of grassland curing. Although grassland fire outbreaks are strongly correlated with degree of grass curing, other variables that affect degree of curing include the amount of available fuel (fuel load), wind direction and speed, temperature, and most crucially precipitation (Cheney and Sullivan, 2008; Li, 2020).

5.5 Conclusion

Accurate quantitative estimation and assessing degree of curing is crucial for fire danger assessment. This study has attempted an assessment of the spatio-temporal pattern of grassland curing for fire danger assessment in GGHNP. Index-then-Blend (IB) data fusion method was applied to downscale MODIS spatial resolution of Sentinel-2. A trade-off between MODIS (fine temporal resolution) and Sentinel-2 (fine spatial resolution) data. Four GCIs was quantified from vegetation greenness, soil and vegetation water content indices GCI_GVMI (NDVI and GVMI), GCI_NDMI (NDVI and NDMI), GCI_SIWSI (NDVI and SIWSI), and GCI_SWCI (NDVI and SWCI) following the "MapVictoria.

The GCIs results revealed May as the onset month of grass curing, September as the peak month of highest degree of curing and February the month of lowest degree of curing as well as the steady increase of degree of curing from May to October. The created fire danger maps showed that more than 90% of the entire park fell under high to extremely high fire danger, spatially distributed throughout the park.

The inverse relationship between the GCIs, and precipitation, and soil moisture as well as the positive relationship between precipitation and soil moisture showed that the more the precipitation, the wetter the soil the less the curing. The fire danger maps are validated using (FIRM) active fire points and all candidate indices succeeded in measuring degree of curing as no fire fell under insignificant fire danger with GCI_NDMI outperforming other indices. Finally, the study paved a way for the utilization of highly spatial resolution (10m) fused remotely sensed for estimation of degree of curing for the preparedness of fire management plan of park and other fire agencies within mountainous grassland environment. The study can also be useful for the livestock agricultural practitioners and the games for pasture management. Although the topographic effects on the timing of degree of curing in mountainous grassland ecosystem was not deciphered in this study, the effects of topographical parameters (elevation, slope and aspects) on the climatic factors that influence degree of curing warrant the future investigation.

CHAPTER 6

INTEGRATED GRASSLAND FIRE DANGER ASSESSMENT MODELS

This chapter is based on:

Olga D. Mofokeng, Samuel A. Adelabu and Colbert M. Jackson. (accepted). *Integrated grassland fire danger assessment of Golden Gate Highlands National Park using geospatial techniques* (Fire – 2824067). Fire (ISSN – 2571-6255)

Abstract

Grassland Protected Areas (PAs) employ fires as the management tool to achieve its conservation and societal goals. Globally, anthropogenic climate changes have altered fire regimes in the grassland biome. Integrated fire risk assessment systems provide an integral approach to fire prevention and mitigate the negative impacts of fire. However, fire risk assessment is extremely challenging owing to the myriad of factors that influence fire ignition and behaviour. Most fire danger systems do not consider fire causes; therefore, they are inadequate in validating the estimation of fire danger, Thus, fire danger assessment models should comprise the potential causes of fire. Understanding the key drivers to fire occurrence is a key factor to the sustainable management of the grassland ecosystems. Hence, the aim of this chapter was to assess the fire danger of grassland Afromontane protected area employing three (3) statistical (Frequency Ratio (FR), Weight of Evidence (WoE) and Logistic Regression (LR)) and three (3) machine learning (Decision Tree (DT), Random Forest (RF) and Support Vector Machine (SVM) models in and determine suitable prediction model. MaxEnt was used to identifying the driving factors that influence the fire danger modelling. The complex interrelationship of drivers with fire danger was investigated. The area under the receiver operating characteristics curve (ROC/AUC) revealed that DT showed the highest precision on model fit (AUC=0.93) and success rate (AUC=0.96), while WoE recorded the highest prediction rate (AUC = 0.74). The WoE model showed that 53% of the study area is susceptible to fire. The land surface temperature (LST) and vegetation condition index (VCI) were the most influential factors. Spatial relation pattern suggests the fire regime of the study area is probable fuel-dominated grassfire. Thus, a grassland fire danger management strategy based on fuel conditions should be advocated aiming at correctly weigh the effects of fuel in fire ignition and spread prior to fire season.

Key words*: Grassland fires, fire drivers, Remote Sensing, GIS, machine learning, statistical methods,*

6.1 Introduction

Grassland cover around a third of the Earth’s land area and account for over 80% of global burnt area (Leys *et al.*, 2018). Grassland ecosystems are valuable natural resources and have crucial ecosystem functioning, including livestock grazing areas, water supply and regulation, biodiversity reserves, tourism sites, recreation areas, religious sites, wild food sources, and natural medicine sources carbon storage and climate mitigation, pollination and a host of cultural services (O'Mara, 2012; Pausas and Keeley, 2019). Fire is an inevitable and essential ecological process in grassland ecosystem, in a long-term evolution processes, it has established a harmonious and balanced relationship with a grassland ecosystem (Chang *et al.*, 2023). Hence fire has been used as a principal management tool in African and Australian grasslands (Berlinck and Batista, 2020) in particular Afromontane grasslands (Everson and Everson, 2016).

Fire plays an intricate role in shaping grassland ecosystems landscape and population structure and composition of inhabiting species (Bond and Keeley, 2005; Bond and Keane, 2017). However, in the context of climate change in conjunction with anthropogenic activity, the delicate balance between fire activity and natural ecosystem (i.e. grassland) process has been disturbance hence fire frequency is increasing and fire season is lengthening (Jolly *et al.*, 2015; Sharma and Dhakal, 2021). Increased in fire frequency also means an increase on fire danger thus high probability of negative economic, environmental and social impacts. However, Keeley and Pausas (2019), stated that the negative impacts related to fire are not caused by fire *per se* but rather perturbations of fire regime parameters.

The changes of fire regimes (frequency, severity and extent) are causing devastating economic, environmental, atmosphere and social impacts globally. For instance, in South Africa, the 2017 Knysna fire resulted in the loss of eight (8) lives and destruction of over 800 homes and approximately 5 000 ha of land burnt and economic loss of ZAR 3036 million (Kraaij *et al.*, 2018; Flores Quiroz *et al.*, 2023). While April 2021 Table Mountain National Park fire affected 11 buildings including University of the Cape Town (UCT) library and other historical buildings, and burnt approximately 600 ha of land and 15 people were injured (Flores Quiroz *et al.*, 2023). Hence, it is crucial to accurately predict the occurrence of fire and to understand the underlying driving factors of fire danger in order to mitigate and reduce these impacts on protected grassland ecosystems.

Four key conditions known as “fire switches’ must be met for the occurrence of fire in vegetation, there must be continuous production of biomass (fuel), the fuel must be adequately dry, the weather needs to meet conditions for fire ignition and spread, and sources of ignition (Archibald *et al.*, 2009; Clarke *et al.*, 2020; Pausas and Keeley, 2021). These key conditions are further influenced by both biophysical (i.e. climatic, edaphic. (soil) , topographic and vegetation variation) and anthropogenic factors such as management practises, population density (Clarke *et al.*, 2020). Numerous studies have endeavoured to analyse the relationship between these biophysical and anthropogenic factors and fire occurrence via prediction modelling or rating approaches. These fire danger prediction and rating models are constructed in order to identify areas that are prone or susceptibility to fire or fire danger assessment. Fire danger as the assessment of the conditions under which fire can be ignited and will spread (Chuvieco *et al.*, 2023). The fire danger prediction models require an understanding of the potential drivers or factors and their role in influencing spatio-temporal patterns over a landscape (Trollope *et al.*, 2004; Archibald *et al.*, 2009; Clarke *et al.*, 2020; Duane *et al.*, 2021; Makhaya *et al.*, 2022).

Recently, Chicas and Østergaard Nielsen (2022); (Zacharakis and Tsihrintzis, 2023b) conducted literature review to identify driving factors used to map fire susceptibility and fire danger modeling respectively. Chicas and Østergaard Nielsen (2022) identified 144 factors and categorized the factors into four (4) thematic groups (Climatic, topographic, anthropogenic, and environmental). From 144 factors identified, 33 were used in more than three (3) models. The factors that were used the most were slope, elevation and distance to roads and the least used were soil moisture, shrubs and livestock density. From these 33 factors, 10 mostly commonly used factors, three (3) are from topographic category (slope, elevation and aspect), three (3) are climatic factors (temperature, precipitation and wind speed), two (2) from anthropogenic category (distance to roads, and distance to residential areas) and two (from environmental category (land cover and NDVI).

Though Zacharakis and Tsihrintzis (2023b) did not rank the driving factors as they believe that no existing hard evidence to prove one variable superiority. They proposed ninety-fire drivers and concluded that fire danger is a function of seven thematic groups of driving factors or variables including meteorology, vegetation, topography, hydrology, socio-economy, land use and climate. With the lack of common agreement for the selection of appropriate driving factors, they further cautioned that these variables should not be simultaneously incorporated into the model because of their very high correlations (i.e. the relative humidity and the dew point).

The processing of dependent and explanatory data is the most challenging task in fire danger assessment, modelling and mapping due to various data sources and the modelling complexity (Mohajane *et al.*, 2021). Geographic Information system (GIS) have proven to be a useful tool for processing and overlaying geospatial data to produce a fire danger map. In addition, remote sensing (RS) is a popular data collection method in fire danger modelling. RS is used to classify land cover as it is associated with fuel type and characteristics (Keane *et al.*, 2001); provide elevation data (Sharma *et al.*, 2023), assess vegetation conditions in particular fuel moisture content (Chuvieco *et* *al.*, 2004a; Verbesselt *et al.*, 2007; Yebra *et al.*, 2013; Chang *et al.*, 2023), soil moisture content (Sungmin *et al.*, 2020; Sazib *et al.*, 2021; Sharma and Dhakal, 2021; Vinodkumar *et al.*, 2021) and dependent variables of fire danger model (active fire detection and burnt area estimation. (Szpakowski and Jensen, 2019; Chuvieco *et al.*, 2020; Pettinari and Chuvieco, 2020) offer a review on how RS contribute to fire science and management. With the development of Google Earth Engine (GEE) and Cloud Engine (CE) (Gorelick *et al.*, 2017) platforms that reduce the requirement for expensive information-technology infrastructure, acquiring and processing of RS dataset is rapidly improving the prediction of fire danger models (Sharma *et al.*, 2022).

From the 19th century, global scholars have applied either statistical or simulation or data-driven machine learning methods or combined methods for fire danger or susceptibility modelling and to explore the relationship between fire occurrence and driving factors. Many previous research assigned weights to independent variables using expert opinion (EO) or judgement adopting techniques like multi-criteria decision analysis (MCDA), Analytic hierarchy process (AHP) to map fire danger or susceptibility (Kumari and Pandey, 2020; Zhao *et al.*, 2021b; Maniatis *et al.*, 2022). However, simply overlay method cannot accurately reflect the influence of drivers on fire probability and AHP are critically subjectively and suffers from the deficiency of uncertainty due to the use of the nine-point pairwise rating scale (Hong *et al.*, 2019; Xie *et al.*, 2022).

Statistical bivariate and multivariate methods have been applied for fire danger modelling such as Frequency Ratio (FR) (Romero-Calcerrada *et al.*, 2008; Salavati *et al.*, 2022) and Weight of Evidences (WoE) (Hong *et al.*, 2017; Jaafari *et al.*, 2017; de Santana *et al.*, 2021; Pradeep *et al.*, 2022). (Hong *et al.*, 2019) combined WoE and AHP to improve the fire susceptibility map of Yuichang County in the south of Jiangxi Province China. (Arca *et al.*, 2020) compared FR and MCDA for fire danger modelling in Karabük Province, Turkey and FR (76.42%) outperformed MCDA (73.92%). (Abdo *et al.*, 2022) showed that FR (0.864) outperformed AHP (0.83) for mapping fire susceptibility in the western region of Syria. Regression models have been intensively applied in fire danger modelling due to its easy and interpretation (Guo *et al.*, 2016b; Tien Bui *et al.*, 2016; Zapata-Ríos *et al.*, 2021; Si *et al.*, 2022), logistic generalized additive models (Brillinger *et al.*, 2006; Sá *et al.*, 2018; Woolford *et al.*, 2021), geographical weighted logistic regression (Rodrigues *et al.*, 2018; Cao *et al.*, 2020; Chang *et al.*, 2023).

Simulation models have been used to quantitatively compute fire likelihood and behaviour. These models have been encapsulated in different applications ranging from rules of thumb and 'pocket or field guide' to full-fledges software suite (Cardil *et al.*, 2021). The most used simulation models include BehavePlus (Andrews, 2013), FARSITE (Finney, 1998) , Flapmap (Finney, 2006; Xofis *et al.*, 2020), ForeFire (Balbi *et al.*, 2009) , Phoenix (Tolhurst *et al.*, 2008) , Prometheus (Tymstra *et al.*, 2010), Spark (Hilton *et al.*, 2015), Wildfire Analyst (Ramírez *et al.*, 2011). Other simulation approaches such as F-Sim , Burn-P3, Burn-Pro has been used to compute fire ignition and spread (Zacharakis and Tsihrintzis, 2023b). A variety of studies have employed machine learning methods including Decision Trees (DT), Random Forest (RF) and support vector machine (SVM) (Sokolova and Lapalme, 2009; Hong *et al.*, 2018; Jaafari *et al.*, 2018; Coffield *et al.*, 2019; Jaafari and Pourghasemi, 2019) as well as Maximum Entropy (MaxEnt) (Adab *et al.*, 2018; Vacchiano *et al.*, 2018; Makhaya *et al.*, 2022). For a thorough review of machine learning in fire science see (Jain *et al.*, 2020). On the other hand, Alkhatib *et al.* (2023) briefly reviewed machine learning that are used to identify and forecast forest fire.

Model comparative studies have been conducted to determine the best-fitted model for fire danger modeling. For example, Chicas *et al.* (2022) compared AHP, RF, Fuzzy AHP models, and their analysis revealed RF (83.1%) as the best model for wildfire susceptibility modeling in Belize ecosystems and protected area. The study by (Pham *et al.*, 2020)**,** evaluated the abilities of Bayes Network (BN), Naivë Bayes, DT, and Multivariate Logistic Regression (MLP) for the prediction and mapping fire danger across the Pu Mat National Park, Nghe An province in Vietnam and BN had the highest performance, followed by DT and MLP had poor performance. The performance of four models linear and quadratic discriminant analysis (LDA and QDA), FR and WoE was investigated to model fire susceptibility in the Yihuang area in China (Hong *et al.*, 2017). They res revealed that WoE had the best performance (82.2%), followed by FR (80.9%), QDA (78.3%) and LDA (78%). A simple DT model outperformed RF, Gradient Boasting and other models in predicting fire occurrence in Alaska (Coffield *et al.*, 2019). Gholamnia *et al.* (2020) compared various 9 machine learning models including SVM, DT, and RF, as well as statistical approach LR. RF had the highest accuracy of 88%, followed by SVM (79%) and LR with the lowest accuracy (65%). The performance of three machine learning models (bagged classification trees (BCT), RF and NN) and two statistical approach (LR and logistic GAM) were compared in the study by (Phelps and Woolford, 2021). The results suggested that logistic GAMs can have similar performance to machine learning models for fire occurrence prediction and recommended logistic GAMs for operational fire management.

A review by (Chicas and Østergaard Nielsen, 2022) noted an increase in the use of fire danger models for fire susceptibility or danger mapping since 2001, however, they have observed that there are fire-prone areas where this type of research is not being implemented especially in Africa and Latin America. These studies focused more on forest fires and have not been widely applied to grassland fires especially montane environments. Mountain ecosystems have long been known to be highly sensitive to the direct impact of climatic warming and drying, such that fires in these ecosystems are expected to increase globally (Abatzoglou *et al.*, 2019). Therefore, South African mountain ecosystems are not spared. Furthermore, montane ecosystems in SA as with other countries fire frequency, severity and extent (fire regimes) are observable increasing because of climate-induced impacts on fire switches (Adler *et al.*, 2022). Fire regimes in these Afromontane ecosystems are not well studied and the conditions under which fires occur at these landscapes are still not quite fully understand. One of the key components of the fire risk assessment is accurately quantify the likelihood or probability of fire occurrence (Phelps and Woolford, 2021). To fill this 'specific gap' in fire preparedness, this study aims to provide solution for reduction, mitigation and minimizing the risk of grassfire through the assessment of fire danger of grassland Afromontane protected area using three (3) statistical (FR, WoE and LR) and three (3) machine learning (DT, RF and SVM) models and determine the best-fitting model by comparing their predictive efficacy. Based on 15-year historical fire data and weather, soil, topography, anthropogenic and fuel factors, this research identified the most driving factors for the probability of fire danger and examined the spatial interrelation between fire occurrence and drivers.

6.2 Methodology

The conceptual approach of this study was based on fire danger component of integrated fire risk assessment system as developed by (Chuvieco *et al.*, 2010) and adapted from (Chuvieco *et al.*, 2014; Adab *et al.*, 2018; Chuvieco *et al.*, 2023) as shown in Figure 6.1. The datasets as presented in Table 6.1. consist of inconsistent spatial resolution therefore all datasets were resampled to 10m to match the fuel condition map generated in chapter 5.

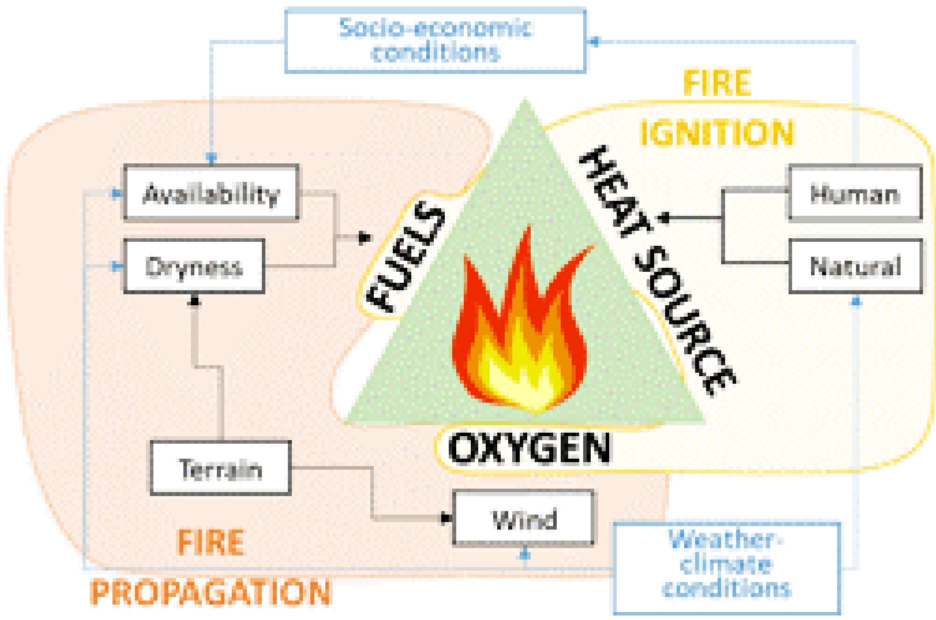

Figure 6.1: Integrated Grassfire danger assessment model (Chuvieco *et al.*, 2023)

6.2.1 Data collection

i) Historical Fire

Fire data was acquired from the Visible Infrared Imaging Radiometer Suite (VIIRS) 375m thermal anomalies/ active fire product (VIIRS-NPP 375m) downloaded from the Fire Information for Resource Management System (FIRMS) (https://firms.modaps.eosdis.nasa.gov/download/) . The attribute information of each fire point contain latitude, longitude, acquisition date and time, satellite instrument, confidence, version, brightness_T31, Fire Radiative Power (FRP), day/night. The confidence information is used to determine the quality of individual hotspot or fire pixel with the value set at low (<15K), nominal (>15K, free of potential sunlight contamination) and high (day or night time saturated pixels (Schroeder and Giglio, 2017). The data became available from 2012 henceforth, data spanning from 2012 to 2021 was utilized for the study.

Table 6.1: List of data type, RS sensor or product with spatial resolution and data source

Category	Driver	Sensor/Product	Resolution	Data Download Source
Fire	Fire Points	VIIRS-NPP	350m	(https://firms.modaps.eosdis.nasa.gov/download/
Topographic	Elevation (DEM)	NASA STRM	30m	https://earthexplorer.usgs.gov/
	Aspect (degrees)	DEM		
	Slope			
	Topographic Position Index (TPI)			
	Topographic Ruggedness Index (TRI)			
	Topographic Wetness Index (TWI)			
Fuel	Grass Curing Index (GCI)	MOD09A1; Sentinel-2	500m;10m	GEE https://developers.google.com/earth-engine/datasets
	Global Vegetation Moisture Index (GVMI)			
	Vegetation Condition Index (VCI)			
	Proximity from River (prox_river)	DEM		https://earthexplorer.usgs.gov/
Soil	Bare Soil Index (BSI)	Sentinel-2	10m	GEE https://developers.google.com/earth-engine/datasets
	Soil bulk density (BD) (cg/kg)	International Soil Reference and Information Centre (ISRIC), SoilGrids	250m	https://soilgrids.org/
	Clay content (g/kg)			
	Coarse fragments (cm^3/dm^3)			
	Sand (g/kg)			
	Silt (g/kg)			
	Soil Moisture Content (SMC) (mm)	TerraClimate	4000m	(https://app.climateengine.org/climateEngine

Category	Driver	Sensor/Product	Resolution	Data Download Source
	Total Plant Available Water Holding Capacity (TAWCP)	African SoilGrids of ISRIC World Soil Information	1000m	http://africasoils.net/services/data/soil-databases
Weather	Land Surface Temperature (LST) (ºC)	MODIS MOD11A2	100m	GEE https://developers.google.com/earth-engine/datasets
	Lightning	South African Weather Services	500m	
	Wind Speed (mm)	TerraClimate	4000m	(https://app.climateengine.org/climateEngine
Anthropogenic	Proximity from Road (prox_road)	Open Street Map; SANParks		https://download.geofabrik.de/africa/south-africa.html
	Proximity from other infrastructure (Built Environment, tourist facilities) (Prox_structure)			

ii) Grassland Fuel

Fuel moisture content, degree of curing and health condition are crucial drivers in grassland fires. MODIS Terra MOD09A1 Version 6 product and Sentinel -2 was utilized to calculate Vegetation Condition Index (VCI), Grass Curing Index (GCI) and Global Vegetation Moisture Index (GVMI) as well as the Bare Soil Index (BSI). The data spanning from 2007 to 2021 for the month of June to October was downloaded from Google Earth Engine (GEE) platform. The period was selected because they reflect the fire season of the region (Strydom and Savage, 2016). GEE is a cloud-based computing platform that gives convenient web-based access to a numerous catalogue of satellite imagery and other geospatial data in a format that is analysis –ready (Gorelick *et al.*, 2017). Distance from the watercourse is vital parameters as its affect the fuel moisture content (Clarke *et al.*, 2019) and can also acts as a fire breaks. Data on rivers was extracted from DEM.

iii) Topographic Data

National Aeronautics and Space Administration (NASA) Shuttle Radar Topography Mission (STRM) 30 meters free available from USGS EarthExplorer (http://earthexploer.usg.gov) was utilized for the retrieval of elevation. Aspect, slope, Topographic Wetness Index (TWI), Topographic Ruggedness Index (TPI), and Topographic Position Index (TPI) were extracted or computed from elevation. These variables were selected due to its known influence on fuel type, load and moisture, in particular when and when topography interacts with microclimates (Moreira *et al.*, 2011).

iv) Soil Properties Data

Soil moisture, texture and soil hydraulic properties such as Fractional Available Water Capacity (FAW) or Profile Available Water (PAW) are example of important indirect drivers of fire ignition and propagation. The influence of soil in fire danger is governed by the soil and vegetation relationship, thus fuel for fire. Soil Moisture data from the month June to October for the period of 2007 to 2021 from TerraClimate with spatial resolution of 4000m was downloaded from Climate Engine (CE) (https://app.climateengine.org/climateEngine) (Huntington *et al.*, 2017). Soil physical properties including soil bulk density, coarse fragments, clay, coarse, sand and silt content was acquired from the International Soil Reference and Information Centre (ISRIC), SoilGrids (https://soilgrids.org/) at 250m spatial resolution (Hengl *et al.*, 2017). While total plant available water holding capacity (TAWCP) was acquired from African SoilGrids of ISRIC World Soil Information (http://africasoils.net/services/data/soil-databases/).

v) Climatic/Weather Data

Land Surface Temperature (LST) was used as proxy to fuel temperature, one of primary factor leading to fire ignition (Wang *et al.*, 2013) and was extracted from MODIS MOD11A2 version 6.1. product (2007-2021) from GEE at spatial resolution of 1000m. Wind is known to be one of the most important factors in determining fire dynamics (Moon *et al.*, 2013; Cruz and Alexander, 2019). One of the most controlling parameters that specifies the direction, spread rate and configuration of fire (Ghodrat *et al.*, 2021). Wind speed data from the month June to October for the period of 2007 to 2021 from TerraClimate with spatial resolution of 4000m was downloaded from CE**.**

vi) Sources of ignition data

Fire-ignition sources can either be caused by human or natural. Natural ignition source includes lightning strikes. Lightning data for this study was obtain from Chapter 2 (Mofokeng *et al.*, 2022)**.** Anthropogenic ignition sources are related to human presences and activities such as distance from the road or tourist infrastructure or housing density. A vector road and infrastructure map attained from South African National Parks (SANParks) Scientific Service Department. As a support, Open Street Map data (OSM) was used to download the road, infrastructure and building maps (https://download.geofabrik.de/africa/south-africa.html).

6.2.2 Data preparation for dependent variable

Firstly, a regular shape file with the cell size of 0.0001 degrees were created using create fishnet tool, Sampling in Data Management toolbox of ArcMap 10.7. to create study area polygons. Extract multi values to point data tool was applied to extract values of all environmental drivers of fire danger to fire point layer. Fire point data were then joined using Spatial Join Analysis tool of ArcMap 10.7 with delineated study area polygons to create a binary layer (10m) indicating the presence and absence fire polygons. All the polygons with null values on Lat, Long and acquisition date were treated as non-fire polygons and denoted a value of 0 for newly created field name “Fire occurrence” and “1” for presence of fire polygon. A binary layer attribute table with associated drivers’ values was then converted into “XLS” format. “Fire_Occurence” field was dependant variable and all drivers are independent variables for models and statistical analysis.

6.2.3 Data preparation for independent variables (drivers of fire danger)

i) Fuel factors

MOD09A1 and Sentinel-2 were processed following the synthesis methods from Chapter 5 (see Appendix 2) to compute GCI_NDMI, GVMI, and NDVI for VCI. VCI is good indicator of how dryness affect vegetation (Clarke *et al.*, 2019; Martín *et al.*, 2019) (Kogan, 1990) and was calculated following Equation 6.1.

$$VCI = \left(\frac{NDVI - NDVI_{min}}{NDVI_{max} - NDVI_{min}}\right) * 100 \qquad \text{Equation 6.1}$$

where VCI is the Vegetation Condition Index, NDVI is the index of greenness and $NDVI_{min}$ is the index minimum and $NDVI_{max}$ is the index of maximum greenness. Lower values of VCI indicate severe dryness for vegetation or poor vegetation condition.

Degree of curing (DoC) as refers to the process of grass senescence, or die-off and the transition of live fuels into the dead fuel component of fuel bed (Duff *et al.*, 2020). DoC is one the key drivers of fire ignition and spread and has been long used in Australia Fire Danger Rating System (Noble *et al.*, 1980)Martin et al., 2015). High percentage of curing is associated with high fuel flammability and high rate of fire spread. It was demonstrated that fire propagation can occur to curing level as low as 20% (Cruz *et al.*, 2015). Vegetation moisture is one of the most essential indicator of potential fire ignition and propagation, hence several fuel moisture prediction models have been developed for fire danger rating systems (Zacharakis and Tsihrintzis, 2023a). Ceccato *et al.* (2002a) developed the GVMI and demonstrated that the index can directly measure vegetation moisture content regardless of species composition. Wang *et al.* (2013)incorporated GVMI for fire danger assessment. Higher fuel moisture may decrease the likelihood of fuel ignition.

The mean composite of GCI, GVMI, VCI and BSI images were averaged to obtain a single raster for respective index. Since the images were downloaded and processed using the extent of the study, the Clip Raster by Mask layer of QGIS 3.28 was applied to produced Curing, fuel moisture, vegetation condition and Bare soil maps of the study area.

ii) Topographic factors

Elevation is a vertical distance above sea level at a location on ground, lightning strikes are frequent at high elevation, which may increase lightning-ignition likelihood (Clarke *et al.*, 2019). Vegetation in high elevation has higher rate of humidity, lower temperature and density hence is associated with few fire occurrences. Slope is the degree of inclination or steepness of an area expressed in degree (Trollope *et al.*, 2004). Fires are more likely to spread uphill due to convection **,** the steeper slope leads to more fuel preheating (Morandini *et al.*, 2018).

Aspect defined as the compass direction that slope faces defined as the compass direction that slope faces (Trollope *et al.*, 2004) the cosine transformation of land which is commonly expressed as the compass direction, (The COMET Program, 2022). The aspect facing the sun have lower humidity, as a result increases the dryness of combustible materials leading to low fuel moisture which increase ignition likelihood (Clarke *et al.*, 2019). Aspect and Slope were derived from Elevation using ArcMap Spatial Analysis Surface Tool.

TPI, and TRI were derived from the elevation using Raster analysis GDAL TPI and TRI tool of QGIS version3.28.5. TPI is a measure of topographic slope position calculated as a difference from the mean elevation of cells in a specified neighbourhood (De Reu *et al.*, 2013). Positive values of TPI indicate a ridge, negative values indicate a valley and values around zero indicate relative flat landscape (Bowman *et al.*, 2021). Lightning is more prevalent on ridges which may increase ignition likelihood (Clarke *et al.*, 2019). Ridges or canyons can change prevailing wind patterns by funnelling air , increasing wind speed and thereby fire acceleration (Viegas and Pita, 2004). The TPI is calculated following Equation 6.2. (Weiss, 2001):

$$TPI = M_0 - \sum_{n=0}^{n}(\frac{M_n}{n}) \qquad \text{Equation 6.2}$$

where M_0 represents the elevation of the model point being assessed, Mn denotes the elevation of the grid, and n indicates the total number of surrounding points considered in the evaluation.

If each square represents a grid cell on a DEM, then TRI is calculated following Equation 6.3 (Riley *et al.*, 1999):

$$TRI = Y[\sum(x_{ij} - x_{00})^2]^{0.5} \qquad \text{Equation 6.3}$$

where x_{ij} is the elevation of each neighbour cell to cell (0,0).

TRI an index for quantitative measure of topographic heterogeneity calculated as a sum of change in elevation between grid cell and its eight neighbour grid cells (Riley *et al.*, 1999). Lower values of TRI the indicates smooth surfaces or levelled area and as result it was classified as the very high fire danger (Babu and Roy, 2020) .

TWI is the most commonly used hydrologically-based topographic index and is described as a function of slope and specific catchment area that describes the tendency of a cell to accumulate water (Mattivi *et al.*, 2019). Hence it has been used as proxy to soil moisture TWI was computed following (Beven and Kirkby, 1979) Equation6.4 using ArcMap 10.7.1.

$$TWI = In\left(\frac{\propto}{tan\beta}\right) \qquad \text{Equation 6.4}$$

where α is the cumulative upslope area of drainage through a point, and tan β is the slope angle at that point. Higher TWI values, the wetter the surface thereby higher soil moisture. High soil moisture makes the surrounding vegetation harder to ignite (Zhao *et al.*, 2021a).

Elevation map was created first and re-projected to UTM Zone 35S and other topographic maps were created thereafter as explained above. All topographic maps were classified into fire classes using quantile except Aspect. Aspect map was categorized into nine classes, namely, Flat, North, North-east, North-west, South, South-east, South-west, East, and West.

iii) Climatic/Weather Factors

In this study, Code Editor of GEE, a web-based integrated development environment for writing and running was used for LST extraction from MOD11A2 (Appendix 3). An increase in LST indicates reduction in fuel moisture content thus increase the likelihood of fire ignition. Hence LST has been used as a driver for fire danger assessment in numerous studies (Wang *et al.*, 2013; Sayad *et al.*, 2019; Dang *et al.*, 2021; Kondylatos *et al.*, 2022; Sharma *et al.*, 2022). Because of the fanning effect, wind significantly affects the fire ignition and spread (Ghodrat *et al.*, 2021). Wind accelerate the preheating of fuel, reduce fuel moisture resulting in drier fuel, thus increase the likelihood of fire ignition and spread. Similarly, to fuel parameters, composite images from June to October for the period of 2007 to 2021 for both LST and Wind speed were averaged to a single raster, clipped by mask layer and resampled to produce 10m LST and Wind speed maps.

iv) **Sources of ignition data processing**

Lightning Hazard Map developed from Chapter 3 (Mofokeng *et al.*, 2022) was used in this study. Roads not only serve as the source of fire ignition, roads can also act as barrier or fire breaks and can also aide in containing the fire as the roads increase the accessibility allowing the fire control or fighters easier access to fire (Kumari and Pandey, 2020). With regards to roads as ignition sources of fire, roads may increase the likelihood of intentional "arson" ignition especially far from the road and accidentally ignition near the through the discard of cigarette butts. Other infrastructure and building such as tourist facilities, offices, staff dwellings are associated with increased population which may increase likelihood of accidental fire ignition. Spatial Analyst Tool, Hydrology, was used to derive river networks applying strahler method.

The proximity from the roads (regional, local, trails and management roads), rivers (perennial) and infrastructure/building (tourist's facilities, hotels, staff dwellers and any building) maps were derived by firstly converting vector to raster using rasterize tool. The proximity tool of raster analysis of QGIS 3 software was used to calculate Euclidean distance to road networks, river networks and infrastructure/buildings. Proximity Maps of maximum distance of 500m and 1000m to infra/building, and river and road respectively were then created at spatial resolution of 10m.

v) Soil factors

Soils play a decisive role in soil-plant-atmosphere systems by allowing extraction of water and nutrients by roots while providing support for plant growth (Indoria *et al.*, 2020) thus fuel condition for fire danger. Wildfire occurs in soils with high sand contents, relatively low clay and silt content (Mathu, 2020). Sandy soils are known to have low water available capacity and therefore vegetation on soils with low available water capacity are susceptible to water stress (Mulder *et al.*, 2019). The higher the sand content the lower the available water capacity, and therefore increased the likelihood of fire ignition. Relative high clay and silt content is associated with high soil water retention and available water capacity thus less vegetation stress and decrease the likelihood of fire ignition. Tanveera *et al.* (2016) has shown a positive correlation between sand content and soil bulk density, therefore high bulk density high vegetation water stress. Bulk Density is a measure of soil compactness and is calculated as the ratio of dry soil mass per unit volume and an indicator of soil quality (Mora and Lázaro, 2014)**.** Wildfire tends to occur less on smaller particle sizes as compared to large particles, the higher the coarse soil content the likelihood of increase in fire occurrence. Clay, Silt, Sand content and coarse fragments, as well as soil bulk density images were extracted using the extent of the study area, the maps were generated by applying Clip Raster by mask layer tool of QGIS, resample to spatial resolution of 10m and reclassified using quantile.

Bare soil is crucial for understanding of ecosystem structure and has become a key driver of ecological functioning (Biancari *et al.*, 2020). Bare soil can be used as the barriers and can limit the direction and rate of spread as well as an indicator of fuel continuity and load (The COMET Program, 2022)**.** BSI has been used to discriminate bare soil from other land cover and land use classes (Novkovic *et al.*, 2021) and is not widely used as driving factor for fire danger assessment. The values of BSI increases as the density of vegetation decreases and ground exposure increases (Kumari and Pandey, 2020). This study has adapted the modified bare soil index as proposed by Nguyen *et al.* (2021) and computed using the following Equation using GEE platform.

$$MBI = \frac{SWIR1 - SWIR\ 2 - NIR}{SWIR1 + SWIR2 = NIR} + f \qquad \text{Equation 6.5}$$

where SWIR1 and SWIR2 are shortwave infrared red band 6 and 7 for MODIS and band 11 and 12 for Sentinel-2 and *f* is an additional factor (*f*=0.5).

6.2.4 Multicollinearity Analysis

Multicollinearity assessment is the test predominately used for detection spatial correlation among independent variables (driving factors) used to model the response variable (fire danger) occurrence (Daoud, 2017). In this study variance inflation factor (VIF) was used as a diagnostic tool for Multicollinearity assessment of Ordinary Least Squares (OLS) linear regression analysis. VIF elaborates by how much variances of estimated regression coefficient is inflated due to the correlation between the predictors in the model (Akinwande *et al.*, 2015). OLS analysis was executed using OLS Modelling Spatial Relationship tool of ArcMap 10.

6.2.5 Fire Danger modelling techniques

Fire danger maps were created using Susceptibility Zoning (SZ) QGIS plugin developed for landslides zoning (Titti and Alessandro, 2021). Nonetheless it can be utilized to map any kind of susceptibility. The SZ plugin has been selected because of its usability, collector of QGIS processing scripts in Python which runs as a part of GIS platform and as it can predict and validate susceptibility using six (6) different models such as WoE, FR, LR, RF,SVM and DT (Titti *et al.*, 2022). Hence, this study utilized all these methods for fire danger mapping. (Titti and Alessandro, 2021; Titti *et al.*, 2022) fully explained the simulation process of the plug-in.

6.2.5.1 An overview of adopted machine learning

i) Weight of Evidence (WoE).

WoE is a is a quantitative data-driven approach based on Bayesian principles The weight of evidence (WoE) is a quantitative data-driven approach based on Bayesian principles to integrate spatial datasets (Salavati *et al.*, 2022) and to estimate the relative importance of independent variables on a dependant variable (occurrence). It utilized conditional probabilities statistics to determine weight values of geographic evidence layers that are closely associated with the predicted events (Romero-Calcerrada *et al.*, 2008; Salavati *et al.*, 2022). These weight values are then used to calculate the probability of events within a given area by superimposing the weight value of each evidence layer that represent the contribution of corresponding evidence factor to event occurrence (Bonham-Carter, 1994). Hence is based on the concepts of prior and posterior probability (Romero-Calcerrada *et al.*, 2008; Hong *et al.*, 2017). The weights were determined using Equations 6.6 and 6.7.

$$Wi^{+} = In\left(\frac{\text{Npix1}}{\text{Npix1+Npix2}} \Big/ \frac{\text{Npix3}}{\text{Npix3+Npix4}}\right) \qquad \text{Equation 6.6}$$

$$\mathrm{W}i^{-} = \mathrm{In}\left(\frac{\text{Npix2}}{\text{Npix1+Npix2}} \Big/ \frac{\text{Npix4}}{\text{Npix3+Npix4}}\right) \qquad \text{Equation 6.7}$$

where W^{+} indicates that there is a driving factor at the site of the fire, and the magnitude of this weight indicates the correlation between that factor and the occurrence of the fire. W^{-} indicate the absence of the desired factor at the site of the fire, indicating inverse level of correlation. N_{pix1}= the number of pixel with fire in class, N_{pix2}= the number of pixels with fire in the map minus the number of pixels with fire in the class, N_{pix3} = the number of pixels in the class minus the number of pixels with fire in the class, and N_{pix4} = the total number of pixels in map minus the number of pixel with fire in the class.

The difference between positive and negative weight which is termed weight contrast (W_f) which indicates the magnitude of the spatial relationship between the driving factor and the fire occurrence is calculated using Equation 6.8.

$$W_f = W^+ - W^+ \qquad \text{Equation 6.8}$$

ii) Frequency Ratio (FR)

FR is a binary statistical model based on the favourability function (Pradeep *et al.*, 2022). Like WoE, FR describes the importance of classes for each driving factor in relation to the occurrence of fire. However FR defines the ratio of the probability of fire occurrence to the probability of non-occurrence fire for a given fire driving factors (de Santana *et al.*, 2021; Mohajane *et al.*, 2021). (Mohajane *et al.*, 2021; Xie *et al.*, 2022) fully explained the calculation of the FR model.

iii) Logistic Regression (LR)

LR is a modelling technique that is part of the family of generalized linear models (Phelps and Woolford, 2021) and is one of the popular statistical models utilized effectively to predict fire occurrence and examine the driving factors for fire ignition and propagation. In regression model , an equation for predicting the value of the dependant variable based on one or more independent predictor variables is developed(Pham *et al.*, 2020). In the context of fire danger assessment modelling, the goal of LR is to find the best fitting model that can describe the relationship between the existence (1) or absence (0) of fire (i.e. dependent variable,) and a set of independent variables (fire driving factors) (Hong *et al.*, 2019; Pham *et al.*, 2020). (Hong *et al.*, 2019) provide the general form of LR equation.

iv) Decision Tree (DT)

Decision Tree (DT) is a non-parametric, supervised learning approach utilized for classification and prediction. Its easy interpretability and simplicity make DT more transparent for application in decision-support systems (Coffield *et al.*, 2019) and has a Boolean function (if each decision is binary, i.e., true or false) (Xie *et al.*, 2022). DT is based on the human-understandable tree-rules (If/Then rules) to extract predictive information. A tree-like structure is designed that kick starts with all training samples and select the variable that best fit the class and make subdirectories (Debeljak and Džeroski, 2011). The tree branches are constructed from the test performed at each step by the algorithm on the middle nodes. At each split in the tree, all input attributes are evaluated for their influence on the predictable attribute (Tang and Maclennan, 2005; Gholamnia *et al.*, 2020). Predictions of the model are seen at the leaves of the tree also known as final nodes. A detailed description of the DT algorithms for wildfire predictions and classification has been described (Jaafari *et al.*, 2018).

v) Random Forest (RF)

For mapping and modelling wildfires, RF is one of the most effective non-parametric ensemble learning techniques proposed by Breiman in 2001 as an inheritance and improvement of the traditional DT (Breiman, 2001). The efficiency of RF is influenced by two parameters: the number of trees in the forest (ntree) and the number of random variables per split node (mtry) (Su *et al.*, 2018; Tan and Feng, 2023) . Sharma *et al.* (2023) thoroughly explained the RF algorithm for the RF classification and regression algorithms.

vi) Support Vector machine (SVM)

Based on structural risk reduction approaches and statistical learning theory, SVM is one of the most reliable supervised ML techniques for creating a linear hyperplane to divide two classes, e.g. fire and non-fire (Jaafari and Pourghasemi, 2019). The core idea of SVM model is to establish the classification hyperplane as a decision surface to maximize the isolation edge between positive and negative examples by providing a high generalization performance (Pang *et al.*, 2022). The SVM can quite well solve high dimensional and non-linear pattern recognition problems (Xie *et al.*, 2022) by using its kernel functions. Kernel functions can map the original input space to a new feature space, making samples that are otherwise linearly indistinguishable potentially distinguishable in the kernel space (Tan and Feng, 2023).

6.2.6 Development of the Grassland fire danger modelling maps

Substantial methods have been used to segment the danger classes into discrete classes. For example, Eskandari *et al.* (2021) used natural breaks to classify the Golestan fire-susceptibility map into four classes. Gholamnia *et al.* (2020) also used the natural breaks as classifier method for fire susceptibility map of Amol County in Iran. In this study ROC curves were not only used to assess model performance, it was also used to produce a robust classification of the fire danger map (Titti *et al.*, 2021). SZ plugin developed a new genetic algorithm (GA) based classifier which is an iterative meta-heuristic algorithm based on the numerical reproduction of Charles Darwin's natural selection theory (Titti *et al.*, 2022). This study applied this GA-based classifier using "classify vector by ROC" tool to classify the susceptible/danger index into five (5) danger classes: Insignificant, Low, Moderate, High and Extreme High. The classifier is based on quantile classification method. Bustillo Sánchez *et al.* (2021) applied quantile classification method for spatial assessment of wildfire susceptibility in Santa Cruz Bolivia. A zonal statistic tool in ArcMap 10. was used to determine the area coverage of each fire danger class.

6.2.7 Model Performance assessment

The evaluation criteria are a key factor in assessing the performance and validation of prediction model (Sokolova and Lapalme, 2009; Zhang *et al.*, 2019). Cross-validation is one of the common techniques used for model performance and validation. A simple model fit and random split in test methods was used for this study as embedded in SZ plugin. The ability of fire danger model to predict the spatial distribution of fire and to evaluate robustness of the model fitting capacity were done using the Area Under the Curve (AUC) calculated from the Receiving Operating Characteristic (ROC) (Zhang *et al.*, 2019; Sharma *et al.*, 2022). ROC/AUC technique is a productive method for portraying the efficiency of probability map predicted by a particular model (Pourtaghi *et al.*, 2016). The ROC curve portrays the trade-offs or relation between True Positives Rates and False Positives (FPs) rather than arbitrarily selecting a particular threshold (Zhang *et al.*, 2019). SZ plugin Plot ROC curve as following Equation 6.9 (Titti *et al.*, 2021).

$$TP_{rates} = \frac{TP}{TP+FN} \quad FP_{rates} = \frac{FP}{FP+TN} \qquad \text{Equation 6.2}$$

where TP_{rates} =Sensitivity. TP =True Positive, FN =False Negative, FR_{rates} =Specificity, FP = (False Positive).

Furthermore, randomly splitting of dataset into two datasets: (70% and 30%) to train and validate the model (Titti *et al.*, 2021) which illustrated the success rate and prediction rate curves (Pourtaghi *et al.*, 2016). The success rate that uses the training datasets indicate how well the modelling results fit the training dataset. The prediction rate that uses the validation dataset measures how well the model predicts future fires across the landscape (Jaafari and Pourghasemi, 2019). ROC/AUC values less than 0.6 (>0.6) indicate poor performance, 0.6 – 0.7 a moderate, 0.7 – 0.8 a good, 0.8 - 0.9 a very good and greater than 0.9 shows an excellent model performance (Jaafari and Pourghasemi, 2019).

6.2.8 Importance and contribution of driving factors in fire danger modelling

Like GEE classifier, SZ plugin suffer the limitation of variable importance analysis. The relative importance and contribution of each driving factors for predicting fire danger model was determined by using Maximum Entropy (MaxEnt) algorithm (Adab *et al.*, 2018; Vacchiano *et al.*, 2018; Molina *et al.*, 2019; Mpakairi *et al.*, 2019; Makhaya *et al.*, 2022) and its principle states that the best probability distribution is one with highest entropy (Phillips *et al.*, 2006). Chapter 4 provide the details on data preparation for MaxEnt modelling. Furthermore, WoE and FR algorithms has the capability to determine the spatial association between classes of each driving factor and fire occurrence. Wf (weight of contrast) value and FR was used to determine the spatial correlation between the driving factor and the fire danger probability (Hong *et al.*, 2017; Gholamnia *et al.*, 2020; de Santana *et al.*, 2021; Salavati *et al.*, 2022).

6.2.9 Correlation analysis

The relationship between twenty (20) driving factors and Susceptibility Index (SI) value from fire danger map was analyzed and correlation graph was generated using Pearson Correlation coefficient. The multi-environment trial analysis (metan) package of software –R was used to perform the correlation analysis.

6.3 Results

6.3.1 Multicollinearity assessment

The multicollinearity test revealed that three (3) (Sand, Silt and Clay) out of 23 selected driving factors (Table 6.1.) failed to meet the multicollinearity threshold. Henceforth these 3 factors were excluded from the analysis. The list of factors that met the multicollinearity threshold VIF value of less than 7.5 indicating little redundancy amongst variable as explained in the OLS analysis results are presented in Table 6.2.

Table 6.2: Variable Inflation Factor (VIF) for selected factors influencing fire danger modelling

Variable	VIF	Variable	VIF
Aspect	1.06	Proximity from River	1.52
Bare Soil Index	1.68	Proximity from road	1.23
Soil Bulk density	6.14	Slope	6.13
Coarse	2.43	Soil moisture content	2.75
Elevation	8.91	TAWCP	1.09
GCI	5.99	TPI	1.10
GVMI	3.64	TRI	6.43
Proximity from structures / Infra	1.15	TWI	1.47
Lightning	1.66	VCI	2.48
LST	2.77	Wind speed	1.95

6.3.2 Fire danger prediction modelling

Wildfire danger maps based on six datasets or models consistently depicted the presence of all five (insignificant to extreme high) fire danger classes across the entire study area as presented in Figure 6.2. and 6.3. The decision tree (DT), frequency ratio (FR) and random forest (RF) models showed the greater area coverage in the extremely high danger level or class, while logistic regression (LR), support vector machine (SVM), and weight of evidence (WoE) models showed the greater area coverage in the moderate danger class (Figure 6.2). Figure 6.2 illustrated that DT yielded to the highest extremely high fire danger area coverage (41.11%), followed by RF (35.68%), FR (32.92%), WoE (26.76%), SVM (16.67) and LR (11.48%). However, the results of WoE model illustrated that approximately 82,72% of the study area were in moderate, high and extremely high fire danger classes. On the other hand, FR, DT, SVM, RF and LR models recorded that 73.12%, 70.40%, 69.62%, 68.58% and 66.15% of the study area were in these three fire danger classes (moderate, high, extremely high) respectively. It is evident that all these models had identified that extremely high fire danger areas are mostly concentrated in the southern, south-western of the park (Figure6.3), which is dominated by rocky highland grassland plant community including grass species such as F *caprine*, *T Triandra, M disticha and X viscosa* and eastern part of the study area dominated by grass species such as *A junciformis, D monodactyla, H contortus, M natalensis,* and *A capillus-veneris* found at outcrop/middle plateau grassland as well as the grass species found in Plateau grassland community including *C dactylon*, *H Hirta*, *E.capensis*, *E.racemos* and *S africana*. In additional, the percentage of different fire danger classes of these six machine learning models were calculated. Figure 6.2 illustrated that DT yielded to the highest extremely high fire danger area coverage (41.11%), followed by RF (35.68%), FR (32.92%), WoE (26.76%), SVM (16.67) and LR (11.48%)..

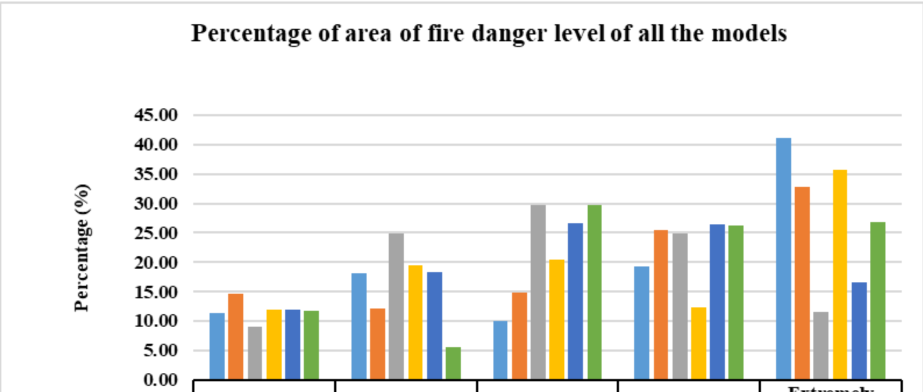

	Insignificant	Low	Moderate	High	Extremely High
DT	11.42	18.17	9.92	19.38	41.11
FR	14.69	12.19	14.80	25.40	32.92
LR	9.02	24.83	29.78	24.89	11.48
RF	11.90	19.52	20.50	12.40	35.68
SVM	12.01	18.36	26.55	26.41	16.67
WoE	11.70	5.59	29.74	26.22	26.76

Figure 6.2: Percentage area of fire danger level of all the models

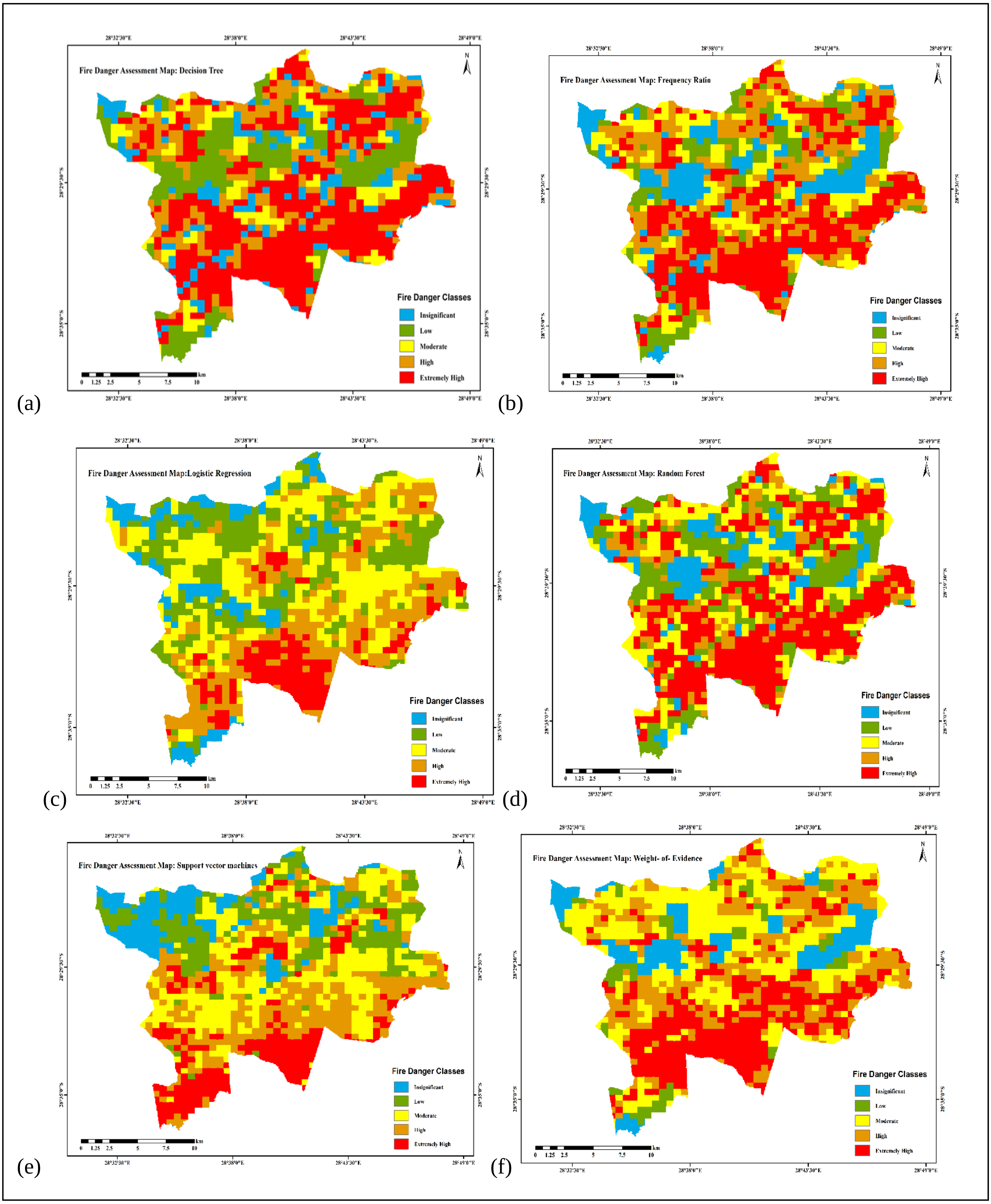

Figure 6.3: Fire danger mapping over GGHNP (a) DT; (b) FR; (c) LR; (d) RF; (e) SVM; and (f) WoE

6.3.3 Models Evaluation

Table 6.3 represent the ROC/AUC values of all the models and Figure 6.4 portray the ROC/AUC curve value from the goodness of model fit results. DT had outperformed other models with AUC value of 0.93, while SVM and LR had poor performed with both yielded a AUC value of 0.63. Other three models, FR, RF and WoE had all performed very good with AUC values of 0.92, 0.91 and 0.83 respectively. Figure 6.5 and Table 6.3 present the performance assessment results of each model using 70/30 training and test dataset. From the success rate ROC/AUC curve, DT has outperformed other models with the highest value of 0.96, FR has 0.95, RF has 0.94, WoE has 0.83, LR has 0.65, whereas as SVM has 0.64 which is the lowest. From the prediction rate, the AUC value of DT is 0.50 the lowest of the all models. Similarly, both RF and SVM demonstrated poor prediction performance with the AUC values of 0.53 and 0.59 respectively. While LR and FR achieved moderate prediction performance having AUC value of 0.60 and 0.66 respectively. WoE has demonstrated good prediction rate outperforming all the models with AUC value of 0.74. On the basis of the above accuracy analysis, a deduction is that WoE is the best model among these six models

Table 6.3: ROC/AUC values of the models

	ROC/AUC		
Model	**Accuracy/Model Fit**	**Success Rate**	**Prediction Rate**
DT	0.93	0.96	0.50
FR	0.92	0.95	0.66
LR	0.63	0.65	0.60
RF	0.91	0.94	0.53
SVM	0.63	0.64	0.59
WoE	0.83	0.83	0.74

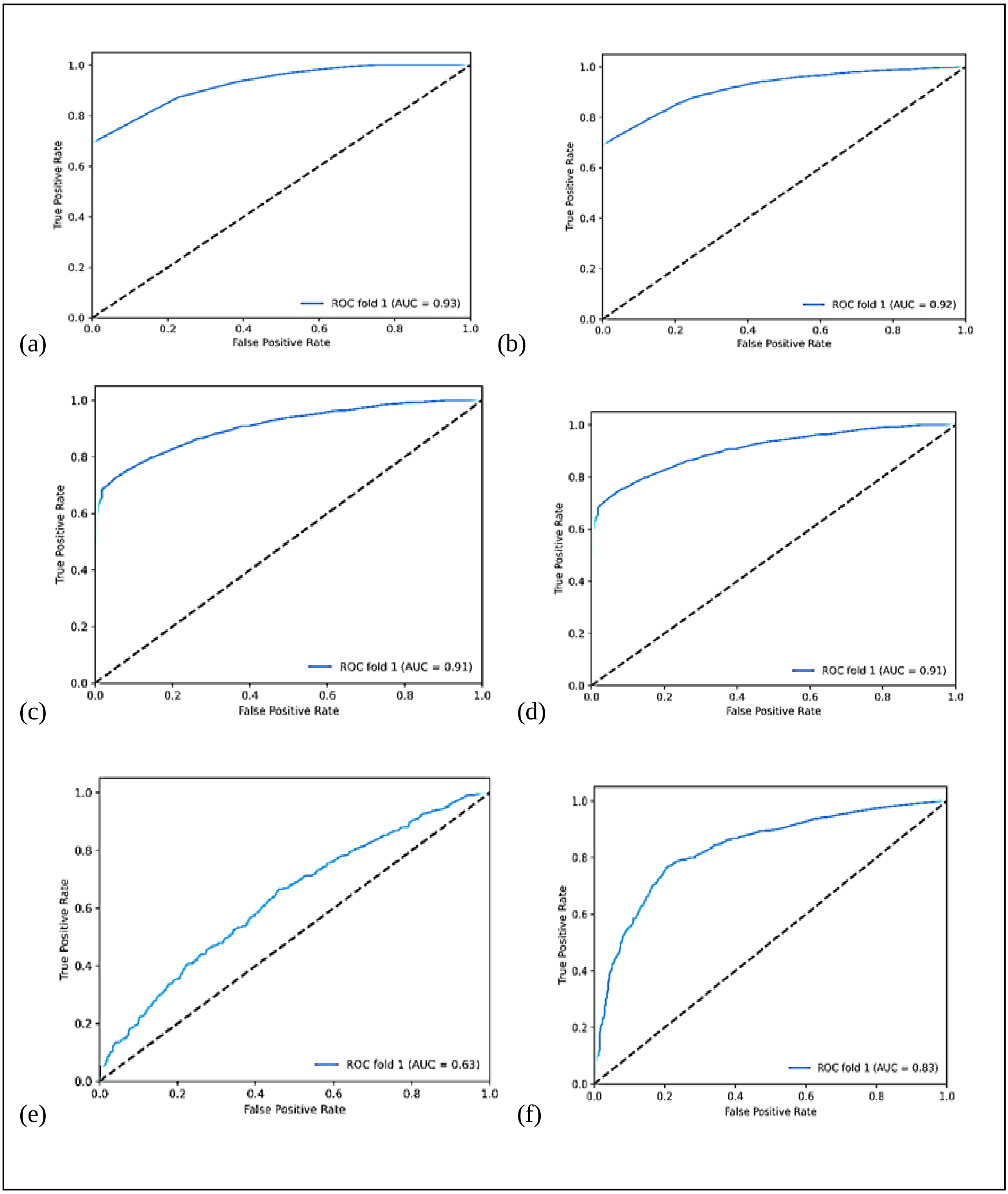

Figure 6.4: ROC/AUC curve of goodness of the model fit performance (a) DT; (b) FR; (c) LR; (d) RF; (e) SVM; and (f) WoE

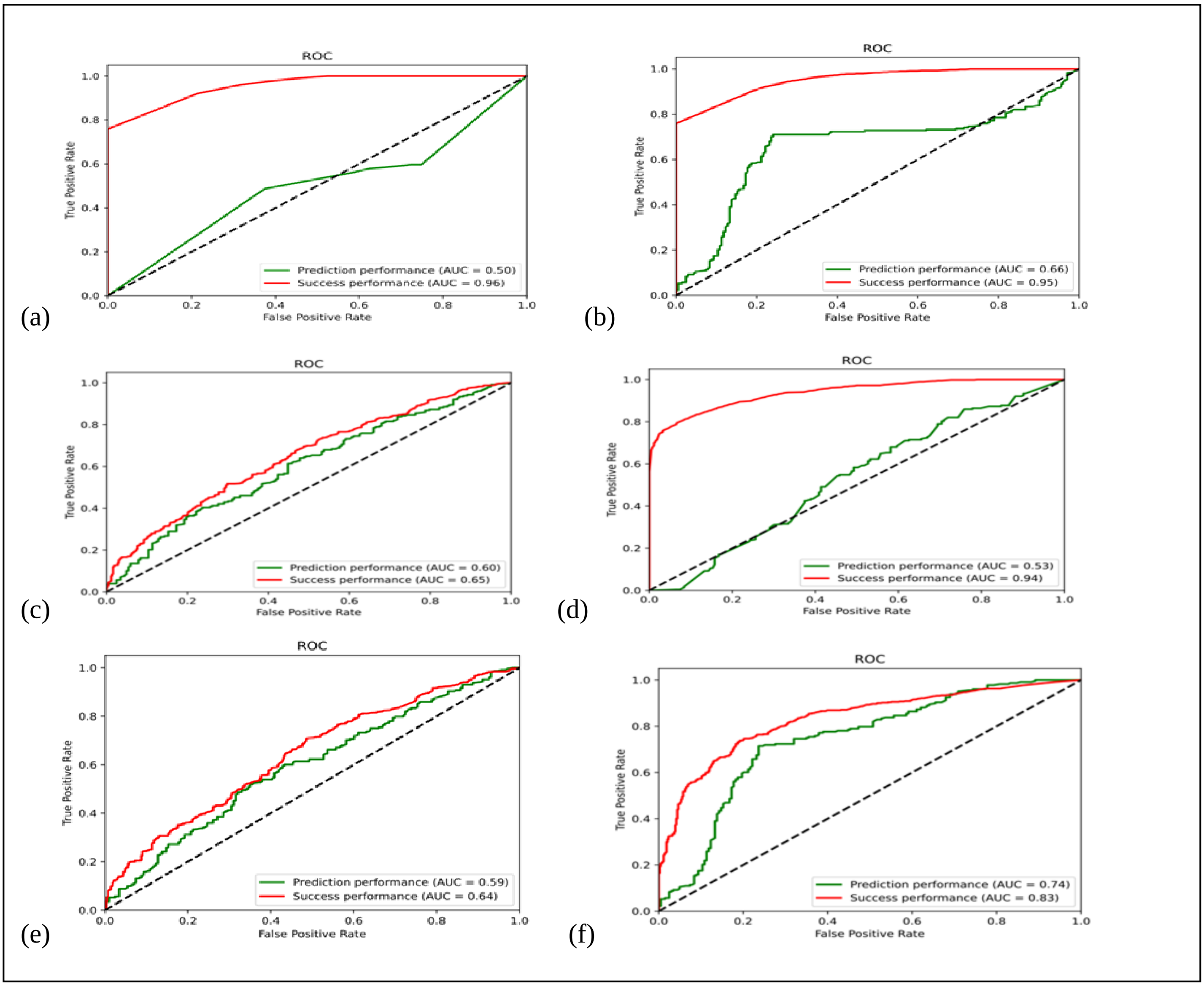

Figure 6.5: ROC/AUC curve of prediction and success rate (a) DT; (b) FR; (c) LR; (d) RF; (e) SVM; and (f) WoE

6.3.4 Importance and contribution of driving factors in fire danger assessment modelling

According to the results of MaxEnt model analysis on the drivers' contribution and importance in fire danger prediction model as illustrated in Table 6.4., LST was the top most and top three (3) driver, accounting 18.8% and 9 % for contribution and importance in the model. Following LST in the order of most contributing driving factors aspect, soil moisture content, bulk density, wind speed, lightning, proximity from river, proximity from road and VCI. While TAWCP had a least contribution to the followed by BSI, elevation, slope, coarse fragments, GCI, TRI, TPI, TWI, proximity from structures and GVM. Soil bulk density was the top most important driver accounting 11.8%, Following Soil bulk density in range from most to least important driving factor is GVMI (10.4%), LST (9%); proximity from road (8.5%), aspect (8%), proximity from river (7.2%), GCI (6.9%); soil moisture content (6.7%), wind speed (5.3%), proximity from structure (4.1), VCI (3.9%), TWI and TRI contributed equally (3.7%), elevation (3.2%), slope (2.4%), BSI (2.2%), TPI (1.6%), coarse fragments (1%), lightning (0.6); and TAWCP (0%).

Table 6.4: Percentage contribution and permutation importance of each driving factor to the fire danger model

Variable	Percent contribution	Permutation importance
Bulk Density	7.7	11.8
GVMI	3.8	10.4
LST	19.9	9
prox_road	4.7	8.5
Aspect	11.4	8
prox_river	5.6	7.2
GCI	2	6.9
SMC	9.1	6.7
Wind Speed	7.3	5.3
prox_structures	3.6	4.1
VCI	4.3	3.9
TRI	2.4	3.7
TWI	3.4	3.7
Elevation	1.3	3.2
Slope	1.8	2.4
BSI	1.2	2.2
TPI	2.6	1.6
Coarse	1.9	1
Lightning	5.8	0.6
TAWCP	0.3	0

Figure 6.6 reveals the results of the jack-knife test regarding the order of importance of the driving factor in the model. VCI was the strongest and influential driving factor of the fire danger model for the study area, therefore, if excluded from the model, its performance is considerably reduced (Adab *et al.*, 2018).

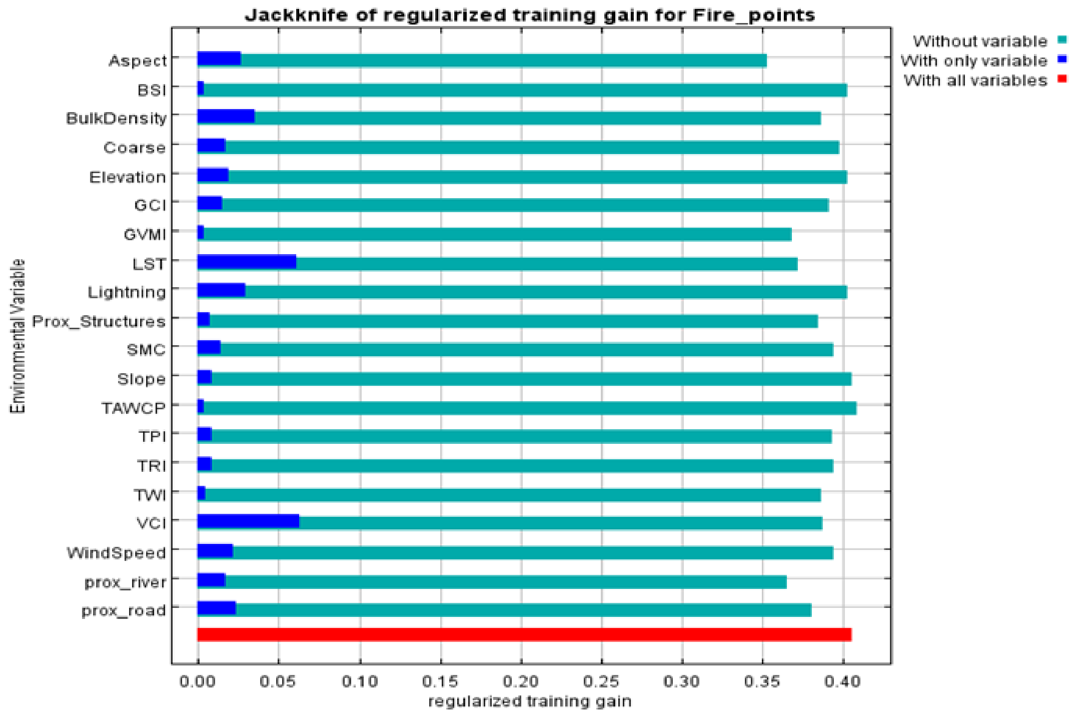

Figure 6.6: The jackknife of regularized training gains for modelling of the spatial distribution of fire

6.3.5 Spatial relationship between each effective factor classes/categories and fire occurrence

The results of spatial relationship of each class of driving factors and fire danger location using WoE and RF are shown in Appendix.4. If the FR is greater than one (>1), there is high correlation and if it is less than one (<1), there is low correlation or no causative relationship (Hong *et al.*, 2017). If the Wf of WoE is positive, the class of driving factor has a role in the occurrence of fire, with positive relation or direct causation. When Wf is zero the factor is not significant for the analysis, and if the Wf is negative means a negative correlation in that the factor reduce wildfire ignition and spread, or no effect or impact on the occurrence of fire (Ye *et al.*, 2017; Salavati *et al.*, 2022). The results of classes of aspect revealed that the class in relief oriented towards Northeast (NE), South (S), Southeast (SE) and Southwest (SW) had the positive Wf value for Wf and FR >1 with highest value observed in NE class. NE facing slope aspect (0.368;1.139) was followed by S (0.103;1.1040), SE (0.101; 1.042) and SW (0.016; 1.007). This indicate that the relief oriented towards NE has a strongest and causative relationship with the fire occurrence and higher probability of fire danger in these areas. While flat zone recorded a negative Wf values and FR <1 (-1.050; 0.552).

As to other topographic factors, for the elevation classes of the positive Wf value and FR >1 was recorded at the altitudes floor ranging from 1976 to 2815m with the highest probability observed at the altitudes floor 1976 – 2094m (0.295; 1.103) followed by the altitudes floor of 2098 – 2815m (0.152; 1.053). The lowest causative relationship was observed at the altitude of 1779- 1875m (-

0.297; 0.894). The slope class of 13.77-21.20 degrees (0.325; 1.113) and 0-4.68 degrees (-0.392; 0.860) had the highest and the lowest impact on the probability of fire occurrence respectively. The highest and lowest correlation was observed in the classes of 0.63 - 2.0 (0.295; 1.103) and 2.0 - 13 (-0.264; 0.907) respectively for the TPI. For TRI, the highest and the lowest probability of the fire danger was observed for the classes of 31.71 - 117.81 (0.310; 1.108) and 1 - 6.86 (-0.331; 0.882) respectively. With respect to TWI, positive causative relationship to the fire danger was recorded by the classes of 3.26 - 5.06 (0.277; 1.097), 6.22-791 (0.043; 1.015) and 10.71 - 17.91 (0.006;1.002). While classes of 7.91 - 10.71 (-0.250; 0.910) and 5.06 - 6.22 (-0.072;0.975) had no effect on the probability of fire danger.

Soil properties analysis results revealed that in terms of soil bulk density the highest and the lowest correlation was observed in the class of 121 - 132 (0.516;1.186) and 141 - 145 (-0.472-0.840) respectively. In terms of soil moisture content, the highest and the lowest impacts on the occurrence of fires was observed in the class of 3.71 - 4.614 (0.422;1.139) and 3.181 - 3.411 (-0.292;0.898). The classes of soil with the coarse fragments between the classes of 103 - 121 and 121 - 194 with Wf values and FR of 0.162;1.057 and 0.161;1.056 respectively had high probability of fire danger location. The negative correlation was observed by the areas with the course fragments between 43 to 103 with the Wf and FR values of -0.223;0.921, -0.057; 0.980 and -0.03;0.987 for the classes of 90 - 103, 43 - 75 and 75 - 90 respectively. For TAWCP, classes of 2 4- 25 (0.263; 1.089) and 25-28 (0.249;1.068) recorded the positive correlation with fire danger whereas classes of 21 - 24 (-0.618; 0.748) and 28 - 33 (-0.263; 0.92)1 showed no effects to the fire danger.

Considering the fuel factors correlation with fire occurrence, all classes in the BSI factor had impact on the probability of fire occurrence except the class of 0.391 - 0.466 (-0.427; 0.848). The highest positive correlation was observed in the class area of 0.373 - 0.382 (0.249; 1.087), followed by 0.334 - 0.365 (0.141; 1.050), 0.382 - 0.391(0.030; 1.010), and 0.365 - 0.373 (0.014; 1.050). Similar to BSI, all the classes of GCI yielded to the positive correlation with the fire danger location except the area between 0 - 30 % (-0.572; 0.816). The highest probability recorded at the area between 60-80% (0.815; 1.304), followed by 50 - 60% (0.562;1.211), 30 - 50% (0.030; 1.007) and 80 -100% (0.022 ;1.010). In contrary to BSI and GCI, all the classes of GVMI factor had no effect to the fire occurrence except in the class of -0.051 - 0.109 with the positive value of Wf (0.704) and FR>1 (1.238). In VCI, the positive correlation was recorded at the area ranging between 28 - 82% with the highest probability of fire danger in class of 39 - 82% (0.671;1.228), 28 - 33% (0.281;1.098), 33 - 39% (0.180; 1.063). The lowest probability of fire danger was recorded in the class of 9.0 -23% (-0.567;0.798) and 23 -28% (0.525; 0.798).

The proximity factors fluctuate more than any other factors, instead of simple positive or negative trend each factor varies spatially from negative to positive in diverse classes. The results for proximity from the roads showed that the fluctuation trends in between the classes. Negative correlation was observed at distances between 0 - 200m (-0.200;0.925) and positive correlation at the distance of between 200 – 400m (0.060;1.024). Similarly, negative and positive correlation was observed at the distance between 400 - 600 (-0.032;0.987) and 600 - 800m (0.140;1.057) and more than 1000m (0.154; 1.036). In terms of proximity from the river, the distance from 200 and 800m recorded positive correlation with the fire danger or potential. The area with the highest probability was observed at the distance between 400 to 600m (0.372; 1.146) from the river. The distance from 800 - 1000m (-0.269; 0.888) and more showed negative correlation with fire potential. As far as the proximity from the tourists' infrastructure and built environment, distance less than 100m (0-100m, 0.177;1.077), between 300 and 400m (0.108;1.047) and more than 500m (0.432;1.009) revealed positive correlation with fire occurrence. The distance between them (i.e.) 100 - 300m (100 - 200, -(0.642;0.718): 200 - 300 (-1.029;0.561), and 400 - 500 (-0.232;0.898) indicate negative impact on the probability of fire occurrence.

The results of the Lightning factor classes revealed that the positive correlation with the probability of fire occurrence was observed at the classes of level 1 (almost danger free lightning zone), Level 4 (severe danger lightning zone) and Level 5 (extremely lightning danger area) with the highest FR value of 1.218 and WoE value of 0.609 recorded at level 5. The lowest correlation with the fire probability was recorded at level 2 lightning minimal danger (-0.618; 0.747), level 3 moderate danger lightning (-0.241;0.917). For LST, highest and the lowest correlation was recorded at the classes of 22 – 23^{o} C (0.37; 1.130) and 19 – 22^{o}C (-0.209;0.926) respectively. In terms of the wind speed, the area with the highest probability of fire occurrence were observed at speed between 4.29 and 11.89 with the highest correlation recorded at the of 6.32 – 11.89 (0.252;1.088) and lowest correlation at the class of 3.59 – 4.29 (-0.131;0.954). Overall, the highest probability of fire danger was observed at the GCI class of 60 – 80% with the Wf value 0.815 and FR value of 1.304 followed by GVMI class of -0.005- 0.109 (0.704;1.238), VCI class of 39 – 82% (0.671;1.228), level 5 of lightning danger (0.609;1.218) and level 1 of lightning danger area (0.587; 1.243l).

6.3.6 Correlation between driving factors and the predicted fire danger map

As depicted by Pearson correlation graph, VCI, GCI, SMC, GVMI, lightning, proximity from river, coarse fragments, elevation, slope, wind speed and TRI had strong statistically significant and positive relationship with the predicted fire danger map with p-value less than 0.001 ($p<0.001$). While soil bulk density and BSI revealed strong statistical and negatively association with the predicted fire danger map. Proximity to road revealed medium statistically significant and negative correlation and a weak statistical significant and negative correlation with LST was observed. TAWCP, TPI, proximity to structures showed non statistically significant correlation with fire danger mapping

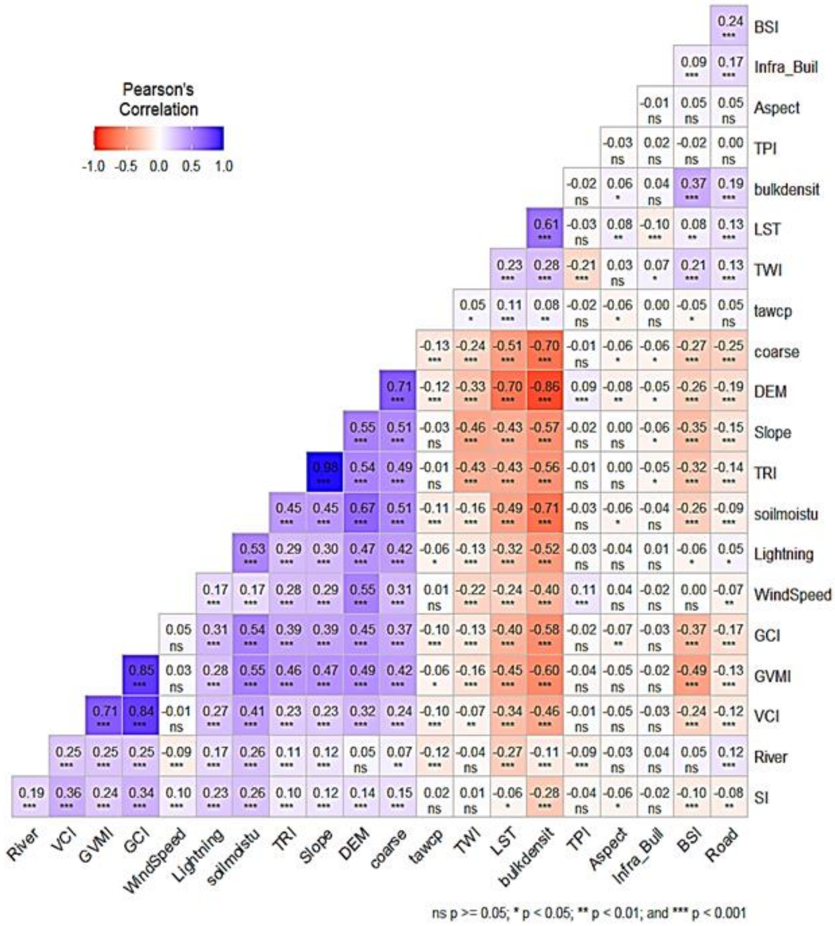

Figure 6.7: Pearson correlation graph among driving factors and fire danger map (WOE model)

6.4 Discussion

6.4.1 Model performance assessment

Considering the importance of grassland ecosystems and the application of fire as the one of the ecological management tool, this study combined twenty (20) driving factors that influence fire occurrence to construct and map fire danger assessment over the grassland GGHNP using conventional machine learning decision tree (DT), random forest (RF), support vector machine (SVM) and statistical frequency ratio (FR), logistic regression (LR) and weight of evidence (WoE) These models, especially RF, SVM and DT (Adab *et al.*, 2018; Hong *et al.*, 2018; Coffield *et al.*, 2019; Jaafari and Pourghasemi, 2019; Eskandari *et al.*, 2020; Milanović *et al.*, 2021; Sharma *et al.*, 2022; Xie *et al.*, 2022) have been largely tested and proven effective in fire danger research. WoE and FR on the other hand, although had outperformed other ML models in predicting complex environmental phenomenon such landslide and gullies (Lee and Pradhan, 2007; Dube *et al.*, 2014; Titti *et al.*, 2022) the application of these methods in fire danger mapping is very limited (Hong *et al.*, 2017; de Santana *et al.*, 2021; Salavati *et al.*, 2022). Despite RF being the typical the most accurate and superior performing algorithm in fire danger modelling (Zacharakis and Tsihrintzis, 2023b) and ranked fourth (4) by (Chicas and Østergaard Nielsen, 2022).

Similarly, superiority performance of RF was expected, however, the result from this study revealed that the RF method had medium performance in comparison with DT and FR in both overall model goodness of fit and success rate accuracy assessments. Furthermore, RF model was the second least poor performed model in prediction rate of fire danger mapping. This is line with previous study were RF was outperformed by other models (Dutta *et al.*, 2016; Pourtaghi *et al.*, 2016; Coffield *et al.*, 2019). Although DT, FR models outperformed RF, all three models performed poorly in prediction rate accuracy assessment, in fact DT had worst prediction accuracy and FR performance was satisfactory, second best from WoE. Poor performance of LR model in this current study was also observed in various fire danger modelling (Guo *et al.*, 2016b; Jafari Goldarag *et al.*, 2016; Gholamnia *et al.*, 2020; Shmuel and Heifetz, 2022) . While WoE had relatively less accuracy in comparison with DT, FR and RF, had outperformed all the models in prediction rate. This demonstrates that WoE can perform just as well as machine learning models for fire danger assessment and mapping. The capability of WoE in achieving balanced accuracy make it a better choice for fire danger mapping in this study area. Furthermore, Phelps and Woolford (2021) has shown that statistical approaches (i.e. logistic GAMs) can perform just as well as the machine learning for fire occurrence predictions and they should be preferred models for fire management operations.

WoE was the best model in prediction rate, however, it was outperformed by DT, FR and RF models in accuracy and success rate. This trend might be explained by the complexity-accuracy trade-offs and the implications of complexity in interpretability and prediction. The trade-off is based on the tendency of complex models to outperform simple models (Gauriau *et al.*, 2024), and interpretable models are worse performers than difficult to understand "black-box models"(Bell *et al.*) Complex models achieve the best performance at the high price of complexity while model interpretability and complexity are positively correlated. However, that trend holds under the assumption that models have been properly parameterized and trained (Gauriau *et al.*, 2024). For example, DT is regarded as interpretable model and are prone to overfitting if not properly parameterized. RF is robust to overfitting and model of choice in fire danger modelling however RF is complex and not interpretable because of aggregation step makes it very difficult to trace the outcome of the model back to the input features (Gauriau *et al.*, 2024). In contrast, WoE is simple and interpretable model. If the data meet the requirements of simple model (linearity) therefore WoE is adept to reveal higher performance.

Because this model can analyze manifold and generalize information and present outcomes as probabilities, thus, offering a robust analytic framework with straightforward interpretation (Wang *et al.*, 2024).

A classification analysis of the developed fire danger maps revealed that the largest percentage of area coverage of the study area was observed from the extreme fire danger class of DT Model (41.11%) succeeded by RF (35.68%) with the lowest percentage of area coverage derived from LR model (11.48%). The findings reveal that these models operate on mathematical concepts that do not necessarily lead to the same performance in environmental settings (Jaafari *et al.*, 2019). Furthermore, these asymmetric performance of models is attributed to model computational algorithm. Decision-tree based models like RF algorithm randomly draws samples, generate multiple decision tree and combine them through averaging or voting in that way reduce overfitting. The basic algorithm of LR model consider a linear relationship between a fire occurrence and its driving factors (Hong *et al.*, 2019) that does not meet the complex nature of phenomena and therefore underestimate the probability of fire danger ((Jaafari *et al.*, 2019). In comparison with SVM can quickly and efficiently implement "transduction inference using a simple and robust algorithm (Li *et al.*, 2020)). However, SVM requires considered to test different kernel functions and model parameters to find the best model and creating the approach impractical for dealing with large sample of datasets (Tan and Feng, 2023)

The efficacy of WoE in fire danger mapping research had been demonstrated by several authors (Dickson *et al.*, 2006; Hong *et al.*, 2017; Jaafari *et al.*, 2017; Salavati *et al.*, 2022). Hong *et al.* (2017) generated fire risk map for China using FR, WoE, linear and quadratic differential analysis models. Their findings showed that WoE had the highest yield (2.82). Leveraging on its ability to deal with generalized and manifold information and represents a robust framework for studying natural hazards, Jaafari *et al.* (2017) used WoE to model fire probability in Zagros Mountains of Iran. The results of their study confirmed the good predictive ability of the WoE model with AUC value of 84.2 and 80.4% for success rate and prediction rate. The authors recommended the model due to its relatively straightforward to implement and interpret results, simplicity and predictive power, easy to incorporate multi-source of information and to apply in GIS environment, objectivity (Ye *et al.*, 2017). Salavati *et al.* (2022) assessed fire danger potential using WoE and Statistical Index (SI) models and compare them their findings demonstrated the superiority of WoE over SI. The main weakness of WoE is that it neglects the internal correlation among the driving factors that are incorporated in the model to predict natural hazards (Hong *et al.*, 2019). However, incorporating WoE model with other ML models or hybrid models could be an effective solution to cope with this problem. Studies have also suggested coupling WoE with AHP (Hong *et al.*, 2019) and constructing multimodal ensembles (Yu *et al.*, 2022). Hence, in future an appropriate ensemble of WoE like FR based by (Mohajane *et al.*, 2021; Xie *et al.*, 2022) can be built and tested for the improvement of fire danger modelling accuracies.

6.4.2 Driving factors of fire danger assessment and modelling

To understand the probability of fire danger it is imperative to analysis the importance, contribution and spatial relation between fire occurrences and its driving factors. This study explored the importance, spatial pattern and relationship among twenty (20) drivers for fire danger mapping of GGHNP using MaxEnt, WoE and FR and Pearson correlation to determine key drivers to fire occurrence. In terms of source of ignition, proximity from the roads have been confirmed as the key important factor to the prediction of fire danger, while lightning contributed more to the fire danger modelling. Proximity from the road networks and other infrastructures such as building and tourist facilities showed inverse relationship to fire danger, i.e. closer to the road, the higher the probability of fire occurrence. However, the proximity from the roads fail to show clear negative or positive trends within the classes of proximities (WoE, FR). Similar fluctuation trend was observed by Ye *et al.* (2017), where they stated that the trend indicated the existence of more complication and that fire ignition pattern vary with distance (space), strengthening the novelty of the relationship between human activities and wildfire occurrence is not linear (Bowman *et al.*, 2011b; Ye *et al.*, 2017). The findings of fire ignition pattern in terms of classes, fit both tenents or assumptions that fire ignitions exist in near to infrastructure as shown by many researches, for instance (Costafreda-Aumedes *et al.*, 2017; Ye *et al.*, 2017; Clarke *et al.*, 2019; de Santana *et al.*, 2021; Dorph *et al.*, 2022) . In contrast with the common conclusion that highest probability of fire ignition is at intermediate level of population density , a review by Ganteaume *et al.* (2013) provide some of researchers. The findings by Pradeep *et al.* (2022) also revealed that areas located far away from settlements and roads of Eravikulam National Park in India had a spatial correlation with fire occurrence with the FR values >1.

The observed fire ignition pattern for this study can be explained using a saturation curve as described by (Pausas and Keeley, 2021), in that if weather conditions are not severe , few ignitions are unlikely to generate a wildfire however there is level of ignitions in which the probability of fire increases abruptly. Some areas may therefore be limited by natural ignition and saturated by frequent lightning strikes or saturated by human population density, in which case a small reduction in ignitions may not reduce fire activity. Even relatively small number of ignitions if coupled with extremely fire weather can generate fires. GGHNP is a mountainous protected area, saturated by frequent lightning strikes as spatial autocorrelation analysis by Mofokeng et al. (2022) revealed that the clustering of lightning strikes at the park is at the distance of about 1.2km. As the park the presence of human is limited and therefore has smaller human population density thus less-fragmented landscape. Therefore, reduced ignition occurrence may be sufficiently compensated for by less-fragmented fuel resulting in more extensive fires. It takes fewer people to provide sufficient ignition source and lightning can provide adequate sources of ignition in smaller human population. Although lightning was on the least important driver of fire danger probability, in concord with (Archibald *et al.*, 2009), lightning account over 5% towards fire danger assessment model. Spatially, as per expectation, most of fire occurred at class 5, extremely high lightning danger zone, however, class 1 free-zone lightning danger area also show positive correlation with fire danger probability. On the basis of this observation, it can be concluded that fire ignition pattern of GGHNP is driven by both anthropogenic and natural source of ignition.

Lightning and elevation had positive correlation, this is in concord with the general conclusion that as elevation increases the lightning strikes increase. Catry *et al.* (2009) found that elevation have a positive influence on ignition distribution and lightning-caused fire are prevalent in high elevation. Elevation, slope, aspect, TPI, TWI and TRI are topographic drivers incorporated in this study. Elevation was the third most important topographic factor and thirteenth 13th out of 20 drivers. Generally, fire danger is higher at lower elevations because is associated with low humidity (Eskandari *et al.*, 2021). However, this study found a significant positive correlation between fire danger and elevation and response curve shape (Appendix 5) illustrated that the fire danger increase as the elevation rise. Spatially pattern illustrated a slight non-linear variation between elevation. The analysis revealed that although fire danger increased with the rise in elevation it slightly dropped at the highest altitude class (>2098). Fang *et al.* (2015) observed the similar contradictory pattern in the boreal forest of the Great Xing'an Mountains, China. The authors suggested that the positive correlation between elevation and fire danger might be possibly attributed to the complex interaction of elevation with fuel and fire weather. Mpakairi *et al.* (2019) also found a positive correlation between elevation and fire occurrence while determining fire hotspot of Kavango Zambezi Transfontier Conservation Area (KAZA-TFCA) of Zimbabwe region. Recent study by Alizadeh *et al.* (2023) reported an increased elevational synchronization of fire danger across ecoregions in western United States (US) mountains, pointing out to a weakened flammability barrier in high elevation owing to climate warming. This imply that higher elevation that were historically wet enough to buffer fire danger have become conducive to fire activity in recent decades (Alizadeh *et al.*, 2021).

Aspect was the top most topographic driver and the third most important driving factor for fire danger prediction model, however, showed weaker negative correlation with the predicted fire danger assessment mapping. Chafer *et al.* (2004) found non-significant relationship between fire and aspect in Sydney basin, Australia. Aspect was found to be collinear with other drivers and was discarded for fire danger analysis (Eskandari *et al.*, 2021). In South Africa (Northern hemisphere) north-facing slope have more direct sunlight exposure, high temperature, less rainfall and low humidity (Trollope *et al.*, 2004) and therefore has relatively sparser and drier vegetation which is favourable for fire activities. Thus expected to have highest fire danger probability. This study satisfied the expectation as NE direction had a greatest correlation with the fire occurrence probability which is in line with fire danger assessment literature. Slope was the second least of importance topographic driver, following elevation on the list of driving factors used in this study. Slope had a significant influence and positive correlation with the predicted fire danger map. Similarly Argañaraz *et al.* (2015) found significant positive correlation between slope and fire frequency. Typically, fires are more likely to spread on intermediate slope than on flat or very steeper slope (Clarke *et al.*, 2019), spatially analysis of this study revealed the similar pattern as fire danger probability increase with the rise in slope steepness and decrease at the very steeper slope (highest slope of the study area). Similar pattern was reported whereby very steeper slope had less fire activities (Oliveira *et al.*, 2013). Fuel-discontinuity might have played a role as rocky outcrops is not adequate to initiate a fire and is less flammable.

Although TWI was the 2nd top most important topographic driver in fire danger modelling (MaxEnt) with the response curve showing inverse relationship with fire occurrence, however, no relationship was found between TWI and the predicted fire danger map. Similarly, no relationship was found between TPI and the predicted fire danger. This findings are consistent with (Eskandari *et al.*, 2020, 2021; Makhaya *et al.*, 2022) and Eskandari *et al.* (2021) further suggested the disqualification use of these drivers in fire danger modelling. TRI, a topographic driver that has not yet received much quantitative attention in fire danger research, was the third most influential topographic driver, demonstrating its superiority among frequently used topographic drivers (elevation and slope). TRI was the second top strongest driver associated with the Fire Weather Index (FWI) threshold for increasing large fires in Portugal (Fernandes, 2019). In general, fire danger probability decrease with TRI, in this study the response curve illustrated similar pattern. In contrast, significant positive correlation between TRI and the predicted fire danger assessment map was observed, Spatially, highest fire danger areas where on the highest class of TPI. This pattern might be due to the effect of climate warming as explained to the effect of elevation on fire danger assessment. Although TRI had collinearity with other topographic drivers (Sharma *et al.*, 2023), its superiority to elevation underscore the incorporation in fire danger modelling.

BSI, GCI, GVMI and VCI were incorporated in the fire danger assessment modelling as the proxies of fuel continuity, dryness, moisture content and load. GVMI was the top most important fuel driver however had the second highest contribution to the model. Generally, the fire danger probability increase as GVMI decrease, the response curve illustrated the similar trend, however, a positive correlation between GVMI and the predicted fire danger map was observed. Spatially analysis also illustrated variation as fire danger probability increase positively and decrease at near highest value and further increase at the highest GVMI values. This non-linear pattern might be associated with the threshold (Pausas and Keeley, 2021) related to fuel moisture. The highest GVMI of the study area of 0.12 imply that the vegetation may ignite and propagate easily as the fuel moisture content exceeds the fire ignition and spread moisture thresholds which fire can be sustained. However, it should be noted that FMC threshold for fire ignition and spread is species-dependant (Chuvieco *et al.*, 2004a). Consistent with Clarke *et al.* (2020), the relationship between fuel dryness (GCI) and predicted fire danger map was positive. Spatially pattern illustrated that probability of fire danger increase as the GCI increase, however decreased above 80%. In that researchers suggested that conditions conducive to extremely fuel dryness in grasslands may be insufficient for the fuel growth required to support fire danger. This could be explained by resource gradient constraints principle (Krawchuk and Moritz, 2011; Kelley *et al.*, 2019).

According to Kumari and Pandey (2020) the probability of fire is expected to be high in areas with low BSI , as these area will be highly vegetated and hence the availability of fuel to sustain fire. This study met the expectation as a significant inverse relation between BSI and predicted fire danger map was observed and response curve showed that the fire activity decrease as the BSI value increase. The spatial analysis also showed a drastic decrease of fire activity at the very highest class of BSI. This could be explained by fuel-constraints principles (Krawchuk and Moritz, 2011) and that higher BSI value is associated with the bare soil cover and therefore act as barrier for fire spread (The COMET Program, 2022). Concerning VCI, the strongest contributor for fire danger modelling the predicted fire danger map show a significant positive relation with VCI, while spatial analysis revealed highest fire activity at the highest value of VCI. This pattern is not surprising, in contrast with woody-communities, in grass community drought is associated with reduced fire activity (Pausas and Keeley, 2021). The researchers stated that this is due to the fact that grasses are highly flammable each year during dry season, and fire activity in most dependent on grass biomass and fuel continuity; in grassland ecosystem, drought reduces fuel continuity and thus less fire spread. Furthermore, Bowman *et al.* (2020) found greatly increased areal extent burned in forest but decrease areal extent burnt in grassland (savannas) in their study of 2019-2020 Australia’s fire season .

Soil Bulk density was of the top most importance driving factor of the model. Bulk density captures soil porosity, which can relate to root growth and therefore influence plant intake of nutrient and water which in turn affect grass production thus fuel condition (Mora and Lázaro, 2014). Bulk density was also one of the strongest predictors of fuel components for all fuel strata modelling in examining the climatic and edaphic gradient variation in wildland fuel hazard in south-eastern Australia (McColl-Gausden *et al.*, 2020). The study found that the probability of extreme fuel hazard decreased as soil bulk density increased. Similarly, significant negative correlation between bulk density and predicted fire danger map was observed in this study with spatial relations showing the highest value of BD having no impact on probability of fire danger. While lowest bulk density class had a greater fire activity. Instead of clay content, this study used coarse fragments as a proxy for soil fertility as soil fertility positively affects grass production, (Archibald *et al.*, 2009). Coarse fragments was the third least important driving factors of the model. In agreement with the hypothesis of Archibald *et al.* (2009), significant positive correlation between coarse fragments and predicted fire danger map was observed in this study, therefore, fire danger probability increased with the increase of coarse fragments. The spatial relation also revealed that the highest fire activity was revealed at the highest classes of coarse fragments. TAWCP showed no significant relation with predicted fire danger map and the only driver that showed 0% importance for the model. This is because Africa Soil Profile database is associated with the shortcoming of data gaps, analysis uncertainty, harmonised data and spatial uncertainty (Leenaars *et al.*, 2014).

Although Chicas and Østergaard Nielsen (2022) classified soil moisture as one of the most least driving factor used in fire danger modelling. However, the application of soil moisture data in fire danger rating systems is gaining traction in fire risk science (Krueger *et al.*, 2022). Soil moisture does not only influence vegetation growth conditions and thus accumulation of fire fuel but also determined the vegetation moisture content and hence the flammability of the vegetation (Chuvieco *et al.*, 2004a; Krueger *et al.*, 2015; Sungmin *et al.*, 2020). Generally, the probability of fire danger decrease as the soil moisture increase. In contrast, significant positive relation between soil moisture and the predicted fire danger was observed in this study. This findings confirmed the global regression models suggesting positive relationship occurrence between soil moisture and fire occurrence in the montane grassland biomes (Krawchuk and Moritz, 2011). This positive trend might have been attributed to chronic lower soil moisture (3.18-4.62mm). (Krueger *et al.*, 2016) has showed that during dormant season, low dormant season soil moisture may reduce vegetation moisture content, increase their flammability and accompanied by extreme weather could provide conducive environment for enhancement of fire activity. Based on this pattern, it is vital important to the use of a combination of current, near-time and antecedent soil moisture data to determine the fire-soil moisture relations.

Generally, it is evident that climatic or weather driving factors had the highest contributions to the fire danger modelling particularly temperature-associated drivers (Turco *et al.*, 2017). In this study, LST was the top most contributor and third most important driver to the model. It is expected that temperature correlate positively with fire danger probability as high temperature increases the probability of fire danger as it increase the effect on evapotranspiration rate and flammability (Hong *et al.*, 2017). This study, on the contrary, revealed a weak significant negative relationship between LST and the predicted fire danger map. Similar relation was observed recently where temperature was negatively related to fire occurrence (Chang *et al.*, 2023). The researched suggested that the most probable reason might be the climate characteristics of rain and heat synchronization, in that when the moisture is high, fuel does not ignite easily in hot weather. Spatially relation analysis also illustrated variation as positive correlation was observed at the area with 22-24^{o}C and negative at the area with the lowest LST class (19-22^{o}C) and highest class (24-25^{o}C). The assumption is that this spatial variation might be due to the local specific biophysical and social conditions of the study area (Zapata-Ríos *et al.*, 2021). In this study, the study area is characterized by a diversity of topography and scenic and heritage or cultural (caves) landscapes. As expected wind speed was positively related to the predicted fire danger map. The higher wind the higher the evapotranspiration rate, the more oxygen is supply for fuel combustion, and higher flame rate and depth as well as the dispersal of embers speed increase (Kelley *et al.*, 2019). Spatially, variation was observed on which fire occurrence decreased in the highest class of wind value. The observation confirmed that severe wind events do not usually accompany extreme fire occurrence (Kelley *et al.*, 2019) due to the role of synoptic circulation interacting with topography (Knight, 2022).

Overall spatial analysis had revealed that the probability of fire danger is higher at the area with the degree of curing rate of 60-80%, fuel moisture content of - 0.0051- 0.109, vegetation with above 35% VCI values indicating low drought to normal condition of vegetation VCI and both at lightning danger free-zone and at extremely high lightning danger. This spatial pattern suggests that the fire regime of the study area is probable fuel- dominated. grassland fires. However, such deduction should be made with caution since fire is a complex ecological disturbance governed by cross-scale interaction such as fire-fuel-atmosphere interaction and these case are beyond the scope of the current studies.

6.5 **Conclusion**

Understanding the probability of fire ignition and spread is critical important in identify fire prone regions especially in mountainous grassland ecosystem and a useful intervention for effective fire preparedness, mitigation planning and sustaining protected area ecological and cultural integrity. This study is probable among the first attempts to map the grassfire danger over the mountainous protected area using statistical (WoE, FR and LR) and conventional machine learning (DT, RF and SVM) models and compare them. The ROC/AUC result revealed that weight of evidence (WoE)

(0.74) had achieved the highest prediction rates while decision tree (DT) outperformed other models in success rate (0.96) and model-fit accuracy rate (0.93). The grassland fire danger maps created by all models revealed extremely high fire danger area concentrated in the south-western, south and eastern part of Golden Gate Highlands National Park (GGHNP), while DT model classified the largest area coverage of 41.11%. This results revealed that statistical models and machine learning models have individual advantages in fire danger prediction and modelling. The analysis also revealed trade-off between these techniques. Statistical method was found better in predictive rates (WoE) while machine learning technique (DT) was found better in success rate and model-fit performance assessment. The capability of WoE in achieving a consistency performance suggests that WoE should be preferred fire danger modelling technique. However, consistency competitive of WoE with the machine learning techniques qualified WoE to be incorporated into hybrid machine learning approach such FR-Bayern Optimization Algorithm (BO) – RF or SVM or XBoost (Xie *et al.,* 2022). for improving fire danger assessment mapping in the Golden Gate Highlands National Park (GGHNP). The developed integrated grassland fire danger maps revealed that almost 50% of the park is high to extremely prone to fire observably concentrated in the southern, SW and eastern part of the park.

Application of WoE and frequency ratio (FR) model allowed for discerning the spatial relationship between fire occurrence and driving factors varied over the different topographic, human, soil, weather, and fuel condition classes. While MaxEnt method assist in the relative importance assessment of driving factors on the fire danger modelling However, the impact of driving factors on fire danger is complex and cannot be apprehended explained by simple monotonic relationship. Overall, spatial analysis revealed that fuel conditions, grass curing index (GCI) class of 60-80%, global vegetation moisture index (GVMI) class of -0.005 – 0.109 and vegetation condition index (VCI) class of 39 -82% as well as level 5 and level 1 of lightning danger area had highest impact on the probability of fire danger. In that the results revealed that the study area’s fire regime was fuel-driven—this suggests that a fire management strategy should be based on a fuel management strategy that considers the local fuel conditions. Therefore, there is an urgent need to identify and determine the thresholds of fuel conditions, especially grass fuel, for fire prevention and control in the study area. Also, suggests that fire ignition source of the study area was caused by both anthropogenic and natural caused, with natural-ignition source dominating fire occurrence owing to heterogeneity with the mountainous terrain of GGHNP.

Knowing where and how the key drivers affect wildfire is significant for fire suppression and preparedness and for Sustainable Development Goal 15; life on land, including protection of natural landscapes and biodiversity and conservation of mountainous ecosystems. In conclusion, this study provides novel perspective to fire danger assessment and modelling methods and offers reference for enhancing the fire management strategies in the protected grassland Afromontane of GGHNP.

CHAPTER 7: SYNTHESIS AND CONCLUSION

7.1 Natural caused source of ignition

The increase of extreme (wild)fire events due to the global changes is becoming evident and is altering fire regimes in thus affect fire occurrence and behaviour. There is a strong consensus that global change is increasing the probability of fire occurrence and danger (Smith *et al.*, 2020)**.** Climate change for example affect fire by directly and indirectly changing the frequency and location of natural and human caused ignition through changing lightning strikes profile and changing human behaviour. The primary aim of the chapter 3 was to determine the spatio-temporal patterns of lightning strikes activity and developed the lightning hazard map of the GGHNP. Lightning fires play a critical role as an ecological disturbance in such a policy of not extinguishing fire started by fire has created more diverse habitant that support a variety of plants and its pollinators (Stephens *et al.*, 2021). Similar policy applies to all SANParks managed protected areas include GGHNP. The data and information derived from this research are intended as basis on how to restore fire as the ecological disturbance under prescribe burning plan on the area that are highly prone to lightning strikes without compromising the its socio-economical goals. Under a climate condition, lightning activities are expected to be extreme owing to the formation of pryrocumulus (PyroCu) or pyrocumulonimbus (pyroCb) clouds. PyroCu may become PyroCb that trigger local storms and thunderstorms. If thunderstorms can cause lightning (Duane *et al.*, 2021), increasing the probability of lightning caused fire to occur.

7.2 Human caused source of ignition

It is no secret that the majority of the fire are ignited by human activity. Human-induced ignitions are associated with human presences and activities often related to indicators like human settlement such as proximity to roads, railways or housing density and etc. Chapter 4 aimed to model temporal dimension of human-caused fire triggers in order to determine the temporal variation and influence of anthropogenic factors on fire occurrence. This research showed that distance from roads (ROADS) strongly influenced weekdays of both seasonal scenarios, while distance from tourist's infrastructure (INFRA) had strong influence in the weekends. This temporary dimension of human caused fire ignition are associated with weather conditions and tourism seasonality of the human behaviour as described by (Martín *et al.*, 2019). Beside influencing fire ignition up to 85%, human-caused fires in Africa can increase the probability of fire danger and occurrence if their coincide with more than recurrent extreme severe weather condition (Archibald *et al.*, 2012; Duane *et al.*, 2021).

7.3 Estimation and spatio-temporal patterns of degree of grass curing (DoC) for fire danger assessment

The research downscaled the coarse spatial data (MODIS) to the fine spatial Sentinel-2 using Index-then-Blend (IB) data fusion method to estimate and assess the spatio-temporal patterns of grass curing. The most critical fuel-based driving factor of the fire occurrence but rarely used in the fire danger assessment and mapping. The method could be used in downscaling available global environmental variables products. Therefore, the study paved a way for the utilisation of fine spatial resolution (10m) remotely sensed data for the estimation of degree of curing instead of meteorologically derived dead fuel moisture content for the preparedness of fire management plan of the GGHNP and other fire agencies within mountainous grassland environment. The study can also be useful for the livestock agricultural practitioners and the games for pasture management. The months of February, September and May were revealed as the lowest, highest, and onset months of the degree of curing of curing of the GGHNP. This temporal trend of degree of curing resembles the climate pattern of the study area (Figure 2.4) and also significant positive correlation between GCIs and precipitation was observed in Figure 5.5.

Since industrialization (1850 -1900) the Earth has experienced a long-term warming trend, with an estimated increase in the global mean surface temperature of 1.09 ^{o}C, and reaching 1.1^{o}C in 2011 – 2020 (Intergovernmental Panel on Climate Change (IPCC), 2007). On a global scale climate warning is expected to greatly affect fuel condition as warming increases evapotranspiration rates leading to drier climate and fuels (Pausas and Keeley, 2021). In contrast, changes in rain patterns are more variable as drought has contrasting effect between forest and grass ecosystems. Ruffault *et al.* (2018) found that increasing drought condition projected by climate change scenarios might affect the dryness of fuel compartments and lead to higher frequency of mega fires in Mediterranean region. In grassland, drought is associated with reduced fire activity because grasses become highly flammable each year during dry season, in that drought reduce fuel continuity and thus fire activity (Pausas and Keeley, 2021).

7.4 Integrated grassland fire danger assessment models

The study mapped the grassfire danger and compare three (3) statistical (FR, LR & WoE and three (3) machine learning (DT, RF and SVM) methods for its efficacy in predicting grassland fire over the mountainous grassland ecosystem. The study revealed trade-off between these methods. Machine learning methods outperformed statistical methods except on predictive rate assessment. The consistency satisfactory performance of WoE model suggest that is suitable and should be the preferred fire danger modelling technique.

The land surface temperature (LST) and vegetation condition index (VCI) were the most influential factors of the fire danger model. The study revealed that fires in the study area were primarily driven by fuel and ignition sources of both natural and human-caused, as revealed by spatial pattern analysis of WoE and FR. The ability of statistical methods to compete at the same par with machine learning methods suggests that both methods are suitable for predicting fire danger over mountainous grassland ecosystem. This study is possibly the first of its kind to predict fire danger in the context of Afromontane protected grassland ecosystem employing integrated approaches including machine learning, statistical, Climate Engine (CE) and Google Earth Engine. Coarse spatial resolution data often leads to inadequately estimation of input variables especially fuel of fire danger modelling at the landscape scale.

7.5 Recommendations

In general, the findings and conclusions of this research study are in agreement with, advance and contribute to scientific knowledge in ecosystem and environmental conservation in particular fire management in mountainous and protected grassland ecosystem. The study could pave a way for conservationist, environmental managers in drawing or improvement on operational integrated grassland fire danger assessment strategy in order to understand the complex interrelation of fire drivers with fire occurrence probability and predict fire danger. For managerial application and future research purpose, the following recommendations are suggested:

1. This study utilised all lightning strikes to develop LHM. However, the study did not consider the polarity, multiplicity and the strengthen of the lightning strikes. Therefore, the future studies should develop LHM based of the positivity and negativity of the lightning or based on long continuing current (LCC) or short continuing current (SCC) would advance the understanding of spatio-temporal patterns of CG lightning activity and accuracy prediction of natural-cause fire ignition.

2. The study developed temporal human-caused fire ignition model in which the park management can adopt for prevention and evaluation of anthropogenic induced fire ignitions controls, as model provide knowledge on human-caused fire ignition drivers that may have impact on the potential fire ignitions according to the season and days of the week. Further research should parse the explanatory variables, for instance, distance to main road, secondary

road, hiking trails, distance to hotels, campsite could improve the model and the knowledge on human-induce fire ignitions.

3. Fire danger maps derived from GCI estimation could be used by park management for fuel treatment strategy and allocate priority area of grass fuel treatment. BI data fusion method can be used for estimating other environmental variables and for downscaling purpose. Further studies should investigate the effects of topographical parameters on the timing of degree of curing in Afromontane grassland ecosystem.

4. The integrated grassland fire danger model indicates that fire regime of the study area is fuel-driven and fires are caused both by lightning and human activities. In these regards the fire management strategy within the park should be based on fuel management or fuel reduction plan that correctly weigh the effects of fuel in fire ignition and fire behaviour prior to fire season. Therefore, there is an urgent need to determine and quantify the critical thresholds of fire switches especially grass fuel conditions such fuel moisture, fuel load and fuel continuity to aide in fire prevention and controlling strategies as well as the fuel treatment at the study area. The application of hybrid and ensemble of machine learning and statistical methods; and deep learning techniques which are easily accessibility from free platform such as GEE and R-Software might improve prediction accuracy of fire danger modelling over the study area and other similar landscapes.

5. Owing to the predicted rising of global warming. further study should look at how grassland fire behaves under a rising temperature and its associated effect on the four fire drivers of fire occurrences.

REFERENCES

Abatzoglou, JT,Dobrowski, SZ,Parks, SA & Hegewisch, KC 2018. TerraClimate, a high-resolution global dataset of monthly climate and climatic water balance from 1958–2015. *Journal of Scientific data,* 5**,** 1-12.

Abatzoglou, JT,Williams, AP & Barbero, R 2019. Global emergence of anthropogenic climate change in fire weather indices. *Geophysical Research Letters,* 46**,** 326-336.

Abdo, HG,Almohamad, H,Al Dughairi, AA & Al-Mutiry, M 2022. GIS-based frequency ratio and analytic hierarchy process for forest fire susceptibility mapping in the western region of Syria. *Sustainability,* 14**,** 4668.

Achu, AL,Thomas, J,Aju, CD,Gopinath, G,Kumar, S & Reghunath, R 2021. Machine-learning modelling of fire susceptibility in a forest-agriculture mosaic landscape of southern India. *Ecological Informatics,* 64**,** 101348.

Adab, H,Atabati, A,Oliveira, S & Moghaddam Gheshlagh, A 2018. Assessing fire hazard potential and its main drivers in Mazandaran province, Iran: a data-driven approach. *Environmental monitoring and assessment,* 190**,** 1-20.

Adab, H,Kanniah, KD & Solaimani, K 2013. Modelling forest fire risk in the northeast of Iran using remote sensing and GIS techniques. *NaturalHazards,* 65**,** 1723-1743.

Adagbasa, GE,Adelabu, SA & Okello, TW. Spatio-temporal assessment of fire severity in a protected and mountainous ecosystem. 2018 2018. IEEE, 6572-6575.

Adelabu, SA,Adepoju, KA & Mofokeng, OD 2020. Estimation of fire potential index in mountainous protected region using remote sensing. *Geocarto International,* 35**,** 29-46.

Adler, C,Wester, P,Bhatt, I,Huggel, C,Insarov, G,Morecroft, M,Muccione, V,Prakash, A,Masson-Delmotte, V & Zhai, P 2022. Cross-chapter paper 5: Mountains, climate change 2022: impacts, adaptation and vulnerability. *Contribution of Working Group II to the Sixth Assessment Report of the Intergovernmental Panel on Climate Change*.

Aguado, I,Chuvieco, E,Borén, R & Nieto, H 2007. Estimation of dead fuel moisture content from meteorological data in Mediterranean areas. Applications in fire danger assessment. *International Journal ofWildland Fire***,** 390-397.

Akinwande, MO,Dikko, HG & Samson, A 2015. Variance inflation factor: as a condition for the inclusion of suppressor variable (s) in regression analysis. *Open journal of statistics,* 5**,** 754.

Aldersley, A,Murray, SJ & Cornell, SE 2011. Global and regional analysis of climate and human drivers of wildfire. *Science of the Total Environment,* 409**,** 3472-3481.

Alizadeh, MR,Abatzoglou, JT,Adamowski, J,Modaresi Rad, A,AghaKouchak, A,Pausata, FSR & Sadegh, M 2023. Elevation-dependent intensification of fire danger in the western United States. *Nature communications,* 14**,** 1773.

Alizadeh, MR,Abatzoglou, JT,Luce, CH,Adamowski, JF,Farid, A & Sadegh, M 2021. Warming enabled upslope advance in western US forest fires. *Proceedings of the National Academy of Sciences,* 118**,** e2009717118.

Alkhatib, R,Sahwan, W,Alkhatieb, A & Schütt, B 2023. A Brief Review of Machine Learning Algorithms in Forest Fires Science. *Applied Sciences,* 13**,** 8275.

Allan, G,Johnson, A,Cridland, S & Fitzgerald, N 2003. Application of NDVI for predicting fuel curing at landscape scales in northern Australia: can remotely sensed data help schedule fire management operations? *International Journal of Wildland Fire,* 12**,** 299-308.

Alonso, C,López, P,Benito, RM & Tarquis, AM 2019. Correlation between vegetation index and soil moisture index using sentinel-2. *Journal of Estudios en la Zona No Saturada Del Suelo,* 14.

Amrhein, E. 2017. *The geography of cloud-to-ground lightning in Yellowstone National Park.* Doctor, George Mason University.

An, S,Zhang, X,Chen, X,Yan, D & Henebry, GM 2018. An exploration of terrain effects on land surface phenology across the Qinghai–Tibet plateau using Landsat ETM+ and OLI data. *Journal of Remote Sensing,* 10**,** 1069.

Anderson, G & Klugmann, D 2014. A European lightning density analysis using 5 years of ATDnet data. *Natural Hazards and Earth System Sciences,* 14**,** 815-829.

Anderson, SA,Anderson, WR,Hollis, JJ & Botha, EJ 2011. A simple method for field-based grassland curing assessment. *International Journal of Wildland Fire,* 20**,** 804-814.

Andrews, PL 2013. Current status and future needs of the BehavePlus Fire Modeling System. *International Journal of Wildland Fire,* 23**,** 21-33.

Arca, D,Hacısalihoğlu, M & Kutoğlu, ŞH 2020. Producing forest fire susceptibility map via multi-criteria decision analysis and frequency ratio methods. *Natural Hazards,* 104**,** 73-89.

Archibald, S 2016. Managing the human component of fire regimes: lessons from Africa. *Philosophical Transactions of the Royal Society B: Biological Sciences,* 371**,** 20150346.

Archibald, S,Lehmann, CE,Belcher, CM,Bond, WJ,Bradstock, RA,Daniau, A-L,Dexter, KG,Forrestel, EJ,Greve, M & He, T 2018. Biological and geophysical feedbacks with fire in the Earth system. *Environmental Research Letters,* 13**,** 033003.

Archibald, S,Lehmann, CE,Gómez-Dans, JL & Bradstock, RA. Defining pyromes and global syndromes of fire regimes. Proceedings of the National Academy of Sciences, 2013. 6442-6447.

Archibald, S,Nickless, A,Scholes, RJ & Schulze, R 2010. Methods to determine the impact of rainfall on fuels and burned area in southern African savannas. *International Journal of Wildland Fire,* 19**,** 774-782.

Archibald, S,Roy, DP,WILGEN, V,Brian, W & SCHOLES, RJ 2009. What limits fire? An examination of drivers of burnt area in Southern Africa. *Global Change Biology,* 15**,** 613-630.

Archibald, S,Staver, AC & Levin, SA. Evolution of human-driven fire regimes in Africa. Proceedings of the National Academy of Sciences, 2012. 847-852.

Argañaraz, JP,Gavier Pizarro, G,Zak, M,Landi, MA & Bellis, LM 2015. Human and biophysical drivers of fires in Semiarid Chaco mountains of Central Argentina. *Science of The Total Environment,* 520**,** 1-12.

Arganaraz, JP,Landi, MA,Bravo, SJ,Gavier-Pizarro, GI,Scavuzzo, CM & Bellis, LM 2016. Estimation of Live Fuel Moisture Content From MODIS Images for Fire Danger Assessment in Southern Gran Chaco. *IEEE JOURNAL OF SELECTED TOPICS IN APPLIED EARTH OBSERVATIONS AND REMOTE SENSING***,** 1-11.

Arndt, N,Vacik, H,Koch, V,Arpaci, A & Gossow, H 2013. Modeling human-caused forest fire ignition for assessing forest fire danger in Austria. *iForest-Biogeosciences and Forestry,* 6**,** 315.

Babu, KVS & Roy, A 2020. Static Fire Danger Estimation Based on the Historical MODIS Hotspot Data Using Geospatial Techniques for the Uttarakhand State, India. *International Society for Environmental Information Science,* 4**,** 11-21.

Bachmann, A & Allgower, B 2001. A consistent wildland fire risk terminology is needed! *Fire Management Today***,** 28-33.

Balbi, JH,Morandini, F,Silvani, X,Filippi, JB & Rinieri, F 2009. A physical model for wildland fires. *Combustion and Flame,* 156**,** 2217-2230.

Banu, T,Banu, C & Banu, C 2014. GIS-based assessment of fire risk in National Park Domogled-Cerna Valley. *Journal of Horticulture, Forestry and Biotechnology,* 18**,** 52-56.

Bardgett, RD,Bullock, JM,Lavorel, S,Manning, P,Schaffner, U,Ostle, N,Chomel, M,Durigan, G,L. Fry, E,Johnson, DJNRE & Environment 2021. Combatting global grassland degradation. *Nature Reviews Earth Environment,* 2**,** 720-735.

Bartsch, A,Balzter, H & George, C 2009. The influence of regional surface soil moisture anomalies on forest fires in Siberia observed from satellites. *Environmental Research Letters,* 4**,** 045021.

Bell, A,Solano-Kamaiko, I,Nov, O & Stoyanovich, J. It's just not that simple: an empirical study of the accuracy-explainability trade-off in machine learning for public policy. 2022. 248-266.

Bentley, ML & Stallins, JA 2005. Climatology of cloud-to-ground lightning in Georgia, USA, 1992–2003. *International Journal of Climatology: A Journal of the Royal Meteorological Society,* 25**,** 1979-1996.

Berlinck, CN & Batista, EKL 2020. Good fire, bad fire: It depends on who burns. *Flora,* 268**,** 151610.

Bhavika, B 2010. *The influence of terrain elevation on lightning density in South Africa*, University of Johannesburg (South Africa).

Bian, H,Zhang, H,Zhou, D,Xu, J & Zhang, Z 2013. Integrating models to evaluate and map grassland fire risk zones in Hulunbuir of Inner Mongolia , China. *Fire Safety***,** 207-216.

Biancari, L,Aguiar, MR & Cipriotti, PA 2020. Grazing impact on structure and dynamics of bare soil areas in a Patagonian grass-shrub steppe. *Journal of Arid Environments,* 179**,** 104197.

Bird, JCM 1996. Geomorphological aspects of veld burning in Golden Gate Highlands National Park, South Africa.

Blumenthal, R,Trengrove, E,Jandrell, IR & Saayman, G 2012. Lightning medicine in South Africa. *SAMJ: South African Medical Journal,* 102**,** 625-626.

Bond, WJ & Keane, RE 2017. Fires, ecological effects of. *Reference module in life sciences***,** 1-11.

Bond, WJ & Keeley, JE 2005. Fire as a global 'herbivore': the ecology and evolution of flammable ecosystems. *Trends in ecology evolution,* 20**,** 387-394.

Bonham-Carter, G 1994. *Geographic information systems for geoscientists: modelling with GIS*, Elsevier.

Bot, K & Borges, JG 2022. A systematic review of applications of machine learning techniques for wildfire management decision support. *Inventions,* 7**,** 15.

Bowman, D,Williamson, G,Yebra, M,Lizundia-Loiola, J,Pettinari, ML,Shah, S,Bradstock, R & Chuvieco, E 2020. Wildfires: Australia needs national monitoring agency. *Nature,* 584**,** 188-191.

Bowman, DM,Balch, J,Artaxo, P,Bond, WJ,Cochrane, MA,D'antonio, CM,DeFries, R,Johnston, FH,Keeley, JE & Krawchuk, MA 2011a. The human dimension of fire regimes on Earth. *Journal of biogeography,* 38**,** 2223-2236.

Bowman, DMJS,Balch, J,Artaxo, P,Bond, WJ,Cochrane, MA,D'antonio, CM,DeFries, R,Johnston, FH,Keeley, JE & Krawchuk, MA 2011b. The human dimension of fire regimes on Earth. *Journal of biogeography,* 38**,** 2223-2236.

Bowman, DMJS,Williamson, GJ,Abatzoglou, JT,Kolden, CA,Cochrane, MA & Smith, AMS 2017. Human exposure and sensitivity to globally extreme wildfire events. *Nature Ecology & Evolution,* 1**,** 0058.

Bowman, DMJS,Williamson, GJ,Gibson, RK,Bradstock, RA & Keenan, RJ 2021. The severity and extent of the Australia 2019–20 Eucalyptus forest fires are not the legacy of forest management. *Nature Ecology & Evolution,* 5**,** 1003-1010.

Bradstock, RA 2010. A biogeographic model of fire regimes in Australia: current and future implications. *Global Ecology and Biogeography,* 19**,** 145-158.

Breiman, L 2001. Random forests. *Machine learning,* 45**,** 5-32.

Brillinger, DR,Preisler, HK & Benoit, JW 2006. Probabilistic risk assessment for wildfires. *Environmetrics: The official journal of the International Environmetrics Society,* 17**,** 623-633.

Brown, JL 2014. SDM toolbox: a python-based GIS toolkit for landscape genetic, biogeographic and species distribution model analyses. *Methods in Ecology and Evolution,* 5**,** 694-700.

Bustillo Sánchez, M,Tonini, M,Mapelli, A & Fiorucci, P 2021. Spatial assessment of wildfires susceptibility in Santa Cruz (Bolivia) using random forest. *Geosciences,* 11**,** 224.

Camia, A,DURRANT, HT & San-Miguel-Ayanz, J 2013. *Harmonized classification scheme of fire causes in the EU adopted for the European Fire Database of EFFIS*.

Cao, Q,Zhang, L,Su, Z,Wang, G & Guo, F 2020. Exploring spatially varying relationships between forest fire and environmental factors at different quantile levels. *International journal of wildland fire,* 29**,** 486-498.

Carbutt, C,Henwood, WD & Gilfedder, LA 2017. Global plight of native temperate grasslands: going, going, gone? *Biodiversity Conservation,* 26**,** 2911-2932.

Carbutt, C,Tau, M,Stephens, A & Escott, B 2011. The conservation status of temperate grasslands in southern Africa. *Grassroots,* 11**,** 17-23.

Cardil, A,Monedero, S,Schag, G,de-Miguel, S,Tapia, M,Stoof, CR,Silva, CA,Mohan, M,Cardil, A & Ramirez, J 2021. Fire behavior modeling for operational decision-making. *Current Opinion in Environmental Science & Health,* 23**,** 100291.

Carmona, A,González, ME,Nahuelhual, L & Silva, J 2012. Efectos espacio-temporales de los factores humanos en el peligro de incendio en Chile mediterráneo. *Bosque (Valdivia),* 33**,** 321-328.

Carr, DB,Olsen, AR & White, D 1992. Hexagon mosaic maps for display of univariate and bivariate geographical data. *Cartography and Geographic Information Systems,* 19**,** 228-236.

Catry, FX,Rego, FC,Bação, FL & Moreira, F 2009. Modeling and mapping wildfire ignition risk in Portugal. *International Journal of Wildland Fire,* 18**,** 921-931.

Ceccato, P,Flasse, S & Grégoire, J-M 2002a. Designing a spectral index to estimate vegetation water content from remote sensing data: Part 2. Validation and applications. *Remote Sensing of Environment,* 82**,** 198-207.

Ceccato, P,Gobron, N,Flasse, S,Pinty, B & Tarantola, S 2002b. Designing a spectral index to estimate vegetation water content from remote sensing data: Part 1: Theoretical approach. *Remote Sensing of Environment,* 82**,** 188-197.

Ceccato, P,Leblon, B,Chuvieco, E,Flasse, S & Carlson, JD 2003. Estimation of Live Fuel Moisture Content. *Wildland Fire Danger Estimation & Mapping. The role of remote sensing data.* Singapore: World Scientific Publising Co. Pe. Ltd.

Cecil, DJ,Buechler, DE & Blakeslee, RJ 2014. Gridded lightning climatology from TRMM-LIS and OTD: Dataset description. *Atmospheric Research,* 135**,** 404-414.

Cha, D,Wang, X & Kim, JW 2017. Assessing lightning and wildfire hazard by land properties and cloud to ground lightning data with association rule mining in Alberta, Canada. *Sensors,* 17**,** 2413.

Chafer, CJ,Noonan, M & Macnaught, E 2004. The post-fire measurement of fire severity and intensity in the Christmas 2001 Sydney wildfires. *International Journal of Wildland Fire,* 13**,** 227-240.

Chaivaranont, W,Evans, JP,Liu, YY & Sharples, J 2018. Estimating grassland curing with remotely sensed data. *Journal of Natural Hazards Earth System Sciences,* 18**,** 1535-1554.

Chandrasekar, K,Srikanth, P,Chakraborty, A,Choudhary, K & Ramana, K 2022. Response of crop water indices to soil wetness and vegetation water content. *Journal of Advances in Space Research*.

Chang, C,Chang, Y,Xiong, Z,Ping, X,Zhang, H,Guo, M & Hu, Y 2023. Predicting Grassland Fire-Occurrence Probability in Inner Mongolia Autonomous Region, China. *Remote Sensing,* 15**,** 2999.

Chaparro, D,Piles, M & Vall-llossera, M 2016. Chapter 13 - Remotely Sensed Soil Moisture as a Key Variable in Wildfires Prevention Services: Towards New Prediction Tools Using SMOS and SMAP Data A2 - Srivastava, Prashant K. *In:* Petropoulos, GP & Kerr, YH (eds.) *Satellite Soil Moisture Retrieval.* Elsevier.

Chen, H,Zhang, H,Shen, S-h,Yu, W & Zou, C. Construction and validation of a new model for cropland soil moisture index based on MODIS data. Remote Sensing and Modeling of Ecosystems for Sustainability VI, 2009. SPIE, 258-265.

Chen, Y,Morton, DC,Andela, N,Van Der Werf, GR,Giglio, L & Randerson, JT 2017. A pan-tropical cascade of fire driven by El Niño/Southern Oscillation. *Nature Climate Change,* 7**,** 906-911.

Cheney, N,Gould, J & Catchpole, W 1993. The influence of fuel, weather and fire shape variables on fire-spread in grasslands. *International Journal of Wildland Fire,* 3**,** 31-44.

Cheney, N,Gould, J & Catchpole, WR 1998. Prediction of fire spread in grasslands. *International Journal of Wildland Fire,* 8**,** 1-13.

Cheney, P & Sullivan, A 2008. *Grassfires: fuel, weather and fire behaviour*, Csiro Publishing.

Chicas, SD & Østergaard Nielsen, J 2022. Who are the actors and what are the factors that are used in models to map forest fire susceptibility? A systematic review. *Natural Hazards,* 114**,** 2417-2434.

Chicas, SD,Østergaard Nielsen, J,Valdez, MC & Chen, C-F 2022. Modelling wildfire susceptibility in Belize's ecosystems and protected areas using machine learning and knowledge-based methods. *Geocarto International,* 37**,** 15823-15846.

Chladil, M & Nunez, MJIJoWF 1995. Assessing grassland moisture and biomass in Tasmania-the application of remote-sensing and empirical-models for a cloudy environment. *International Journal of Wildland Fire,* 5**,** 165-171.

Chowdhury, EH & Hassan, QK 2015. Operational perspective of remote sensing-based forest fire danger forecasting systems. *ISPRS Journal of Photogrammetry and Remote Sensing,* 104**,** 224-236.

Christian, HJ,Blakeslee, RJ,Boccippio, DJ,Boeck, WL,Buechler, DE,Driscoll, KT,Goodman, SJ,Hall, JM,Koshak, WJ & Mach, DM 2003. Global frequency and distribution of lightning as observed from space by the Optical Transient Detector. *Journal of Geophysical Research: Atmospheres,* 108**,** ACL-4.

Chuvieco, E. Remote sensing inputs to fire danger rating. New strategies for European remote sensing. Proceedings of the 24th Symposium of the European Association of Remote Sensing Laboratories, Dubrovnik, Croatia, 25-27 May 2004, 2005. Millpress Science Publishers, 33-40.

Chuvieco, E,Aguado, I & Dimitrakopoulos, AP 2004a. Conversion of fuel moisture content values to ignition potential for integrated fire danger assessment. *Canadian Journal of Forest Research,* 34.

Chuvieco, E,Aguado, I,Jurdao, S,Pettinari, M,Yebra, M,Salas, J,Hantson, S,De La Riva, J,Ibarra, P & Rodrigues, M 2014. Integrating geospatial information into fire risk assessment. *International journal of wildland fire,* 23**,** 606-619.

Chuvieco, E,Aguado, I,Jurdao, S,Pettinari, ML,Yebra, M,Salas, J,Hantson, S,de la Riva, J,Ibarra, P & Rodrigues, M 2012. Integrating geospatial information into fire risk assessment. *International journal of wildland fire,* 23**,** 606-619.

Chuvieco, E,Aguado, I,Salas, J,García, M,Yebra, M & Oliva, P 2020. Satellite remote sensing contributions to wildland fire science and management. *Current Forestry Reports,* 6**,** 81-96.

Chuvieco, E,Aguado, I,Yebra, M,Nieto, H,Salas, J,Martín, MP,Vilar, L,Martínez, J,Martín, S,P.:, I,de la Riva, J,Baeza, J,Rodríguez, F,Molina, JR,Herrera, MA & Zamora, R 2010. Development of framework for fire risk assessment using remote sensing and geographic imformation system technologies. *Ecological Modelling***,** 46-58.

Chuvieco, E,Cocero, D,Riano, D,Martin, P,Martinez-Vega, J,de la Riva, J & Perez, F 2004b. Combining NDVI and surface temperature for the estimation of live fuel moisture content in forest fire danger rating. *Remote Sensing of Environment***,** 322-331.

Chuvieco, E & Congalton, RG 1989. Application of Remote Sensing & Geographic Information Systems to Forest Fire Hazard Mapping. *Remote Sensing Environment,* 29**,** 147-159.

Chuvieco, E,Riano, D,Aguado, I & Coppin, P 2002. Estimation of fuel moisture content from multitemporal analysis of Landsat Thematic Mapper reflectance data: Applications in Fire danger assessment. *International Journal of Remote Sensing,* 23**,** 2145-2162.

Chuvieco, E,Yebra, M,Martino, S,Thonicke, K,Gómez-Giménez, M,San-Miguel, J,Oom, D,Velea, R,Mouillot, F & Molina, JR 2023. Towards an integrated approach to wildfire risk assessment: when, where, what and how may the landscapes burn. *Fire,* 6**,** 215.

Clarke, H,Gibson, R,Cirulis, B,Bradstock, RA & Penman, TD 2019. Developing and testing models of the drivers of anthropogenic and lightning-caused wildfire ignitions in south-eastern Australia. *Journal of environmental management,* 235**,** 34-41.

Clarke, H,Penman, T,Boer, M,Cary, GJ,Fontaine, JB,Price, O & Bradstock, R 2020. The proximal drivers of large fires: A pyrogeographic study. *Frontiers in Earth Science,* 8**,** 90.

Coffield, SR,Graff, CA,Chen, Y,Smyth, P,Foufoula-Georgiou, E & Randerson, JT 2019. Machine learning to predict final fire size at the time of ignition. *International Journal of Wildland Fire,* 28**,** 861-873.

Costafreda-Aumedes, S,Comas, C & Vega-Garcia, C 2017. Human-caused fire occurrence modelling in perspective: A review. *International Journal of Wildland Fire,* 26**,** 983-998.

Costafreda-Aumedes, S,Comas, C & Vega-Garcia, C 2018. Human-caused fire occurrence modelling in perspective: a review. *International Journal of Wildland Fire,* 26**,** 983-998.

Cruz, M,Sullivan, A,Hurley, R,Plucinski, M & Gould, J 2017. *The effect of fuel load and structure on grassland fire behaviour and fire danger-Final report,* Canberra, Australia, CSIRO Land and Water, .

Cruz, MG & Alexander, ME 2019. The 10% wind speed rule of thumb for estimating a wildfire's forward rate of spread in forests and shrublands. *Annals of Forest Science,* 76**,** 1-11.

Cruz, MG,Alexander, ME & Kilinc, M. 2022. Wildfire Rates of Spread in Grasslands under Critical Burning Conditions. *Fire* [Online], 5.

Cruz, MG,Gould, JS,Kidnie, S,Bessell, R,Nichols, D & Slijepcevic, A 2015. Effects of curing on grassfires: II. Effect of grass senescence on the rate of fire spread. *International Journal of Wildland Fire,* 24**,** 838-848.

Daemane, M,Bezuidenhout, H,Bissett, C,Strydom, T,Nariandas, D,Tshabalala, M & Sikhosana, T 2018. Proposed changes to the Fire Management Plan of the Golden Gate Highlands National Park. Pretoria: SANParks.

Daemane, ME,Bezuidenhout, H,Bissett, C,Strydom, T,Nariandas, D,Tshabalala, M & Sikhosana, T 2018. Proposed changes to the Fire Management Plan of Golden Gate Highlands

National Park. . Pretoria: SANParks.

Daemane, ME,Ramoelo, A & Adelabu, S 2021. The spatial distribution of the woodland communities and their associated environmental drivers in the Golden Gate Highlands National Park, South Africa. *Koedoe,* 63**,** 1-9.

Dang, ATN,Kumar, L,Reid, M & Mutanga, O 2021. Fire danger assessment using geospatial modelling in Mekong delta, Vietnam: Effects on wetland resources. *Remote Sensing Applications: Society and Environment,* 21**,** 100456.

Daoud, JI. Multicollinearity and regression analysis. 2017 2017. IOP Publishing, 012009.

Davies, DK,Ilavajhala, S,Wong, MM & Justice, CO 2008. Fire information for resource management system: archiving and distributing MODIS active fire data. *IEEE Transactions on Geoscience and Remote Sensing,* 47**,** 72-79.

De Reu, J,Bourgeois, J,Bats, M,Zwertvaegher, A,Gelorini, V,De Smedt, P,Chu, W,Antrop, M,De Maeyer, P & Finke, P 2013. Application of the topographic position index to heterogeneous landscapes. *Geomorphology,* 186**,** 39-49.

de Santana, RO,Delgado, RC & Schiavetti, A 2021. Modeling susceptibility to forest fires in the Central Corridor of the Atlantic Forest using the frequency ratio method. *Journal of Environmental Management,* 296**,** 113343.

De Vasconcelos, MP,Silva, S,Tome, M,Alvim, M & Pereira, JCJ 2001. Spatial prediction of fire ignition probabilities: comparing logistic regression and neural networks. *Photogrammetric Engineering Remote Sensing,* 67**,** 73-81.

Debeljak, M & Džeroski, S 2011. Decision Trees in Ecological Modelling. *In:* Jopp, F, Reuter, H & Breckling, B (eds.) *Modelling Complex Ecological Dynamics: An Introduction into Ecological Modelling for Students, Teachers & Scientists.* Berlin, Heidelberg: Springer Berlin Heidelberg.

Del Hoyo, LV,Isabel, MPM & Vega, FJM 2011. Logistic regression models for human-caused wildfire risk estimation: analysing the effect of the spatial accuracy in fire occurrence data. *European Journal of Forest Research,* 130**,** 983-996.

Dewan, A,Ongee, ET,Rahman, MM,Mahmood, R & Yamane, Y 2018. Spatial and temporal analysis of a 17-year lightning climatology over Bangladesh with LIS data. *Theoretical and Applied Climatology,* 134**,** 347-362.

Dickson, BG,Prather, JW,Xu, Y,Hampton, HM,Aumack, EN & Sisk, TD 2006. Mapping the probability of large fire occurrence in northern Arizona, USA. *Landscape Ecology,* 21**,** 747-761.

Dijkshoorn, J,van Engel, V & Hutting, J 2008. Soil and Landform properties for LADA partner countries (ARgentina, China, Cuba, Senegal, and The Gambia, South Africa and Tunisia Wageningen: ISRIC-World Soil Information and FOA.

Dilley, A,Millie, S,O'brien, D & Edwards, M 2004. The relation between Normalized Difference Vegetation Index and vegetation moisture content at three grassland locations in Victoria, Australia. *International Journal of Remote Sensing,* 25**,** 3913-3930.

Dissing, D & Verbyla, DL 2003. Spatial patterns of lightning strikes in interior Alaska and their relations to elevation and vegetation. *Canadian Journal of Forest Research,* 33**,** 770-782.

Dixon, A,Faber-Langendoen, D,Josse, C,Morrison, J & Loucks, C 2014. Distribution mapping of world grassland types. *Journal of Biogeography,* 41**,** 2003-2019.

Dorigo, W,Himmelbauer, I,Aberer, D,Schremmer, L,Petrakovic, I,Zappa, L,Preimesberger, W,Xaver, A,Annor, F & Ardö, JJ 2021. The International Soil Moisture Network: serving Earth system science for over a decade. *Hydrology Earth System Sciences* 25**,** 5749-5804.

Dorph, A,Marshall, E,Parkins, KA & Penman, TD 2022. Modelling ignition probability for human-and lightning-caused wildfires in Victoria, Australia. *Natural Hazards and Earth System Sciences,* 22**,** 3487-3499.

Driver, A,Mukhandi, F & Botts, EA 2019. AN INITIAL ASSESSMENT OF BIODIVERSITY-RELATED EMPLOYMENT IN SOUTH AFRICA. Pretoria

Developed by the South African National Biodiversity Institute (SANBI) in collaboration with the Development Policy Research Unit (DPRU), University of Cape Town.

Du, X,Wang, S,Zhou, Y & Wei, H 2007. Construction and validation of a new model for unified surface water capacity based on MODIS data. 32**,** 205-207.

Duane, A,Castellnou, M & Brotons, L 2021. Towards a comprehensive look at global drivers of novel extreme wildfire events. *Climatic Change,* 165**,** 43.

Dube, F,Nhapi, I,Murwira, A,Gumindoga, W,Goldin, J & Mashauri, DA 2014. Potential of weight of evidence modelling for gully erosion hazard assessment in Mbire District–Zimbabwe. *Physics and Chemistry of the Earth, Parts A/B/C,* 67**,** 145-152.

Dudley, N,Ali, N,Kettunen, M & MacKinnon, K 2017. Editorial essay: Protected areas and the sustainable development goals. *Parks,* 23**,** 10-12.

Dudley, N,S. Stolton,A. Belokurov,L. Krueger,N. Lopoukhine,K. MacKinnon,and, TS & [editors], NS 2009. Natural Solutions: Protected areas helping people cope with climate change. *In:* IUCN-WCPA, TNC, UNDP, Wildlife Conservation Society, The World Bank and WWF (ed.). Gland, Switzerland, Washington DC and New York.: IUCN-WCPA.

Duff, T,Bessell, R & Cruz, M 2019. Grass Curing/Cured Fuels. In 'Encyclopedia of Wildfires and Wildland-Urban Interface (WUI) Fires'.(Ed. SL Manzello) pp. 1–7. Springer International Publishing: Cham.

Duff, TJ,Bessell, R & Cruz, MG 2020. Grass curing/cured fuels. *Encyclopedia of Wildfires and Wildland-Urban Interface (WUI) Fires.* Springer.

Durrheim, G 2010. Monitoring for sustainable indigenous forest management in the Garden Route National Park. *Scientific Services, South African National Parks, Knysna*.

Dutta, R,Das, A & Aryal, J 2016. Big data integration shows Australian bush-fire frequency is increasing significantly. *Royal Society open science,* 3**,** 150241.

Elith, J,Phillips, SJ,Hastie, T,Dudík, M,Chee, YE & Yates, CJ 2011. A statistical explanation of MaxEnt for ecologists. *Diversity and distributions,* 17**,** 43-57.

Environmental Systems Research Institute (ESRI) 2013. ArcGIS 10.2 Desktop Help Redlands, CA.: ESRI, Inc.

Erickson, HE & White, R 2008. *Soils under fire: soils research and the Joint Fire Science Program*, US Department of Agriculture, Forest Service, Pacific Northwest Research Station.

ESA, TESA. *Sentinel Online - Sentinel-2 MSI User Guide* [Online]. Available: https://sentinel.esa.int/web/sentinel/user-guides/sentinel-2-msi;jsessionid=1ADA9B2E6C21CAC7C8A41E91F51B041C.jvm2 [Accessed June 29 2022].

Eskandari, S & Chuvieco, E 2015. Fire danger assessment in Iran based on geospatial information. *International Journal of Applied Earth Observation and Geoinformation,* 42**,** 57-64.

Eskandari, S,Pourghasemi, HR & Tiefenbacher, JP 2020. Relations of land cover, topography, and climate to fire occurrence in natural regions of Iran: Applying new data mining techniques for modeling and mapping fire danger. *Forest Ecology and Management,* 473**,** 118338.

Eskandari, S,Pourghasemi, HR & Tiefenbacher, JP 2021. Fire-susceptibility mapping in the natural areas of Iran using new and ensemble data-mining models. *Environmental Science and Pollution Research,* 28**,** 47395-47406.

Everson, CS & Everson, T 2016. The long-term effects of fire regime on primary production of montane grasslands in South Africa. *African Journal of Range Forage Science,* 33**,** 33-41.

Everson, TM,Everson, C,Dicks, H & Poulter, AJSAFJ 1988. Curing rates in the grass sward of the Highland Sourveld in the Natal Drakensberg. 145**,** 1-8.

Evert, C & Gijben, M. Official South African lightning ground flash density map 2006 to 2017. 2017 2017. 5-9.

Evert, R & Schulze, G. Impact of a new lightning detection and location system in South Africa. 2005 2005. IEEE, 356-363.

Fan, L,Wigneron, J-P,Xiao, Q,Al-Yaari, A,Wen, J,Martin-StPaul, N,Dupuy, J-L,Pimont, F,Al Bitar, A & Fernandez-Moran, R 2018. Evaluation of microwave remote sensing for monitoring live fuel moisture content in the Mediterranean region. *Remote Sensing of Environment,* 205**,** 210-223.

Fang, L,Yang, J,Zu, J,Li, G & Zhang, J 2015. Quantifying influences and relative importance of fire weather, topography, and vegetation on fire size and fire severity in a Chinese boreal forest landscape. *Forest Ecology and Management,* 356**,** 2-12.

Fawcett, T 2006. An introduction to ROC analysis. *Pattern recognition letters,* 27**,** 861-874.

Fensholt, R & Sandholt, I 2003. Derivation of a shortwave infrared water stress index from MODIS near-and shortwave infrared data in a semiarid environment. *Remote Sensing of Environment,* 87**,** 111-121.

Fernandes, PM 2019. Variation in the Canadian fire weather index thresholds for increasingly larger fires in Portugal. *Forests,* 10**,** 838.

Finney, MA 1998. *FARSITE, Fire Area Simulator--model development and evaluation*, US Department of Agriculture, Forest Service, Rocky Mountain Research Station.

Finney, MA. An overview of FlamMap fire modeling capabilities. *In:* Andrews, PL & Butler, BW, eds. Fuels Management-How to Measure Success:, 2006 2006 Portland. US Department of Agriculture, Forest Service, Rocky Mountain Research Station, 213-220.

Flannigan, MD,Krawchuk, MA,de Groot, WJ,Wotton, BM & Gowman, LM 2009. Implications of changing climate for global wildland fire. *International Journal of Wildland Fire,* 18**,** 483-507.

Flores Quiroz, N,Gibson, L,Conradie, WS,Ryan, P,Heydenrych, R,Moran, A,van Straten, A & Walls, R 2023. Analysis of the 2017 Knysna fires disaster with emphasis on fire spread, home losses and the influence of vegetation and weather conditions: A South African case study. *International Journal of Disaster Risk Reduction,* 88**,** 103618.

Food and Agricultural Organisation (FAO) 2007. Fire management-global assessment 2006. Rome: FAO.

Food and Agriculture Organization (FAO). 2005. *Wildland Fire Management Terminology* [Online]. Available: https://www.fao.org/faoterm/en/ [Accessed].

Forkel, M,Dorigo, W,Lasslop, G,Chuvieco, E,Hantson, S,Heil, A,Teubner, I,Thonicke, K & Harrison, SP 2019. Recent global and regional trends in burned area and their compensating environmental controls. *Environmental Research Communications,* 1**,** 051005.

Frost, P,Kleyn, L,van den Dool, R,Burgess, M,Vhengani, L,Steenkamp, K,Wessels, K & Rd, MN 2018. The Elandskraal fire, Knysna. *CSIR Report.*

Gang, C,Zhou, W,Chen, Y,Wang, Z,Sun, Z,Li, J,Qi, J & Odeh, I 2014. Quantitative assessment of the contributions of climate change and human activities on global grassland degradation. *Environmental Earth Sciences,* 72**,** 4273-4282.

Ganteaume, A,Camia, A,Jappiot, M,San-Miguel-Ayanz, J,Long-Fournel, M & Lampin, C 2013. A review of the main driving factors of forest fire ignition over Europe. *Environmental management,* 51**,** 651-662.

Ganteaume, A & Syphard, AD 2018. Ignition sources. *Encyclopedia of Wildfires Wildland-Urban Interface Fires***,** 1-17.

Gao, B 1996. NDWI- Normalized difference water index for remote sensing of vegetation liquid. *Remote Sensing of Environment,* 58**,** 322 - 331.

Gauriau, O,Galárraga, L,Brun, F,Termier, A,Davadan, L & Joudelat, F 2024. Comparing machine-learning models of different levels of complexity for crop protection: A look into the complexity-accuracy tradeoff. *Smart Agricultural Technology,* 7**,** 100380.

Gaznayee, HAA,Zaki, SH,Al-Quraishi, AMF,Aliehsan, PH,Hakzi, KK,Razvanchy, HAS,Riksen, M & Mahdi, KJW 2023. Integrating Remote Sensing Techniques and Meteorological Data to Assess the Ideal Irrigation System Performance Scenarios for Improving Crop Productivity. 15**,** 1605.

Genton, MG,Butry, DT,Gumpertz, ML & Prestemon, JP 2006. Spatio-temporal analysis of wildfire ignitions in the St Johns River water management district, Florida. *International Journal of Wildland Fire,* 15**,** 87-97.

Getis, A & Ord, JK 1992. The analysis of spatial association by use of distance statistics. *Geographical analysis,* 24**,** 189-206.

Ghodrat, M,Shakeriaski, F,Nelson, DJ & Simeoni, A 2021. Existing improvements in simulation of fire–wind interaction and its effects on structures. *Fire,* 4**,** 27.

Gholamnia, K,Gudiyangada Nachappa, T,Ghorbanzadeh, O & Blaschke, T. 2020. Comparisons of Diverse Machine Learning Approaches for Wildfire Susceptibility Mapping. *Symmetry* [Online], 12.

Gijben, M 2012. The lightning climatology of South Africa. *South African Journal of Science,* 108**,** 1-10.

Gijben, M,Dyson, LL & Loots, MT 2017. A statistical scheme to forecast the daily lightning threat over southern Africa using the Unified Model. *Atmospheric Research,* 194**,** 78-88.

Gill, T. 2009. *Initial steps in the development of a comprehensive lightning climatology of South Africa.* University of the Witwatersrand.

Gorelick, N,Hancher, M,Dixon, M,Ilyushchenko, S,Thau, D & Moore, R 2017. Google Earth Engine: Planetary-scale geospatial analysis for everyone. *Remote sensing of Environment,* 202**,** 18-27.

Guo, F,Su, Z,Wang, G,Sun, L,Lin, F & Liu, A 2016a. Wildfire ignition in the forests of southeast China: Identifying drivers and spatial distribution to predict wildfire likelihood. *Applied Geography,* 66**,** 12-21.

Guo, F,Wang, G,Su, Z,Liang, H,Wang, W,Lin, F & Liu, A 2016b. What drives forest fire in Fujian, China? Evidence from logistic regression and Random Forests. *International Journal of Wildland Fire,* 25**,** 505-519.

Guyette, R,Muzika, R & Dey, D 2002. Dynamics of an Anthropogenic Fire Regime. *Ecosystems,* 5**,** 472-486.

Hardisky, M & Smart, R 1983. The Influence of Soil Salinity, Growth Form, and Leaf Moisture on the Spectral Radiance of Spartina alterniflora Canopies. *Photogrammetric Engineering Remote Sensing,* 49**,** 77-83.

Haubrock, S,Chabrillat, S,Kuhnert, M,Hostert, P & Kaufmann, HJJJoars 2008. Surface soil moisture quantification and validation based on hyperspectral data and field measurements. 2**,** 023552.

Hengl, T,Mendes de Jesus, J,Heuvelink, GB,Ruiperez Gonzalez, M,Kilibarda, M,Blagotić, A,Shangguan, W,Wright, MN,Geng, X & Bauer-Marschallinger, B 2017. SoilGrids250m: Global gridded soil information based on machine learning. *PLoS one,* 12.

Hernandez-Leal, PA,Arbelo, M & Gonzalez-Calvo, A 2006. Fire risk assessment using satellite data. *Advances in Space Research,* 13**,** 741-746.

Hilton, JE,Miller, C,Sullivan, AL & Rucinski, C 2015. Effects of spatial and temporal variation in environmental conditions on simulation of wildfire spread. *Environmental Modelling & Software,* 67**,** 118-127.

Holgate, C,De Jeu, R,Van Dijk, A,Liu, Y,Renzullo, L,Dharssi, I,Parinussa, R,Van Der Schalie, R,Gevaert, A & Walker, J 2016. Comparison of remotely sensed and modelled soil moisture data sets across Australia. *Remote Sensing of Environment,* 186**,** 479-500.

Holgate, CM,van Dijk, AI,Cary, GJ & Yebra, M 2017. Using alternative soil moisture estimates in the McArthur Forest Fire Danger Index. *International Journal of Wildland Fire,* 26**,** 806-819.

Hong-wei, Z,Huai-liang, C & Shuang-he, S 2011. Drought remote sensing monitoring based on the surface water content index (SWCI) method. *Remote Sensing Technology Application,* 23**,** 624-628.

Hong, H,Jaafari, A & Zenner, EK 2019. Predicting spatial patterns of wildfire susceptibility in the Huichang County, China: An integrated model to analysis of landscape indicators. *Ecological Indicators,* 101**,** 878-891.

Hong, H,Naghibi, SA,Moradi Dashtpagerdi, M,Pourghasemi, HR & Chen, W 2017. A comparative assessment between linear and quadratic discriminant analyses (LDA-QDA) with frequency ratio and weights-of-evidence models for forest fire susceptibility mapping in China. *Arabian Journal of Geosciences,* 10**,** 1-14.

Hong, H,Tsangaratos, P,Ilia, I,Liu, J,Zhu, AX & Xu, C 2018. Applying genetic algorithms to set the optimal combination of forest fire related variables and model forest fire susceptibility based on data mining models. The case of Dayu County, China. *Science of The Total Environment,* 630**,** 1044-1056.

Hosking , R 1990. Grassland Curing Index-a district model that allows forecasting of curing. *An International Journal of Mathematical Computer Modelling,* 13**,** 73-82.

Hua, X,Ohlemüller, R & Sirguey, P 2022. Differential effects of topography on the timing of the growing season in mountainous grassland ecosystems. *Environmental Advances,* 8**,** 100234.

Huang, Y,Wu, S & Kaplan, JO 2015. Sensitivity of global wildfire occurrences to various factors in the context of global change. *Atmospheric Environment,* 121**,** 86-92.

Huete, AR 2012. Vegetation indices, remote sensing and forest monitoring. *Geography Compass,* 6**,** 513-532.

Hunt, ER,Wang, L,Qu, JJ & Hao, X 2012. Remote sensing of fuel moisture content from canopy water indices and normalized dry matter index. *Journal of Applied Remote Sensing,* 6**,** 061705-061705.

Hunt, JRE & Rock, NE 1989. Detection of Changes in Leaf Water Content Using Near-and Midle-infrared Reflectances. *Remote Sensing to Environment,* 30.

Huntington, JL,Hegewisch, KC,Daudert, B,Morton, CG,Abatzoglou, JT,McEvoy, DJ & Erickson, T 2017. Climate engine: Cloud computing and visualization of climate and remote sensing data for advanced natural resource monitoring and process understanding. *Bulletin of the American Meteorological Society,* 98**,** 2397-2410.

Indoria, AK,Sharma, KL & Reddy, KS 2020. Chapter 18 - Hydraulic properties of soil under warming climate. *In:* Prasad, MNV & Pietrzykowski, M (eds.) *Climate Change and Soil Interactions.* Elsevier.

Intergovernmental Panel on Climate Change (IPCC) 2007. Synthesis Report . Climate Change 2007. Contribution of Working Groups I, II and III to the Fourth Assessment Report of the Intergovernmental Panel on Climate Change. *In:* Pachauri, RK & Reisinger, A (eds.). Geneva: IPCC.

International Union for Conservation of Nature (IUCN). 2020. *Natural Solutions: Protected Area helping to meet the Sustainable Development Goals* [Online]. Gland, Switzerland: IUCN. Available: https://www.iucn.org/sites/default/files/2022-09/6.-natural_solutions_-_sdgs_final_2.pdf [Accessed 10 August 2022].

Jaafari, A,Gholami, DM & Zenner, EK 2017. A Bayesian modeling of wildfire probability in the Zagros Mountains, Iran. *Ecological informatics,* 39**,** 32-44.

Jaafari, A,Mafi-Gholami, D,Thai Pham, B & Tien Bui, D 2019. Wildfire probability mapping: Bivariate vs. multivariate statistics. *Remote Sensing,* 11**,** 618.

Jaafari, A & Pourghasemi, HR 2019. 28 - Factors Influencing Regional-Scale Wildfire Probability in Iran: An Application of Random Forest and Support Vector Machine. *In:* Pourghasemi, HR & Gokceoglu, C (eds.) *Spatial Modeling in GIS and R for Earth and Environmental Sciences.* Elsevier.

Jaafari, A,Zenner, EK & Pham, BT 2018. Wildfire spatial pattern analysis in the Zagros Mountains, Iran: A comparative study of decision tree based classifiers. *Ecological Informatics,* 43**,** 200-211.

Jafari Goldarag, Y,Mohammadzadeh, A & Ardakani, AS 2016. Fire risk assessment using neural network and logistic regression. *Journal of the Indian Society of Remote Sensing,* 44**,** 885-894.

Jain, P,Coogan, SCP,Subramanian, SG,Crowley, M,Taylor, S & Flannigan, MD 2020. A review of machine learning applications in wildfire science and management. *Environmental Reviews,* 28**,** 478-505.

Jarihani, AA,McVicar, TR,Van Niel, TG,Emelyanova, IV,Callow, JN & Johansen, K 2014. Blending Landsat and MODIS data to generate multispectral indices: A comparison of “Index-then-Blend” and “Blend-then-Index” approaches. *Remote Sensing,* 6**,** 9213-9238.

Javor, V,Stoimenov, L,Džaković, N,Dinkić, N,Javor, D & Betz, H-D 2018. LINETGIS analysis of lightning flash density in Serbia based on ten years data. *Serbian Journal of Electrical Engineering,* 15**,** 201-211.

Jia, S,Kim, SH,Nghiem, SV & Kafatos, M 2019. Estimating live fuel moisture using SMAP L-band radiometer soil moisture for Southern California, USA. *Remote Sensing,* 11**,** 1575.

Jin, H 2010. Drivers of Global Wildfire-Statistical Analyses. *Unpublished MSc Thesis.* Lund University: Division of Physical Geography and Ecosystem Analysis, Department of Earth an Ecosystem Sciences.

Jolly , W. Overview of NFDRS2016. National NFDRS2016 Workshop, 2018 Tuscan, AZ,USA.

Jolly, WM,Cochrane, MA,Freeborn, PH,Holden, ZA,Brown, TJ,Williamson, GJ & Bowman, DM 2015. Climate-induced variations in global wildfire danger from 1979 to 2013. *Nature communications,* 6**,** 7537.

Jolly, WM,Nemani, R & Running, SW 2005. A generalized, bioclimatic index to predict foliar phenology in response to climate. *Global Change Biology,* 11**,** 619-632.

Jurdao, S,Chuvieco, E & Arevalillo, JM 2012. Modelling Fire Ignition Probability from Satellite Estimates of Live Fuel Moisture Content. *Fire Ecology,* 8**,** 77-97.

Kay, C,Bredenkamp, GJ & Theron, GK 1993. The plant communities of the Golden Gate Highlands National Park in the north-eastern Orange Free State. *South African Journal of Botany,* 59**,** 442-449.

Keane, RE,Burgan, R & van Wagtendonk, J 2001. Mapping wildland fuels for fire management across multiple scales: Integrating remote sensing, GIS, and biophysical modeling. *International Journal of Wildland Fire***,** 301-319.

Keeley, JE & Pausas, JG 2019. Distinguishing disturbance from perturbations in fire-prone ecosystems. *International Journal of Wildland Fire,* 28**,** 282-287.

Keetch, JJ & Byram, GM 1968. A drought index for forest fire control. *In:* United State Department of Agriculture, FS (ed.). Southeasten Forest Experiement Station.

Kelley, DI,Bistinas, I,Whitley, R,Burton, C,Marthews, TR & Dong, N 2019. How contemporary bioclimatic and human controls change global fire regimes. *Nature Climate Change,* 9**,** 690-696.

Kelly, LT,Fletcher, M-S,Menor, IO,Pellegrini, AFA,Plumanns-Pouton, ES,Pons, P,Williamson, GJ & Bowman, DMJS 2023. Understanding Fire Regimes for a Better Anthropocene. *Annual Review of Environment and Resources,* 48.

Kerdiles, H & Grondona, MO 1995. NOAA-AVHRR NDVI decomposition and subpixel classification using linear mixing in the Argentinean Pampa. *International Journal of Remote Sensing,* 16**,** 1303-1325.

Kidnie, S,Cruz, MG,Gould, J,Nichols, D,Anderson, W & Bessell, R 2015. Effects of curing on grassfires: I. Fuel dynamics in a senescing grassland. *International Journal of Wildland Fire,* 24**,** 828-837.

Kidnie, S & Wotton, BM 2015. Characterisation of the fuel and fire environment in southern Ontario's tallgrass prairie. *International Journal of Wildland Fire,* 24**,** 1118-1128.

Kigotsi, JK,Soula, S & Georgis, J-F 2018. Comparison of lightning activity in the two most active areas of the Congo Basin. *Natural Hazards and Earth System Sciences,* 18**,** 479-489.

Kilinc, M & Beringer, J 2007. The spatial and temporal distribution of lightning strikes and their relationship with vegetation type, elevation, and fire scars in the Northern Territory. *Journal of climate,* 20**,** 1161-1173.

Knight, J 2022. Scientists' warning of the impacts of climate change on mountains. *PeerJ,* 10**,** e14253.

Kogan, FN 1990. Remote sensing of weather impacts on vegetation in non-homogeneous areas. *International Journal of Remote Sensing,* 11**,** 1405-1419.

Kondylatos, S,Prapas, I,Ronco, M,Papoutsis, I,Camps-Valls, G,Piles, M,Fernández-Torres, MÁ & Carvalhais, N 2022. Wildfire danger prediction and understanding with Deep Learning. *Geophysical Research Letters,* 49**,** e2022GL099368.

Kotroni, V & Lagouvardos, K 2008. Lightning occurrence in relation with elevation, terrain slope, and vegetation cover in the Mediterranean. *Journal of Geophysical Research: Atmospheres,* 113.

Kraaij, T,Baard, JA,Arndt, J,Vhengani, L & Van Wilgen, BW 2018. An assessment of climate, weather, and fuel factors influencing a large, destructive wildfire in the Knysna region, South Africa. *Fire Ecology,* 14**,** 1-12.

Kraaij, T & van Wilgen, BW 2014. Drivers, ecology, and management of fire in fynbos. *Fynbos: Ecology, evolution, conservation of a megadiverse region.*

Krawchuk, MA & Moritz, MA 2011. Constraints on global fire activity vary across a resource gradient. *Ecology,* 92**,** 121-132.

Krueger, ES,Levi, MR,Achieng, KO,Bolten, JD,Carlson, J,Coops, NC,Holden, ZA,Magi, BI,Rigden, AJ & Ochsner, TE 2022. Using soil moisture information to better understand and predict wildfire danger: a review of recent developments and outstanding questions. *International Journal of Wildland Fire*.

Krueger, ES,Ochsner, TE,Carlson, J,Engle, DM,Twidwell, D & Fuhlendorf, SD 2016. Concurrent and antecedent soil moisture relate positively or negatively to probability of large wildfires depending on season. *International Journal of Wildland Fire,* 25**,** 657-668.

Krueger, ES,Ochsner, TE,Engle, DM,Carlson, J,Twidwell, D & Fuhlendorf, SD 2015. Soil moisture affects growing-season wildfire size in the southern Great Plains. *Soil Science Society of America Journal,* 79**,** 1567-1576.

Kumar, V,Dharssi, I,Yebra, M & Fox-Hughes, P 2020. Exploring the soil moisture-live fuel moisture relationship. Melbourne: Bushfire and Natural Hazards CRC.

Kumari, B & Pandey, AC 2020. Geo-informatics based multi-criteria decision analysis (MCDA) through analytic hierarchy process (AHP) for forest fire risk mapping in Palamau Tiger Reserve, Jharkhand state, India. *Journal of Earth System Science,* 129**,** 1-16.

Le Maitre, DC,Kruger, FJ & Forsyth, GG 2014. Interfacing ecology and policy: developing an ecological framework and evidence base to support wildfire management in South Africa. *Austral Ecology,* 39**,** 424-436.

Lee, S & Pradhan, B 2007. Landslide hazard mapping at Selangor, Malaysia using frequency ratio and logistic regression models. *Landslides,* 4**,** 33-41.

Leenaars, JGB,Kempen, B,van Oostrum, AJM & Batjes, NH 2014. Africa Soil Profiles Database: A compilation of georeferenced and standardised legacy soil profile data for Sub-Saharan Africa. *Arrouays et al.(eds.), 2014b***,** 51-57.

Levi, MR & Bestelmeyer, BT 2016. Biophysical influences on the spatial distribution of fire in the desert grassland region of the southwestern USA. *Landscape Ecology,* 31**,** 2079-2095.

Leys, BA,Marlon, JR,Umbanhowar, C & Vannière, B 2018. Global fire history of grassland biomes. *Ecology and Evolution,* 8**,** 8831-8852.

Li, S 2020. Analysis of Landsat 8 detection of the interannual variability of grassland curing in Greater Melbourne, Australia. *International Journal of Digital Earth,* 13**,** 1321-1338.

Li, S 2021. Inter-satellite variability of grassland curing maps produced by different satellite sensors–Victoria, Australia. *International Journal of Digital Earth,* 14**,** 899-920.

Li, Y,Feng, Z,Chen, S,Zhao, Z & Wang, F 2020. Application of the artificial neural network and support vector machines in forest fire prediction in the guangxi autonomous region, China. *Discrete Dynamics in Nature and Society,* 2020**,** 1-14.

Li, Z-L,Tang, B-H,Wu, H,Ren, H,Yan, G,Wan, Z,Trigo, IF & Sobrino, JA 2013. Satellite-derived land surface temperature: Current status and perspectives. *Remote Sensing of Environment,* 131**,** 14-37.

Lopes, S,Viegas, DX,de Lemos, LT & Viegas, MTJ 2014. Equilibrium moisture content and timelag of dead Pinus pinaster needles. *International Journal of Wildland Fire,* 23**,** 721-732.

Lu, Y & Wei, C 2021. Evaluation of microwave soil moisture data for monitoring live fuel moisture content (LFMC) over the coterminous United States. *Science of The Total Environment,* 771**,** 145410.

Luo, K,Quan, X,He, B & Yebra, M 2019. Effects of live fuel moisture content on wildfire occurrence in fire-prone regions over southwest China. *Forests,* 10**,** 887.

MacKinnon, K,Smith, R,Dudley, N,Figgis, P,Hockings, M,Keenleyside, K,Laffoley, D,Locke, H,Sandwith, T & Woodley, S. Strengthening the global system of protected areas post-2020: A perspective from the IUCN World Commission on Protected Areas. Parks Stewardship Forum, 2020.

Makhaya, Z,Odindi, J & Mutanga, O 2022. The influence of bioclimatic and topographic variables on grassland fire occurrence within an urbanized landscape. *Scientific African,* 15**,** e01127.

Malakhov, DV & Tsychuyeva, NY 2020. Calculation of the biophysical parameters of vegetation in an arid area of south-eastern Kazakhstan using the normalized difference moisture index (NDMI). *Central Asian Journal of Environmental Science Technology Innovation,* 1**,** 189-198.

Mancini, LD,Corona, P & Salvati, L 2018. Ranking the importance of Wildfires' human drivers through a multi-model regression approach. *Environmental Impact Assessment Review,* 72**,** 177-186.

Maniatis, Y,Doganis, A & Chatzigeorgiadis, M 2022. Fire Risk Probability Mapping Using Machine Learning Tools and Multi-Criteria Decision Analysis in the GIS Environment: A Case Study in the National Park Forest Dadia-Lefkimi-Soufli, Greece. *Applied Sciences,* 12**,** 2938.

Mansuy, N,Miller, C,Parisien, M-A,Parks, SA,Batllori, E & Moritz, MA 2019. Contrasting human influences and macro-environmental factors on fire activity inside and outside protected areas of North America. *Environmental Research Letters,* 14**,** 064007.

Martin, D,Chen, T,Nichols, D,Bessell, R,Kidnie, S & Alexander, J 2015. Integrating ground and satellite-based observations to determine the degree of grassland curing. *International Journal of Wildland Fire,* 24**,** 329-339.

Martin, DA 2019. Linking fire and the United Nations sustainable development goals. *Science of the Total Environment,* 662**,** 547-558.

Martín, Y,Zúñiga-Antón, M & Rodrigues Mimbrero, M 2019. Modelling temporal variation of fire-occurrence towards the dynamic prediction of human wildfire ignition danger in northeast Spain. *Geomatics, Natural Hazards Risk,* 10**,** 385-411.

Martínez-Fernández, J,Chuvieco, E & Koutsias, N 2013. Modelling long-term fire occurrence factors in Spain by accounting for local variations with geographically weighted regression. *Natural Hazards and Earth System Sciences,* 13**,** 311.

Martínez, J,Vegan-García , C & Chuvieco, E 2009. Human-caused wildfire risk rating for prevention planning in Spain. *Journal of Enviornmental Management***,** 1241-1252.

Massada, AB,Syphard, AD,Stewart, SI & Radeloff, VC 2012. Wildfire ignition-distribution modelling: a comparative study in the Huron–Manistee National Forest, Michigan, USA. *International Journal of Wildland Fire,* 22**,** 174-183.

Massada, AB,Syphard, AD,Stewart, SI & Radeloff, VC 2013. Wildfire ignition-distribution modelling: a comparative study in the Huron–Manistee National Forest, Michigan, USA. *International journal of wildland fire,* 22**,** 174-183.

Mathu, LFA 2020. How soil texture and groundwater level drive wildfire occurrence in North-western Europe. *Wageningen University & Research, Wageningen (NL)*.

Mattivi, P,Franci, F,Lambertini, A & Bitelli, G 2019. TWI computation: a comparison of different open source GISs. *Open Geospatial Data, Software and Standards,* 4**,** 1-12.

Mayet, N 2016. Spatial and temporal patterns of lightning strikes in the eastern Lesotho Highlands, southern Africa. *South African Geographical Journal= Suid-Afrikaanse Geografiese Tydskrif,* 98**,** 321-336.

McAllister, S & Weise, DR 2017. Effects of season on ignition of live wildland fuels using the forced ignition and flame spread test apparatus. *Combustion Science and Technology,* 189**,** 231-247.

McColl-Gausden, SC,Bennett, LT,Duff, TJ,Cawson, JG & Penman, TD 2020. Climatic and edaphic gradients predict variation in wildland fuel hazard in south-eastern Australia. *Ecography,* 43**,** 443-455.

McGranahan, DA,Ramaano, R,Tedder, MJ & Kirkman, KP 2016. Variation in grassland fuel curing in South Africa. *Fire Ecology,* 12**,** 40-52.

Meng, L,Liu, H,Zhang, X,Ren, C,Ustin, S,Qiu, Z,Xu, M & Guo, D 2019. Assessment of the effectiveness of spatiotemporal fusion of multi-source satellite images for cotton yield estimation. *Computers and Electronics in Agriculture,* 162**,** 44-52.

Merlin, O,Malbéteau, Y,Notfi, Y,Bacon, S,Khabba, SE & Jarlan, L. 2015. Performance Metrics for Soil Moisture Downscaling Methods: Application to DISPATCH Data in Central Morocco. *Remote Sensing* [Online], 7.

Milanović, S,Marković, N,Pamučar, D,Gigović, L,Kostić, P & Milanović, SD. 2021. Forest Fire Probability Mapping in Eastern Serbia: Logistic Regression versus Random Forest Method. *Forests* [Online], 12.

Misra, G,Cawkwell, F & Wingler, A 2020. Status of phenological research using Sentinel-2 data: A review. *Remote Sensing,* 12**,** 2760.

Mofokeng, DO,Olusola, A & Adelabu, S 2022. Development of Lightning Hazard Map for Fire Danger Assessment Over Mountainous Protected Area Using Geospatial Technology. *Remote Sensing of African Mountains: Geospatial Tools Toward Sustainability.* Springer.

Mohajane, M,Costache, R,Karimi, F,Pham, QB,Essahlaoui, A,Nguyen, H,Laneve, G & Oudija, F 2021. Application of remote sensing and machine learning algorithms for forest fire mapping in a Mediterranean area. *Ecological Indicators,* 129**,** 107869.

Molaudzi, OD & Adelabu, SA 2018. Review of the use of remote sensing for monitoring wildfire risk conditions to support fire risk assessment in protected areas. *South African Journal of Geomatics,* 7**,** 222-242.

Molina, JR,Lora, A,Prades, C & y Silva, FR 2019. Roadside vegetation planning and conservation: New approach to prevent and mitigate wildfires based on fire ignition potential. *Forest ecology and management,* 444**,** 163-173.

Moloi, M,Ogbeide, O & Otomo, PV 2020. Probabilistic health risk assessment of heavy metals at wastewater discharge points within the Vaal River Basin, South Africa. *International journal of hygiene and environmental health,* 224**,** 113421.

Moon, K,Duff, T & Tolhurst, K. Characterising forest wind profiles for utilisation in fire spread models. Twentieth International Congress on Modelling and Simulation. Adelaide: Australia, 2013.

Mora, JL & Lázaro, R 2014. Seasonal changes in bulk density under semiarid patchy vegetation: the soil beats. *Geoderma,* 235**,** 30-38.

Moran, PAP 1950. Notes on continuous stochastic phenomena. *Biometrika,* 37**,** 17-23.

Morandini, F,Silvani, X,Dupuy, J-L & Susset, A 2018. Fire spread across a sloping fuel bed: Flame dynamics and heat transfers. *Combustion and Flame,* 190**,** 158-170.

Moreira, F,Viedma, O,Arianoutsou, M,Curt, T,Koutsias, N,Rigolot, E,Barbati, A,Corona, P,Vaz, P & Xanthopoulos, G 2011. Landscape–wildfire interactions in southern Europe: implications for landscape management. *Journal of environmental management,* 92**,** 2389-2402.

Mpakairi, KS,Tagwireyi, P,Ndaimani, H & Madiri, HT 2019. Distribution of wildland fires and possible hotspots for the Zimbabwean component of Kavango-Zambezi Transfrontier Conservation Area. *South African Geographical Journal,* 101**,** 110-120.

Mucina, L & Rutherford, MC 2006. *The vegetation of South Africa, Lesotho and Swaziland*, South African National Biodiversity Institute.

Mulder, VL,van Eck, CM,Friedlingstein, P,Arrouays, D & Regnier, P 2019. Controlling factors for land productivity under extreme climatic events in continental Europe and the Mediterranean Basin. *Catena,* 182**,** 104124.

Müller, MM,Vilà-Vilardell, L & Vacik, H 2020. Towards an integrated forest fire danger assessment system for the European Alps. *Ecological Informatics,* 60**,** 101151.

Mushtaq, F,Lala, MGN & Anand, A 2018. Spatio-temporal variability of lightning activity over J&K region and its relationship with topography, vegetation cover, and absorbing aerosol index (AAI). *Journal of Atmospheric and Solar-Terrestrial Physics,* 179**,** 281-292.

Myeni, L,Moeletsi, ME & Clulow, AD 2021. Development and analysis of a long-term soil moisture data set in three different agroclimatic zones of South Africa. *South African Journal of Science,* 117**,** 1-8.

National Wildfire Coordinating Group (NWCG). 2006. *Glossary of wildland fire terminology* [Online]. Available: https://www.fs.usda.gov/Internet/FSE_DOCUMENTS/fswdev3_009827.pdf [Accessed].

Neary, DG & Leonard, J 2020. Effects of fire on grassland soils and water: A review. *In:* Missiakô, KV (ed.) *Grasses and Grassland Aspects.* IntechOpen.

Nelson Jr, RM & Adkins, CW 1988. A dimensionless correlation for the spread of wind-driven fires. *Canadian Journal of Forest Research,* 18**,** 391-397.

Newnham, GJ,Grant, IF,Martin, DN & Anderson, SA 2010. Improved methods for assessment and prediction of grassland curing. *Bushfire Cooperative Research Centre, Melbourne, VIC*.

Newnham, GJ,Verbesselt, J,Grant, IF & Anderson, SA 2011. Relative Greenness Index for assessing curing of grassland fuel. *Remote Sensing of Environment,* 115**,** 1456-1463.

Nguyen, CT,Chidthaisong, A,Kieu Diem, P & Huo, L-Z 2021. A modified bare soil index to identify bare land features during agricultural fallow-period in southeast Asia using Landsat 8. *Land,* 10**,** 231.

Nieman, WA,Van Wilgen, BW & Leslie, AJ 2021. A review of fire management practices in African savanna-protected areas. *KOEDOE-African Protected Area Conservation,* 63**,** 1655.

Nieto, H,Aguado, I,Chuvieco, E & Sandholt, I 2010. Dead fuel moisture estimation with MSG–SEVIRI data. Retrieval of meteorological data for the calculation of the equilibrium moisture content. *Agricultural and Forest Meteorology,* 150**,** 861-870.

Noble, I,Gill, A & Bary, G 1980. McArthur's fire-danger meters expressed as equations. *Australian Journal of Ecology,* 5**,** 201-203.

Nolan, RH,de Dios, VR,Boer, MM,Caccamo, G,Goulden, ML & Bradstock, RA 2016. Predicting dead fine fuel moisture at regional scales using vapour pressure deficit from MODIS and gridded weather data. *Remote Sensing of Environment,* 174**,** 100-108.

Novkovic, I,Markovic, GB,Lukic, D,Dragicevic, S,Milosevic, M,Djurdjic, S,Samardzic, I,Lezaic, T & Tadic, M 2021. Gis-based forest fire susceptibility zonation with iot sensor network support, case study—nature park Golija, Serbia. *Sensors,* 21**,** 6520.

O'Mara, FP 2012. The role of grasslands in food security and climate change. *Annals of Botany,* 110**,** 1263-1270.

Oliveira, S,Moreira, F,Boca, R,San-Miguel-Ayanz, J & Pereira, JMC 2013. Assessment of fire selectivity in relation to land cover and topography: a comparison between Southern European countries. *International Journal of Wildland Fire,* 23**,** 620-630.

Olsen, JL,Ceccato, P,Proud, SR,Fensholt, R,Grippa, M,Mougin, E,Ardö, J & Sandholt, I 2013. Relation between seasonally detrended shortwave infrared reflectance data and land surface moisture in semi-arid Sahel. *Remote Sensing,* 5**,** 2898-2927.

Pang, Y,Li, Y,Feng, Z,Feng, Z,Zhao, Z,Chen, S & Zhang, H 2022. Forest fire occurrence prediction in China based on machine learning methods. *Remote Sensing,* 14**,** 5546.

Parisien, M-A,Miller, C,Parks, SA,DeLancey, ER,Robinne, F-N & Flannigan, MD 2016. The spatially varying influence of humans on fire probability in North America. *Environmental Research Letters,* 11**,** 075005.

Pausas, JG & Keeley, JE 2019. Wildfires as an ecosystem service. *Frontiers in Ecology and the Environment,* 17**,** 289-295.

Pausas, JG & Keeley, JE 2021. Wildfires and global change. *Frontiers in Ecology and the Environment,* 19**,** 387-395.

Pausas, JG & Ribeiro, E 2013. The global fire–productivity relationship. *Global Ecology Biogeography,* 22**,** 728-736.

Pellizzaro, G,Cesaraccio, C,Duce, P,Ventura, A & Zara, P 2007. Relationships between seasonal patterns of live fuel moisture and meteorological drought indices for Mediterranean shrubland species. *International Journal of Wildland Fire,* 16**,** 232-241.

Peng, J,Loew, A,Merlin, O & Verhoest, NEC 2017. A review of spatial downscaling of satellite remotely sensed soil moisture. *Reviews of Geophysics,* 55**,** 341-366.

Peng, W,Wei, Y,Chen, G,Lu, G,Ye, Q,Ding, R,Hu, P & Cheng, Z 2023. Analysis of Wildfire Danger Level Using Logistic Regression Model in Sichuan Province, China. *Forests,* 14**,** 2352.

Pereira, P,Mierauskas, P,Ubeda, X,Mataix-Solera, J & Cerda, A 2012. Fire in Protected Areas-the Effect of Protection and Importance of Fire Management. *Environmental Research, Engineering and Management,* 59**,** 52-62.

Pettinari, ML & Chuvieco, E 2020. Fire danger observed from space. *Surveys in Geophysics,* 41**,** 1437-1459.

Pham, BT,Jaafari, A,Avand, M,Al-Ansari, N,Dinh Du, T,Yen, HPH,Phong, TV,Nguyen, DH,Le, HV & Mafi-Gholami, D 2020. Performance evaluation of machine learning methods for forest fire modeling and prediction. *Symmetry,* 12**,** 1022.

Phelps, N & Woolford, DG 2021. Comparing calibrated statistical and machine learning methods for wildland fire occurrence prediction: A case study of human-caused fires in Lac La Biche, Alberta, Canada. *International journal of wildland fire,* 30**,** 850-870.

Phillips, SJ,Anderson, RP & Schapire, RE 2006. Maximum entropy modeling of species geographic distributions. *Ecological modelling,* 190**,** 231-259.

Pourtaghi, ZS,Pourghasemi, HR,Aretano, R & Semeraro, T 2016. Investigation of general indicators influencing on forest fire and its susceptibility modeling using different data mining techniques. *Ecological Indicators,* 64**,** 72-84.

Pradeep, GS,Danumah, JH,Nikhil, S,Prasad, MK,Patel, N,Mammen, PC,Rajaneesh, A,Oniga, V-E,Ajin, RS & Kuriakose, SL 2022. Forest fire risk zone mapping of Eravikulam National Park in India: A comparison between frequency ratio and analytic hierarchy process methods. *Croatian Journal of Forest Engineering: Journal for Theory and Application of Forestry Engineering,* 43**,** 199-217.

Price, C & Federmesser, B 2006. Lightning-rainfall relationships in Mediterranean winter thunderstorms. *Geophysical Research Letters,* 33.

Qi, Y,Dennison, PE,Spencer, J & RiaÃ±o, D 2012. Monitoring live fuel moisture using soil moisture and remote sensing proxies. *Fire Ecology,* 8**,** 71-87.

Qie, X,Toumi, R & Yuan, T 2003. Lightning activities on the Tibetan Plateau as observed by the lightning imaging sensor. *Journal of Geophysical Research: Atmospheres,* 108.

Rademeyer, C, ; & van Zyl, W 2014. Golden Jubilee for Golden Gate-A concise history of Golden Gate Highlands National Park , 1963 -2013. *Mediterranean Journal of Social Science,* 5**,** 1169 -1177.

Rakov, VA & Uman, MA 2003. *Lightning: physics and effects*, Cambridge university press.

Ramírez, J,Monedero, S & Buckley, D. New approaches in fire simulations analysis with Wildfire Analyst. Proceedings of the 5th International Wildland Fire Conference, 2011 Sun City, South Africa. 9-13.

Republic of South Africa, R, Department of Forest, Fisheries, the Environment. 2020. *SA NAtional Land Cover Datasets* [Online]. Department of Forest, Fisheries, the Environment

Available: https://egis.environment.gov.za/sa_national_land_cover_datasets [Accessed 01 June 2021].

Ricotta, C,Bajocco, S,Guglietta, D & Conedera, M 2018. Assessing the Influence of Roads on Fire Ignition: Does Land Cover Matter? *Fire,* 1**,** 24.

Riley, SJ,DeGloria, SD & Elliot, R 1999. Index that quantifies topographic heterogeneity. *intermountain Journal of sciences,* 5**,** 23-27.

Robinne, F-N,Burns, J,Kant, P,Flannigan, M,Kleine, M,de Groot, B & Wotton, D. Global fire challenges in a warming world. 2018. IUFRO.

Rodrigues, M,Jiménez-Ruano, A,Peña-Angulo, D & de la Riva, J 2018. A comprehensive spatial-temporal analysis of driving factors of human-caused wildfires in Spain using Geographically Weighted Logistic Regression. *Journal of Environmental Management,* 225**,** 177-192.

Romero-Calcerrada, R,Novillo, CJ,Millington, JDA & Gomez-Jimenez, I 2008. GIS analysis of spatial patterns of human-caused wildfire ignition risk in the SW of Madrid (Central Spain). *Landscape ecology,* 23**,** 341-354.

Ruffault, J,Curt, T,Martin-StPaul, NK,Moron, V & Trigo, RM 2018. Extreme wildfire events are linked to global-change-type droughts in the northern Mediterranean. *Natural Hazards and Earth System Sciences,* 18**,** 847-856.

Russell, IA & Skelton, PH 2005. Freshwater fishes of Golden Gate Highlands national park. *Koedoe,* 48**,** 87-94.

Rutherford, MC,Mucina, L & Powrie, LW 2006. Biomes and bioregions of southern Africa. *The vegetation of South Africa, Lesotho and Swaziland,* 19**,** 30-51.

Rutherford, MC & Westfall, RH 1994. *Biomes of southern Africa: an objective categorization,* National Botanical Institute.

Sá, ACL,Turkman, MAA & Pereira, JMC 2018. Exploring fire incidence in Portugal using generalized additive models for location, scale and shape (GAMLSS). *Modeling Earth Systems and Environment,* 4**,** 199-220.

Sabaghy, S,Walker, JP,Renzullo, LJ,Akbar, R,Chan, S,Chaubell, J,Das, N,Dunbar, RS,Entekhabi, D,Gevaert, A,Jackson, TJ,Loew, A,Merlin, O,Moghaddam, M,Peng, J,Peng, J,Piepmeier, J,Rüdiger, C,Stefan, V,Wu, X,Ye, N & Yueh, S 2020. Comprehensive analysis of alternative downscaled soil moisture products. *Remote Sensing of Environment,* 239**,** 111586.

Salavati, G,Saniei, E,Ghaderpour, E & Hassan, QK 2022. Wildfire risk forecasting using weights of evidence and statistical index models. *Sustainability,* 14**,** 3881.

Sandwith, T & Besançon, C 2010. Making peace: protected areas contributing to conflict resolution. *Arguments for Protected Areas.* Routledge.

Sayad, YO,Mousannif, H & Al Moatassime, H 2019. Predictive modeling of wildfires: A new dataset and machine learning approach. *Fire Safety Journal,* 104**,** 130-146.

Sazib, N,Bolten, JD & Mladenova, IE 2021. Leveraging NASA soil moisture active passive for assessing fire susceptibility and potential impacts over Australia and California. *IEEE Journal of Selected Topics in Applied Earth Observations and Remote Sensing,* 15**,** 779-787.

Schroeder, W & Giglio, L 2017. Visible Infrared Imaging Radiometer Suite (VIIRS) 375 m & 750 m Active Fire Detection Data Sets Based on NASA VIIRS Land Science Investigator Processing System (SIPS) Reprocessed Data—Version 1. 2017. Washington, DC, USA: NASA.

Sharma, LK,Gupta, R & Fatima, N 2022. Assessing the predictive efficacy of six machine learning algorithms for the susceptibility of Indian forests to fire. *International journal of wildland fire,* 31**,** 735-758.

Sharma, S,Carlson, J,Krueger, ES,Engle, DM,Twidwell, D,Fuhlendorf, SD,Patrignani, A,Feng, L & Ochsner, TE 2020. Soil moisture as an indicator of growing-season herbaceous fuel moisture and curing rate in grasslands. *International Journal of Wildland Fire,* 30**,** 57-69.

Sharma, S & Dhakal, K 2021. Boots on the ground and eyes in the sky: A perspective on estimating fire danger from soil moisture content. *Fire,* 4**,** 45.

Sharma, SK,Aryal, J,Shao, Q & Rajabifard, A 2023. Characterizing Topographic Influences of Bushfire Severity Using Machine Learning Models: A Case Study in a Hilly Terrain of Victoria, Australia. *IEEE Journal of Selected Topics in Applied Earth Observations and Remote Sensing,* 16**,** 2791-2807.

Sharples, JJ 2009. An overview of mountain meteorological effects relevant to fire behaviour and bushfire risk. *International Journal of Wildland Fire,* 18**,** 737-754.

Sharples, JJ,McRae, RHD & Weber, RO 2010. Wind characteristics over complex terrain with implications for bushfire risk management. *Environmental Modelling & Software,* 25**,** 1099-1120.

Shmuel, A & Heifetz, E. 2022. Global Wildfire Susceptibility Mapping Based on Machine Learning Models. *Forests* [Online], 13.

Si, L,Shu, L,Wang, M,Zhao, F,Chen, F,Li, W & Li, W 2022. Study on forest fire danger prediction in plateau mountainous forest area. *Natural Hazards Research,* 2**,** 25-32.

Silva, JS,Rego, FC,Fernandes, P & Rigolot, E 2010. *Towards integrated fire management-Outcomes of the European project Fire Paradox*, European Forest Institute.

Sjöström, J & Granström, A 2023. A phenology-driven fire danger index for northern grasslands. *International Journal of Wildland Fire,* 32**,** 1332-1346.

Skowno, A,Poole, C,Raimondo, D,Sink, K,van Niekerk, L,van Deventer, H,Smith-Adao, L,Harris, L,Tolley, K & Zengeya, T 2019. National Biodiversity Assessment 2018: an assessment of South Africa's ecosystems, species and genes. *Synthesis Report. South African National Biodiversity Institute, an entity of the Department of Environmental Affairs, Pretoria*.

Slater, R 2002. Between a rock and a hard place: contested livelihoods in Qwaqwa National Park, South Africa. *Geographical Journal,* 168**,** 116-129.

Smith, AJP,Jones, MW,Abatzoglou, JT,Canadell, JG & Betts, RA 2020. Climate change increases the risk of wildfires: September 2020. *ScienceBrief*.

Sokolova, M & Lapalme, G 2009. A systematic analysis of performance measures for classification tasks. *Information processing & management,* 45**,** 427-437.

South African National Parks (SANParks). 2020. *Golden Gate Highlands National Park Management Plan 2020-2029* [Online]. Pretoria: SANParks. Available: https://www.sanparks.org/assets/docs/conservation/park_man/gghnp_approved_plan.pdf [Accessed March 2021].

South African National Parks, S 2013. Golden Gate Highland National Park Management Plan 2013 -2023.

Spatial Temporal Evidence for Planning South Africa (stepSA). 2015. *Climate Indicators: Köppen-Geiger climate classification* [Online]. CSIR. Available: http://stepsatest.csir.co.za/climate_koppen_geiger.html [Accessed March 2022].

Sriwongsitanon, N,Gao, H,Savenije, H,Maekan, E,Saengsawan, S & Thianpopirug, S 2015. The Normalized Difference Infrared Index (NDII) as a proxy for soil moisture storage in hydrological modelling. *Hydrology Earth System Sciences Discussions,* 12.

Statistics South Africa (StatisticsSA) 2021. Natural Capital Series 2: Accounts for Protected Areas, 1900 to 2020. *In:* The South African National Biodiversity Institute and the Department of Forestry, FatE (ed.). Pretoria. : Statistics South Africa,

.

Stavi, I 2019. Wildfires in grasslands and shrublands: A review of impacts on vegetation, soil, hydrology, and geomorphology. *Water,* 11**,** 1042.

Steiner, JL,Wetter, J,Robertson, S,Teet, S,Wang, J,Wu, X,Zhou, Y,Brown, D & Xiao, X. 2020. Grassland Wildfires in the Southern Great Plains: Monitoring Ecological Impacts and Recovery. *Remote Sensing* [Online], 12.

Stephens, SL,Thompson, S,Boisramé, G,Collins, BM,Ponisio, LC,Rakhmatulina, E,Steel, ZL,Stevens, JT,van Wagtendonk, JW & Wilkin, K 2021. Fire, water, and biodiversity in the Sierra Nevada: a possible triple win. *Environmental Research Communications,* 3**,** 081004.

Stocks, B,Mason, J,Todd, J,Bosch, E,Wotton, B,Amiro, B,Flannigan, M,Hirsch, K,Logan, K & Martell, D 2002. Large forest fires in Canada, 1959–1997. *Journal of Geophysical Research: Atmospheres,* 107**,** FFR 5-1-FFR 5-12.

Stolton, S & Dudley, N 2010. *Vital Sites: The Contribution of Protected Areas to Human Health: a Research Report by WWF and Equilibrium Research*, WWF.

Stott, P 2000. Combustion in tropical biomass fires: a critical review. *Progress in Physical Geography,* 24**,** 355-377.

Strydom, S & Savage, MJ 2016. A spatio-temporal analysis of fires in South Africa. *South African Journal of Science,* 112**,** 1-8.

Strydom, T,Riddell, ES,Rowe, T,Govender, N,Lorentz, SA,le Roux, PAL & Wigley-Coetsee, C 2019. The effect of experimental fires on soil hydrology and nutrients in an African savanna. *Geoderma,* 345**,** 114-122.

Sturtevant, BR & Cleland, DT 2007. Human and biophysical factors influencing modern fire disturbance in northern Wisconsin. *International Journal of Wildland Fire,* 16**,** 398-413.

Su, Z,Hu, H,Wang, G,Ma, Y,Yang, X & Guo, F 2018. Using GIS and Random Forests to identify fire drivers in a forest city, Yichun, China. *Geomatics, Natural Hazards and Risk,* 9**,** 1207-1229.

Sullivan, A 2010. Grassland fire management in future climate. *Advances in Agronomy,* 106**,** 173-208.

Sungmin, O,Hou, X & Orth, R 2020. Observational evidence of wildfire-promoting soil moisture anomalies. *Scientific Reports,* 10.

Suttie, JM,Reynolds, SG & Batello, C 2005. *Grasslands of the World*, Food & Agriculture Org.

Syphard, AD & Keeley, JE 2016. Historical reconstructions of California wildfires vary by data source. *International Journal of Wildland Fire,* 25**,** 1221-1227.

Szpakowski, DM & Jensen, JLR 2019. A review of the applications of remote sensing in fire ecology. *Remote sensing,* 11**,** 2638.

Tan, C & Feng, Z 2023. Mapping Forest Fire Risk Zones Using Machine Learning Algorithms in Hunan Province, China. *Sustainability,* 15**,** 6292.

Tang, Z & Maclennan, J 2005. *Data mining with SQL Server 2005*, John Wiley & Sons.

Tanveera, A,Kanth, TA,Tali, PA & Naikoo, M 2016. Relation of soil bulk density with texture, total organic matter content and porosity in the soils of Kandi Area of Kashmir valley, India. *Int. Res. J. Earth Sci,* 4**,** 1-6.

Taylor, SW & Alexander, ME 2006. Science, technology, and human factors in fire danger rating: the Canadian experience. *International Journal of Wildland Fire,* 15**,** 121-135.

The COMET Program. 2022. *S-290 Unit 2: Topographic influences on wildland fire behaviour* [Online]. The University Corporation for Atmospheric Research. Available: https://www.meted.ucar.edu/fire/s290/unit2/index.htm [Accessed 11 September 2022].

Thompson, MP,Calkin, DE,Finney, MA,Ager, AA & Gilbertson-Day, JW 2011. Integrated national-scale assessment of wildfire risk to human and ecological values. *Stochastic Environmental Research and Risk Assessment,* 25**,** 761-780.

Tien Bui, D,Le, K-TT,Nguyen, VC,Le, HD & Revhaug, I 2016. Tropical forest fire susceptibility mapping at the Cat Ba National Park Area, Hai Phong City, Vietnam, using GIS-based kernel logistic regression. *Remote Sensing,* 8**,** 347.

Titti, G & Alessandro, S 2021. Cnr-irpi-padova/sz: Sz Plugin. Zenodo.

Titti, G,Sarretta, A,Lombardo, L,Crema, S,Pasuto, A & Borgatti, L 2022. Mapping susceptibility with open-source tools: a new plugin for QGIS. *Frontiers in Earth Science,* 10**,** 842425.

Titti, G,van Westen, C,Borgatti, L,Pasuto, A & Lombardo, L 2021. When enough is really enough? On the minimum number of landslides to build reliable susceptibility models. *Geosciences,* 11**,** 469.

Tolhurst, K,Shields, B & Chong, D 2008. Phoenix: development and application of a bushfire risk management tool. *Australian journal of emergency management,* 23**,** 47-54.

Trollope, W,Trollope, L & Hartnett, D 2002. *Fire behaviour a key factor in the fire ecology of African grasslands and savannas,* Rotterdam, Forest Fire Research Wildland Fire Safety ,Millpress.

Trollope, WSW,de Ronde, C & Geldenhys, CJ 2004. Fire Behavior. *In:* Goldammer, RC & de Ronde, C, ; (eds.) *Wildland Fire Management Handbook for SubSahara Africa.*: Global Fire Monitoring Centre (GFMC).

Turco, M,von Hardenberg, J,AghaKouchak, A,Llasat, MC,Provenzale, A & Trigo, RM 2017. On the key role of droughts in the dynamics of summer fires in Mediterranean Europe. *Scientific Reports,* 7**,** 81.

Turner, D,Lewis, M & Ostendorf, B 2011. Spatial indicators of fire risk in the arid and semi-arid zone of Australia. *Ecological Indicators,* 11**,** 149-167.

Tymstra, C,Bryce, RW,Wotton, BM,Taylor, SW & Armitage, OB 2010. Development and structure of Prometheus: the Canadian wildland fire growth simulation model. *Natural Resources Canada, Canadian Forest Service, Northern Forestry Centre, Information Report NOR-X-417.(Edmonton, AB)*.

United Nations Enviroment Program - World Conservation Monitoring Centre (UNEP-WCMC) 2021. Protected Area Profile for South Africa from the World Database on Protected Areas.

United Nations International Strategy for Disaster Risk Reduction (UNISDR) 2009. Terminology on Disater Risk Reduction

Vacchiano, G,Foderi, C,Berretti, R,Marchi, E & Motta, R 2018. Modeling anthropogenic and natural fire ignitions in an inner-alpine valley. *Natural Hazards and Earth System Sciences,* 18**,** 935-948.

Van Dijk, A,Yebra, M,Cary, GJ & Shah, S 2019. Towards comprehensive characterisation of flammability and fire danger. Melbourne, VIC, Australia: Bushfire Natural Hazards.

Van Wagtendonk, JW & Cayan, DR 2008. Temporal and spatial distribution of lightning strikes in California in relation to large-scale weather patterns. *Fire Ecology,* 4**,** 34-56.

Van Wilgen, **B**,Biggs, H,O'Regan, S & Mare, N 2000. A fire history of the savanna ecosystems in the Kruger National Park, South Africa, between 1941 and 1996. *South African Journal of Science,* 96**,** 167-178.

van Wilgen, BW,Forsyth, GG & Prins, P 2012. The management of fire-adapted ecosystems in an urban setting: the case of Table Mountain National Park, South Africa. *Ecology and Society,* 17.

Van Wilgen, BW,Govender, N,Forsyth, GG & Kraaij, T 2011. Towards adaptive fire management for biodiversity conservation: Experience in South African National Parks. *koedoe,* 53**,** 96-104.

Verbesselt, J,Somers, B,Lhermitte, S,Jonckheere, I,Van Aardt, J & Coppin, P 2007. Monitoring herbaceous fuel moisture content with SPOT VEGETATION time-series for fire risk prediction in savanna ecosystems. *Remote Sensing of Environment,* 108**,** 357-368.

Vermote, E. 2019. *MOD09A1 MODIS/Terra Surface Reflectance 8-day L3 Global 500m SIN Grid V006* [Online]. NASA EODIS Land Processes DAAC. [Accessed June 10 2020].

Victoria County Fire Authority (CFA). 2020. *CFA Grasslang Curing Guide* [Online]. CFA. Available: https://www.cfa.vic.gov.au/about-us/what-we-do/grassland-curing-observations [Accessed 20 June 2022].

Viegas, DX & Pita, LP 2004. Fire spread in canyons. *International Journal of wildland fire,* 13**,** 253-274.

Vilar, L,Gómez, I,Martínez-Vega, J,Echavarría, P,Riaño, D & Martín, MP 2016. Multitemporal modelling of socio-economic wildfire drivers in central Spain between the 1980s and the 2000s: comparing generalized linear models to machine learning algorithms. *PLoS One,* 11**,** e0161344.

Vinodkumar, V,Dharssi, I,Yebra, M & Fox-Hughes, P 2021. Continental-scale prediction of live fuel moisture content using soil moisture information. *Agricultural and Forest Meteorology,* 307**,** 108503.

Walker, JP. 1999. *Estimating soil moisture profile dynamics from near-surface soil moisture measurements and standard meteorological data.* University of Newcastle.

Wang, l,Zhou, Y,Zhou, W & Wang, S 2013. Fire danger assessment with remote sensing: a case study in Northern China. *Natural Hazards,* 65**,** 819-834.

Wang, S,Wang, W,Wu, Y & Zhao, S 2022. Surface Soil Moisture Inversion and Distribution Based on Spatio-Temporal Fusion of MODIS and Landsat. *Sustainability,* 14**,** 9905.

Wang, W,Fang, X,Wei, X & Ye, J 2024. Optimized stratification approach enhances the weight-of-evidence method: Transparently uncovering wildfire probability and drivers-wildfire relationships in the southwest mountains of China. *Ecological Indicators,* 158**,** 111500.

Weise, DR & Biging, GS 1994. Effects of wind velocity and slope on fire behavior. *Fire Safety Science,* 4**,** 1041-1051.

Weiss, A. Topographic position and landforms analysis. ESRI User Conference, 9–13 July 2001 2001 San Diego, CA, USA. 227–245.

White, RP,Murray, S,Rohweder, M,Prince, S & Thompson, K 2000. *Grassland ecosystems*, World Resources Institute Washington, DC, USA.

Williams, ER 1994. Global circuit response to seasonal variations in global surface air temperature. *Monthly Weather Review,* 122**,** 1917-1929.

Willis, C,van Wilgen, B,Tolhurst, K,Everson, C,D'Abreton, P,Pero, L & Fleming, G 2001. The development of a national fire danger rating system for South Africa. *Department of Water Affairs and Forestry, Pretoria*.

Wilson, EH & Sader, SA 2002. Detection of forest harvest type using multiple dates of Landsat TM imagery. *Remote Sensing of Environment,* 80**,** 385-396.

Wittich, K-P 2011. Phenological observations of grass curing in Germany. *International Journal of Biometeorology,* 55**,** 313-318.

Woolford, DG,Martell, DL,McFayden, CB,Evens, J,Stacey, A,Wotton, BM & Boychuk, D 2021. The development and implementation of a human-caused wildland fire occurrence prediction system for the province of Ontario, Canada. *Canadian Journal of Forest Research,* 51**,** 303-325.

Wotton, BM 2009. Interpreting and using outputs from the Canadian Forest Fire Danger Rating System in research applications. *Environmental and Ecological Statistics,* 16**,** 107-131.

Wu, M,Niu, Z,Wang, C,Wu, C & Wang, L 2012. Use of MODIS and Landsat time series data to generate high-resolution temporal synthetic Landsat data using a spatial and temporal reflectance fusion model. *Journal of Applied Remote Sensing,* 6**,** 063507-063507.

Wu, M,Wu, C,Huang, W,Niu, Z & Wang, C 2015. High-resolution Leaf Area Index estimation from synthetic Landsat data generated by a spatial and temporal data fusion model. *Computers and electronics in agriculture,* 115**,** 1-11.

Wu, M,Yang, C,Song, X,Hoffmann, WC,Huang, W,Niu, Z,Wang, C,Li, W & Yu, B 2018. Monitoring cotton root rot by synthetic Sentinel-2 NDVI time series using improved spatial and temporal data fusion. *Scientific reports,* 8**,** 2016.

Xiao, X,Boles, S,Liu, J,Zhuang, D & Liu, M 2002. Characterization of forest types in Northeastern China, using multi-temporal SPOT-4 VEGETATION sensor data. *Remote Sensing of Environment,* 82**,** 335-348.

Xie, L,Zhang, R,Zhan, J,Li, S,Shama, A,Zhan, R,Wang, T,Lv, J,Bao, X & Wu, R 2022. Wildfire risk assessment in Liangshan Prefecture, China based on an integration machine learning algorithm. *Remote Sensing,* 14**,** 4592.

Xofis, P,Tsiourlis, G & Konstantinidis, P 2020. A Fire Danger Index for the early detection of areas vulnerable to wildfires in the Eastern Mediterranean region. *Euro-Mediterranean Journal for Environmental Integration,* 5**,** 32.

Xu, Z,Zhou, G & Shimizu, H 2010. Plant responses to drought and rewatering. *Plant signaling behavior,* 5**,** 649-654.

Yang, C,Deng, K,Peng, D,Jiang, L,Zhao, M,Liu, J & Qiu, X 2022. Spatiotemporal Characteristics and Heterogeneity of Vegetation Phenology in the Yangtze River Delta. *Remote Sensing,* 14**,** 2984.

Ye, J,Wu, M,Deng, Z,Xu, S,Zhou, R & Clarke, KC 2017. Modeling the spatial patterns of human wildfire ignition in Yunnan province, China. *Applied Geography,* 89**,** 150-162.

Yebra, M,Chuvieco, E & Rian˜o, D 2008. Estimation of live fuel moisture content from MODIS images for fire risk assessment. *Agricultural and Forest Meteorology***,** 523-536.

Yebra, M,E.;, P,Dennison, PE,Chuvieco, E,Riaño, D,Zylstra, P,Hunt Jr, ER,Danso, FM,Qi, Y & Jurdao, S 2013. A global review of remote sensing of live fuel moisture content for fire danger assessment: Moving towards operational products. *Remote densing of Environment***,** 455 - 468.

Yebra, M,Quan, X,Riaño, D,Larraondo, PR,van Dijk, AI & Cary, GJ 2018. A fuel moisture content and flammability monitoring methodology for continental Australia based on optical remote sensing. *Remote Sensing of Environment,* 212**,** 260-272.

Yebra, M,Scortechini, G,Badi, A,Beget, ME,Boer, MM,Bradstock, R,Chuvieco, E,Danson, FM,Dennison, P & Resco de Dios, V 2019. Globe-LFMC, a global plant water status database for vegetation ecophysiology and wildfire applications. *Scientific data,* 6**,** 155.

Yu, B,Chen, F,Li, B,Wang, L,Wu, M,Mingquan, W,Bo, Y,Fang, C & Bin, L 2017. Fire risk prediction using remote sensed products: A case of Cambodia. *Photogramm. Eng. Remote Sens,* 83**,** 19-25.

Yu, Y,Mao, J,Wullschleger, SD,Chen, A,Shi, X,Wang, Y,Hoffman, FM,Zhang, Y & Pierce, E 2022. Machine learning–based observation-constrained projections reveal elevated global socioeconomic risks from wildfire. *Nature communications,* 13**,** 1250.

Yunhao, C,Jing, L & Guangxiong, P 2007. Forest fire risk assessment combining remote sensing and meteorological information. *New Zealand Journal of Agricultural Research,* 50**,** 1037-1044.

Zacharakis, I & Tsihrintzis, VA 2023a. Environmental forest fire danger rating systems and indices around the globe: a review. *Land,* 12**,** 194.

Zacharakis, I & Tsihrintzis, VA 2023b. Integrated wildfire danger models and factors: A review. *Science of the total environment***,** 165704.

Zapata-Ríos, X,Lopez-Fabara, C,Navarrete, A,Torres-Paguay, S & Flores, M 2021. Spatiotemporal patterns of burned areas, fire drivers, and fire probability across the equatorial Andes. *Journal of Mountain Science,* 18**,** 952-972.

Zhang, G,Wang, M & Liu, K 2019. Forest fire susceptibility modeling using a convolutional neural network for Yunnan province of China. *International Journal of Disaster Risk Science,* 10**,** 386-403.

Zhang, Y,Lim, S & Sharples, JJ 2016. Modelling spatial patterns of wildfire occurrence in south-eastern Australia. *Geomatics, Natural Hazards and Risk,* 7**,** 1800-1815.

Zhao, L,Yebra, M,van Dijk, AIJM,Cary, GJ & Hughes, D 2022. Controlled field experiment clarifies the influence of soil moisture on litter moisture content. *Agricultural and Forest Meteorology,* 314**,** 108782.

Zhao, L,Yebra, M,van Dijk, AIJM,Cary, GJ,Matthews, S & Sheridan, G 2021a. The influence of soil moisture on surface and sub-surface litter fuel moisture simulation at five Australian sites. *Agricultural and Forest Meteorology,* 298**,** 108282.

Zhao, P,Zhang, F,Lin, H & Xu, S 2021b. GIS-Based Forest Fire Risk Model: A Case Study in Laoshan National Forest Park, Nanjing. *Remote Sensing,* 13**,** 3704.

Zhao, S,Wang, Q,Zhang, F,Yao, Y,Qin, Q,You, L,Li, J,Li, Z,Wu, Y & Liu, S 2013. Drought Mapping Using Two Shortwave Infrared Water Indices with MODIS Data under Vegetated Season. *Journal of Environmental Informatics,* 21.

Zhou, X-H,McClish, DK & Obuchowski, NA 2009. *Statistical methods in diagnostic medicine,* John Wiley & Sons.

Zhu, X,Chen, J,Gao, F,Chen, X & Masek, JG 2010. An enhanced spatial and temporal adaptive reflectance fusion model for complex heterogeneous regions. *Remote Sensing of Environment,* 114**,** 2610-2623.

APPENDICES

Appendix 1. List of studies on fire danger prediction and mapping comparing statistical and machine learning models.

Authors	**Study Area**	**Driving Factors**	**Methods**	**Key findings**
(Tien Bui *et al.*, 2016)	Cat Ba National Park, Vietnam	Slope, Aspect, Topographic Wetness Index (TPI), Distance to road, distance to populated area, land cover, NDVI, Surface Temperature, Wind Speed, Rain fall	SVM and Kernel Logistic Regression (KLR)	KLR outperformed SVM with overall accuracy of 92.20%. NDVI, TWI and land cover most significant factors
(Chicas *et al.*, 2022)	Belize ecosystem and protected Area , Central America	Elevation, Slope, precipitation, temperature, distance to roads, residential area and agriculture, NDVI and land cover	AHP, RF, Fuzzy AHP (FAHP)	RF outperformed other models AUC=83.1%), FAHP (71.2), AHP(66.8)
(Eskandari *et al.*, 2020)	The Zagros Mountains , Iran	Slope angle, aspect, elevation, climate, TWI distance from rivers and roads	SVM, GLM, Functional Data Analysis (FDA); RF	AUC of 0.777 for FDA and GLA however GLA; SVM (0.75) and RF (0.74) Distance from roads had highest mean importance values.
(Pham *et al.*, 2020)	The Pu Mat National Park, Vietnam	Elevation, slope degree, aspect, average annual temperature, drought index rive density, land cover, and distance from roads and residential areas	Bayes Network (BN), Naïve Bayes (NB), Decision Tree (DT) and Multivariate Logistic Regression (MLP)	BN was dominant with AUC=0.96, DT(0.94), NB(0.939); MLR (0.936)
(Hong *et al.*, 2017)	Yihuang Area in Jiangxi Province , China	Slope degree, altitude, TWI, plan curvature, land use, NDVI, annual rainfall and temperature, distance from roads and rivers, wind effect, and soil texture	Linear and quadratic discriminant analysis (LDA and QDA). Frequency Ratio (FR) and weights of evidence (WoE)	WoE had highest accuracy rate (82.2%); FR(80.9), QDA (78.3) and LDA (78). Altitude, slope degree and temperature had the highest contribution to the model Aspect and soil had the lowest contribution.
(Coffield *et al.*, 2019)	Alaska, United, State of America	Slope, elevation, aspect, temperature, vegetation type, vapour pressure deficit, surface air temperature, precipitation and wind speed	DT, RF, K-nearest neighbours,(KNN), gradient boosting (GB) , multilayer perceptron (MLP)	DT had highest accuracy performance followed RF, KNN, GB and (MLP perceptron
(Chang *et al.*, 2023)	Inner Magnolia Autonomous Region, North of China	Mean annual temperature and precipitation, daily average specific	Global logistic regression (GLS), geographically weighted logistic	Daily humidity and temperature were of highest importance while slope and aspect

		humidity, temperature, and wind speed, daily cumulative precipitation, distance to the nearest settlement, road, river, and railways, population density, global vegetation moisture content (GVMI), NDVI, elevation, aspect index and slope.	regression (GWLR) and RF	were of lowest import with no impact on fire danger probability.
(Gholamnia *et al.*, 2020)	Amol County, Mazandaran Province, Iran	Slope % and degree, altitude, aspect, plan curvature, TWI, landforms, distance to river, village, recreational, and road, annual rainfall, and temperature, wind effect and potential solar radiation .	Artificial neural network (ANN), dmine-regression (DR), DM neural, least angle regression (LARS, MLP, RF, radial basis function (RBF), self-organizing maps (SAM), SVM, DT and LR.	RF and LR had highest and lowest accuracy (88% and 65%) respectively
(Mohajane *et al.*, 2021)	Tanger-Tetouan-Al Hoceima region, North Morocco	Slope angle, aspect, elevation, distance to road and residential, rainfall, temperature, wind speed, land use and NDVI.	FR, FR-MLP, FR-LR, FR-classification and regression trees (CART), FR-SVM and FR-RM.	RF-FR achieved the best performance (AUC=0.98), SVM-FR (0.95), MLP-FR(0.85), CART-FR (0.847), and LR-FR (0.80).
(Phelps and Woolford, 2021)	Lac La region of Alberta, Canada	Highways, railways, roads, cut lines, power line, wildland-urban interface (3), fuel types, precipitation, temperature, wind speed and fire weather systems codes and indices (7).	Classification trees, RF, NN,LR, logistic generalized additive models (GAM).	They suggested that statistical methods may have a similar performance to machine learning.
(Achu *et al.*, 2021)	Wayanad district of Kerala state, India	Ambient air temperature, wind speed, rainfall, RH, atmospheric water vapour (WVP), elevation, slope angle , TWI, aspect LULC, distance from road and villages.	ANN, GLM, multivariate adaptive regression spines (MARS), NBS, KNN, SVM, RF , GBM, adaptive boosting (AdaBoost) and maximum entropy (MaxEnt)	A weighted approach to describe fire danger from models outcome and the approach improved accuracy area AUC =89% in comparison with individual models (AUC= 71.5 – 86.9%). LULC was the primary factor influencing fire danger probability.

Appendix 2. Google Earth Engine scripts for calculating Grass Curing Index (GCI)

```
// Load Sentinel-2 data
var s2 = ee.ImageCollection('COPERNICUS/S2');



//calculate NDVI and map as a band into the collection
var addNDVI = function(s2) {
  var ndvi = s2.normalizedDifference(['B8', 'B4']).rename('NDVI');
  return s2.addBands(ndvi);
};

var s2 = s2.map(addNDVI);



//calculate GVMI and map as a band into the collection
var addGVMI = function(s2) {
// Sentinel 2 GVMI = ((NIR+0.1)-(SWIR+0.02))/((NIR+0.1)+(SWIR+0.02)).
    var GVMI = s2.expression(
    '((NIR+0.1)-(SWIR+0.02))/((NIR+0.1)+(SWIR+0.02))', {
      'NIR': s2.select('B8'),
      'SWIR': s2.select('B12')
      }).rename('GVMI');
      return s2.addBands(GVMI);
};

var s2 = s2.map(addGVMI);

//Select the Pre fire dates
var s2 = s2.filterDate('2017-12-01', '2017-12-31')
```

```
        .filterBounds(geometry)
        .select(['NDVI', 'GVMI'])
        .median();



print(s2);

// Load MODIS data
var modis = ee.ImageCollection('MODIS/061/MOD09A1');

//calculate NDVI and map as a band into the collection
var addNDVI = function(modis) {
  var ndvi = modis.normalizedDifference(['sur_refl_b02', 'sur_refl_b01']).rename('NDVI');
  return modis.addBands(ndvi);
};

var modis = modis.map(addNDVI);

//calculate GVMI and map as a band into the collection
var addGVMI = function(modis) {
// Sentinel 2 GVMI = ((NIR+0.1)-(SWIR+0.02))/((NIR+0.1)+(SWIR+0.02)).
    var GVMI = modis.expression(
    '((NIR+0.1)-(SWIR+0.02))/((NIR+0.1)+(SWIR+0.02))', {
      'NIR': modis.select('sur_refl_b02'),
      'SWIR': modis.select('sur_refl_b07')
      }).rename('GVMI');
      return modis.addBands(GVMI);
};
```

```
var modis = modis.map(addGVMI);

//Select the Pre fire dates
var modis = modis.filterDate('2017-12-01', '2017-12-31')
            .filterBounds(geometry)
            .select(['NDVI', 'GVMI']);


print(modis);


// let's create a function to rename Modis bands to match up Sentinel 2.
function rename(image){
  return image.select(
    ['NDVI', 'GVMI'],
    ['NDVI', 'GVMI']);
}

// Apply the rename function
var modisRenamed = modis.map(rename);


// Merge Sentinel2 and Modis NDVI and GVMI images
var S2_modis = modisRenamed.merge(s2);
print('Merged collections',S2_modis);


// Display the composite image
```

```
Map.centerObject(geometry, 10);
var S2_modis = S2_modis.max().clip(geometry);
var ndviVis = {min:0, max:0.5,  palette: ['white', 'green']};
Map.addLayer(S2_modis.select('NDVI'), ndviVis, 'NDVI');
Map.addLayer(S2_modis.select('GVMI'), ndviVis, 'GVMI');

//Grass curing Index = (NDVI* – 88.41) + (GVMI* – 67.71) + 113.80
var GCI = S2_modis.expression(
   '(NDVI*- 88.41) + (GVMI*- 67.71) + 113.80', {
     'NDVI': S2_modis.select('NDVI'),
     'GVMI': S2_modis.select('GVMI')
}).rename('GCI');

var GCIVis = {min:50, max:100,  palette: ['red', 'yellow', 'green']};
Map.addLayer(GCI.clip(geometry), GCIVis, 'GCI');
// Reduce the region. The region parameter is the Feature geometry.
print(GCI);

//Export the image, specifying scale and region.
Export.image.toDrive({
image: GCI,
description: 'GCI_GVMI',
scale: 10,
region: geometry
});

//Export the image, specifying scale and region.
Export.image.toDrive({
image: S2_modis.select('NDVI'),
```

```
description: 'NDVI',
scale: 10,
region: geometry
});

//Export the image, specifying scale and region.
Export.image.toDrive({
image: S2_modis.select('GVMI'),
description: 'GMVI',
scale: 10,
region: geometry
});
```

Appendix 3. Google Earth Engine scripts for calculating Land Surface Temperature (LST)

```
//Important the LST image collection
var modis = ee.ImageCollection("MODIS/061/MOD11A1")
.filterDate("2021-06-01" , "2021-10-31")
.filterBounds(geometry)
.select('LST_Day_1km');

//kelvin to celcius
var LST = modis.map(function(img){
  return img
  .multiply(0.02)
  .subtract(273.15)
  .copyProperties(img,['system:time_start'])

})

print(
      ui.Chart.image.series({
        imageCollection: LST,
        region: geometry,
        reducer: ee.Reducer.mean(),
        scale: 1000, // nominal scale MODIS imagery
        xProperty: 'system:time_start' // default
      }));

print(LST)
```

```
// As a reduced Image
var export_Image = LST.reduce(ee.Reducer.mean());
print("export_Image map", export_Image);
Export.image.toDrive ({
   image: export_Image,
   description: 'LST_MOD',
   scale: 10,
   region: geometry,
  maxPixels:1e13

});
```

Appendix 4: Spatial relationship between each driving factor and grassfire location using WoE and FR

Fire Drivers	Class	WoE							FR				
		Npx1	**Npx2**	**Npx3**	**Npx4**	**W+**	**W-**	**Wf**	**Npx1**	**Npx2**	**Npx3**	**Npx4**	**FR**
Aspect	Flat	4	796	9	627	-1.040	0.009	-1.050	4	13	800	1436	0.552
	N	62	738	51	585	-0.034	0.003	-0.037	62	113	800	1436	0.985
	NE	118	682	68	568	0.322	-0.047	0.368	118	186	800	1436	1.139
	E	123	677	112	524	-0.136	0.027	-0.162	123	235	800	1436	0.940
	SE	84	716	61	575	0.091	-0.010	0.101	84	145	800	1436	1.040
	S	54	746	39	597	0.096	-0.007	0.103	54	93	800	1436	1.042
	SW	60	740	47	589	0.015	-0.001	0.016	60	107	800	1436	1.007
	W	110	690	95	541	-0.083	0.014	-0.097	110	205	800	1436	0.963
	NW	132	668	106	530	-0.010	0.002	-0.012	132	238	800	1436	0.996
	N	53	747	48	588	-0.130	0.010	-0.140	53	101	800	1436	0.942
BD	121 -132	150	650	77	559	0.437	-0.079	0.516	150	227	800	1436	1.186
	132 - 135	155	645	94	542	0.271	-0.055	0.326	155	249	800	1436	1.117
	135 -138	145	655	118	518	-0.023	0.005	-0.029	145	263	800	1436	0.990
	138 - 141	190	610	165	471	-0.088	0.029	-0.118	190	355	800	1436	0.961
	141 -145	160	640	182	454	-0.358	0.114	-0.472	160	342	800	1436	0.840
BSI	0.334 - 0.365	169	631	120	516	0.113	-0.028	0.141	169	289	800	1436	1.050
	0.365 - 0.373	159	641	125	511	0.011	-0.003	0.014	159	284	800	1436	1.005
	0.373 - 0.382	175	625	114	522	0.199	-0.049	0.249	175	289	800	1436	1.087
	0.382 - 0.391	161	639	125	511	0.024	-0.006	0.030	161	286	800	1436	1.010
	0.391 - 0.466	136	664	152	484	-0.341	0.087	-0.427	136	288	800	1436	0.848
Coarse fragments	43-75	149	651	124	512	-0.046	0.011	-0.057	149	273	800	1436	0.980
	75-90	155	645	127	509	-0.030	0.007	-0.038	155	282	800	1436	0.987
	90-103	154	646	146	490	-0.176	0.047	-0.223	154	300	800	1436	0.921
	103-121	169	631	118	518	0.130	-0.032	0.162	169	287	800	1436	1.057
	121 - 194	173	627	121	515	0.128	-0.033	0.161	173	294	800	1436	1.056
Elevation	1654 - 1779	151	649	132	504	-0.095	0.023	-0.118	151	283	800	1436	0.958
	1779 - 1875	145	655	146	490	-0.236	0.061	-0.297	145	291	800	1436	0.894

Fire Drivers	Class	WoE							FR				
		Npx1	Npx2	Npx3	Npx4	W+	W-	Wf	Npx1	Npx2	Npx3	Npx4	FR
	1875 - 1976	158	642	128	508	-0.019	0.005	-0.024	158	286	800	1436	0.992
	1976 - 2098	177	623	111	525	0.237	-0.058	0.295	177	288	800	1436	1.103
	2098 - 2815	169	631	119	517	0.121	-0.030	0.152	169	288	800	1436	1.053
GCI	0 -30	181	619	217	419	-0.411	0.161	-0.572	181	398	800	1436	0.816
	30 -50	406	394	318	318	0.015	-0.015	0.030	406	724	800	1436	1.007
	50 -60	110	690	53	583	0.501	-0.061	0.562	110	163	800	1436	1.211
	60 -80	93	707	35	601	0.748	-0.067	0.815	93	128	800	1436	1.304
	80 -100	9	791	7	629	0.022	0.000	0.022	9	16	800	1436	1.010
GVMI	-0.151 - -0.103	139	661	146	490	-0.279	0.070	-0.348	139	285	800	1436	0.875
	-0.103 - -0.085	155	645	136	500	-0.099	0.025	-0.124	155	291	800	1436	0.956
	-0.085 - -0.072	155	645	128	508	-0.038	0.009	-0.047	155	283	800	1436	0.983
	-0.072 - -0.051	153	647	137	499	-0.119	0.030	-0.149	153	290	800	1436	0.947
	-0.051 - 0.109	198	602	89	547	0.570	-0.134	0.704	198	287	800	1436	1.238
Prox_structures	0 -100	3	797	2	634	0.176	-0.001	0.177	3	5	800	1436	1.077
	100 -200	6	794	9	627	-0.635	0.007	-0.642	6	15	800	1436	0.718
	200 -300	5	795	11	625	-1.018	0.011	-1.029	5	16	800	1436	0.561
	300-400	7	793	5	631	0.107	-0.001	0.108	7	12	800	1436	1.047
	400-500	9	791	9	627	-0.229	0.003	-0.232	9	18	800	1436	0.898
	>500	770	30	600	36	0.020	-0.412	0.432	770	1370	800	1436	1.009
Lightning	1	9	791	4	632	0.582	-0.005	0.587	9	13	800	1436	1.243
	2	47	753	66	570	-0.569	0.049	-0.618	47	113	800	1436	0.747
	3	165	635	158	478	-0.186	0.055	-0.241	165	323	800	1436	0.917
	4	425	375	335	301	0.009	-0.010	0.018	425	760	800	1436	1.004
	5	154	646	73	563	0.517	-0.092	0.609	154	227	800	1436	1.218
LST	19-22	148	652	139	497	-0.167	0.042	-0.209	148	287	800	1436	0.926
	22-23	180	620	106	530	0.300	-0.073	0.373	180	286	800	1436	1.130
	23-24	177	623	112	524	0.228	-0.056	0.285	177	289	800	1436	1.099
	24-25	146	654	142	494	-0.202	0.051	-0.253	146	288	800	1436	0.910

Fire Drivers	Class	WoE							FR				
		Npx1	**Npx2**	**Npx3**	**Npx4**	**W+**	**W-**	**Wf**	**Npx1**	**Npx2**	**Npx3**	**Npx4**	**FR**
	25	149	651	137	499	-0.145	0.036	-0.182	149	286	800	1436	0.935
Prox_ River	0-200	118	682	102	534	-0.084	0.015	-0.099	118	220	800	1436	0.963
	200-400	112	688	73	563	0.199	-0.029	0.228	112	185	800	1436	1.087
	400-600	83	717	47	589	0.339	-0.033	0.372	83	130	800	1436	1.146
	600-800	77	723	51	585	0.183	-0.018	0.200	77	128	800	1436	1.080
	800-1000	45	755	46	590	-0.251	0.017	-0.269	45	91	800	1436	0.888
	>1000	365	435	317	319	-0.088	0.081	-0.169	365	682	800	1436	0.961
Proximity _Road	0-200	117	683	110	526	-0.168	0.032	-0.200	117	227	800	1436	0.925
	200-400	81	719	61	575	0.054	-0.006	0.060	81	142	800	1436	1.024
	400-600	77	723	63	573	-0.029	0.003	-0.032	77	140	800	1436	0.987
	600-800	63	737	44	592	0.130	-0.010	0.140	63	107	800	1436	1.057
	800-1000	69	731	70	566	-0.244	0.026	-0.270	69	139	800	1436	0.891
	>1000	393	407	288	348	0.081	-0.073	0.154	393	681	800	1436	1.036
Slope	0 - 4.68	138	662	150	486	-0.313	0.080	-0.392	138	288	800	1436	0.860
	4.68 - 8.54	152	648	139	497	-0.140	0.036	-0.176	152	291	800	1436	0.938
	8.54 - 13.77	157	643	125	511	-0.001	0.000	-0.002	157	282	800	1436	0.999
	13.77 - 21.20	178	622	109	527	0.261	-0.064	0.325	178	287	800	1436	1.113
	21.20 - 70.21	175	625	113	523	0.208	-0.051	0.259	175	288	800	1436	1.091
SMC	3.181 - 3.411	153	647	153	483	-0.229	0.063	-0.292	153	306	800	1436	0.898
	3.411 - 3.448	118	682	91	545	0.030	-0.005	0.036	118	209	800	1436	1.013
	3.488 - 3.517	190	610	166	470	-0.094	0.031	-0.126	190	356	800	1436	0.958
	3.517 - 3.763	120	680	100	536	-0.047	0.009	-0.056	120	220	800	1436	0.979
	3.713 - 4.616	219	581	126	510	0.323	-0.099	0.422	219	345	800	1436	1.139
TAWCP	21-24	50	750	70	566	-0.566	0.052	-0.618	50	120	800	1436	0.748
	24-25	196	604	127	509	0.205	-0.058	0.263	196	323	800	1436	1.089
	25-28	322	478	219	417	0.156	-0.093	0.249	322	541	800	1436	1.068
	28-33	232	568	220	416	-0.176	0.082	-0.258	232	452	800	1436	0.921
TPI	-20.38 - -1.25	168	632	118	518	0.124	-0.030	0.154	168	286	800	1436	1.054

Fire Drivers	Class	WoE							FR				
		Npx1	Npx2	Npx3	Npx4	W+	W-	Wf	Npx1	Npx2	Npx3	Npx4	FR
	-1.25 - -0.25	145	655	130	506	-0.120	0.029	-0.149	145	275	800	1436	0.946
	-0.25 -0.63	160	640	130	506	-0.022	0.006	-0.027	160	290	800	1436	0.990
	0.63 - 2.0	177	623	111	525	0.237	-0.058	0.295	177	288	800	1436	1.103
	2.0 - 13	150	650	147	489	-0.209	0.055	-0.264	150	297	800	1436	0.907
TRI	1- 6.86	139	661	144	492	-0.265	0.066	-0.331	139	283	800	1436	0.882
	6.86-12.33	162	638	130	506	-0.009	0.002	-0.012	162	292	800	1436	0.996
	12.33-18.66	153	647	133	503	-0.089	0.022	-0.112	153	286	800	1436	0.960
	18.66-31.71	167	633	118	518	0.118	-0.029	0.147	167	285	800	1436	1.052
	31.71-117.81	179	621	111	525	0.248	-0.061	0.310	179	290	800	1436	1.108
TWI	3.26 -5.06	173	627	110	526	0.223	-0.054	0.277	173	283	800	1436	1.097
	5.06-6.22	158	642	133	503	-0.057	0.015	-0.072	158	291	800	1436	0.975
	6.22-7.91	164	636	126	510	0.034	-0.009	0.043	164	290	800	1436	1.015
	7.91-10.71	142	658	138	498	-0.201	0.049	-0.250	142	280	800	1436	0.910
	10.71-17.91	163	637	129	507	0.005	-0.001	0.006	163	292	800	1436	1.002
VCI	9.0-23	129	671	161	475	-0.451	0.116	-0.567	129	290	800	1436	0.798
	23-28	129	671	156	480	-0.419	0.106	-0.525	129	285	800	1436	0.812
	28-33	175	625	111	525	0.226	-0.055	0.281	175	286	800	1436	1.098
	33-39	170	630	117	519	0.144	-0.036	0.180	170	287	800	1436	1.063
	39-82	197	603	91	545	0.543	-0.128	0.671	197	288	800	1436	1.228
Wind Speed	1.45-3.59	153	647	135	501	-0.104	0.026	-0.131	153	288	800	1436	0.954
	3.59-4.29	142	658	143	493	-0.236	0.059	-0.296	142	285	800	1436	0.894
	4.29-5.16	166	634	122	514	0.079	-0.020	0.098	166	288	800	1436	1.035
	5.16-6.32	174	626	113	523	0.202	-0.050	0.252	174	287	800	1436	1.088
	6.32-11.89	165	635	123	513	0.064	-0.016	0.080	165	288	800	1436	1.028

Appendix 5: MaxEnt model response curves of fire drivers

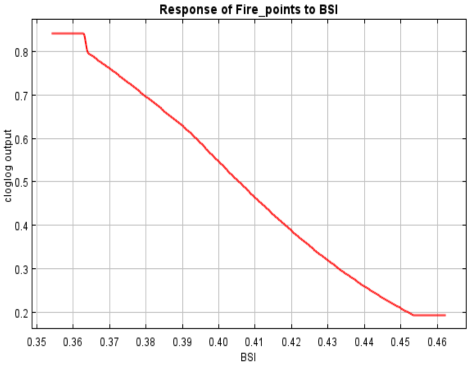

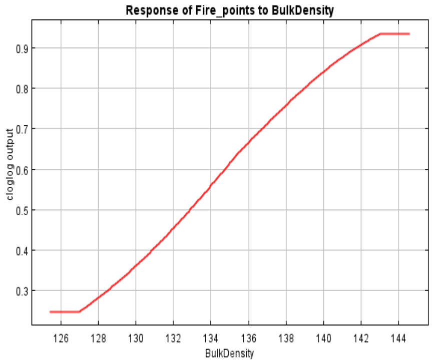

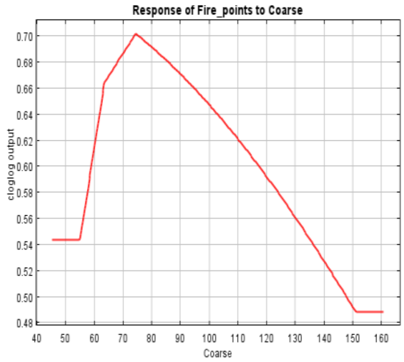

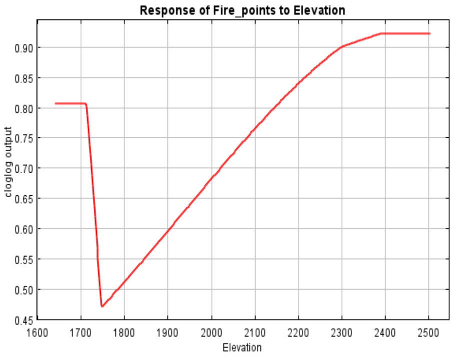

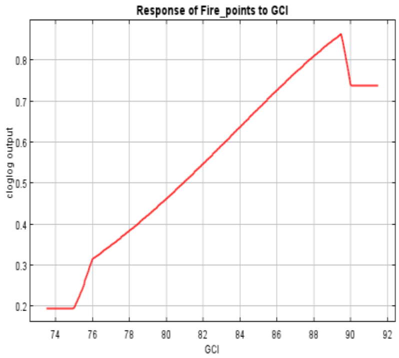

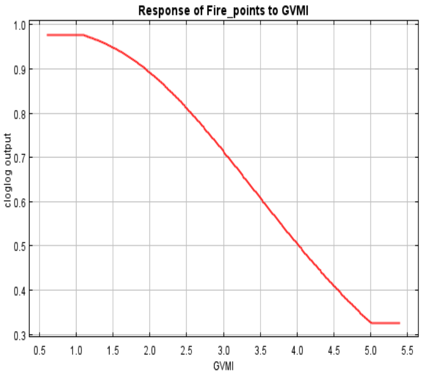

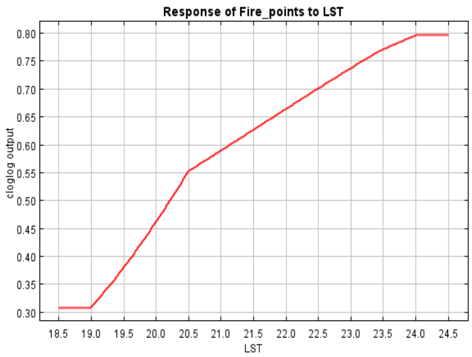

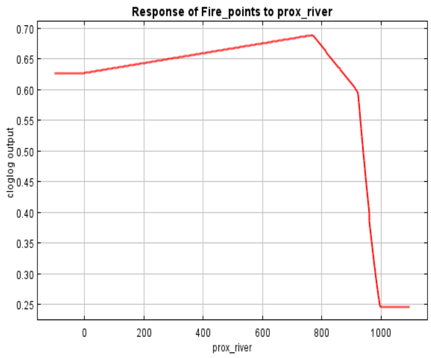

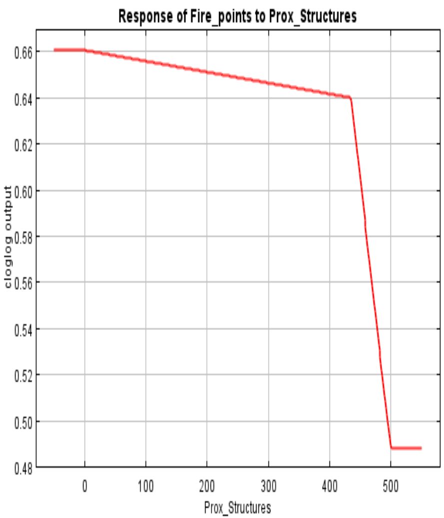

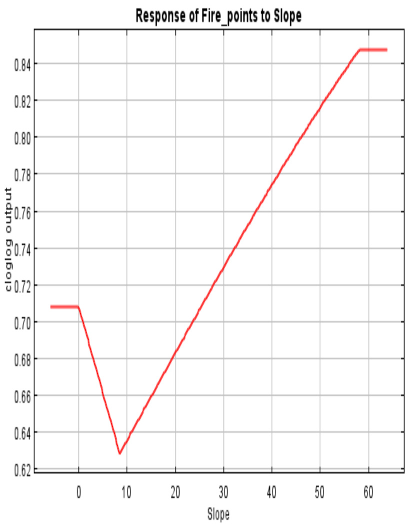

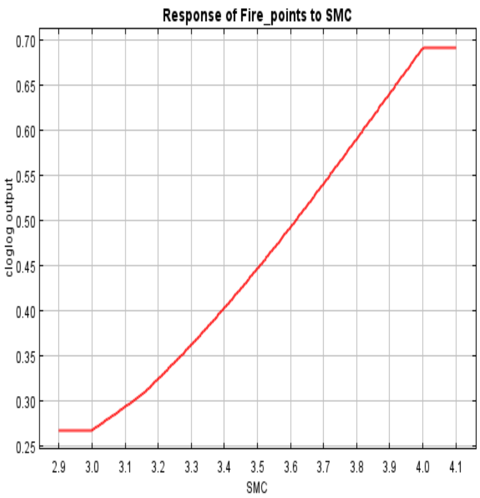

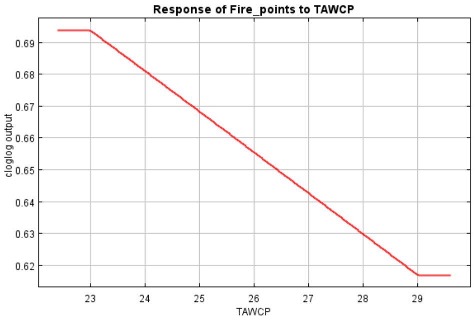
Response of Fire_points to TAWCP
cloglog output
TAWCP

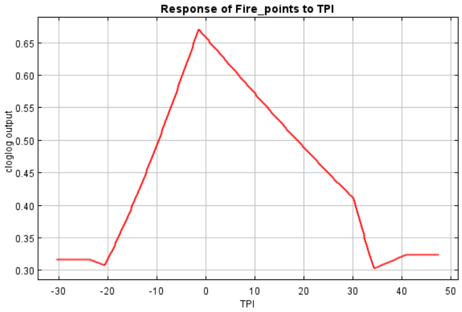
Response of Fire_points to TPI
cloglog output
TPI


Response of Fire_points to TRI
cloglog output
TRI


Response of Fire_points to TWI
cloglog output
TWI

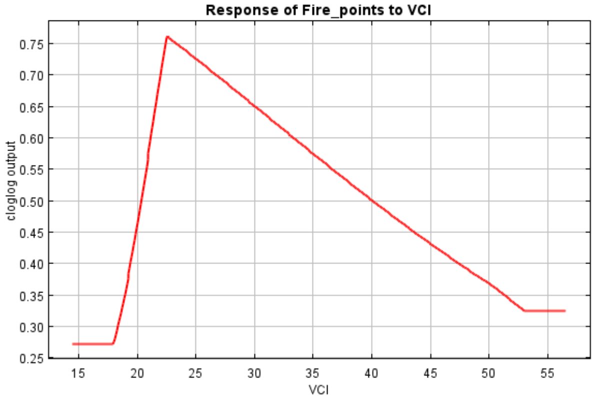
Response of Fire_points to VCI
cloglog output
VCI


Response of Fire_points to WindSpeed
cloglog output
WindSpeed